Polymorphic metabolism and the eco-evolutionary influence of social feeding strategies

Submitted by Richard James Lindsay to the University of Exeter as a thesis for the degree of Doctor of Philosophy in Biological Sciences.

April 2016

I certify that all material in this thesis which is not my own work has been identified and that no material has been previously submitted and approved for the award of a degree by this or any other University.

Richard J. Lindsay

Summary

Microbes live in complex environments where competitive and cooperative interactions occur that dictate their success and the status of their environment. By furthering our understanding of the interactions between microbes, questions into the evolution of cooperation, disease virulence and biodiversity can be addressed. This will help develop strategies to overcome problems concerning disease, socioeconomics and conservation. We use an approach that combines evolutionary ecology theory with genetics and molecular biology to establish and develop model microbial ecological systems to examine feeding strategies, in what has been termed synthetic ecology. Using the model fungal plant pathogen system of rice blast disease, we generated less virulent gene deletion mutants to examine the sociality of feeding strategies during infection and test a nascent virulence reduction strategy based on competitive exclusion. We revealed that the success of the pathogen is unexpectedly enhanced in mixed strain infections containing the virulent wild-type strain with a less virulent gene deletion mutant of the metabolic enzyme invertase. Our finding is explained by interference between different social traits that occur during sucrose feeding. To test the generality of our result, gene deletion mutants of putative proteases were generated and characterised. We found that if virulence related genes acted 'privately', as predicted by social theory, the associated mutants would not make viable strains to use for this virulence reduction strategy by competitive exclusion. Our study then went on to study the fitness of digesting resources extracellularly, as many microbes do, given that this strategy is exposed to social exploitation by individuals who do not pay the metabolic costs. This was investigated by developing an experimental system with *Saccharomyces cerevisiae.* Though internalising digestion could suppress cheats, the relative fitness of opposing strategies was dependent upon the environmental and demographic conditions. Using this polymorphic system, the influence of competitors on the stability of cooperation, and the influence of cheats on the maintenance of diversity were assessed. To test the fitness of internal versus external digestion in a more natural setting, we generated an internally digesting strain of the rice blast fungus. In addition to suppressing cheats, the strain had enhanced fitness and virulence over the wild-type. We propose that this is caused by a shift in a trade-off between yield and rate. We show how a synthetic ecology approach can capture details of the biology underlying complex ecological processes, while having control over the factors that drive them, so that the underlying mechanisms can be teased apart.

Contents

Acknowledgements

I am grateful to the NERC for funding this research.

I would like thank the numerous people that have helped me along the way. Thank you to my supervisors Ivana Gudelj and Nick Talbot for their support and guidance.

Thanks to those who taught an ecologist to ‘do’ molecular biology and genetics, especially to Michael Kershaw, Lauren Ryder, Magdalena Martin-Urdiroz, Miriam Oses-Ruiz, Xia Yan, Darren Soanes and George Littlejohn.

For theoretical discussions, technical support and general encouragement I want to thank Rob Beardmore, Bogna Pawlowska, Tina Penn, Yogesh Gupta, Carlos Reding-Roman, Mark Hewlett, Michael Sieber, Andy Foster, Barbara Saddler, Vincent Were, Lisa Butt, Yasin Dagdas, Wasin Sukulkoo, Magdalena Basiewicz, David Mwongera and all the others who I have missed!

Thanks to Meg Hunter and Maurice Lindsay for all of their support.

Thank you to Philippa Holder for all of her help and for putting up with me.

Finally, to my other friends and my family, thank you for everything you have done.

List of Figures, Tables and Appendices

Glossary

Allee effect - where per capita growth rate is maximal at intermediate population densities and reduced at lower densities

Anastomosis – the fusion between fungal hyphae

Apoplast - in plants, this is the diffusional space between plant cells and outside the plasma membrane

Appressorium – a specialised infection structure generated by pathogenic fungi to penetrate host surfaces.

Ascomycete – a phylum of the kingdom Fungi

Autophagy - a process that allows the controlled degradation and recycling of cellular components

Autophagosome – a vesicle involved in autophagy

Auxotrophy – the inability of an organism the anabolise (metabolically synthesise) an organic compound required for its growth

Axenic – a culture comprised of a single species or strain.

Biotroph – a pathogen that obtains nutrients from living host cells

Cheat – a non-cooperating individual or behaviour that exploits the cooperative actions of others

Conidium – an infecting agent of pathogenic fungi comprised of a three celled spore in *M. oryzae*

Conidiation – the production of conidia

Effectors – proteins produced by pathogens to facilitate infection by manipulating the host

Hardin's competitive exclusion principle - at equilibrium multiple species are unable to coexist for a single limiting resource

Hemibiotroph – a pathogen that is initially biotrophic but then switches to necrotrophic

Hyphae – the branching filamentous growth structure of fungi

Mycelium – vegetative growth of fungi consisting of a mass of hyphae

Necrotroph – a pathogen that kills host cells from which it acquires nutrients

'Non-producer' – used to describe a strain that does not produces a particular gene product

Osmolyte – a compound that influences osmotic pressure

Osmotrophy – a feeding mechanism where external digested or dissolved nutrients are taken up by osmosis

Periplasm – the subcellular space between the cell wall and the plasma membrane

Permease – a membrane transport protein

Phagocytosis – a feeding mechanism where nutrients are engulfed for intracelluar digestion

Preproenzyme – an inactive precursor of an enzyme that possesses a signal sequence

Private-goods – substances produced by an individual that only they can use

'Producer' – used to describe a strain that produces a particular gene product

Prototrophy – the ability of an organism to anabolise (metabolically synthesise) all of the organic compounds required for its growth

Public-goods – substances produced by an individual to generate a benefit that is available to all within a locality.

Rate-efficiency trade-off - a fitness trade-off in resource use and ATP production

Signal peptide – a short amino acid sequence at the N-terminal of proteins destined for the secretory pathway

Simpson's paradox – a statistical paradox where a trend is observed in different groups, however when the groups are combined this trend is lost or reverses

Social dilemma – a conflict between what is best for the group and what is best for an individual

Sporulation – the production of reproductive spores

Tragedy of the Commons - A scenario where cooperation is unstable because individuals selfishly look out for their own short term interests, despite cooperation being beneficial in the long term.

Transfer experiment – repeated batch cultures where a portion of an established population is inoculated into fresh media over numerous cycles to monitor population dynamics

'Transporter' – a strain that uses a transporter protein to take up a resource for 'private' metabolism

Virulence – The degree of damage that a pathogen inflicts upon its host

Virulence factors – molecular products of pathogens which cause damage to hosts

Zymogen – an inactive precursor of an enzyme

List of Abbreviations

μ - micro(n)

Abs – absorbance

ATP – adenosine triphosphate

b – (nucleotide) base

bp – base pair

BSA – Bovine serum albumin

C – carbon

CCR – carbon catabolite repression

cDNA – complementary DNA

CFU – colony formingcolony-forming units

CM - complete media

CMAC - 7-amino-4-chloromethylcoumarin

CO39 – a rice cultivar susceptible to infection by the rice blast fungus wild-type strain Guy11

CTAB - hexadecyltrimethylammonium bromide

d.f. - degrees of freedom

d.p.i. / h.p.i. – days/hours post inoculation

DAPI - 4',6-diamidino-2-phenylindole

DIC - Differential interference contrast

DIG – digoxigenin

DMSO – Dimethyl sulfoxide

DNA – deoxyribonucleic acid

DNase – deoxyribonuclease

EDTA - Ethylenediaminetetraacetic acid

ER – endoplasmic reticulum

F.w/v – fresh weight by volume

Fw – fresh weight

g – gram

g – standard gravity

gDNA – genomic DNA

GFP – green fluorescent protein

Guy11 – Wild-type strain of *Magnaporthe oryzae*

h – hour(s)

k – kilo

L – litre(s)

LB – Luria-Bertani (media)

LF – left flank

m – milli or metre

M – molar

min – minute(s)

MM – minimal media

MM-C – MM without a carbon source

MM-N – MM without a nitrogen source

MM-NC – MM without carbon and nitrogen source

n – nano or number of replicates

N – nitrogen

N:C – nitrogen to carbon ratio

NMR – Nitrogen metabolite repression

OD – optical density

ORF – open reading frame

PCR – polymerase chain reaction

r.p.m. – revolutions per minute

RF – right flank

RFP – red fluorescent protein

RNA – ribonucleic acid

RNase – ribonuclease

RNA-seq – RNA sequencing

ROS – reactive oxygen species

RT – reverse transcription

s.e.m. – standard error of the mean

sdH_2O – sterile distilled water

SDS - sodium dodecyl sulfate

sec – second(s)

SMM – supplemented minimal media

SOC – Super optimal broth with catabolite repression

Tris - Tris(hydroxymethyl)aminomethane

u – unit(s)

UTR – untranslated region

v/v- volume by volume

w/o – without

w/v- weight by volume

YPD - Yeast extract peptone dextrose

Δ – proceeds the name of a gene that has been deleted

Introduction

Microorganisms are ubiquitous; they have essential roles in biogeochemical processes and are involved in many symbiotic, parasitic and pathogenic relationships with other organisms over the spectrum of biological complexity. These range from pathogenic organisms that endanger human health and food security; to symbiotic relationships between mycorrhizal fungi or rhizobial bacteria and plants, which are thought to have enabled plants to colonise the land over 400 million years ago (1). Interactions between organisms dictate their success, the outcomes of which can alter evolutionary trajectories of all parties involved and, subsequently, the status of the environment they inhabit. This means that an understanding of microbial ecology can provide insight into some of the biggest questions of biology such as the evolution of cooperation, disease virulence, nutrient cycling, multicellularity and the maintenance of diversity. Further insight into the dynamics and implications of these ecological interactions represent promising avenues of research. The outcomes of novel findings provide theoretical and empirical support to novel strategies to overcome socioeconomic and ecological issues, including the management of disease (2, 3) in addition to the management of natural and agricultural ecosystems (4, 5).

Beyond the importance in their own right, microbes can also provide ideal model systems for studying broader questions concerning evolutionary ecological processes. Microbial systems have numerous benefits. They have short generation times, sequenced genomes, techniques for genetic analysis have been developed, there is an absence of moral dispute and, importantly from a synthetic biology perspective, strains are available or can be generated with altered genomes so that

the influence of genotypic and phenotypic diversity, such as that of a social trait, can be examined (6, 7). Model microbial systems are traditionally associated with being models for understanding genetics and molecular biology (8, 9). Yet using these systems to address ecological questions provides opportunities to control the degree of complexity of a system, a feature not possible to the same extent in field experiments (7). Moreover, working in parallel with molecular biology and genetics facilitates an understanding of ecological principles in the light of the detailed physiology of the organisms being studied. It may be important to point out that the semantics of microbial social behaviours often suggest conscious choice to perform a behaviour. Though certainly possible for metazoans, this is clearly not the case for microbes and during this thesis it is merely implied from an evolutionary sense.

As will be examined in further detail during this thesis, studies of ecological processes, such as cooperation and virulence evolution, can be overly complicated by multiple variables within and between organisms and their community. This often means that singling out particular driving forces behind observed effects can be problematic (e.g. (10, 11)), and the multi-dimensional nature of an individual's fitness can lead to genotypes being wrongly characterised (12). Synthetic biology provides an opportunity to unpick the complexity of ecological systems by constructing them so that single parameters can be carefully controlled and manipulated, in the absence of the full complexity of their natural existence. The key interactions between members of communities can therefore be known, facilitating quantification, and empowering the predictive capabilities of mathematical modelling. Examples of such microbial systems engineered to examine natural phenomena of ecology and evolution include the construction of systems of *Escherichia coli* strains to study Simpson's paradox (13), snowdrift game dynamics in sucrose metabolism by yeast

(14), and obligatory cross-feeding (15). Our study sets out to address further evolutionary and ecological questions using a synthetic ecology approach. This includes constructing strains or using generated strains from previous studies that are genotypically distinct in a social trait, yet traceable in mixed populations so that the relative fitness of co-existing strains can be determined. In this project we have used these systems, coupled with a systems biology approach of mathematical modelling, to examine theories of cooperation, the evolution of virulence and the maintenance of diversity using the fundamental trait of nutrient acquisition and metabolism.

Structure of the thesis:

In Chapter 1 we identify and characterise an invertase deletion mutant in the rice blast fungus to gain an understanding of sucrose feeding and its importance during disease

In Chapter 2 we investigate the social nature of sucrose metabolism in the rice blast fungus and examine a novel disease management strategy based upon cooperation and virulence theory.

In Chapter 3 we study the generality of findings from Chapters 1 and 2 by characterising another virulence related gene, this time associated with protein metabolism, where we highlight the importance of sociality in virulence reduction strategies.

In Chapter 4 we develop a system with polymorphisms in sucrose metabolism with yeast to study the fitness consequences of privatising invertase production, and how these polymorphisms can underpin mechanisms for the maintenance of diversity and cooperation.

In Chapter 5 we generate a strain of the rice blast fungus that privately metabolises sucrose to gain an understanding of the fitness consequences of private vs public feeding strategies during infection.

Each experimental chapter has an introduction to give the relevant background of the subject and motivation, as well as a discussion and a chapter specific methods section.

The thesis then concludes with a general discussion to tie together the overall findings, and finally a general methods section for protocols that are involved in numerous chapters.

Chapter 1

Using an understanding of evolution and ecology to tackle disease

1.1 | Introduction

1.1.1 | Targeting disease virulence

Novel, durable and effective strategies to tackle disease – of humans, animals and plants - are essential in the face of antibiotic resistance and the ever evolving capacity of microbial pathogens to overcome resistant crop cultivars (16-23). An alternative to traditional disease management approaches, which is considered to be more evolutionarily robust against resistance due to imposing weaker selective pressure, is to target virulence of a pathogen. This approach aims to both reduce the damage caused to the host and weaken the disease to facilitate secondary interventions, including the deployment of natural immune responses (2, 24-27).

Virulence factors are molecular products of the pathogen that are generally dispensable for vegetative growth in fully supplemented complete media, but which, directly or indirectly, cause damage to hosts during infection. Approaches to anti-virulence strategies include the development of drugs that ‘disarm’ pathogens by targeting the virulence factors they produce (24, 28, 29). Successful clinical trials have been conducted using monoclonal antibody-based drugs, which target toxins produced by *Escherichia coli* (30) and *Clostridium difficile* (31). Iron-scavenging siderophores of pathogens have also been targeted, including by quenching with the iron-mimicking metal gallium which binds to siderophores, but does not have the same reducing capacity as iron (32). Another target has been to enzymatically degrade quorum sensing molecules, which influence cell-to-cell communication (33). Notably, quorum sensing frequently regulates the collective production of secondary virulence factors such as proteases (34-36), so interruption of one virulence related

trait may have secondary effects upon another. Despite some success and evidence of evolutionary robustness of virulence reducing drugs (30-32, 37), resistance (38) and undesirable secondary effects have been reported (39, 40).

1.1.2 | Deploying live organisms to tackle virulence

An alternative to using anti-virulence drugs is to deploy live organisms to lessen virulence. An existing implemented strategy in agriculture is to infect fungal pathogens with mycoviruses that impose a hypovirulent phenotype upon the pathogen. This method, referred to as hypovirulence, has had some success. For example, the mycovirus *Cryphonectria hypovirus 1* has been used to lessen the damage caused by the Chestnut Blight fungus *Chryphonectria parasitica.* This virulence reduction strategy continues to be used in European chestnut orchards. However, the success of mycoviruses as biocontrol agents on crops plants has been restricted by problems with the speed of treatment and transmission to fungal hosts (41, 42).

Another strategy in clinical and agricultural use that deploys live organisms is the introduction of less virulent pathogen strains to reduce the success of more virulent strains. This strategy is based upon competitive displacement of a pathogen, where stains with attenuated virulence, resulting from not performing a metabolically costly behaviour that normally results in host damage, can out-compete more virulent strains (2, 26, 44). During this thesis, it is this form of virulence reduction strategy that is examined in more detail with *Magnaporthe oryzae.* Successful examples of this strategy being implemented include in clinical trials where the use of naturally occurring non-toxigenic strains of *C. difficile* have successfully prevented toxigenic strains from infecting both hamsters and humans (45, 46). The principle of

introducing less virulent strains is also in use with applications to crops, including maize, cotton and peanuts. Here, naturally occurring non-aflatoxin producing strains of *Aspergillus flavus* are used as a biocontrol agent against toxin producing strains. The mechanism of non-toxigenic strain inoculation is thought to be based on competitive exclusion of the virulent toxigenic strain (47-51). These biocontrol strains are commercially available, with *Afla-Guard* being sold by Syngenta as a crop protection product (52). Ecological and evolutionary based therapies such as these, which control rather than eradicate disease, have also been proposed as a treatment strategy against cancer. Such treatments include targeting secreted growth factors with antiangiogenic drugs or promoting the evolution of cell lines that are non-producers of such factors to limit nutrient supply to a tumour (25, 27).

1.1.3 | Ecology and evolution of disease

In general, it is thought that the basis of these strategies of introducing less virulent strains is based upon understanding of ecology and evolution. It aims to turn knowledge of the fitness and virulence consequences of cooperation against disease. The social behaviours of organisms have consequences for both the actor and recipient of the action. Social behaviours have been broadly categorised based on the fitness benefits or detriment they cause to the actor and recipient. They can vary from a negative cost to both, such as interference competition by spiteful production of antagonistic and antibiotic proteins (53, 54); positive to the actor at the expense of the recipient, such as exploitation of a shared resource; or cooperative in which recipients benefit from the action of another and provide direct and/or indirect benefits to the actor (through aiding relative fitness) (55-61).

1.1.4 | Cooperation

Cooperation can be observed throughout nature in organisms of diverse biological complexity. Why an individual would perform a costly act to enhance the fitness of others has received much scientific attention (55-61). Although traditionally believed to be unique to animals, cooperation in microorganisms and even between cancer cells is now apparent and is indeed a growing area of study (3, 25, 27, 55, 62-64). Microbes exhibit numerous traits that can be seen as cooperative (65), including nutrient acquisition (66-69), host attack (70-72) reproduction (73), dispersal (74, 75), the efficient use of resources (76, 77), competition suppression (53, 78, 79), persistence (80) and protection (81, 82). Angiogenic growth factors and immune suppression factors produced by cancer cells have been also suggested to represent public-goods during tumour formation (3, 25, 27). Furthermore, cancer cells are thought to cooperate by secreting proteases to degrade the extracellular membrane to facilitate invasion of epithelial cancer cells (83).

1.1.5 | Public-goods

One of the most common and widely studied forms of microbial cooperation comes in the form of public-goods. These are substances, for example a secreted enzyme, that are generated at a metabolic cost to the individual producing them, yet the benefit they produce is external, allowing access to a previously indigestible food source to neighbours. This brings about an exploitative opportunity where individuals can selfishly avoid such a costly investment in producing public-goods and gain from the investment made by others; all else being equal, putting those ‘cheats’ at a relative selective advantage (66, 67, 72, 84-88). Existing model systems for studying the sociality of microbial public-goods include iron-scavenging siderophore

molecules produced by bacterial pathogens (86), secreted invertase produced by *Saccharomyces cerevisiae* to break down extracellular sucrose (66), cell signalling by quorum sensing molecules of bacteria (70), production of exopolysaccharides to form protective biofilms (81, 89), and production of secreted toxins to attack hosts for successful infection (71, 78). In addition to these established systems, because many gene products of microbes act externally from the cell, the results of their actions are frequently shared by individuals other than the original producer, so any of these products are potential public-goods (e.g. (90-92)).

1.1.6 | Efficient use of resources

Cooperation can also take the form of efficient use of resources, or prudency, which will be explained below. Constraints upon ATP-producing metabolic pathways results in a trade-off between rate (moles of ATP per unit of time) and yield (moles of energy per unit of resource) (77). Energy is obtained by heterotrophs from breaking down substrates into products with lower free energy. This difference in energy can be partly captured by producing ATP. Some of this free energy is required to drive degradation reactions to overcome activation energies. The amount of energy invested dictates the rate of the reaction, at the expense of yield (77). For instance, sugar can be metabolised to produce ATP by slow, high-yielding respiration; or by rapid, low-yielding fermentation. So resources can either be used in a cooperative manner; slowly and efficiently at a detriment to the individual but benefit of the local population; or conversely in a selfish fashion; rapidly and inefficiently in a way that maximises an individual’s growth rate at the impairment of fitness of the collective group (76, 77, 93).

1.1.7 | Mechanisms for the evolution and maintenance of cooperation

Cooperation has received considerable scientific attention because it initially appears to contradict Darwinian natural selection. It poses a problem to classical evolutionary theory, because costly behaviour decreases an individual's relative fitness, all else being equal, so would be selected against (59, 60, 94). This would lead to populations of cooperators being vulnerable to invasion by non-cooperating individuals, who have a competitive advantage by benefitting from the cooperative contributions of others without experiencing the associated cost (59, 60, 95). This leads to a rise of the 'Tragedy of the Commons', where cooperation is unstable because individuals selfishly look out for their own short term interests, despite cooperation being favourable in the long term (96). Theoretical and empirical work has revealed multiple mechanisms that facilitate the evolution of cooperation (58-60).

Cooperative traits could evolve and persist as a result of direct fitness benefits, meaning that the benefits received by the individual performing the cooperative behaviour, will outweigh the penalty of performing it, thus being mutually beneficial (57, 97). In this case there is no social dilemma. However there are numerous occasions when this does not appear to hold true, so further explanations may be required. Indirect fitness benefits of cooperation occur when recipients of cooperative acts share the cooperative gene with the performer, thereby promoting the gene's replication through relatives, referred to as 'Kin Selection' (59, 60, 98). According to Hamilton's Rule, cooperative behaviours can evolve when $r.b > c$, where r is the genetic relatedness between actor and recipient, b is the fitness benefit obtained by the recipient and c is the fitness cost incurred by the actor (59, 60). To facilitate kin selection, interacting individuals need to have relatively high genetic relatedness, which can be achieved via limited dispersal or kin discrimination, which result in

spatially structured populations (59, 60, 99). Limited dispersal results in a higher probability of interacting with genetically related individuals who may also possess a common gene for cooperation, thereby promoting selection (100, 101). This structuring is often inherent in microbes which form clonal patches such as colonies or hyphal networks.

Population structuring or assortment is therefore significant for cooperation between microbes because interactions, such as public-good secretion, act over short distances (102, 103). Microbes also possess the ability to identify relatives by recognising ‘green beard’ genes, such as the flocculation gene *FLO1* in yeast (104) and *csaA* in amoeba (105). These genes aim to keep groups clonal to avoid cooperative acts being exploited by unrelated individuals. Taking this population structuring one step further, public-goods use may have selected for incomplete cell division leading to the evolution of multicellularilty (106).

Group selection, or multi-level selection, has been suggested to be a mechanism for cooperation emergence and persistence (107). This can occur when competition for a global gene pool exists at the sub-population level and the scale of competition is more intense between (global), rather than within (local) patches. This may occur, for example if cooperators having lower relative fitness within mixed-strategy groups and so decrease proportionally. However, over the metapopulation this proportional decrease is outweighed in groups with high proportions of cooperators. These cooperator-rich groups have improved productivity in terms of reproductive output and therefore cooperators persist in the overall gene pool. This scenario, where trends identified within different groups are lost or reversed when the groups are combined as a result of weighted averages, such as the differing productivity of groups with different frequencies of cooperators, is referred to as a Simpson’s

paradox (108). Experimental support of this paradox supporting cooperation includes a synthetically generated public-goods system in *E.coli* (13).

Another mechanism to support cooperation is to repress competition by limiting the success of cheating. This can be through pleiotropy where cooperative traits are linked to other traits so defection in the social behaviour has secondary detrimental effects (109-111). For example, social cheats can be prevented from invading populations because there is an obligatory link, through quorum sensing, between a public- (protease production) and a private-good (adenosine metabolism) (110).

1.1.8 | The influence of cooperation theory for the evolution of virulence

Social behaviours influence population fitness, and given that numerous microbes exist as obligately pathogenic organisms this can subsequently alter the manifestation of virulence caused during disease (72, 86-88, 112-115). Virulence is thought to be the unavoidable result of a pathogen exploiting its host in order to proliferate and transmit to a new host (116-120). Multiple infections, when more than a single genotype of the same species simultaneously infect a single host, are thought to be common in nature (121-123). Individuals share the host environment so that interactions between genotypes, including both competitive and cooperative encounters, can occur as they do in other ecosystems (124). Both forms of cooperation discussed above, public-good production and efficient use of resources, can occur during pathogenesis. They have an impact upon the extent of damage caused to the host during infection. The occurrence of multiple genotype infections leading to breakdown of cooperative traits as a result of social dilemmas has implications for the evolution of virulence. Evolutionary theory of disease virulence, considering social interactions that occur between infecting individuals, predicts that

multiple genotype infection could lead to an increase, or decrease, in virulence depending on the social behaviour considered (114, 115).

1.1.9 | Prudency and the evolution of virulence

Models of virulence evolution considering the social trait of prudent use of resources predict that to maximise fitness, cooperating populations will use host derived nutrients slowly and efficiently resulting in low virulence. However, when genotypic competition is introduced in multiple infections, individuals can be at a selective advantage if they exploit resources quickly, but wastefully. As virulence is the result of host exploitation, this increased consumption rate will lead to higher virulence (117-119, 124-126).

1.1.10 | Public-goods and the evolution of virulence

The augmentation of fitness resulting from a pathogen's public-goods causes an increase in exploitation of the host and, therefore, virulence (87, 88, 112). Accordingly, these public-goods are referred to as virulence factors. Kin selection theory predicts that pathogen population fitness and disease virulence will decrease in mixed genotype infections when public-goods cooperation is a mechanism of pathogenicity (115). This is because during mixed genotype infections, less virulent non-public-good-producing cheats arise and profit from the goods produced by others resulting in reduced net production of these virulence factors which facilitate population growth and infection (87, 88, 112, 113, 127-129).

1.1.11 | Virulence evolution and mixed genotype infection

As discussed above, theory predicts that mixed-genotype infections can lead to an increase or decrease in virulence depending upon the social interactions occurring

between co-infecting pathogens. Experimental evidence has been found to support both theories. For example mixed-genotype infections by fungal plant pathogens have been found to reduce disease severity. This is thought to be caused by competition between strains inhibiting the aggressiveness of the pathogens (130-133). Alternatively mixed infections can lead to increased virulence or a higher pathogen load in fungi (124, 134) and other microbial pathogens (125, 126, 135-137). As alluded to in the thesis introduction, experimental evidence of many ecology based theories such as those just mentioned, can often be confused as to the precise mechanisms responsible for observed results. They frequently lack exact details of the causal mechanism; or phenotypic diversity of the co-infecting pathogens and hence the nature of the resulting social interactions; be they cooperative or competitive. Furthermore, observed differences in pathogen density and virulence may be as a result of phenotypic plasticity of the pathogen upregulating growth rates in mixed genotype infection or hosts being less capable of mounting effective immune responses to diverse infections (138, 139). Consequently, the synthetic ecology approach employed during the research presented in this thesis attempts to circumvent these issues.

1.1.12 | Hamiltonian medicine

Based on the understanding of the ecology and evolution of disease, strategies have been proposed and developed that aim to apply this knowledge of inclusive fitness and disease virulence against the dynamic social lives of pathogens. This is an extension of the more general Darwinian medicine: the application of evolutionary concepts (43), to what has been termed Hamiltonian medicine (2, 26).

Importantly, for both cases of social traits of pathogens discussed above when considering the implications for cheats and virulence evolution, be it for public-goods or prudency, the occurrence of less virulent genotypes within a population of virulent genotypes is expected to reduce the overall virulence of that infection compared to a population exclusively of the more virulent strain (115).

Hamiltonian medicine aims to hamper the fitness of the pathogen/disease population by restricting the benefit they gain through public-good cooperation. It has been proposed that due to the selective advantage that less virulent non-cooperating cheats have within populations, they may be introduced into pathogen populations where they could out-compete the highly virulent cooperators present and hence reduce the severity of the infection by reducing the overall virulence factor production (2, 26). Furthermore, 'cheat therapy' could also reduce the overall pathogen population fitness meaning that they are more susceptible to secondary interventions and host defences. Experimental evidence to support this theory includes laboratory experiments with *Staphylococcus aureus* and *Pseudomonas aeruginosa* infection of wax moth larvae *(Galleria mellonella*) or mice, respectively, with strains lacking the cooperative traits of quorum sensing signal production or response (87, 112), and iron-scavenging siderophore production (88). Clinical studies on human patients with cystic fibrosis found that disease virulence from *Pseudomonas* infections was reduced in infections that contained public-good mutant strains (113). Given the theoretical promise and empirical success for this disease management strategy, we asked if it is failsafe. Our study firstly aimed to create a synthetic ecological system in a pathogenic organism where the impact of non-cooperating exploitative cheats of a virulence causing public-good could be examined to test the principles of 'Hamiltonian medicine'. For this we used the rice blast fungus *M. oryzae*.

1.1.13 | *Magnaporthe oryzae*

Fungal plant pathogens cause devastating disease and extensive yield loss in agriculturally important crops. Rice blast disease, caused by the hemibiotrophic ascomycete *Magnaporthe oryzae,* causes enough rice yield loss to feed 60 million people at a cost of over £40 billion (19). *M. oryzae* is capable of infecting multiple grasses including numerous crops in addition to rice (*Oryza sativa*), such as wheat (*Triticum aestivum*), barley (*Hordeum vulgare*) and finger millet (*Eleusine coracana*) (140). *M. oryzae* is thought of as the most important fungal pathogen in terms of scientific and economic importance (18) and is considered a model fungal plant pathogen system for investigating the biology of fungal virulence (9, 141). Rice blast control strategies need to be developed because resistant rice cultivars are not durable (19, 142). *M. oryzae* can readily be cultured away from its host plant, its complete genome has been sequenced and the development of techniques for genetic analysis are enabling its biology to be deciphered. This includes the analysis of social behaviours making it an ideal system for studying pathogen-pathogen interactions in contrast to the more commonly studied pathogen-host interactions (92, 141, 143-147).

The infection cycle of *M. oryzae* begins with a conidium (three celled spore) germinating on plant leaves where it forms a specialised structure to penetrate the plant cuticle called an appressorium. This process occurs in response to environmental cues including a hard hydrophobic surface (148) and nutrient deprivation (149). It is regulated by the cAMP and *PMK1* MAP kinase signalling pathways which interact with downstream regulatory genes such as the transcription factor *MST12* (150-152). The appressorium creates mechanical force to rupture the plant cuticle by accumulating osmolytes such as glycerol, which in turn amasses

osmotic pressure of up to 8.0 MPa to force the fungal penetration peg through the tough exterior of the leaf (153). Autophagy during this process is important to metabolically fuel pathogenesis by recycling endogenous nutrients before the fungus can utilise the plant derived food resources (146, 154, 155). Thin penetration hyphae emerge from the base of the appressorium allowing tissue colonisation via bulbous invasive hyphae that invaginate the rice plasma membrane. Biotrophic growth occurs through neighbouring plant cells via plasmodesmata for 4-5 days (156). During the biotrophic phase the pathogen acquires nutrients from the host, and suppresses host defences using a diverse range of effectors, the functions of which include masking the presence of the fungus and interfering with plant defence signalling (92, 147). Later on during infection, the fungus becomes necrotrophic killing host cells and resulting in disease lesions from which the pathogen erupts and sporulation occurs for further disease transmission (Figure 1.1) (144, 157). Wild populations of *M. oryzae* exhibit a large amount of genetic diversity, a reason for the challenge faced to yield durable resistant rice cultivars (158, 159).

Figure 1.1

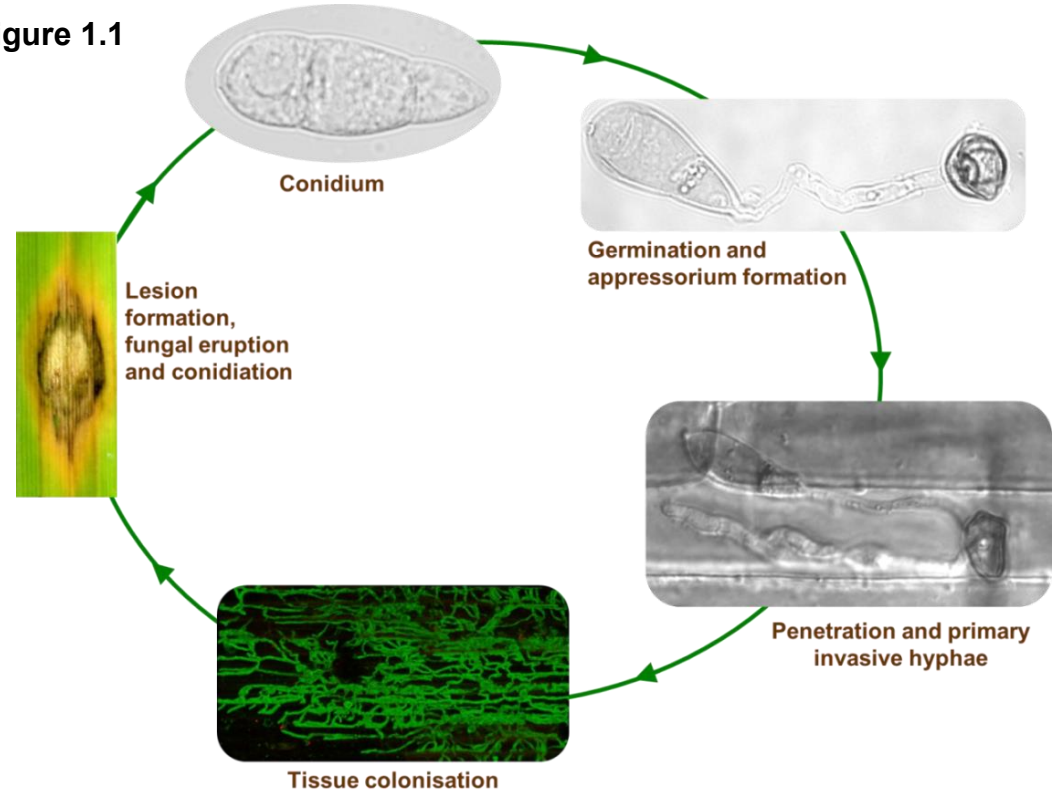

Figure 1.1 | The disease cycle of *Magnaporthe oryzae*. Infection of rice starts and finishes with the release of conidia, the infecting agent analogous to many microbial diseases. Conidia initiate disease by germinating to form a specialised structure, the appressorium, which generates the mechanical force to enable penetration of the host. From the appressorium, primary invasive hyphae grow into the host cells. Hyphae proliferate through host cells enabling the pathogen to colonise the tissue and exploit nutrients. Disease lesions form on the plant from which the fungus erupts and conidia are generated for transmission. Images shown are (clockwise) a three celled conidium, a germinated conidia forming an appressorium *in vitro* on an inducing hydrophobic surface, live-cell image of a successfully penetrated rice plant (CO39 cultivar) leaf sheath 26 h.p.i (DIC), a proliferating cytoplasmic GFP expressing strain of *Magnaporthe oryzae,* ramifying through rice plant cells, and disease lesion on rice leaf 7 d.p.i..

1.1.14 | How plant pathogenic fungi acquire their food

Fungi acquire nutrients via osmotrophy, by secreting enzymes to externally break down complex polymeric nutrients. The simpler molecules liberated are subsequently taken up through selective transporters (Figure 1.2) (160, 161). Proteins often possess an N-terminal sequence called the signal peptide to designate them to the secretory pathway (162). During this thesis, we targeted extracellular metabolic enzymes as potentially cooperatively produced public-goods upon which our system could be based.

Sucrose is the major product of photosynthesis and represents the compound used to transport carbon in plants (163, 164) and therefore may be an important nutrient to sustain and allow proliferation of plant pathogenic fungi (165). Non- infected rice leaves have approximate sucrose concentrations in the region of 40-60 $mmol.kg^{-1}$ FW (approx. 1- 2%) (166). Sucrolytic activity is catalysed by invertase enzymes (β-fructofuranosidase; EC 3.2.1.26), thus invertase genes were targeted for deletion to generate a null mutant which could act as a social ‘cheat’.

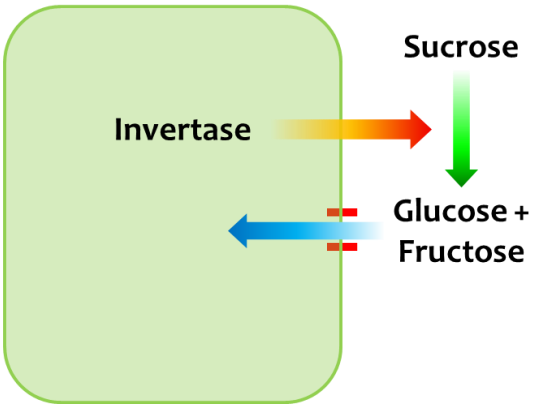

Figure 1.2 | Schematic of invertase catalysed sucrose metabolism. Fungi feed by osmotrophy whereby they secrete depolymerising enzymes, such as invertase, which break down more complex polymers, such as sucrose, into simpler molecules that are taken up through selective transporters, in this case hexose transporters, for internal metabolism.

Invertase breaks down sucrose to form equimolar glucose and fructose by hydrolysis of the glycosidic bond (165), with glucose being the preferentially utilized carbon source for *M. oryzae* (167). Invertase enzymes form part of the glycoside hydrolase family 32 (GH32) group of carbohydrate active enzymes. In Fungi, GH32 enzymes are associated with a plant biotrophic lifestyle, with the exception of mycorrhizal taxa, but including pathogens (165).

For invertase of *M. oryzae* to act as a public-good, it must act externally so that the benefits from the products of sucrose metabolism are communal. Most classified transport proteins in plant associated fungi are specific for monosaccharides; primarily facilitating the uptake of glucose and fructose (168-171). This is with exception including a sucrose transporter identified in the biotrophic pathogen *Ustilago maydis* (172). Invertase activity in *Magnaporthe*-infected rice leaves, coupled with a lack of sucrose found in fungal cultures, suggests *M. oryzae* externally hydrolyses sucrose before it is ingested (173). Bioinformatic and PCR-

based analyses identified the presence of two GH32 genes in *M. oryzae* that were predicted to be extracellular (165). Fungal infection of plants has been reported to result in increased invertase activity (174, 175) including in the *M. oryzae* – rice (*O. sativa*) system (173, 176). Though whether all of this invertase was of host or pathogen origin has not been discriminated. During blast infection, expression of rice cell-wall invertases have been found to be enhanced, believed to be part of a metabolic shift to resist pathogen infection (176); but it is thought to be unlikely that the carbohydrate requirements of fungal pathogens could be exclusively met via host derived enzymes (177). Indeed it does appear that there is a contribution from both parties, as observed in the *Botrytis cinerea* – *Vitis vinifera* (178) and *Uromyces fabae* – *Vicia faba* systems (179).

The nutrient environment experienced by the fungus during infection is still largely unknown (180). Nevertheless, *M. oryzae* has numerous G-protein coupled receptors and possesses carefully controlled carbon and nitrogen metabolism. This enables the fungus to respond to the dynamic and heterogenous nutrient conditions it experiences during infection such as different carbon sources available during light/dark cycling and the occurrence of necrosis (141, 167, 181). The genetic regulatory systems carbon catabolite repression (CCR) and nitrogen metabolite repression (NMR) enable the preferential use of carbon and nitrogen sources by repressing the expression of genes for secondary metabolism such as secreted digestive enzymes. This transition to secondary metabolism is the link between the use of available resources and pathogenesis. These systems are controlled by the sugar sensor trehalose-6-phosphate synthase (*TPS1*) via glucose-6-phosphate sensing, to preferentially consume glucose (carbon), and ammonium and L-glutamine (nitrogen). In the CCR system of *M. oryzae* α-D-glucose and D-fructose

act as repressors, whereas sucrose has de-repressing effects (167, 181-184). Growth triggered by the nutritional environment may also be governed by a TOR signalling pathway (185). For its own gain *M. oryzae* is also understood to elicit metabolic reprogramming and nutrient release by the host plant upon infection with substantial increases in sucrose, glucose and fructose at disease sites (91).

To gain a further understanding of nutrient acquisition and feeding strategies of *M. oryzae* to test the possibility of implementing ‘Hamiltonian medicine’ style interventions for rice blast disease, we firstly set out to create a mutant that did not generate a public-good virulence related product.

1.2 | Results

1.2.1 | Generating an invertase deletion mutant

As mentioned above, *M. oryzae* has previously been predicted to possess two GH32 genes with secreted products namely MGG_05785 (GenBank: XP 369679.1, Uniprot: G4N0X0) and MGG_ 02507 (GenBank: XP 365805.1, Uniprot: G4MKB1) (165, 186). Therefore to functionally identify invertase genes and to generate a non-invertase producing strain, we targeted these genes for deletion using a split-marker gene deletion technique (145, 146) (Figure 1.3). We found that both of these genes are predicted to be secreted based on the protein localization software WoLF PSORT (Table 1.1)(187) and the signal peptide identifying software SIGNALP 4.1 (Figure 1.4) (188).

Figure 1.3 | Schematic of fusion PCR based split-marker targeted gene deletion of putative invertase genes *INV1* (MGG_05785) & *INV2* (MGG_02507) (a & c) and confirmation of gene replacement by Southern blot analysis (b & d). Gene replacements were achieved by replacing putative invertase genes with a 2.8 kb sulfonylurea resistance allele (*ILV1)*. For each gene, in a first round of PCR, a 1 kb genomic fragment upstream (LF) and downstream (RF) of the ORF were amplified. Separately, 1.6 kb overlapping fragments of the 5' and 3' end of the sulfonylurea resistance gene cassette (*ILV1*) were amplified. Amplicons produced were fused in a second round of PCR to produce two larger fragments of 2.6 kb. The constructs were used to transform *M. oryzae* (Strain *ToxA*:*SGFP* background Guy11) and gene replacement achieved by homologous recombination. Gene replacements were confirmed by fragment size differentiation following restriction endonuclease digestion of gDNA with *XhoI* for *INV1* and *SapI* for *INV2*. Wild-type genotype band for *INV1* was at 4.2 kb with mutants at 5.6 kb (transformants #11 & #15 shown here (**b**). Wild-type genotype band for *INV2* was at 5.2 kb with mutants at 20.1 kb (transformants #52, 54 & 56 shown here) (**d**).

Figure 1.3

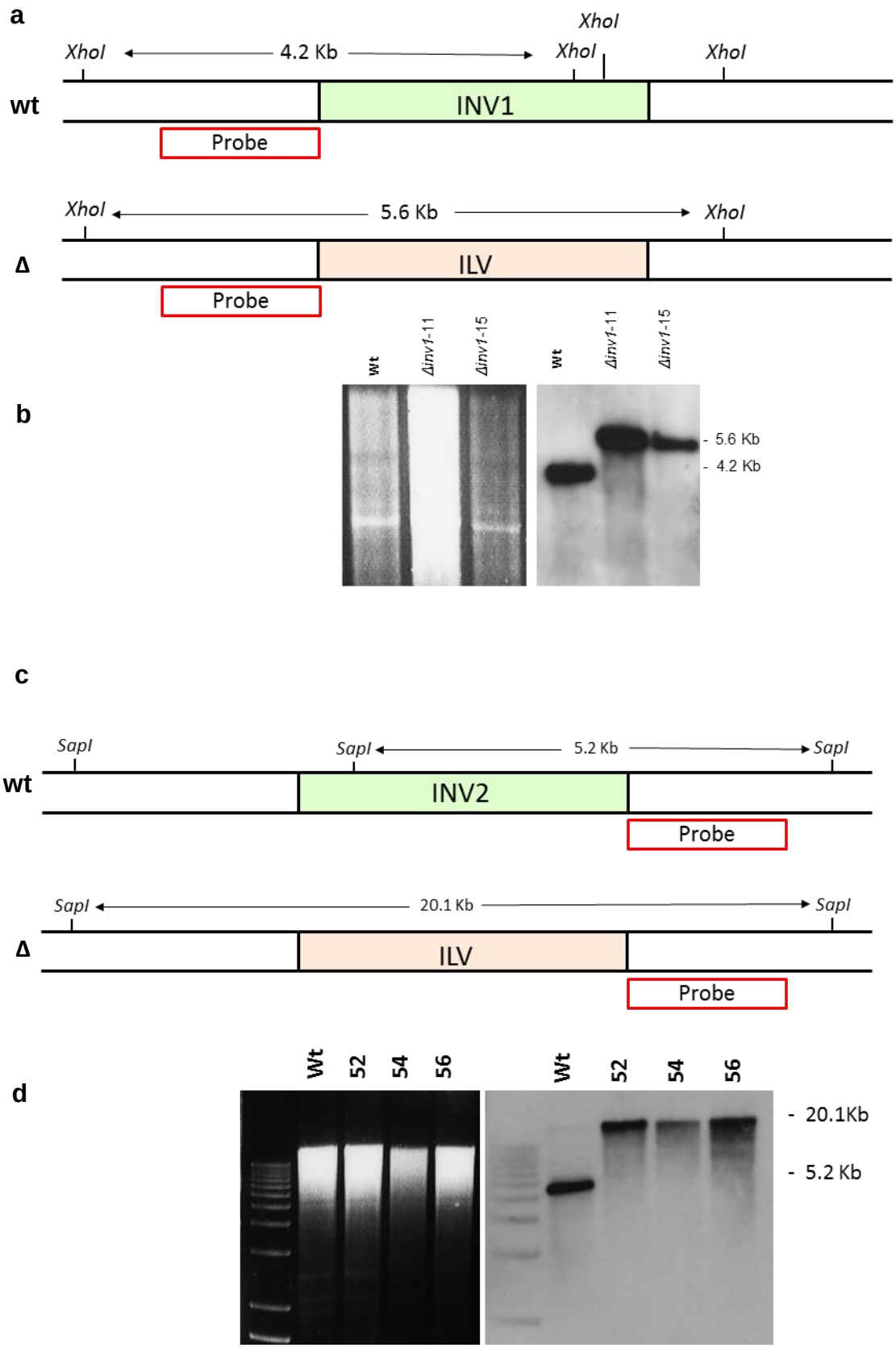
a
XhoI
4.2 Kb
XhoI
XhoI
XhoI
wt
INV1
Probe
XhoI
5.6 Kb
XhoI
Δ
ILV
Probe
b
wt
Δinv1-11
Δinv1-15
wt
Δinv1-11
Δinv1-15
- 5.6 Kb
- 4.2 Kb
c
SapI
SapI
5.2 Kb
SapI
wt
INV2
Probe
SapI
20.1 Kb
SapI
Δ
ILV
Probe
d
Wt
52
54
56
Wt
52
54
56
- 20.1Kb
- 5.2 Kb

Table 1.1 Subcellular localisation prediction of putative invertase genes from Wolf PSORT software (187)

Gene	Wolf PSORT prediction
MGG_05785	extr: 24, mito: 2
MGG_02507	extr: 24, E.R.: 2

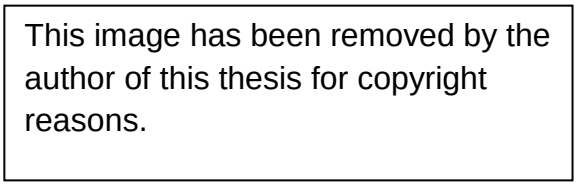

Figure 1.4 | Identification of predicted signal peptides on putative invertase genes of *Magnaporthe oryzae* using SIGNALP 4.1 software (188). Both genes possess putative signal peptides with **a** MGG_05875 (*INV1*) having a cleavage site between amino acids 19-20, with **b** MGG_02507 (*INV2*) having a cleavage site between amino acids 20-21. This suggests that both gene products are destined for the secretory pathway.

1.2.2 | Invertase expression in *M. oryzae*

In order to assess phenotypically to impact of gene deletion *in vitro,* conditions of invertase expression in the wild-type strain had to be established so that impairment in invertase activity of the deletion mutants could be confirmed. Using enzymatic assays on crude secreted enzyme extracts, as predicted of the CCR system of *M. oryzae,* we confirmed that glucose acts as a repressor, whereas sucrose has de-repressing effects (Figure 1.5a) (167, 181-184), with invertase activity peaking around 1% sucrose (Figure 1.5b). This is in agreement with previous findings in *Aspergillus* species (189-191), but in contrast to *S. cerevisiae* invertase expression, which is regulated by the experienced concentration of glucose (192, 193). For plant pathogens, such as *M. oryzae*, this may be because sucrose represents a primary carbon source for the fungus (164, 165). This also demonstrates the ability of *M. oryzae* to respond efficiently to dynamic nutrient conditions it encounters (167, 181).

Figure 1.5

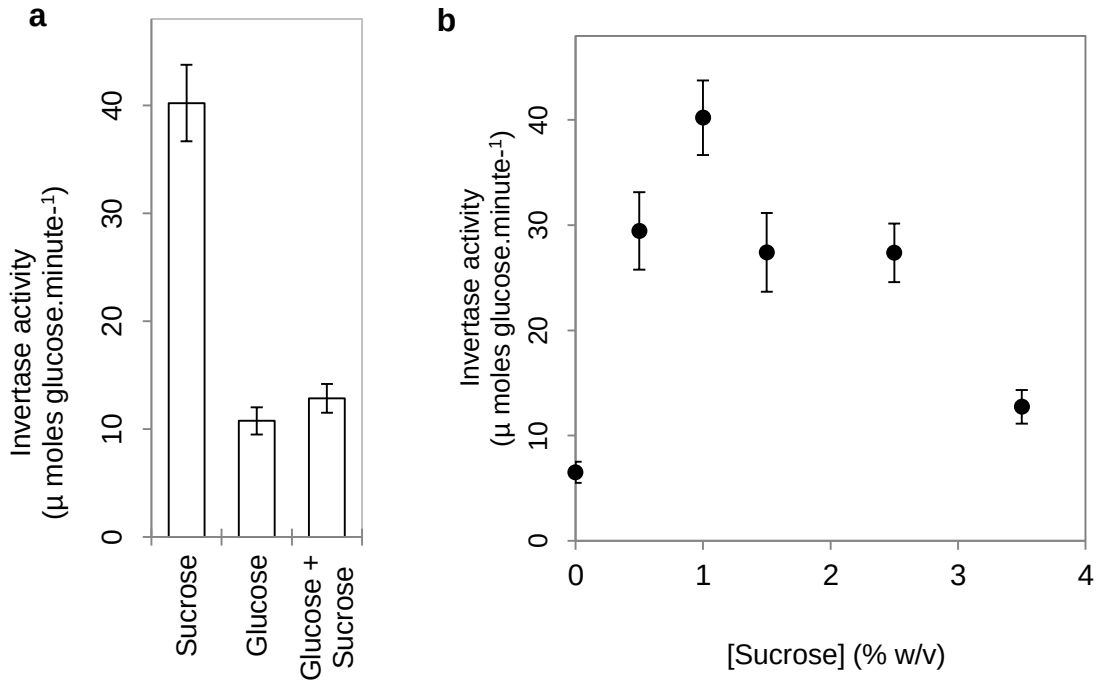

Figure 1.5 | Invertase production and regulation by *M. oryzae*. a, Invertase production by wild-type Guy11 strain was tested by enzymatic assay of culture filtrate under different induction treatments (units are µ moles of glucose/fructose liberated from sucrose per minute, n = 3). *INV1* expression in Guy11 is sucrose induced and glucose repressed, with constitutive expression remaining in non-yielding environments (glucose). **b** Induction under sucrose conditions is concentration dependent with expression peaking at 1% (w/v).

1.2.3 | Assessment of gene deletions on invertase activity and sucrose metabolism

Using sucrose induction treatments (1%), the gene deletion strains of MGG_05785 (Δ*inv1*) and MGG_02507 (Δ*inv2*) were tested for secreted invertase activity, where Δ*inv1* showed a deficiency whereas Δ*inv2* did not (Figure 1.6a). Furthermore, Δ*inv1* showed a growth deficiency, in terms of biomass (Figure 1.6b), sporulation (Figure 1.6c) and morphology in terms of growth defects including lack of melanin and fine, sparsely distributed hyphae, when sucrose was the sole carbon source (Figure 1.6d). The growth defects of Δ*inv1* were alleviated when the constituent of sucrose: glucose, replaced the disaccharide as a sole carbon source (Figure 1.6d). Furthermore, Δ*inv1* showed a growth deficiency on raffinose (Figure 1.6d), which is structurally similar to sucrose, with an additional galactose group, and a β-link with a terminal fructose residue. Therefore, Δ*inv1* was identified as an invertase null mutant and *INV2* was seen as dispensable for invertase activity expression and so disregarded from further analysis.

Figure 1.6

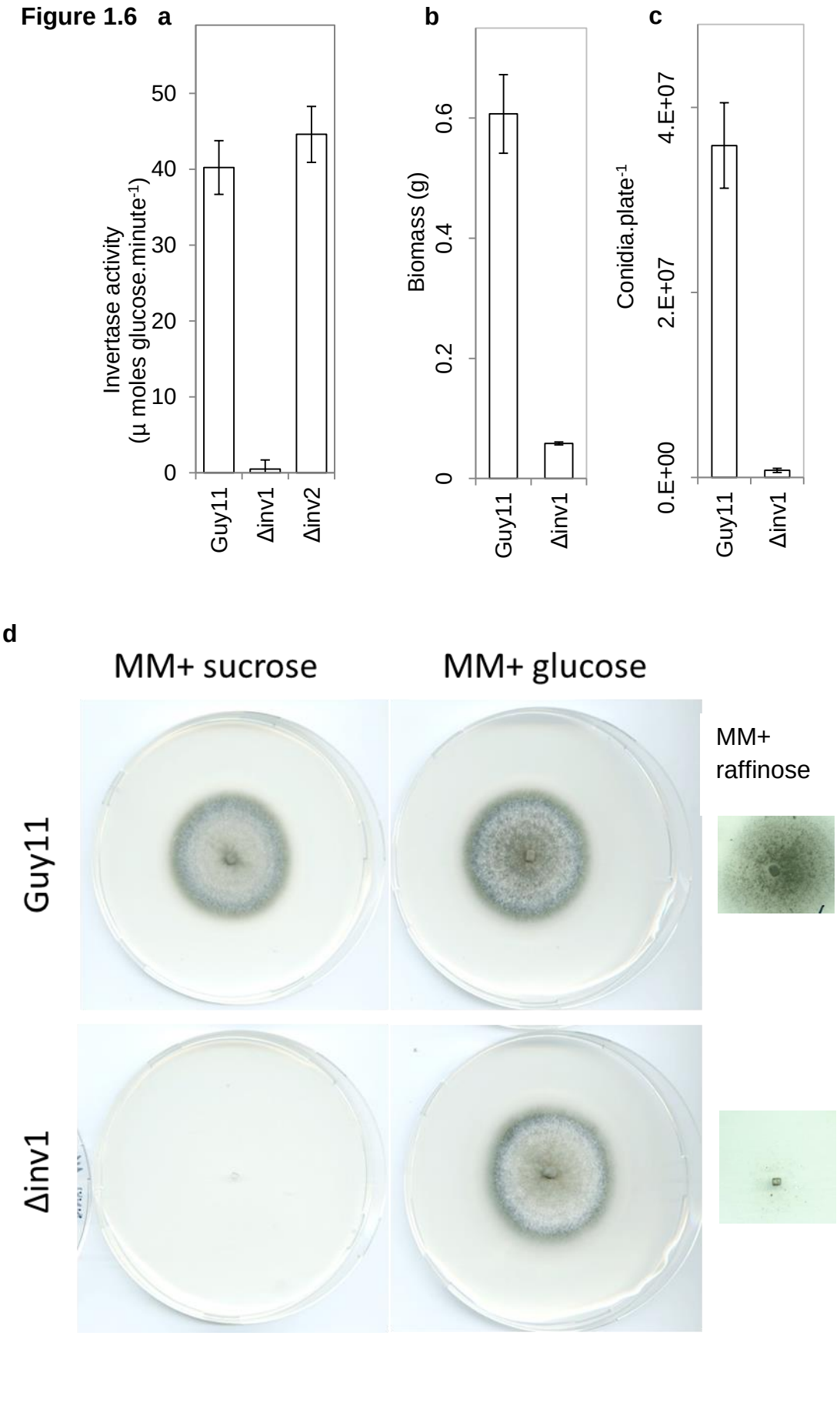
a
Invertase activity
(µ moles glucose.minute-1)
0
10
20
30
40
50
Guy11
Δinv1
Δinv2
b
Biomass (g)
0
0.2
0.4
0.6
Guy11
Δinv1
c
Conidia.plate-1
0.E+00
2.E+07
4.E+07
Guy11
Δinv1
d
MM+ sucrose
MM+ glucose
MM+
raffinose
Guy11
Δinv1

Figure 1.6 | *In vitro* assessment of deletion of putative invertase genes in *M. oryzae.* a Δ*inv1* showed an invertase deficiency in secreted invertase activity from enzymatic assays, whereas Δ*inv2* did not. This deficiency meant that the Δ*inv1* mutant had a fitness reduction on sucrose (mean ± s.e.m.) with respect to generating **b** biomass ($p < 0.0001$, n = 9, one-sided 2-sample t-test) (5 d.p.i.) and **c** conidia ($p < 0.0001$, n = 12, one-sided 2-sample t-test) (12 d.p.i.). **d** Growth morphology of *M. oryzae* wild-type strain Guy11 and the isogenic Δ*inv1* mutant strain. The mutant displays growth deficiency on sucrose media, which is complemented by supply of glucose which does not require catabolism by invertase. Similar deficiencies were also observed on the structurally similar sugar raffinose (inset).

1.2.4 | Confirming the activity of *INV1* by functional complementation

M. oryzae invertase gene function was verified by complementation of Δ*inv1* and an invertase deletion strain of *S. cerevisiae,* Δ*suc2* (BLASTp of *M. oryzae INV1*: *S. cerevisiae* S288c invertase *SUC2*: Identities = 31 %, e-value = 3e-10). In both cases *INV1* restored the ability of the mutants to proliferate when sucrose was the sole carbon source (Figure 1.7).

Figure 1.7

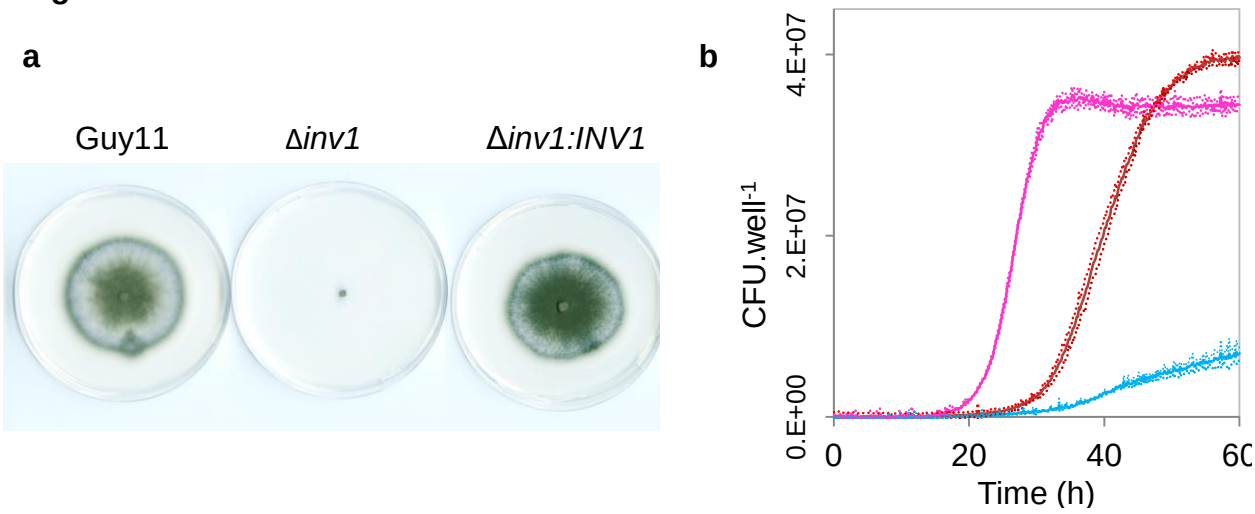

Figure 1.7 | *INV1* successfully complements the Δ*inv1* mutant of *M. oryzae* and an invertase mutant Δ*suc2* of *S. cerevisiae*. a Functional complementation restoring invertase synthesis and growth morphology of Δ*inv1:INV1* on sucrose media. The native promoter, ORF and 3'UTR were cloned and transformed into Δ*inv1,* restoring invertase activity. **b** To verify its function, the ORF of *M. oryzae INV1* was cloned into the yeast expression vector NEV-E with the *PMA1* promoter being

replaced with the constitutive *GPD* promoter. This vector was expressed in the invertase deletion strain DBY1701. This partially restored the growth rate of the deletion strain in sucrose limited media (dark red). The empty vector was transformed into DBY1701 as a negative control (blue). The ancestral *SUC2* invertase bearing strain (DBY1034) with the empty vector was used as the positive control (pink) (n = 3, mean ± 95% CI). BLASTp of *M. oryzae INV1* against *S. cerevisiae* S288c invertase *SUC2*: Identities = 31 %, e-value = 3e-10.

1.2.5 | The subcellular localisation and expression of *INV1:mCherry*

The Δ*inv1* strain was also functionally complemented by constructing a C-terminal *INV1:mCherry* fusion vector (Figure 1.8). This enabled both the sub-cellular localisation and regulation of *INV1:mCherry* to be determined by epifluorescent microscopy. Secretion of *INV1*:*mCherry* uniformly outlined the invasive hyphae 48 h.p.i. presumably being secreted into the extracellular compartment following the conventional secretory pathway of filamentous fungi, reminiscent of apoplastic effectors (194) (Figure 1.8a). This *in planta* expression supports data generated from RNA-seq data of gene expression during plant infection (Figure 1.8b) (M. Oses-Ruiz, X. Yan, D.M. Soanes and N.J.Talbot unpublished). A similar localisation was found in vegetative hyphae grown on MM + sucrose agar plates (Figure 1.8c). However, when analysing hyphae grown in liquid MM + sucrose, expression could be observed intracellularly (Figure 1.8d). This is thought to be caused by the protein rapidly being lost into the environment due to reduced spatial structuring in liquid media, with the intracellular expression being observed as the protein is being synthesised and trafficked through the conventional ER-Golgi secretion pathway (162). Alternatively, *M. oryzae* may form different isoforms of invertase from a single gene, one secreted and one cytoplasmic, as described in *S. cerevisiae* (195).

Figure 1.8

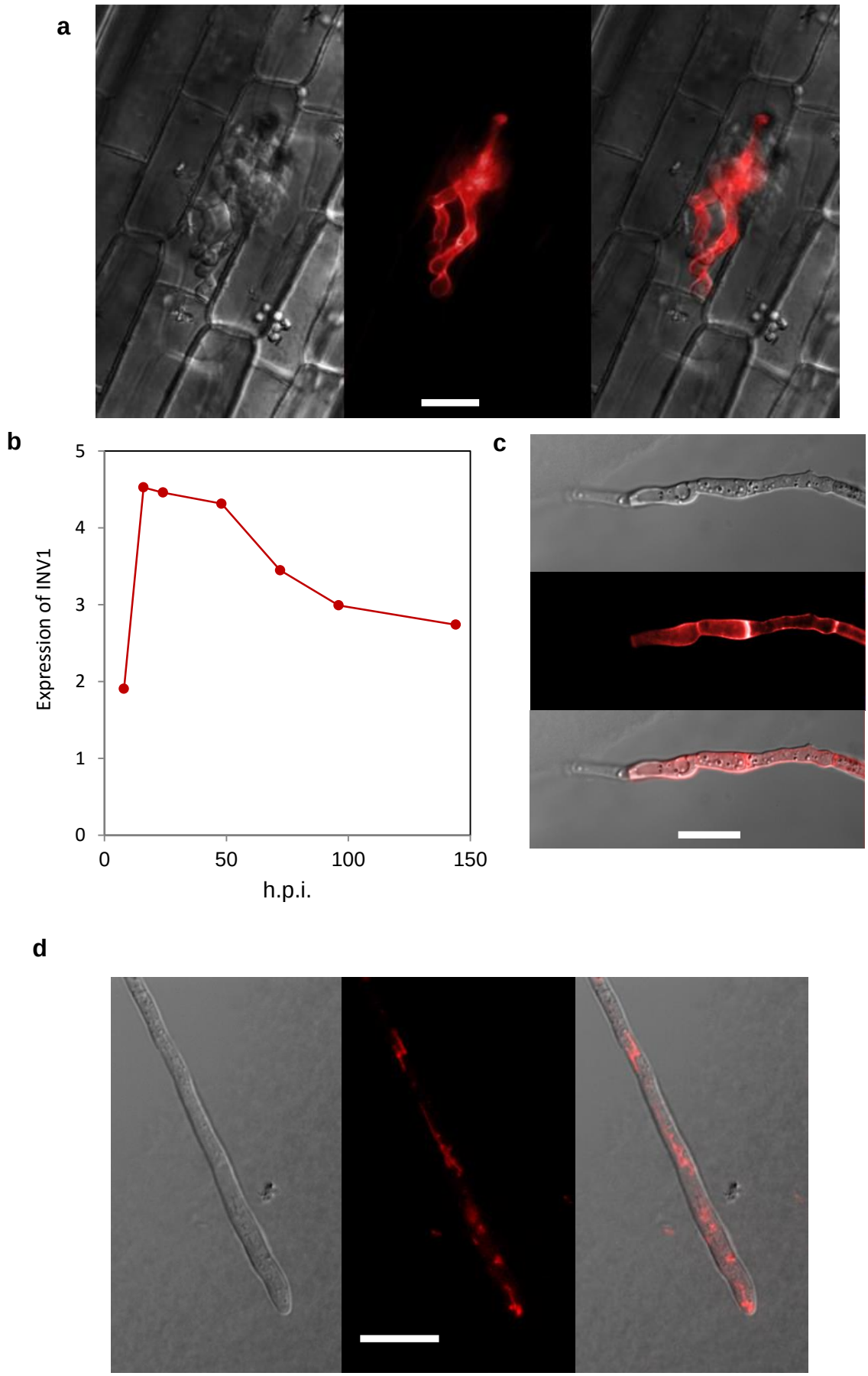

Figure 1.8 | Expression of *INV1* during *in planta* and *in vitro* inoculations. a Expression 48 h.p.i. during leaf sheath infection assay of epidermal rice cells. **b** Expression profile of *INV1* during rice leaf infection (data acquired by RNA-seq by M. Oses-Ruiz, X. Yan & D. Soanes, unpublished). Levels of expression are shown as moderated $\log_2$ ratio of transcript abundance compared to conidia (0 h.p.i.). **c** Expression in vegetative hyphae grown on MM+sucrose agar plates. In both conditions (**a** & **c**) secretion of *INV1:mCherry* outlined the hyphae. **d** Expression in liquid media (MM+sucrose) was detected intracellularly. Scale bars = 30 µm.

1.2.6 | *INV1* contributes to pathogen fitness and virulence during infection

To examine the impact of *INV1* on *in vivo* pathogen fitness and disease virulence, infection assays were performed to ascertain differences between the wild-type and Δ*inv1* (Figure 1.9). The infection cycle of *M. oryzae* is initiated by germination of the conidia followed by the formation of an appressorium to enable penetration of the plant surface (Figure 1.1) (157). Viability of Δ*inv1* conidia was confirmed with appressorium production > 75 % after 24 h (Figure 1.9a) (196). Three different infection assays were performed so that various parameters could be assessed most effectively, namely invasive growth during the initial 48 h.p.i, (Figure 1.9b), disease lesion area as a measure of disease virulence 5 (Figure 1.9c) and 7 (Figure 1.9e) d.p.i,, and conidia production as a measure of pathogen population fitness 9 d.p.i. (Figure 1.9d). Δ*inv1* showed a reduced rate of initial invasive growth (Figure 1.9b), disease lesion area produced (Figure 1.9c & e), and conidia production (Figure 1.9d) following infection compared to the wild-type. All three measurements showed that Δ*inv1* is impaired during the host-pathogen interaction and that *INV1* is essential for full virulence and pathogenicity, and that damage caused to the host is positively correlated with the fitness of the pathogen during disease.

Figure 1.9

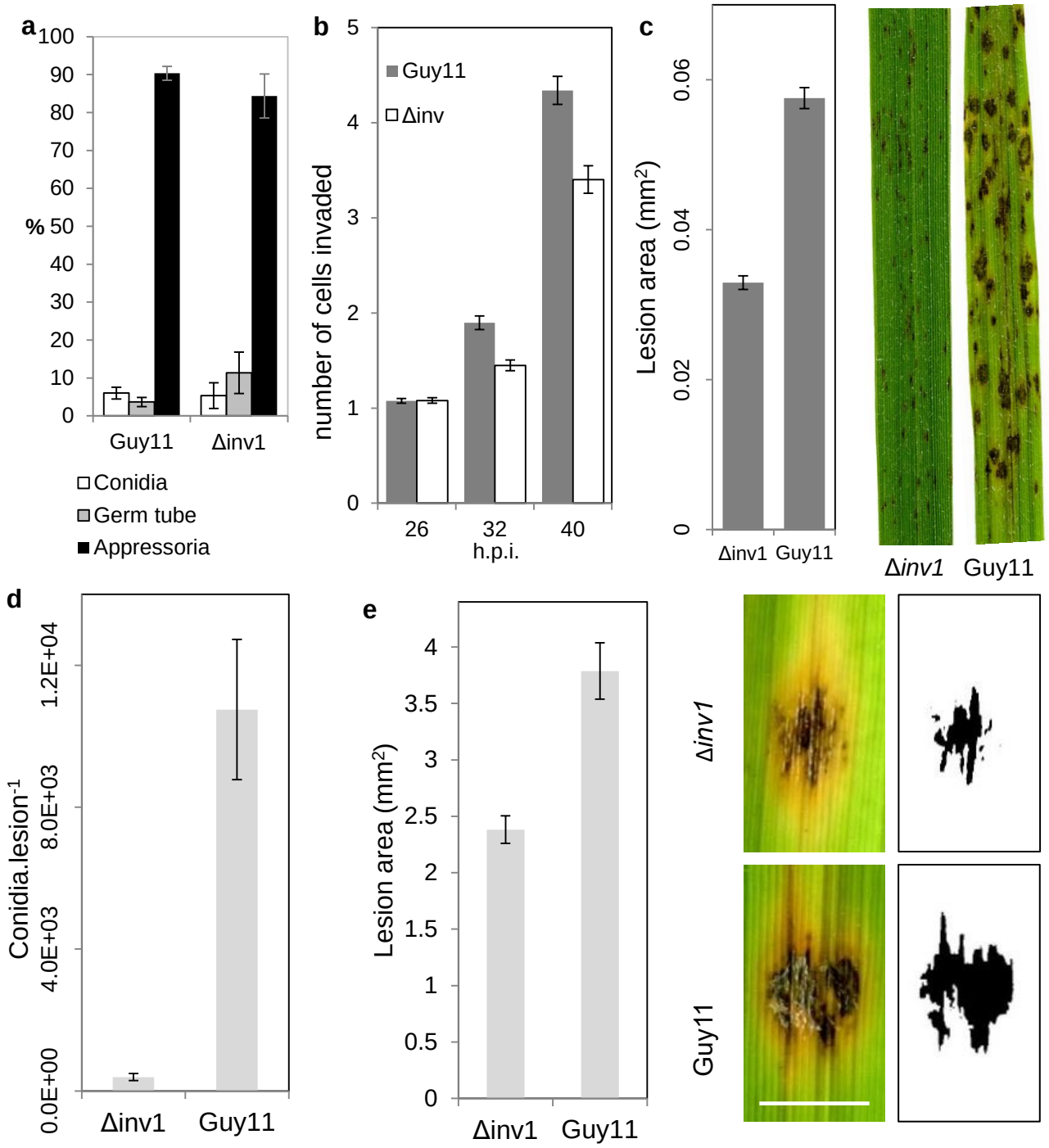

Figure 1.9 | *INV1* is required for full virulence and pathogen fitness during infection of rice plants by *Magnaporthe oryzae*. a, The *Δinv1* mutant is proficient in appressoria formation (> 75 % (196)), measured *in vitro* on hydrophobic surfaces. **b** The *Δinv1* mutant has impaired invasive growth compared to wild-type during the initial infection period, as measured by cell invasion in leaf sheath infections ($p < 0.001$, 32 h.p.i., $W = 30798$, d.f. = 445; 40 h.p.i., $W = 29094.5$, d.f. = 432, Mann-Whitney U test, compiled from three replicated experiments). The Δ*inv1* mutant shows reduced virulence in terms of disease lesion area: **c** Lesion area, quantified

by image analysis, was significantly greater in Guy11 infections than those of the isogenic *Δinv1* mutant ($p < 0.001$, $W = 124563256$, d.f. = 35497, Mann-Whitney U test, compiled from three replicated experiments) with representative typical infection of a spray-inoculated rice seedling cultivar CO39. **d** *In planta* fitness of *M. oryzae* during infections was evaluated by leaf spot inoculation of attached rice leaves with 10^3 conidia (mean ± s.e.m., n = 42, pooled from three experiments). Fitness was quantified by the number of conidia recovered per lesion at the end of the disease cycle. Infections with Guy11 produced significantly more conidia than pure non-producer infections of the Δ*inv1* mutant ($p < 0.0001$, $W = 969$, one-sided Mann-Whitney U test, d.f. = 82, n = 42). **e** Disease virulence by spot inoculation and infection with 10^3 conidia showing reduced virulence as measured by lesion area (mean ± s.e.m.), of Δ*inv1* compared to Guy11 ($p < 0.0001$, one-sided 2-sample t-test with unequal variances, n = 20). Example lesions (7 d.p.i.) from leaf spot infections, scale bar = 3 mm with ImageJ analysis images from which areas were measured. Images of all replicates can be seen in Appendix 2.1.

1.3 | Discussion

These results, from both *in vitro* and *in vivo* measurements, identify *INV1* encodes for the major invertase activity in *M. oryzae* (β-fructofuranosidase; 71.81 kDa). Production of invertase provides a benefit to the population when environmental conditions suit, by hydrolysing sucrose and so providing access to previously inaccessible monosaccharides that fuel growth.

Our findings are in contrast to results suggesting *M. oryzae* possessed two extracellular invertases (165). The growth deficit of Δ*inv1* and phenotypic analysis of the wild-type provides experimental evidence into nutrition acquisition by *M. oryzae* in that it feeds by osmotrophy for sucrose utilisation (Figure 1.2, 1.6, 1.7, 1.9). This contrasts with *U. maydis* which feeds via a high affinity sucrose transporter (172). This may be characteristic of the hemibiotrophic lifestyle of *M. oryzae* because it also obtains nutrients by necrotrophy so prevention of eliciting host defence responses, which are thought to be associated with glucose signalling, may not be as crucial in

comparison to exclusively biotrophic pathogens such as *U. maydis* (140, 160, 172, 197, 198).

The pathogenicity defect of Δ*inv1* also gives an insight into feeding by *M. oryzae* during infection. The nutritional environment experienced by the pathogen during infection is still largely unknown (180). Sucrose, due to its abundance and being the product of photosynthesis, is thought to represent an important carbon source for plant pathogenic fungi (164-166), However, given that *M. oryzae* possesses numerous depolymerising enzymes to digest complex nutrients, such as cellulose and lipids (141, 161), it would seem that the fungus has many carbon sources available to exploit. Therefore, the deficit of Δ*inv1* reveals quite how important a carbon source sucrose is to the pathogen because the inability to utilise it results in a significantly less virulent pathogen that effectively is unable to complete the infection cycle to produce substantial conidia for transmission to new hosts (Figure 1.1 & 1.9d). It is likely that sucrose is relatively more crucial during the initial stages of infection while the plant tissue at the site of infection is still photosynthesising, prior to the fungus switching to a necrotrophic phase when it relies more upon degrading more complex structural carbon sources such as cellulose and lignin (157, 161). Therefore, as a result of the inability to use sucrose, the relative nutrient starvation experienced by Δ*inv1* may mean that the fungus is unable to fuel the production of metabolically costly secondary metabolites to degrade these alternative food sources. In addition, this lack of consumable nutrients available may also weaken Δ*inv1*, the result of which shifts the balance of disease in favour of the host, meaning that it is more capable of eliciting a successful defence response.

So far this study has identified that a single invertase gene of *M. oryzae* appears to be responsible for sucrose metabolism. Deletion of this gene results in an inability of

the null mutant to proliferate, both *in vitro* via the formation of mycelial biomass or conidiation (Figure 1.6), or in the pathogen's natural host, *in planta,* where the deletion mutant had impaired virulence as measured by host damage, and pathogen fitness, as measured by conidiation at the end of the disease cycle (Figure 1.9). In Chapter 2, we next sought to identify whether this invertase production was an exploitable public-good cooperative trait, and if it could be exploited as a disease management strategy by competitive exclusion.

1.4 | Methods

1.4.1 | Targeted deletion of invertase

Invertase genes were targeted using a PCR-based split-marker gene deletion technique (145, 146). The genes MGG_05785 & MGG_02507 were targeted as putative invertase genes. LFs were amplified using primers 50.1 and M13F, RFs with 30.1 & M13R (Table 1.2). Transformants that exhibited sulfonylurea resistance were assessed by digoxigenin-(DIG) labelled Southern blot analysis and evaluated for fragment size differentiation following restriction endonuclease digestion of gDNA.

Screening of putative transformants for Δ*inv1* (MGG_05785) used a probe constructed using primers MGG_05785_50.1 and MGG_05785_M13F so hybridised with the left flank of the ORF. Genomic DNA of putative transformants and a wild-type control were digested with *XhoI* generating a fragment of 5.6 kb or 4.2 kb in the region of the left flank for positive transformants or wild-type respectively. Transformants 11 and 15 generated bands that had migrated according to the size of positive gene replacement (Figure 1.3a & b).

Table 1.2 | Primers used for targeted gene deletion of putative invertase genes from *M. oryzae.* Underlined bases indicate regions of homology for fusion PCR.

Primer name	Nucleotide sequence (5' - 3')
MGG_05785_50.1	TTGGCGTGGAGAAAGAAGTGGGTA
MGG_05785_M13F	GTCGTGACTGGGAAAACCCTGGCGGTGCTGGTATTATTAACGAGGGAC
MGG_05785_30.1	AAAGATCAAGGACAAGGCACCCAA
MGG_05785_M13R	TCCTGTGTGAAATTGTTATCCGCTGGGCGGTCATGTTTGAGAGATAGG
MGG_02507_50.1	AACTACCTACCTACCTACCTACCT
MGG_02507_M13F	GTCGTGACTGGGAAAACCCTGGCGCAATTCCAGCGTATAGTAAACACA
MGG_02507_30.1	GTACGGTAAGCCTTTTTCCCCCTC
MGG_02507_M13R	TCCTGTGTGAAATTGTTATCCGCTGACGGCGACGATGCATAATAAGGT
IL_M13F	CGCCAGGGTTTTCCCAGTCACGAC
ILsplit	TCTGGTTGTATTCTCAGGAC
LVsplit	CATACCAAGCATGTGCAGTG
LV_M13R	AGCGGATAACAATTTCACACAGGA

A similar strategy was implemented for Δ*inv2* (MGG_02507) though the probe was constructed with primers MGG_02507_30.1 and MGG_02507_M13R thus hybridised with the right flank of the ORF during DIG-labelled Southern analysis. *SapI* was used to digest gDNA for screening putative transformants returning fragments containing the probing region of 20.1 kb for positive gene replacement strains and 5.2 kb for wild-type genome (Figure 1.3c & d).

1.4.2 | Yeast functional complementation

The strains of *S. cerevisiae* used were kindly supplied by the Botstein lab (Princeton University, USA) and the Fink lab (Whitehead Institute, USA). DBY1034 has the genotype *MATa his4-539 lys2-801 ura3-52 SUC2,* DBY1701 is a *SUC2* deletion strain with genotype *MATa his4-539 lys2-801 ura3-52 suc2Δ9* (199).

We constructed the *S. cerevisiae* expression vector by modification of the NEV-E vector (200) (Figure 1.10). The plasma membrane ATPase gene promoter (P_{PMA1}) in the NEV-E vector was replaced by digestion and with *HindIII*/*EcoRI* followed by a double ligation of the plasma membrane ATPase gene terminator (T_{PMA1}) and *HindIII*/*EcoRI* fragment containing the constitutive promoter of the glyceraldehyde-3-phosphate dehydrogenase gene (P_{GPD}) (201), PCR amplified using primers GPDP_F and GPDP_R resulting in the plasmid NEV-E-P_{GPD}. To this vector the *INV1* ORF, PCR amplified with Phusion taq using primers MGG_05785.7_F and MGG_05785.7_R, was firstly cloned into pSC-B-amp/kan (Agilent Technologies, USA) and subsequently ligated as a *EcoRI* fragment into NEV-E-$P_{GPD.}$ Orientation was confirmed by PCR analysis using primers GPDP_F and MGG_05785.7_R to generate a 2.7 kb amplicon. Plasmids were transformed into *S. cerevisiae* using a lithium acetate mediated protocol and selection was made with the *URA3* marker on minus-URA media.

Table 1.3 | Primer sequences for the construction of the yeast expressions vector NEVE-P_{GPD} to drive *INV1* expression.

Primer name	Nucleotide sequence (5' - 3')
MGG_05785.7_F	TTAAGCTTATGAAATTCACATTTGTGTCATCG
MGG_05785.7_R	AAGAATTCTTACCATCCGTTCCACCAGGTGTA
GPDp_F	AAGCTTTTACGTTGTAAAACGACGGCCA
GPDp_R	GAATTCAAGACTAACTATAAAAGTAGAA

Figure 1.10

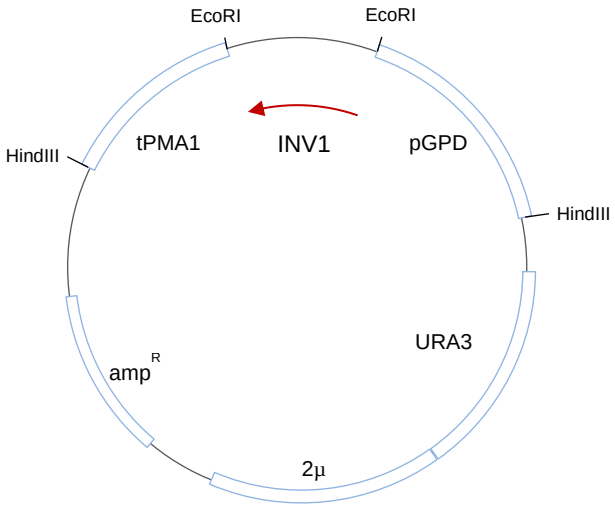

Figure 1.10 | Plasmid map of vector constructed for complementation of Δ*suc2* with *INV1.* Complementation of an invertase deletion mutant of *S. cerevisiae* was achieved by conventional cloning of the *INV1* ORF (*EcoRI/EcoRI* fragment) driven by the *GPD* promoter (*EcoRI/HindIII* fragment) in the modified NEV-E shuttle vector (200).

Supplemented minimal media (SMM) was used for growth experiments with the resulting strains. SMM + sucrose is comprised of 25 mM sucrose, 5 $g.L^{-1}$ ammonium sulfate, 1.7 $g.L^{-1}$ yeast nitrogen base w/o amino acids or ammonium sulfate, 50 $mg.L^{-1}$ L-lysine and 20 $mg.L^{-1}$ L-histidine. The strains were initially grown overnight in this media with glucose (2 % w/v) replacing the sucrose, washed and resuspended before being diluted to an initial cell density of approximately 1.26 x 10^5 $cells.mL^{-1}$ in SMM + sucrose. Growth measurements took place with 640 µL cultures in 48-well suspension culture microplate (Bio-One Greiner) with shaking at 700 r.p.m. OD measurements were made at 620 nm in a FLUOstar Omega microplate reader (BMG Labtech) and converted to cell density using a calibration curve where CFU = 34403199.79 x (OD-blank) (R^2 = 0.99).

1.4.3 | Δ*inv1* functional complementation, subcellular localisation and regulation

Functional complementation was achieved by PCR cloning the *INV1* ORF, with 1.8 kb upstream and 0.5 kb downstream to incorporate the native promoter and terminator sequences, into pSC-B-amp/kan (Agilent Technologies, USA) as an *EcoRI/HindIII* fragment. To this vector, the *BAR* gene conferring bialophos (BASTA) resistance (202) was ligated as a *NotI/SpeI* fragment. The resulting vector, pSC-INV1-BAR (Figure 1.11), was transformed into the Δ*inv1* mutant and transformants were assessed for single integration of the *INV1* gene by Southern blot analysis with digestion of gDNA with *AhdI* and a probe constructed using primers MGG_05785.7_F and MGG_05785.7_R (Figure 1.12 & Table 1.3), and restored wild-type growth morphology on sucrose media (Figure 1.7).

Subcellular localization and regulation of *INV1* was measured by functionally complementing the Δ*inv1* strain by constructing a C-terminal *INV1:mCherry* fusion vector. This plasmid was constructed by In-Fusion cloning using the previously generated vector backbone pSC-INV1-BAR, linearized by digestion with *EcoRI/HindIII* to retain the *BAR* gene. The native *INV1* promoter was retained by PCR amplifying a fragment from 1.8 kb upstream of the ORF with the reverse primer excluding the stop codon. To this an *mCherry*:*trpC* terminator fragment was cloned. The resulting vector was transformed into Δ*inv1* with transformants screened for restored ability to metabolise sucrose. This enabled both the sub-cellular localisation and regulation of *INV1:mCherry* to be determined by epifluorescent microscopy (Figure 1.8).

Figure 1.11

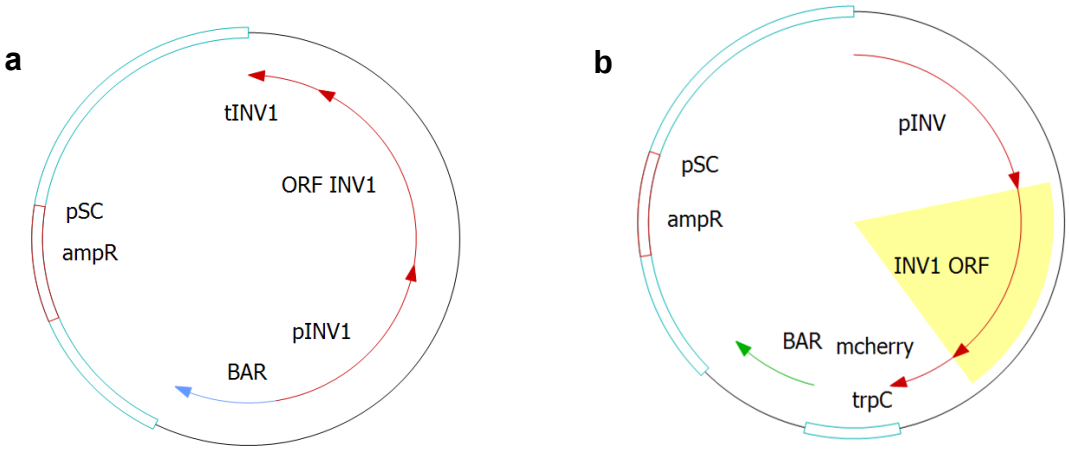

Figure 1.11 | Plasmid maps of *INV1* complementation vector and INV1-mCherry expression vector. a invertase complementation (*EcoRI*/*HindIII* fragment) vector in the pSC-B-amp/kan backbone with *BAR* gene (*NotI*/*SpeI* fragment) creating pSC-INV1-BAR by conventional cloning. **b** INV1-mCherry expression and localisation vector constructed by In Fusion cloning by modification of the pSC-INV1-BAR which was first linearised with *HindIII/EcoRI*, retaining the *BAR* gene, and introducing the pINV1-INV1 and mCherry-trpCt fragments.

Figure 1.12

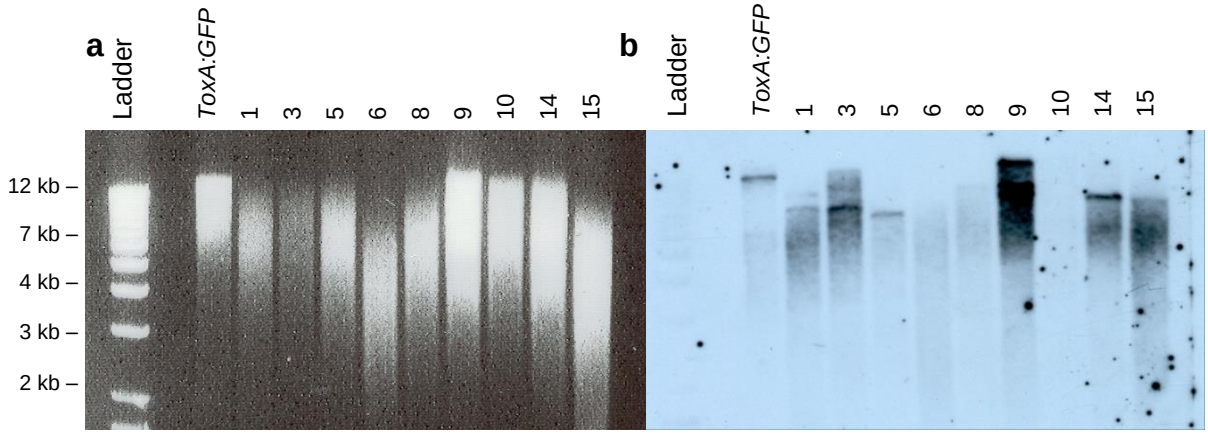

Figure 1.12 | Confirmation of single integration of the pSC-INV1-BAR vector for *INV1* functional complementation. gDNA was digested with *AhdI,* which has no restriction sites within the *INV1* ORF. Southern blot analysis using a probe of the *INV1* ORF revealed that transformants #5 and #14 showed a single band and so single integration of the transformation vector. The ancestral *ToxA:SGFP* strain of the Δ*inv1* mutant was used as a positive control (far left lane). **a** shows ethidium bromide stained electrophoresis gel to confirm DNA integrity. **b** the developed film. Transformants #6, #8 and #15 show signs of degradation with no banding, and #10 shows no band suggesting unsuccessful integration. #1 #3 and #9 show >1 band suggesting multiple-integration, increasing the chances of genome interruption.

Table 1.4 | Primer sequences for generating the *INV1* complementation vector and the INV1-mCherry fusion construct (underlined regions indicate added sequence for restriction sites and/or complementary regions for cloning)

Primer Name	Sequence
INV1_C_F_EcoRI	GAATTCTTCAGATTATGTGTATGGCGGC
INV1_C_R_HindIII	AAGCTTATATGTCGGCTGTCTTTCTCCA
BAR_F_Noti	GCGGCCGCAAGTCGACAGAAGATGATATTGAAGG
BAR_R_Spei	ACTAGTAAGTCGACCTAAATCTCGGTGA
TrpC_R_IF	GGTATCGATAAGCTTCTCGAGTGGAGATGTGGAGT
mCh_F_IF	ATGGTGAGCAAGGGCGAGGA
INV1_C_F_IF (mch fusion)	CCCAATGTGGAATTCCAGATTATGTGTATGGCGGC
INV1_C_R_IF (mCh fusion)	GCCCTTGCTCACCATCCATCCGTTCCACCAGGTGT

Chapter 2

Testing Hamiltonian Medicine: The sociality of sucrose metabolism in *Magnaporthe oryzae* and its influence upon population fitness and disease virulence

2.1 | Introduction

2.1.1 | Invertase as a public-good cooperative trait

The invertase system of *S. cerevisiae* is one of the most studied examples of public-good cooperation. Invertase production can increase yeast group fitness, amplifying growth rate by about 20% when conditions suit (85). However, because monosaccharides liberated are available to all cells (14) an opportunity arises for individuals to gain a fitness advantage by consuming without contributing (66). Notably, approximately 10% of strains do not produce and secrete invertase (203). Coexistence of invertase producers and non-producers in populations has been observed at equilibrium, maintained through negative-frequency dependent selection, saturating benefits gained by additional contributions, and producers getting a disproportionate amount of the benefits generated (an extra 1%) (14, 66, 85).

In Chapter 1, we have identified and characterised *M. oryzae* invertase and generated a deletion mutant Δ*inv1*. In Chapter 2, we investigate the nature of invertase mediated sucrose metabolism in *M. oryzae.* We sought to test the principles of Hamiltonian medicine using this system, but firstly we had to establish if *M. oryzae* sucrose metabolism represented a public-good cooperative trait. To do this it was necessary to confirm that it conforms to common features of other established experimental systems and predictions made by social evolution theory (55, 58). These features include the ability of the public-good to provide a benefit to the population when conditions suit, the production of the public-good comes at a

metabolic cost to the individual generating it yet the benefits can be used by others in the vicinity of its actions, and cheats can gain a selective advantage by not investing in production of the public-good yet exploit the production by others. A number of these features are captured by a measurement of frequency dependent fitness in competition where either cooperation or defection strategies can yield a selective advantage (204). Furthermore, another common feature of public-goods systems is the influence of population spatial structuring, also referred to as assortment of individuals or relatedness, which can influence the relative fitness of either strategy by altering the likelihood of interacting with public-good producers (14, 69, 85, 88, 112). We will examine in Chapter 2 how spatial structuring can influence the relative success of invertase production in *M. oryzae.*

2.1.2 | Testing *M. oryzae* invertase production as a Hamiltonian disease management strategy

As mentioned and observed in Chapter 1, the public-good virulence factors produced by pathogens can be crucial for successful infection (72, 87, 88, 112, 113). Existing theory therefore suggests that these factors may be targeted to reduce the severity of disease (2, 24, 26, 29). In mixed strain populations, low virulence public-good cheats are predicted to out-compete the more virulent wild-type strains by exploitative behaviour resulting in a reduced overall production of these factors. This is predicted to diminish the overall success of pathogens, reducing disease virulence and the pathogen population size (2, 44, 88, 112). This principle contrasts with virulence predictions regarding social cheats in prudent use of resources which are more virulent than cooperators (115), hence an introduction of cheats into pathogen populations in these cases would augment disease virulence.

2.2 | Results

2.2.1 | *M. oryzae* sucrose metabolism as a cooperative trait

To confirm that sucrose metabolism by invertase mediated hydrolysis represented a public-good cooperative trait, classical definitions from social evolution theory had to be satisfied (58). It was confirmed that invertase production and secretion was a useable extracellular public-good trait by inoculating Δ*inv1* in spent media that had been previously utilised by the invertase producing wild-type. The media was resupplied with the original nutrients, including sucrose. Δ*inv1* was able to generate biomass in this sucrose media if it had been previously occupied by invertase secreting Guy11 as a result of the generated public-goods of the 'cooperative' strain, but unable to grow if subsequent to being inhabited by non-public-good-producing Δ*inv1* 'cheats' (Figure 2.1).

Figure 2.1

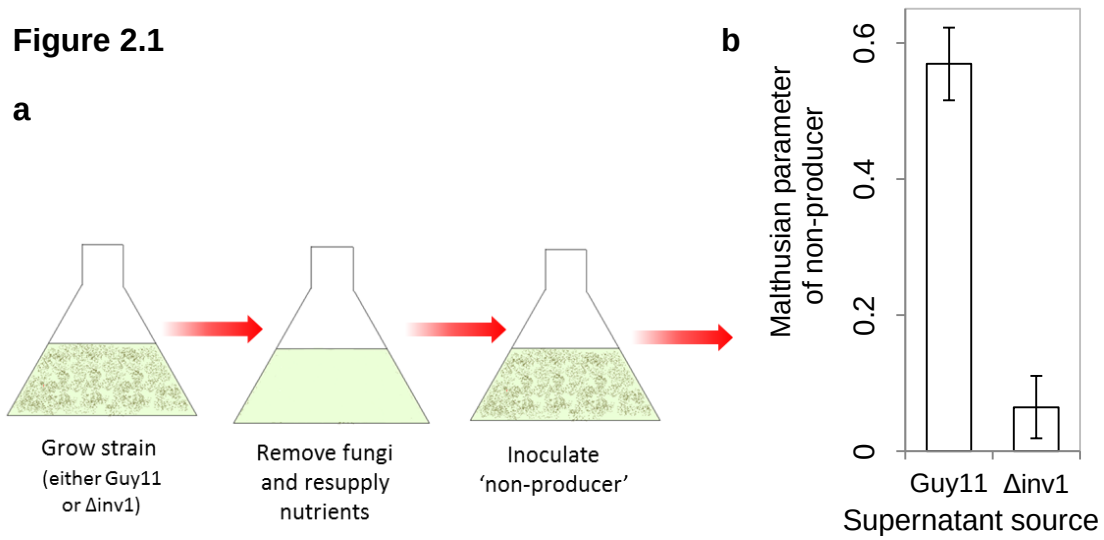

Figure 2.1 | Δ*inv1* is able to use the public-good invertase produced by Guy11. **a** Schematic of experimental design. **b** Δ*inv1* was able to establish biomass in the supernatant (MM + sucrose) of the producer (Guy11) (significantly greater than 0, $p < 0.0001$, $t = 10.63$, one sample t-test), but not in the supernatant of the non-

producer (not significantly different from 0, $p > 0.05$, $t = 1.416$, one-sample t-test). Δ*inv1* could generate significantly more biomass in the supernatant of Guy11 than the supernatant of Δ*inv1* ($p < 0.0001$, $t = 7.158$, two-sample t-test assuming equal variance). Data compiled from three replicated experiments, mean ± s.e.m., $n = 9$.

Cooperator and cheat strains were competed to observe their relative fitness in mixed strain cultures to verify that *M. oryzae*-invertase production is an exploitable public-good cooperative trait (Figure 2.2). To distinguish cooperator and cheat strains in mixed cultures, the wild-type strain was tagged with an RFP (3mCh) and the mutant strains were tagged with a GFP (SGFP). These markers were verified to be selectively neutral by determining the fitness of fluorescent protein tagged wild-type strains by measuring mycelial biomass production in liquid culture and sporulation on agar media. Both measures showed no significant fitness costs (Figure 2.3). In mixed strain competition cultures (see methods for details) with a low degree of population spatial structuring, invertase non-producers out-competed invertase producers on sucrose media (Figure 2.4).

Figure 2.2

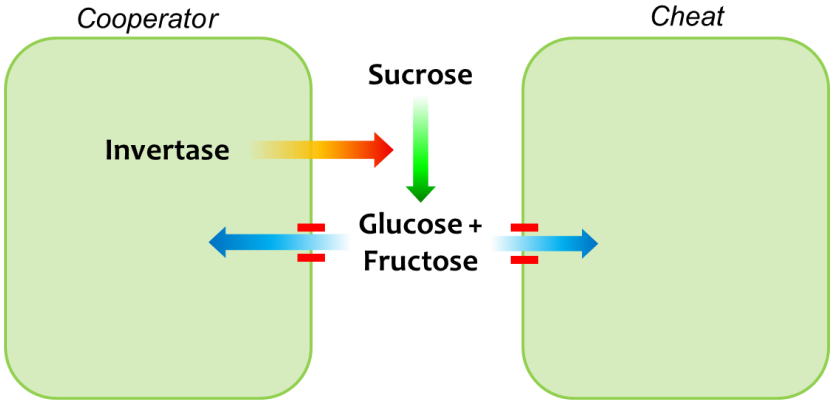

Figure 2.2 | Schematic of the social dilemma of public-good production of invertase secretion (by 'Cooperators') and sucrose hydrolysis. As this osmotrophic process occurs extracellularly, the products are open to exploitation by others ('cheats') in the locality who can avoid the cost of production yet can reap the benefits generated (glucose + fructose).

Figure 2.3

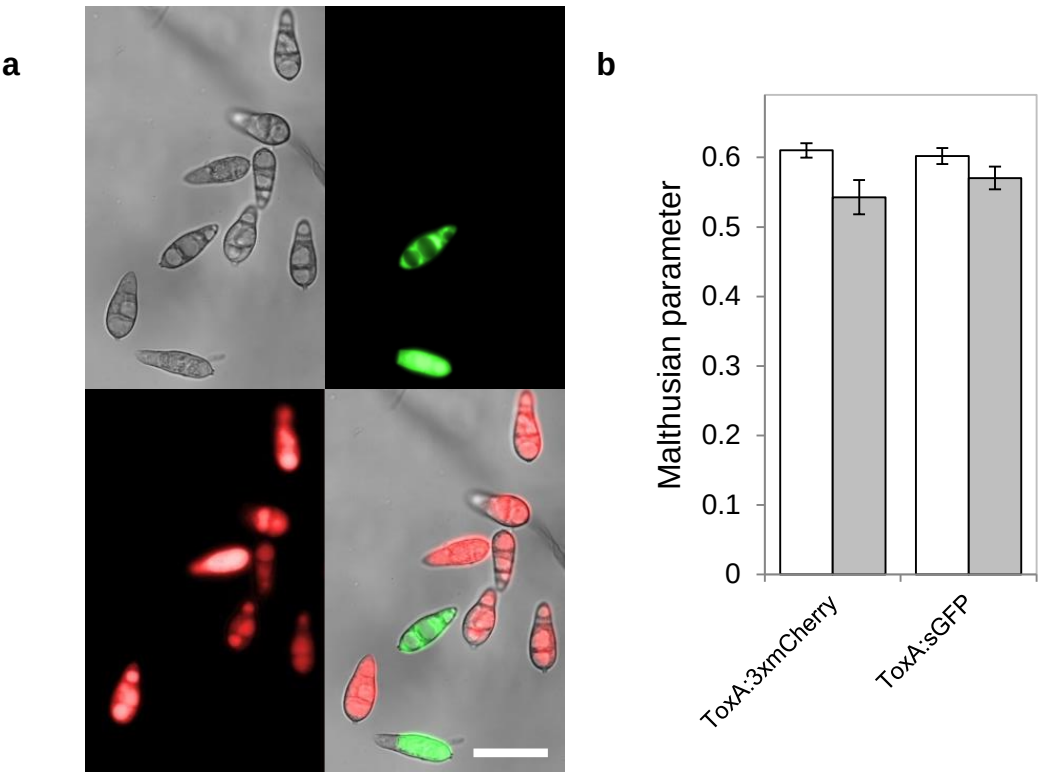

Figure 2.3 | Strains were distinguishable by the presence of fluorescent protein tags. **a**, Wild-type invertase producer strain Guy11 was tagged with *ToxA:3xmCherry* and the non-invertase producing strain Δ*inv1* was tagged with *ToxA:sGFP*. Bright field (DIC) images with RFP / GFP overlay. Scale bar = 30 µm. **b,** these tags were selectively neutral in wild-type strain Guy11 (Two sample t-test) based on biomass (grey bars, p = 0.3319, d.f. = 10, t = 0.5568) and conidia (white bars, p = 0.5845, d.f. = 18, t = 1.0198) production on MM + Sucrose (mean ± s.e.m.).

In more ‘structured’ populations, where generated public-goods are more likely to be obtained by other ‘cooperators’, *M. oryzae* invertase displays negative-frequency dependence of relative fitness (Figure 2.4), meaning that both invertase producers and non-producers were fitter when rare in the population. However, this measure assumes constant fitness of the strains. Therefore, it may not reflect the long-term equilibrium frequencies (205). This result indicates that spatial structuring of populations may be important to retain public-good cooperation with invertase,

analogous to observations of other cooperative systems (14, 69, 72, 85, 88, 204, 206).

Figure 2.4

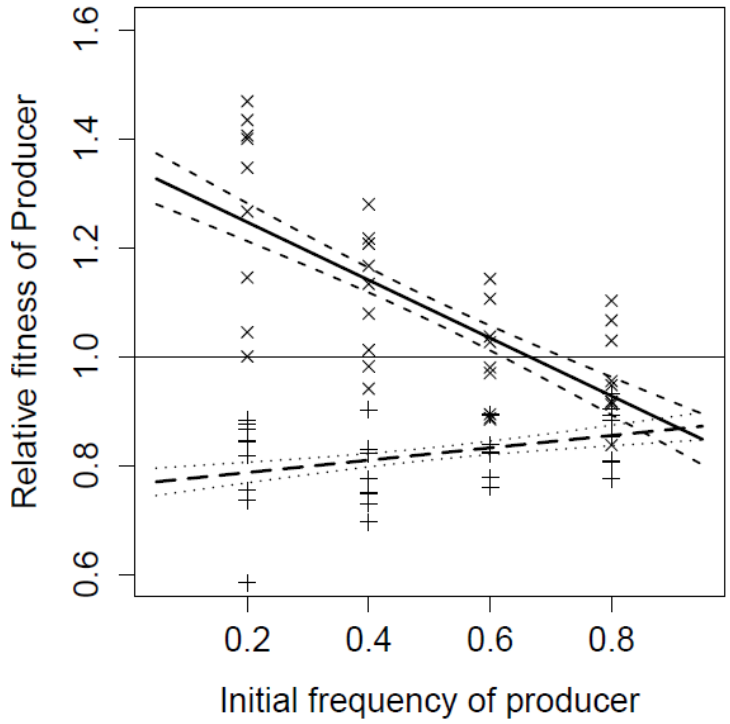

Figure 2.4 | Competition cultures to establish the *in vitro* relative fitness of invertase producers to non-producers. Relative fitness of the invertase producer, Guy11, against the isogenic Δ*inv1* mutant as a function of its initial frequency in a structured (x) (solid line of best fit) and semi-structured (+) (dashed lines of best fit) environment, linear model ± s.e.m. (dotted lines), pooled from three experiments. Experiments were performed on 1% (w/v) MM + sucrose supplemented with 1.5 % (w/v) agar. Conidia were harvested after 12 d. In more structured environments, negative frequency dependent fitness was observed with strains being relatively more fit when rare (one-way ANOVA; $F_{3,32}$= 12.194, $p < 0.001$, n = 9; post-hoc Tukey's; when initial frequency of producer = 0.2, fitness of producer > than when initial frequency is 0.4, 0.6 or 0.8, $p < 0.05$). In less structured environments, the Δ*inv1* mutant had a significant competitive advantage over the invertase producer ($p < 0.0003$, one-sample t-test, n = 9) at all initial frequencies.

Negative-frequency dependent selection is predicted to occur in public-good cooperative systems because when cheats are rare, they will find it easier to exploit

the more abundant cooperators and public-goods (58, 204). The mutual invasability of strains from rare that we found suggests a coexistence of invertase producers and non-producers at steady state (Figure 2.4). This feature, however, was lost at the tested frequencies when strains were competed in a comparatively less structured population (one-way ANOVA; $F_{3,32}$= 2.151, p = 0.1132, n = 9; Figure 2.4), which led to invertase 'cheats' being relatively fitter in all tested initial frequencies of 'cooperators' (p < 0.0003, one-sample t-test, n = 9). This indicates the metabolic cost incurred by producers and sets the stage for Δ*inv1* to be suitable to test virulence reduction strategies based upon competitive exclusion by a less virulent strain. This finding also implies that a degree of assortment, greater than the inherent hyphal network of filamentous fungi, is necessary to maintain invertase production in a mixed-strain population, when nutritional conditions require this trait. However, given that non-producers in axenic culture are unable to digest sucrose (Figure 1.6), this cooperative trait may be essential within a population when this is the primary carbon source available, such as during plant infection. Therefore, although 'cheats' were at a selective advantage at all tested frequencies, it may be that cooperators obtain a competitive advantage when at even lower frequencies. Furthermore, the natural environment within plant tissue is intrinsically structured, which restricts the diffusion of public-goods away from producers and so would increase the proportion of the benefit they receive. This structure *in planta* would favour producers and is expected to represent a higher degree of structuring than that of the *in vitro* conditions which generated these results. Therefore, despite the competitive advantage of cheats *in vitro*, this may not be representative of fitness during infection.

We established that Δ*inv1* could exploit the cooperative invertase secretion of the wild-type *in planta*. This was firstly observed from live cell imaging of leaf sheath

epidermal cells during mixed infection where fluorescence signals from both strains could be observed in close proximity in either neighbouring or the same host cell where exploitation of extracellular products could occur (Figure 2.5a).

Figure 2.5

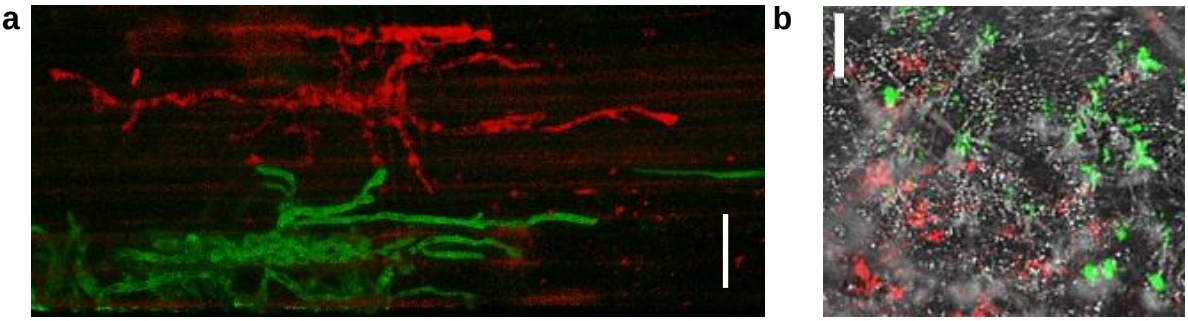

Figure 2.5 | Invertase is an exploitable trait *in planta.* a Live cell imaging of mixed strain infection (48 h.p.i.) of rice sheath epidermal cells indicating close proximity of coinfecting strains; this suggests interactions and invertase exploitation is possible, scale bar = 50 µm. **b** Merged epifluorescence micrograph of sporulating lesion from mixed strain infections (9 d.p.i.) with DIC, showing RFP (wildtype) and GFP (Δ*inv1*) conidia, indicating the presence of both strains within conidia populations produced at the end of the infection cycle, scale bar = 200 µm.

From mixed strain infections, we found that the Δ*inv1* mutant had greater success when in mixed strain infections with the wild-type, based on imaging of sporulating lesions from mixed infections where both strains were present, which in nature would proceed to instigate new infections (Figure 2.5b & Figure 1.1). It was also found that invertase production during infection incurs a cost to the individuals producing it, demonstrated by the fact that Δ*inv1* had a competitive advantage over the wild-type producer (relative fitness (*v*) of Δ*inv1* at 20% initial frequency: $v = 2.11 \pm 0.28$ s.e.m. n = 32). This also shows that invertase secretion remains an exploitable cooperative trait *in planta*. The advantage gained also suggests that the producer and non-

producer stains would coexist at some intermediate frequency and ‘cheats’ would persist in the population.

2.2.2 | Quinate metabolism is a private-good

To further study the extent to which sucrose consumption by Δ*inv1* was a result of the exploitation of external digestion by the invertase producing strain, knockout mutants of three genes for internally metabolised quinic acid (quinate dehydrogenase (*qa3*), 3-dehydroquinase (*qa2*) and 3-dehydroshikimate dehydratase (*qa4*)) (207) (strains generated and provided by M. Martin-Urdiroz, unpublished) were competed with a GFP tagged wild-type. Quinic acid is a cyclic polyol and is a carbon source present in high quantities in leaf litter (208). Unlike Δ*inv1*; Δ*qa2*, Δ*qa3* or Δ*qa4* were unable to outcompete the wild-type in mixed strain cultures (relative fitness < 1 when at an initial frequency of 20%) when reliant upon a gene product that they are deficient in to metabolise the only available carbon source. This gene product is produced by the co-cultured wild-type (Figure 2.6).

Figure 2.6 a

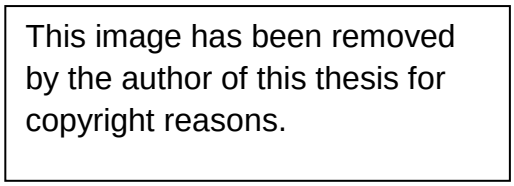

b

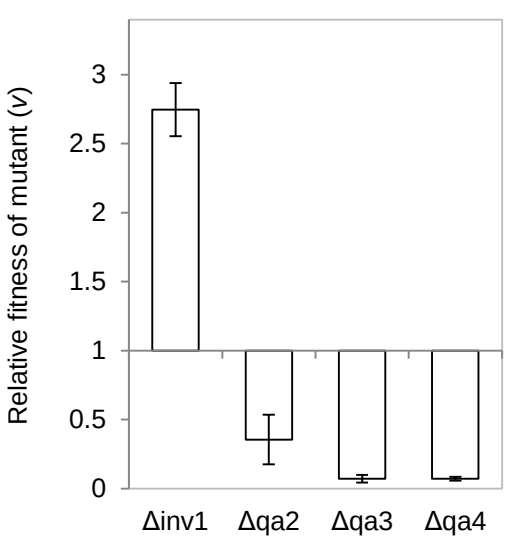

Figure 2.6 | Internal quinate metabolism does not represent an exploitable public-good. a Metabolic pathway and genes involved in catabolising quinate

(image reproduced and adapted from (207)). **b** Quinic acid metabolism it is not exploitable by mutants. Unlike Δ*inv1* ($p < 0.0003$, one sample t-test); Δ*qa2*, Δ*qa3* or Δ*qa4* were unable to gain a selective advantage and outcompete the wild-type in mixed strain cultures when reliant on the wild-type; i.e. when the only available carbon source (sucrose or quinic acid) requires metabolism by a gene product that each mutant is deficient in ($n = 6$, mean ± s.e.m.) (relative fitness of Δ*qa* < Guy11; Δ*qa2*: $p < 0.02$; Δ*qa3*: $p < 0.0001$; Δ*qa4*: $p < 0.0001$, one-sample t-test). When cultured in isolation on MM + quinic acid (1% w/v), wild-type Guy11 generated $2.44 \pm 0.56 \times 10^6$ conidia per plate (mean ± s.e.m.) whereas the Δ*qa2,* Δ*qa3* nor Δ*qa4* did not generate any detected conidia ($n = 3$).

Despite the fact that quinate metabolism is expected to occur internally due to *M. oryzae* possessing putative quinate permeases (207), the mutants were able to gain some benefits of metabolism by the wild-type (Figure 2.6). This is thought to be due to leakage of metabolic intermediates from hyphae, or anastomosis (209). Importantly though, because the gene products predominantly act internally, the mutants were unable to exploit the trait to a level more beneficial than generating the gene products themselves. Thus because quinate metabolism is not truly exploitable it would not conform to a public-good cooperative trait in the same way as sucrose metabolism, instead representing a ‘private-good’, hence further supporting the sociality of the invertase system established.

As all of the necessary conditions were appeased, we concluded that invertase production conformed to the definition of a cooperative system based on social evolution theory.

2.2.3 | Investigating ‘Hamiltonian Medicine’-style virulence reduction strategies by competitive exclusion

Having constructed and phenotypically characterised a non-invertase producing strain of *M. oryzae* in Chapter 1 and confirmed that invertase secretion represents a

public-good cooperative trait in sections 2.2.1 – 2.2.2, we next tested the principles of Hamiltonian Medicine by competitive exclusion as a disease management strategy (2). This strategy relies upon two key components of cooperation and virulence evolution theory. Namely that social cheats can invade a population of cooperators, and that public-good cheats are less virulent than cooperators (115). Does it represent a full-proof strategy as suggested by the existing theory and experimental evidence (e.g. (45, 87, 112))?

To test proposed strategies of Hamiltonian medicine, mixed infections were performed with the fully pathogenic wild-type Guy11 strain where Δ*inv1* would diminish the population levels of invertase production. Existing theory and *in vivo* disease investigations predict and provide evidence to suggest that the success of the pathogen and the subsequent virulence expressed would be lessened (2, 44, 45, 87, 88, 112, 113, 115). On the contrary, we found that with the introduction of the less virulent strain to an infecting population the overall success of the pathogen was amplified above infections initiated purely with the wild-type virulence factor producing strain (Figure 2.7). This increased fitness also translated into a more virulent infection in terms of the size of disease lesions inflicted upon the host (Figure 2.8).

The inoculation method employed for mixed strain infections was a quantitative attached leaf spot assay so that initial population demography and density could be established and manipulated. This localised method enabled intimate interactions to occur between coinfecting spores and permitted the quantification and assessment of the fungal population at the end of the disease cycle. The infection studies were conducted over 9 days following an entire rotation in a polycyclic disease (Figure

1.1), using an assay comparable to wild infections, with an inoculum size enabling successful colonisation and the life cycle to be completed (see methods for details).

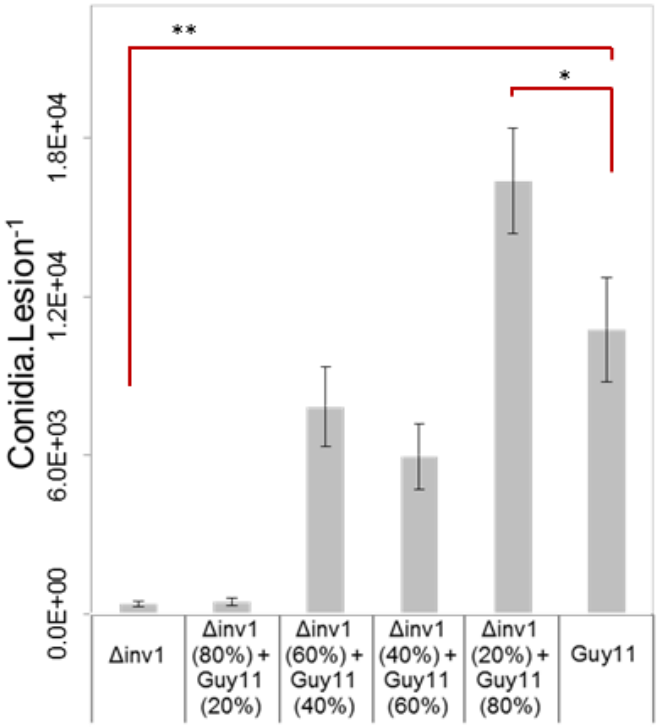

Figure 2.7 | Pathogen fitness measurements of *Δinv1*, Guy11 and a mixed inoculum. *In planta* fitness of *M. oryzae* during infections was evaluated by leaf spot inoculation of attached rice leaves with 10^3 conidia (mean ± s.e.m., n = 42, pooled from three experiments). Fitness was quantified by the number of conidia recovered per lesion at the end of the disease cycle. Infections with Guy11 produced significantly more conidia than pure 'non-producer' infections of the Δ*inv1* mutant (**p < 0.0001, W = 66, one-sided Mann-Whitney U test, n = 42). In addition, at least one out of five infection inocula containing 20%, 40%, 60%, 80% & 100% of producers, generated significantly different conidia numbers from the other four (p<0.0001, Kruskal Wallis test). Furthermore, we can reject the hypothesis that pure 'producer' (Guy11) infections created significantly more or equal conidia numbers compared to a mixture of 'producers' and 'non-producers' by conducting all pairwise comparisons between 100% Guy11 and mixed infections (*p < 0.04, W = 1174, Mann-Whitney U-test with Bonferroni correction, n = 42).

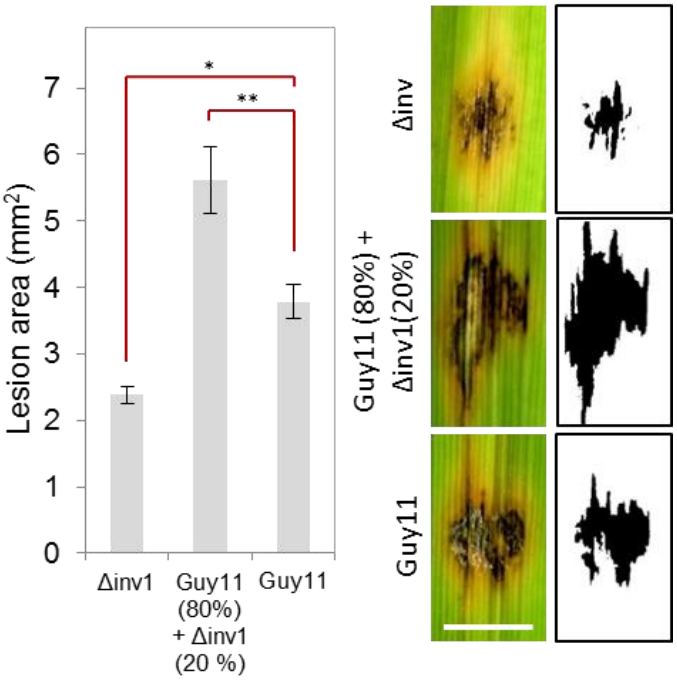

Figure 2.8 | Virulence measurements of Δ*inv1*, Guy11 and a mixed inoculum. Disease virulence by spot inoculation and infection with 10^3 *M. oryzae* conidia showing reduced virulence as measured by lesion area (mean ± s.e.m.), of Δ*inv1* compared to Guy11 (* $p < 0.0001$, one-sided 2-sample t-test with unequal variances, n = 20). Guided by the conidia data in Figure 2.7, we also confirm that the mixed strain infection containing Guy11 at 80% was more virulent than pure Guy11 infections (**$p < 0.002$, one-sided 2-sample t-test with unequal variances, n = 20). Example lesions (7 d.p.i.) from leaf spot infections from pure and mixed populations, scale bar = 3 mm with ImageJ analysis images from which areas were measured. Images of all replicates can be seen in Appendix 2.1.

2.2.4 | Why does Hamiltonian Medicine fail?

Investigation into the possible reasons behind this contradictory finding led to the prediction that this synergistic effect could be the result of multiple interacting social behaviours, which may be frequently observed in microbes (35, 39, 85, 109, 210, 211). Existing theory and experimental evidence that led to the prediction which our finding contradicts, are based on examining the influence of pathogen public-goods acting independently of other social traits that may be being experienced.

2.2.5 | *M. oryzae* faces a secondary social dilemma during sucrose metabolism

The secondary social trait that *M. oryzae* was found to be experiencing was that of prudent use of resources. Resource use is constrained by a rate-efficiency trade-off where resources are converted into energy in the form of ATP either slowly and efficiently or quickly and wastefully (76, 77, 93). This is analogous to a “tragedy of the commons” (96) where the cooperative way to consume resources is efficiently to maximise total population output, but at the costly expense of a slow rate. However, this cooperative metabolism may be exploited by cheats that metabolise resources quickly and inefficiently for their own gain but at the expense of the population. This trade-off is considered to be ubiquitous for resource usage by microbes and a thermodynamic necessity (77, 93). Evidence of this trade-off was found for both the metabolism of sucrose and its constituent hexose, glucose (Figure 2.9).

Figure 2.9

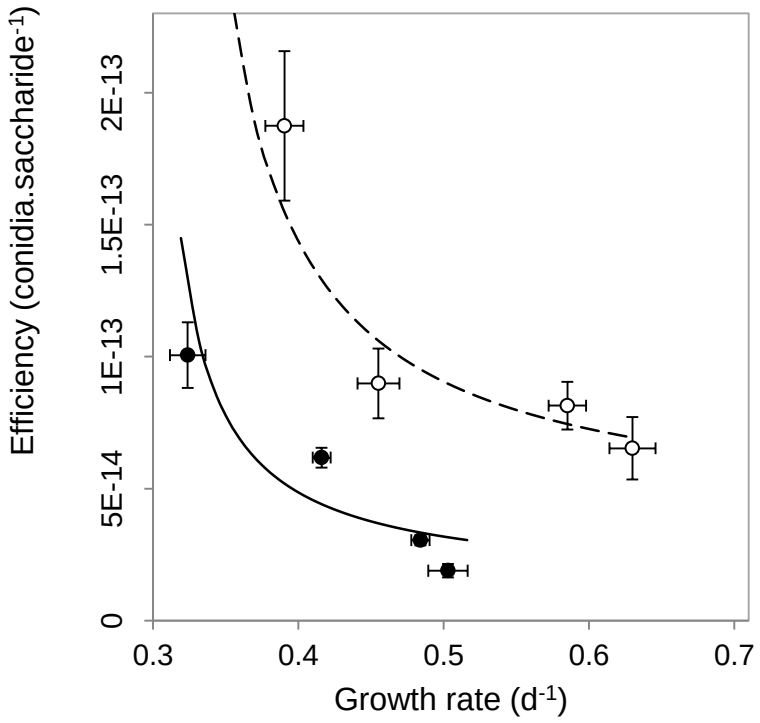

Figure 2.9 | Multi-trait interactions during sucrose metabolism by *M. oryzae.* In addition to public-good invertase production, we found evidence of a rate-efficiency trade-off where resources are used less efficiently when abundant, applicable to growth on glucose (•) (ρ= -0.8, $p < 0.0001$, Spearman rank correlation) and sucrose (o) (ρ= -0.5, $p < 0.05$, Spearman rank correlation). Efficiency units are conidia generated per molecule of saccharide. Growth rates were calculated from the Malthusian growth parameter (mean ± s.e.m., n = 5), which were manipulated by varying uptake rates by culturing on varying resource concentrations (1, 0.5, 0.125 & 0.03125 % w/v). Lines (solid = glucose, dashed = sucrose) represent a fit to data of a trade-off geometry directly inferred from the biophysical mechanisms that cause trade-offs (93). These fits were calculated by I. Gudelj, details of which can be seen in Appendix 2.2.

2.2.6 | Investigating multiple social trait interactions *in silico*

To demonstrate that the interaction between these social traits was sufficient to explain the amplified population fitness, a mathematical model was devised that would include both the social traits of public-good production and self-restraint (Figure 2.10 and Appendix 2.3). This captured the result observed experimentally that the synergistic effect of a mixture of high virulence invertase producers and low virulence non-producers leads to a population fitness peak (Figure 2.10b). The model predicts that removing the influence of the social trait of self-restraint will remove the synergistic effect observed in our system and return the initially anticipated result of fitness peaking in pure producer populations. This was achieved in the model by firstly removing the influence of the efficiency deficiency in high resources concentrations (Figure 2.10c). Secondly, this was achieved by exposing the entire population to the same degree of trade-off as would occur when resources are homogenously distributed in space or removing the public-good trait of osmotrophic metabolism (Figure 2.10d).

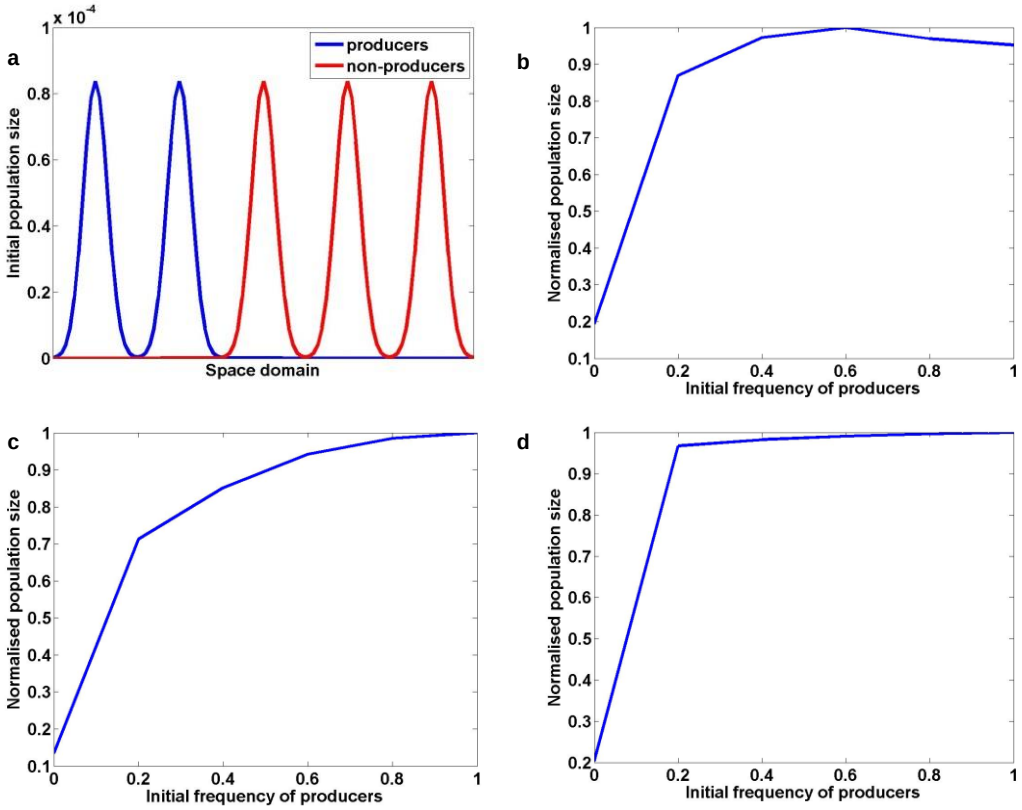

Figure 2.10 | The interactions between two social traits: public-good production and self-restraint; theoretical results. a Initial distribution of producers and non-producers, for producer frequency 0.4. Normalised final population size after exhaustion of resources as a function of initial producer frequency **b** in the spatially structured environment and in presence of rate-efficiency trade-off, **c** in the spatially structured environment and in the absence of rate-efficiency trade-off, **d** in homogeneous environment and in the presence of rate-efficiency trade-off. Mathematical model (Appendix 2.3) was developed by I. Gudelj & B. J. Pawlowska, Numerical simulations were conducted by B. J. Pawlowska.

2.2.7 | Testing predictions of the model *in vitro*

To experimentally verify the predictions of the mathematical model, *in vitro* conditions were established in which the rate-efficiency trade-off, the spatial structuring of the population, and the mode of metabolism could be altered. Firstly, conditions were determined that captured the synergistic effect of the mixed population of producers and non-producers, as observed during infection (Figure 2.6

& 2.7) and in the mathematical model (Figure 2.10). This occurred when the population was sufficiently spatially structured, had a carbon source that requires public-good invertase cooperation (sucrose) and resource concentrations were at the levels where they are consumed inefficiently (1%) (Figure 2.11a). This finding also suggests that the enhanced fitness of mixed infections is not caused by compensatory up-regulation of genes in 'non-producers', for instance to target other host nutrients, because sucrose is the sole carbon source in this *in vitro* environment.

Figure 2.11 | Population fitness of INV1 producing Guy11 and the Δ*inv1* mutant in axenic and mixed-strain populations of intermediate frequencies. a, b, d Populations were established by inoculation with 10^5 conidia with varying initial frequencies of invertase 'producers' and 'non-producers', with population fitness being assessed by the number of conidia recovered per plate. **a,** on 1 % sucrose agar media (mean ± s.e.m., n = 9). Single genotype populations of Guy11 produced more conidia than the Δ*inv1* mutant ($p < 0.0002$, two-sided 2-sample t-test assuming unequal variances, n = 9). In addition, at least one out of five inocula containing 20%, 40%, 60%, 80% & 100% of producers, generated significantly different conidia numbers from the other four ($p < 0.0025$, $F_{(4,\ 40)} = 4.95$, one-way ANOVA). Furthermore, we can reject the hypothesis that pure producer (Guy11) infections created significantly more or equal conidia numbers compared to a mixture of producers and non-producers by conducting all pairwise comparisons between 100% producers and mixed populations (* $p < 0.038$, ** $p < 0.0014$, post-hoc Tukey's, n = 9). **b,** Population fitness on 0.01 % sucrose agar media to remove the influence of a rate-efficiency trade-off. This resulted in mixed populations of producers and 'non-producers' not having significantly different fitness to single genotype population of 'producers' ($p > 0.75$, $F_{(4,\ 40)} = 0.48$, one-way ANOVA, n = 9). **c,** Population fitness in 1 % sucrose liquid media to minimise population spatial structure. Mixed populations of 'producers' and 'non-producers' did not have different fitnesses to pure 'producer' populations ($p > 0.85$, $F_{(4,\ 40)} = 0.33$, one-way ANOVA, n = 9). Cultures were prepared using a mycelial homogenate and fitness measured as biomass production (dry weight). **d,** Population fitness on 1% glucose agar media to remove the need for invertase mediated metabolism and hence spatial heterogeneity in hexoses. Mixed populations of producers and non-producers did not have different fitnesses to pure producer population ($p > 0.9$, $F_{(4,\ 40)} = 0.24$, one-way ANOVA, n= 9). **a - d** results are pooled from three repeated experiments.

Figure 2.11

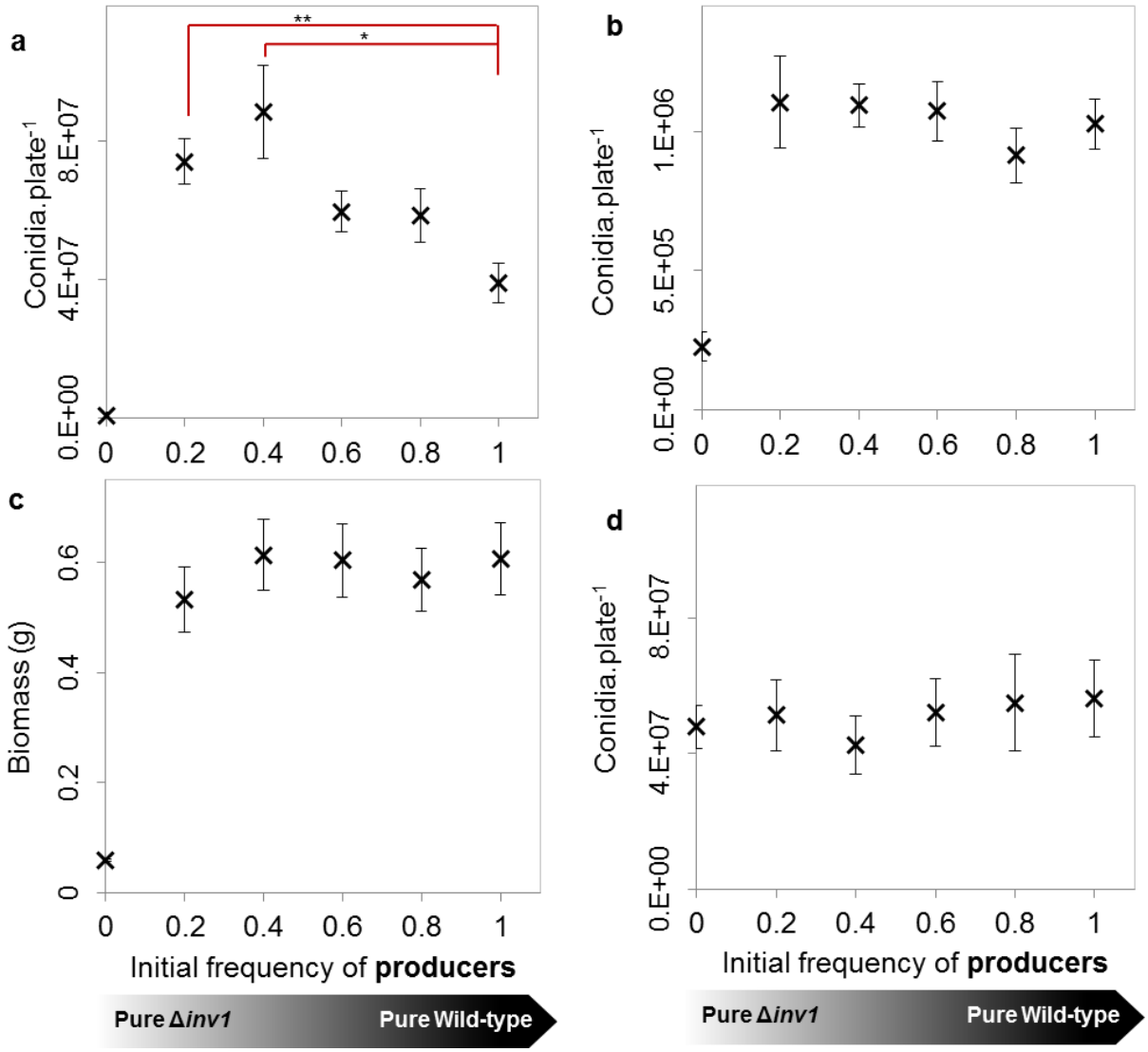

These three features; resource use inefficiency, population spatial structuring and spikes in hexose concentration from sucrose hydrolysis; were confirmed to be necessary to observe the synergistic effect on population fitness of a mixture of invertase 'producers' and 'non-producers' by removing each one independently. The influence of the rate-efficiency trade-off was removed by culturing the population at resource concentrations where the trade-off would be weak or non-existent (0.01% sucrose) (Figure 2.11b) as established from previous tests (Figure 2.9). Likewise, when sucrose concentrations were returned to trade-off levels (1%) but

homogenously spatially distributed in the population so that any influence of the trade-off would be equalised throughout the population (Figure 2.11c); or the public-good invertase metabolism was negated by culturing populations in glucose (Figure 2.11d) where external metabolism is not required as glucose is taken up directly through hexose transporters (161, 212). In each case, the synergistic effect was lost as predicted from the model (Figure 2.10).

2.2.8 | Investigating other possible mechanisms for this result

Cheats alleviating constraints upon resource use efficiency have also been described during modelling of social dynamics within decomposer communities (5). The presence of public-good cheats in this system are predicted to alter the nutrient composition by reducing consumption rates and hence carbon use efficiency, though not invoking a thermodynamic based trade-off. Instead it was suggested that nitrogen limitation caused carbon to be wastefully respired rather than invested in biomass formation, so the relative carbon to nitrogen ratio (C:N) was altered by the presence of cheats making metabolism more efficient (5).

Although nitrogen starvation elicits *M. oryzae* to produce secreted products (213), we found no evidence that *M. oryzae* experiences nitrogen limitation during the *in vitro* experiments reported here with comparable sporulation at 10% of the nitrogen supply of the fully supplemented media. In addition, no overgrowth phenotype resulting from increasing the N:C was apparent (Figure 2.12). These results suggest that the synergy we found does not result from similar mechanism to those predicted in social decomposer communities (5).

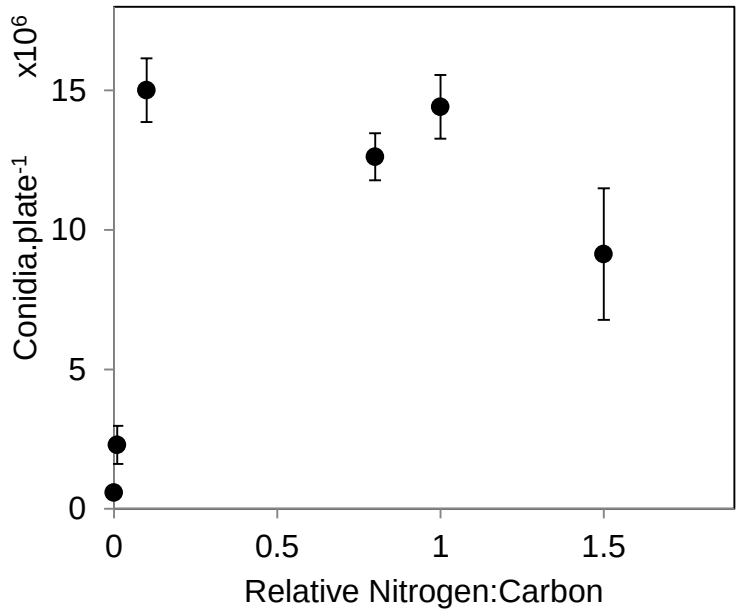

Figure 2.12 | Conidia production by *M. oryzae* in varying Nitrogen : Carbon ratios. *M. oryzae* does not experience nitrogen limitation during the *in vitro* conditions employed in this study. Conidia produced with 10% of the relative nitrogen available of the conditions employed during *in vitro* experiments were at comparable levels (to when relative N:C = 1). Increasing the available nitrogen (N:C) did not increase the production of conidia. N:C was varied with constant C-source concentrations and altering the supply of N (as $NaNO_3$). Mean ± s.e.m., n = 5.

2.3 | Discussion

Our study suggests that rice blast infections, comprised purely of highly virulent individuals, may be limited in their population fitness by resource use inefficiency. This is caused by invertase secretion forming glucose concentration spikes around invertase producers, leading to less efficient use. Therefore, the introduction of lower virulence ‘cheats’, that do not produce invertase, into a population of highly virulent invertase producers does not reduce population fitness. Instead, it alleviates the constraints on efficiency of resource use experienced, making the overall pathogen population fitter, and leading to increased virulence. Furthermore, the mechanism responsible for this synergy has been teased apart with a combination of

mathematical modelling and experimental evidence in tractable *in vitro* conditions so that the implications of multiple social traits can be elucidated. For the first time, we have demonstrated that targeting social virulence factors as a promising novel disease therapy (2, 25, 27, 44, 45, 49, 50, 214) can fail due to complex interactions between different social traits. Others have found that a combination of public-good producers and non-producers can result in maximal microbial population fitness *in vitro* (82, 85). However, our study is the first to find that this amplification of population fitness is relevant in the natural nutritional environment of a pathogen, within its host.

Interactions of multi-trait cooperative behaviours leading to such a counterintuitive observation may have wide applicability for disease management and not be restricted to the synthetic system employed here. This is considering the potential for multi-trait interactions in bacterial and fungal infection, but also in the establishment of tumours during cancer. For instance, pathogenic bacteria employ multiple social traits such as extracellular signalling molecule production responsible for the regulation of exoenzyme and effector production (36, 82, 215).

Linkage between social traits may act to enhance the effect of disease interventions that interfere with cooperative traits (109). However, as we have shown, this multiple-trait interaction may inadvertently have the reverse effect on infection severity. Indeed, others have found that quenching iron scavenging siderophores, which contribute towards virulence, with gallium can induce the production of other virulence factors in *Pseudomonas* populations as a result of iron starvation (39). Furthermore, populations of *E. coli* with a mixture of signalling molecule ‘producers’ – conferring antibiotic resistance – and ‘non-producers’ have been found to grow better than pure ‘producer’ populations (82). Moreover, synergy has been observed

between wild-type and *gac* (global activating) mutants of *Psuedomonas.* Here, a mutation in a regulatory gene responsible for multiple social traits led to a mutually beneficial mixed-strain population, hypothetically caused by interference between different traits (216). Another example is where a similar trend of synergy between public-good 'producers' and 'non-producers' was found in a bacterial entomopathogen through toxin production. However, unlike that finding, public-good 'cheats' of *M. oryzae* can still infect alone, albeit with reduced success, so community level transmission would not have the same extent of trade-off imposed between infectivity and spore production (72). When making predictions of virulence evolution, it is therefore crucial to assess consequences of within host outcomes on the influence of other stages of the infection cycle, such as transmission or infectivity (217).

In addition to microbial disease, tumour cells could face multiple interacting social dilemmas. Firstly, cancer cells produce numerous secreted proteins to facilitate carcinogenesis. These include growth factors, angiogenic factors, proteases and immune suppression factors (3, 27, 83). Secondly, they may face a tragedy of the commons through rapid glucose metabolism given the ubiquity of rate-efficiency trade-offs (93). Therefore, the prospect of applying ecological and evolutionary theory against cancer by either promoting public-good cheats, or medical treatments, such as antiangiogenic drugs that target secreted products, may have devastating consequences (3, 25, 27, 218, 219).

The potential for multi-trait cooperative behaviours is particularly relevant for fungal pathogens because fungi are osmotrophic organisms. This means that they proliferate within a host by secreting a large diversity of extracellular enzymes that break down polymeric nutrients of a host (cellulose, proteins and lipids), before

transporting the resulting simple sugars, amino acids and fatty acids into the cell (161, 220). Fungi, therefore, generate public-goods as a consequence of their break down of host polymers and will be particularly prone to public-goods games and harbouring cheating individuals within large populations. In fact, the secreted proteome of *M. oryzae* is thought to contain over 700 gene products (141), to which cheats may be able to avoid contributing towards. Moreover, the utilisation of newly created resources is likely to be constrained by rate-efficiency trade-offs, which have been found across the microbial world and are considered to be a thermodynamic and biophysical necessity (93).

Genetic and physiological diversity, like that observed in natural populations of *M. oryzae* and emerging from single disease lesions initiated by monoconidial inocula (140, 142), can provide resilience and adaptability to environmental changes. The synergy observed in our study suggests that diversity can also facilitate the pathogen in achieving maximal population fitness.

Although the synthetically created invertase cheat strain of *M. oryzae* has not yet been identified in the wild, as mentioned above, natural populations do exhibit a high degree of genetic diversity (140). Novel pathogenic strains that can infect resistant rice cultivars arise rapidly (20) and such gains in pathogenicity are often caused by transposon-mediated gene deletions or disruption (221, 222) similar to those used to create the synthetic strain in our study. Therefore, it is possible that *M. oryzae* invertase mutants can arise in nature, but since their importance was not previously realised, to my knowledge this has not been investigated further.

In general, natural fungal populations have a high degree of intraspecific diversity in invertase activity (203, 223). Moreover, the non-toxigenic strains of *A. flavus* used in

agricultural biocontrol were recovered from natural populations (47-51) and non-toxigenic strains of *C. difficile* that have been used in human clinical trials also occur naturally (45, 224). Studies investigating *M. oryzae* populations at the end of a disease cycle, isolated from single disease lesions that had been initiated from monoconidial cultures, have reported a high degree of virulence and race variability in the resulting population (142). This instability in pathogenicity could arise as a result of genetic alterations during proliferation of the fungus through the course of the disease cycle. This in turn suggests that even if infections are initiated from a single conidium, as opposed to the 10^3 used in our study; mixed-genotype or mixed-phenotype infections develop naturally, within which the multi-trait social interactions found in our study could occur.

Our study is relevant to polycyclic disease systems where infection is initiated by infecting agents (cell, spore, virus etc.), which exploit a host to replicate and form more infection agents for transmission. We follow the infection dynamics of an entire rotation in a polycyclic disease: from sporulation, spore germination, host infection to eruption and new sporulation. Importantly, it is during this cycle that the counterintuitive results are observed with mixed infections leading to maximal virulence and pathogen fitness, in which resulting populations contain both cooperator and cheat strains (Figure 2.5b) to initiate new infection. The infection assays we performed were carried out over the appropriate period to observe disease reactions (225, 226). However, the single cycle may not represent the longer term evolutionary process (205). Yet we do find that Δ*inv1* can have a selective advantage when present at low frequencies, suggesting coexistence between the strains at certain frequencies. Nonetheless, the amplified pathogen fitness and disease virulence from mixed infections, even within a single life cycle, is particularly

relevant for applications of Hamiltonian medicine in actual agricultural or clinical settings. In these circumstances, longer-term evolutionary dynamics are not necessarily the crucial factor provided the ‘cheat’ strains can establish within the population in individual hosts, as we found. Rather, a single infection or outbreak can result in 100% yield loss (227) or death, the chances of which are increased by a fitter and more aggressive pathogen population.

Virulence reduction strategies have produced positive outcomes in a number of animal (46, 87, 112), human (30, 31, 45) and agricultural (41, 42, 51) settings. Hence, they are emerging as a popular idea for treating disease, particularly with the issues surrounding existing measures such as antibiotic resistance (16, 17). The findings presented here highlight the importance of understanding the evolutionary and ecological outcomes of novel disease treatments, such as anti-virulence strategies, to avoid making mistakes similar to those made in the past with antibiotic use, which led to widespread resistance evolution.

Our results question the safety and durability of using anti-virulence strategies that target social virulence factors for infectious and oncological disease management (2, 24-29). Treating diseases with less virulent genotypes is emerging as popular strategy in a range of systems (e.g. (45, 50)) and is likely to be increasingly straightforward to implement with the development of genome editing technologies such as CRISPR/Cas9 (228), in addition to recovering naturally occurring less virulent cheat strains.

Despite the failure of principles of Hamiltonian medicine exposed in this study with a virulence causing metabolic enzyme, targeting virulence factors of fungi may still provide opportunities for disease management in the future. Beyond feeding,

successful pathogens suppress host immune responses. Plants detect pathogen-associated molecular patterns (PAMPs) which elicit PAMP-triggered immunity (PTI) (229). In response, successful pathogens deliver secreted effectors to interfere with PTI, such as a *M. oryzae* monooxygenase (*ABM*) which inactivates jasmonic acid and so evades jasmonate-based immunity in rice plants (92). These extracellular effectors may be targeted or exploitable by cheats or deletion mutants of these effectors (such as Δ*abm* (92)). If these effectors are targeted chemically or with null-mutants, meaning that the pathogen is unable to evade host immunity, it may induce a form of systemic-acquired resistance in plants leading to successful interventions (230). These alternative targets of anti-virulence therapies, though promising, will require further investigation into their viability and, as highlighted in our study, the possible secondary-trait interactions that may occur.

2.4 | Methods

2.4.1 | Construction of *ToxAp:mCherry* vector

To distinguish cooperator and cheat strains in mixed cultures, the wild-type strain was tagged with an RFP and the mutant strains were tagged with GFP. For the GFP tagged strain, the existing *ToxAp*:*SGFP* strain (ancestral genetic background: Guy11) (231) was used as the ancestral strain from which putative public-good genes were targeted for deletion. The vector to enable constitutive expression of a monomeric RFP was generated by yeast recombinational cloning (Figure 2.13a). Six primers were designed to amplify three fragments of DNA, four of which included 5' overhangs for homologous recombination between the fragments and with the plasmid p1284 that confers *URA3* selection (Table 2.1). PCR amplification was performed as described in detail in Chapter 7, with Phusion® High-Fidelity DNA Polymerase (NEB Inc., USA). A fragment of the phosphinothricin acetyltransferase gene cassette (*BAR*), that confers resistance to glufosinate ammonium, was amplified with a 30 bp 5' overhang on the forward primer complementary to vector p1284. The *toxA* promoter sequence was amplified with a 5' overhang on the forward primer complementary to the downstream region of *BAR* gene from an existing *ToxAp:SGFP* vector and has been shown to drive constitutive expression of downstream genes (231, 232). An RFP (*mCherry*) with fused *trpC* terminator sequence was amplified with forward primer with a 5' overhang complementary to the downstream region of toxA and a reverse primer with a 5' overhang complementary to vector p1284. These three fragments and vector, linearised with *HindIII* and *SacI*, were subsequently transformed into *S. cerevisiae* using a lithium acetate mediated yeast transformation protocol. Following successful construction the plasmid was isolated from *S. cerevisiae* and transformed into *E. coli* (XL10-

Gold® Ultracompetent cells, Agilent Technologies) to retrieve a large quantity of high quality constructed plasmid for *M. oryzae* transformation. Positive clones were inoculated into 50 mL LB/ampicillin and DNA extracted using a PureYield™ Plasmid Midiprep System (Promega, USA). The resulting *ToxAp:mCherry* plasmid (Figure 2.13a) was transformed into the wild-type Guy11 strain.

Figure 2.13

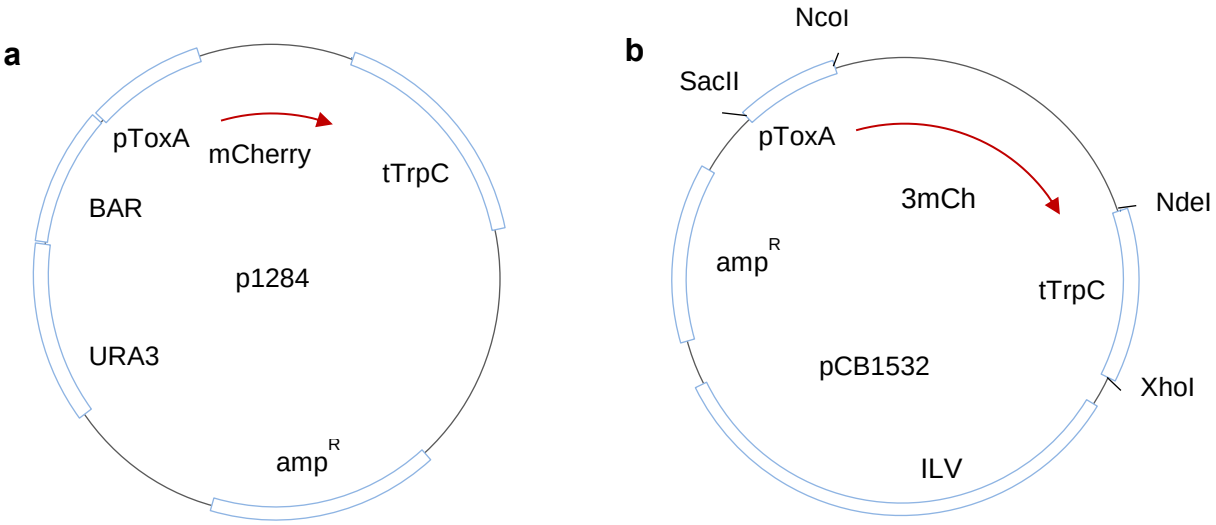

Figure 2.13 | Plasmid maps of vectors for generating an RFP tagged *M. oryzae* strain. **a**, The cytoplasmic promoter driven RFP expression vector ToxAp:mCherry constructed - in the backbone plasmid 1284 pNEB-Nat-Yeast, linearised with *Hind*III/*Sac*I - by yeast recombinational cloning. **b**, to increase RFP signal, a triple tandem repeated *mCherry* (*3mCh*) was used to create *ToxAp*:*3xmCherry* by conventional cloning in the fungal transformation vector pCB1532 (202).

2.4.2 | Assessment of *ToxA:mCherry* transformants

Strains that exhibited bialophos resistance (glufosinate ammonium (50 µg.mL^{-1})) were examined for expression of the fluorescent protein mCherry by epifluorescent

microscopy (Olymus IX81). Fluorescent strains were subsequently assessed by DIG-labelled Southern blot analysis for a single integration of the transformation plasmid. DNA was extracted from transformants before being digested with *EcoRI*, which does not have recognition sites within the *ToxA:mCherry* fragment. The blotting membrane containing fractionated gDNA was hybridised with a DIG-labelled probe constructed using primers ToxA_F.BAR and mCherry_R.1284. Single integration of the vector was confirmed by visualising a single band (Figure 2.14).

Figure 2.14

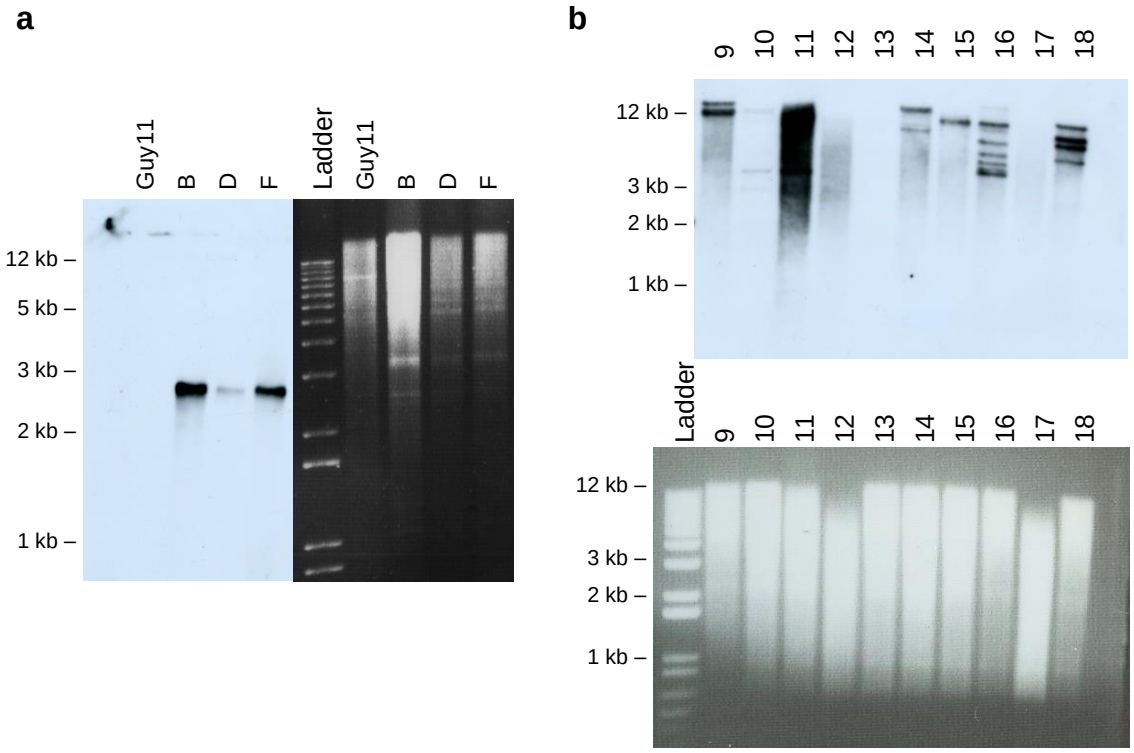

Figure 2.14 | Single integration of the *ToxA*:*RFP* expression vectors. a *ToxA:mCherry* transformants B, D and F are single integrations verified with Southern blot analysis after digestion with *EcoRI* and probed with pToxA-mCherry-tTrpC fragment. Left panel shows the developed film. Right panel shows an image of ethidium bromide stained agarose gel. **b** *ToxA:3xmCherry* transformant #15 shows single integration following digestion with *BamHI* and probed with mCherry-tTrpC fragment. Top panel shows developed film and bottom panel shows an image of ethidium bromide stained agarose gel.

2.4.3 | Construction of *ToxA:3xmCherry*

To amplify the constitutive cytoplasmic RFP signal expression in *M. oryzae,* the *mCherry* RFP was substituted for a triple tandem repeated *mCherry* (*3mCh*) (233) (Figure 2.13b). This vector was generated by ligation of a *3mCh NcoI*/*NdeI* fragment, *toxA* promoter *SacII*/*NcoI* fragment, and *trpC* terminator *NdeI*/*XhoI* fragment, into the transformation vector pCB1532 conferring sulfonylurea resistance (202). Transformants exhibiting resistance were assessed for positive fluorescence signal by epifluorescence microscopy (Olympus IX81) and single integration of the vector was screened for by Southern blot analysis following restriction digest of gDNA with *BamHI* using a probe generated with PCR using primers mCherry_F_ToxA and trpC_R_1284 (Figure 2.14b).

Table 2.1 | Primers used for constructing the *ToxA:mCherry* plasmid.
Underlined regions indicate complementary regions for recombination cloning.

Primer name	Nucleotide sequence (5' - 3')
BAR_F.1284	AACTGTTGGGAAGGGCGATCGGTGCGGGCCGTCGACAGAAGATGA
BAR_R	GTCGACCTAAATCTCGGTGACGGG
ToxA_F.BAR	GTCCTGCCCGTCACCGAGATTTAGGTCGACCGATTGGAATGCATGGAGGAGTTC
ToxA_R	GGACTATATTCATTCAATGTCAGC
mCherry_F.ToxA	GCGATAGCTGACATTGAATGAATATAGTCCATGGTGAGCAAGGGCGAGGAGGAT
mCherry_R.1284	TTCACACAGGAAACAGCTATGACCATGATTGAATTCAATTACTTGTACAGCTCGTCCA

2.4.4 | Mixed strain competitions

Population fitness and strain frequencies of *M. oryzae* were measured by spore production, except for in liquid cultures where dry-weight biomass was measured, as liquid culture is not conducive to conidiogenesis (234). Both traits contribute to the ability to survive and reproduce, so represent appropriate measures of fitness (235). Importantly for pathogenic fungi, sporulation permits transmission to new hosts. Spore production quantification has been used as a direct measure of fungal reproduction and transmissibility (and hence fitness), which is thought to correlate with the degree of host exploitation and resource uptake (11). The time points where measurements were taken, were chosen in order to allow resources to be exhausted so that population fitness is based on yield and not just rate. This time varies between experiments, as detailed below, depending on the resource concentration and environment employed.

Mixed-strain competition experiments on agar plates were performed as described previously for *S. cerevisiae* to establish degrees of population spatial structuring (85) (Figure 2.15). Conidia from 10-12 d CM agar plates were harvested and washed with sdH_2O and resuspended in semi-solid (2 $g.L^{-1}$ agar) MM-C (213) to a concentration of 2.5 x 10^5.mL^{-1}. Conidia were then inoculated onto 25 mL MM + sucrose (10 $g.L^{-1}$ or 0.1 $g.L^{-1}$) or glucose (10 $g.L^{-1}$) agar plates with 10^5 conidia.$plate^{-1}$ in a 4 x 5 array with patch midpoints separated by 12 mm. Two levels of assortment were considered. In the ‘structured’ population each patch consisted entirely of *INV1* or Δ*inv1*, whereas in the ‘semi-structured’ population each patch was made up of a mixture of both *INV1* and Δ*inv1* at the appropriate frequencies (Figure 2.13). Six initial frequencies of *INV1* and Δ*inv1* were tested; 0, 20, 40, 60, 80 and 100 %. For ‘structured’ population treatments, frequencies were established by varying the

number of the 20 patches of either *INV1* or Δ*inv1,* which were located randomly in the array. 'Semi-structured' treatments were initiated by preparing a starter spore suspension of the mixed strains at the appropriate proportions. Data in Figure 2.11 used the 'semi-structured' configuration. Competition cultures were incubated for 12 d, conidia collected and counted as described above, with *INV1* and Δ*inv1* identified by epifluorescence microscopy (Leica M205FA). When investigating quinic acid metabolism, the 'semi-structured' configuration was used with sucrose being replaced with quinic acid (1% w/v) with an initial frequency of 80% 'producers'.

Figure 2.15

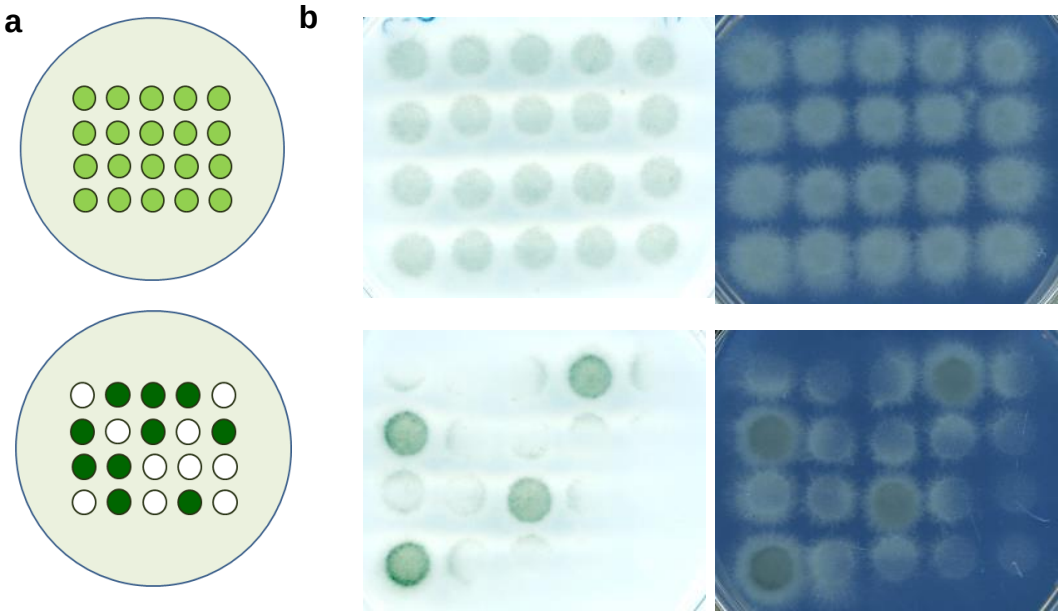

Figure 2.15 | Experimental set up of mixed strain cultures to establish degrees of strain frequency and spatial structuring. a Schematic of inoculation regimen for mixed strain cultures. **b** images of competitions inoculated on MM + sucrose agar plates after 4 d with light or dark background for image clarity. In the 'semi-structured' population (top row) each 'patch' was made up of a mixture of both *INV1* and Δ*inv1* at the appropriate frequencies (light green), whereas, in the 'structured' population (bottom row) each 'patch' consisted entirely of *INV1* (dark green) or Δ*inv1* (white).

To minimise the influence of population structure and hence spikes in glucose concentrations where the rate-efficiency trade-off would peak, competitions were performed in liquid sucrose (10 $g.L^{-1}$) MM at 125 r.p.m. with strains inoculated as wet biomass, established in CM, totaling 1 g in strain proportions of 0, 20, 40, 60, 80 or 100 %. Fitness was measured as dry weight biomass established. Growth curves were established for each proportion of strains to establish the point at which resources had been consumed and biomass peaked. This was 5 d for all combinations except 20 % producer, which required 9 d, and axenic 'non-producer' populations failed to increase in biomass. In case biomass did not capture the subtleness of the synergistic effect, the heterogeneous glucose spikes, which occur in structured conditions when sucrose breakdown by invertase is required, were eliminated. This was achieved by performing the same experiment as the *in vitro* set up that captured the synergy between strains (Figure 2.11a) but in a nutritional environment that does not require external digestion (1% (w/v) glucose, Figure 2.11d).

To investigate the influence of nitrogen starvation and N:C, conidia production was assessed by inoculating wild-type *M. oryzae* conidia (10^5) onto MM-N agar plates supplemented with different nitrogen ($NaNO_3$) concentrations. Relative Nitrogen:Carbon = 1 is the concentration found in MM (10 $g.L^{-1}$ glucose, 6 $g.L^{-1}$ sodium nitrate) (213). Conidia were collected and counted after 12 d.

Appendix 2.1

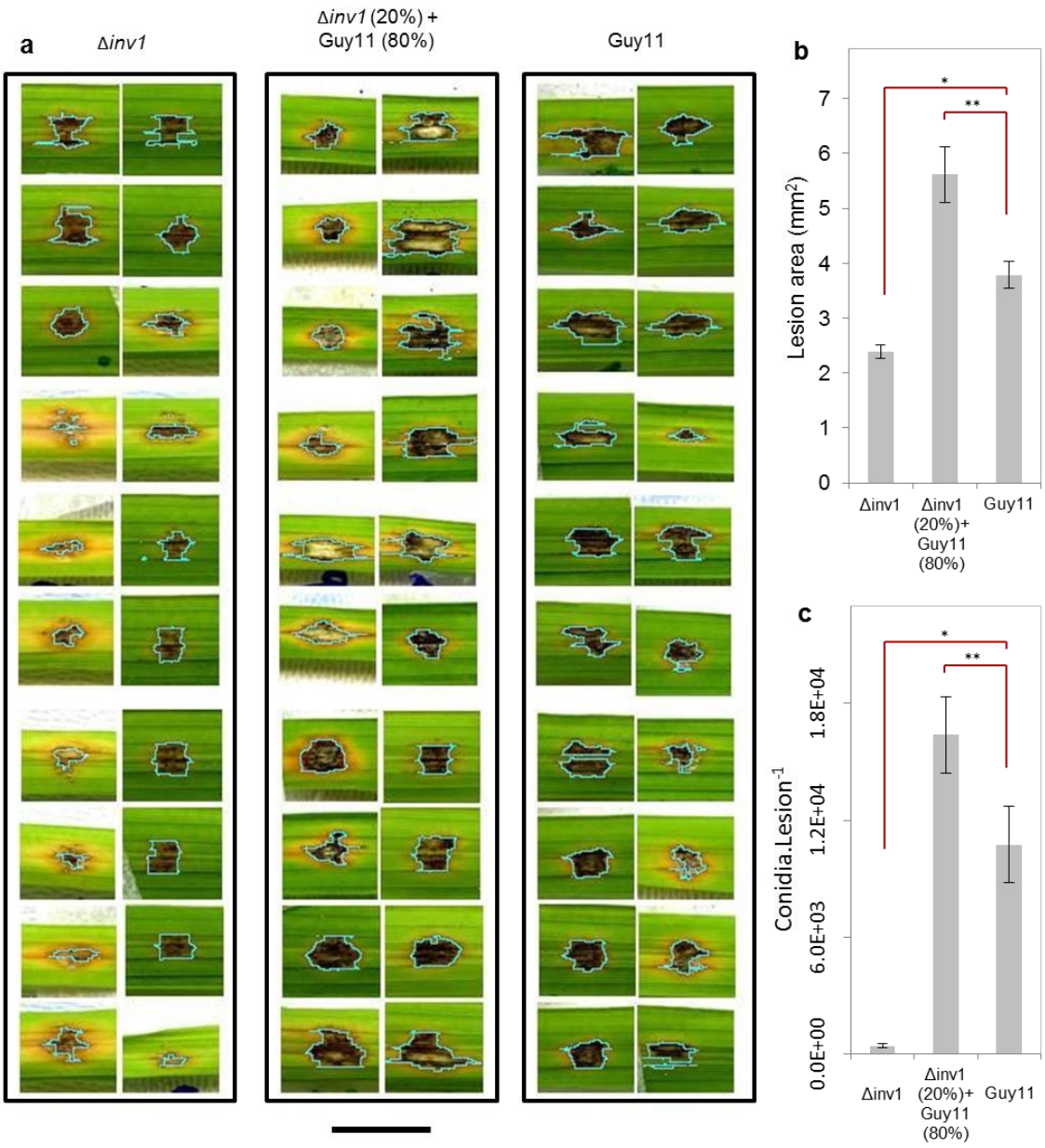

Appendix 2.1 | Extended summary of Fig 2.7 / 2.8. Disease virulence of *M. oryzae* from attached leaf spot inoculations of Guy11, Δ*inv1*, and a mixture of Guy11 (80%) + Δ*inv1* (20%). a Images of disease lesions captured with an Epson Expression 1680 Pro scanner 7 d.p.i., pale blue lines indicate boundaries of lesion area quantified, Scale bar = 7 mm. **b** Disease lesion area quantified with ImageJ. Δ*inv1* imposed reduced virulence as measured by lesion area compared to Guy11 (* $p < 0.0001$, one-sided 2-sample t-test with unequal variances, n = 20). Mixed strain infection containing Guy11 at 80% was more virulent than pure Guy11 (** $p < 0.002$, one-sided 2-sample t-test with unequal variances, n = 20). **c** This virulence difference was as a result of different pathogen population fitness as measured by the number of conidia generated at the end of the disease cycle (9 d.p.i.) where Guy11 was fitter than Δ*inv1* (* $p < 0.0001$, W = 66) with mixed infections with 80% Guy11 being fitter than pure Guy11 populations (** $p < 0.04$, W = 1174, Mann-Whitney U-test with Bonferroni correction, n = 42), all treatments shown in Figure 2.6.

Appendix 2.2

Data fitting for Figure 2.9 was performed by I. Gudelj. Details in Appendix 2.2 were written by I. Gudelj.

Fitting Geometric Trade-offs to Data

Recent paper (93) inferred geometry of the rate-efficiency trade-off, directly from the biophysical mechanisms that cause it. The resulting five parameter geometric trade-off has the form:

$$(growth\ rate, efficiency) = \left(c(H)\frac{HV_{max}}{K_m + H}, c(H) \right),$$

where H is the resource concentration, V_{max} is the maximal rate of sugar uptake while K_m denotes sugar half saturation constant (see (93) for more details).

The resource efficiency is a function of sugar and takes the form as in (93)

$$c(H) = c_{hi}\frac{1}{1+pH} + \frac{pH}{1+pH}c_{lo}.$$

The parameter c_{hi} represents the highest spore number per molecule of resources attainable, achieved at the lowest sugar concentrations, whereas c_{lo} is the spore numbers attained when sugar is abundant, p is a phenotype that controls the rate of decrease in efficiency with increasing sugar supply.

We first fit c_{hi}, c_{lo} and p to the data on efficiency as a function of sugar, then we fit V_{max} and K_m to the growth rate data as a function of sugar, both steps using non-linear fitting routines in MATLAB. The resulting rate-efficiency data fit is shown in Figure 2.9 and typical parameter estimates are given in the table below.

Parameter	Estimate	Standard error estimate	T value	p value
Sucrose				
c_{hi}	3.7058×10^{-5}	8.597×10^{-24}	4.3106×10^{18}	$< 10^{-15}$
p	10^{10}	8.9348×10^{-31}	1.1192×10^{40}	$< 10^{-15}$
c_{lo}	6.6768×10^{-14}	8.0478×10^{-15}	8.2967	$< 10^{-7}$
V_{max}	9.8624×10^{12}	1.1727×10^{-16}	8.4101×10^{28}	$< 10^{-15}$
K_m	0.12247	0.0045833	26.721	$< 10^{-15}$
Glucose				
c_{hi}	2.3203×10^{-5}	4.0433×10^{-24}	5.7385×10^{18}	$< 10^{-15}$
p	10^{10}	4.2022×10^{-31}	2.3797×10^{40}	$< 10^{-15}$
c_{lo}	2.8892×10^{-14}	3.785×10^{-15}	7.6331	$< 10^{-7}$
V_{max}	1.8711×10^{13}	6.072×10^{-17}	3.0816×10^{29}	$< 10^{-15}$
K_m	0.1499	0.0039922	37.547	$< 10^{-15}$

Appendix 2.3

Mathematical model was developed by I. Gudelj & B. J. Pawlowska, Numerical simulations were conducted by B. J. Pawlowska. Details in Appendix 2.3 were written by I. Gudelj.

Multi-trait mathematical model

We investigate whether the synergy between two social traits: public-goods production and self-restraint is sufficient to explain why a mixture of public-goods producers and non-producers enhances population fitness. To this end, we develop a mathematical model based on a simplified version of MacLean *et al*. (85) which allows us to probe the effects of multi-trait interactions on population fitness. The first trait is the extracellular production of a public-good, invertase that breaks down a complex sugar (sucrose) into simple sugars (hexose) and we consider two strains, an invertase producer (the wildtype Guy11) and a non-producer (the Δ*inv1* mutant). The second social trait is intracellular and relates to the efficiency with which a cell exploits newly-acquired simple sugars.

Growth kinetics.

In our model both strains take up resources R and use them to generate ATP using a simple, unbranched pathway (77). The rate of ATP production in the pathway is denoted by J^{ATP} and is given by

$$J^{ATP} = \eta_{ATP}^{R} J^{R}$$

where J^R denotes the rate of the pathway which is a function of resource concentration R and is mathematically represented by $J^R(R)$. The term η_{ATP}^{R} denotes the number of ATP molecules produced in the pathway. In practice, yield of ATP production $\eta_{ATP}^{R}$is not easy to measure as the efficiency, η_e^R whereby $\eta_e^R = b \cdot \eta_{ATP}^{R}$, where b is a constant denoting the amount of biomass formed per unit of ATP. We represent microbial growth as a linear function of the rate of ATP production (77, 85, 236) namely $r \cdot J^{ATP}$, where r is some proportionality constant which we here set to 1.

Sucrose utilization

Both strains can take up sucrose (*S*) and the rate of sucrose pathway is defined by

$$J^S = \frac{V_{max}^S S}{K_m^S + S}$$

where V_{max}^S denotes the maximal rate of the pathway while K_m^S denotes the respective Michaelis-Menten constant. The pathway rate represents the rate at which product is formed, which in this case is the same as the rate at which substrate is consumed. Therefore throughout this article we refer to V_{max}^R as the maximal rate of resource *R* uptake and K_m^R as the measure of affinity for resource *R*. The efficiency of the pathway utilising sucrose is denoted by η^S.

Invertase production

Invertase producers secrete invertase, an enzyme which catalyses the hydrolysis of sucrose (*S*) with each sucrose molecule being broken down to two molecules of hexose (*H*), namely one molecule of glucose and one molecule of fructose. Hexose is then transported into the cell and for simplicity our model does not differentiate between glucose and fructose molecules. The rate of conversion of sucrose into hexose (*Inv*) is a saturating function of sucrose concentration taking the following form:

$$Inv = inv \frac{S}{k + S}$$

where *inv* denotes invertase activity and *k* is a saturation constant. Invertase is costly to produce, and the cost is denoted by *c*, which for simplicity we assume to be a constant.

Hexose utilisation

Both strains can take up hexose (*H*) and the rate of sucrose pathway is defined by

$$J^H = \frac{V_{max}^H H}{K_m^H + H}$$

where V_{max}^H denotes the maximal rate of the pathway while K_m^H denotes the respective Michaelis-Menten constant. The efficiency of the pathway utilising hexose is denoted by η^H and we assume that $J^H > J^S$, allowing for hexose to be the preferential carbon source.

Self-restraint through efficiency of resource utilisation

The efficiency of the hexose pathway is known to depend on the rate of resource uptake, termed rate-efficiency trade-off; therefore η^H is a decreasing function of J^H and motivated by (237) we assume that

$$\eta^H (J^H) = \alpha_1 + \frac{\alpha_2}{1+\exp(\alpha_3 + \alpha_4 \cdot J^H)},$$

where α_i, i = 1..4 are constants.

To predict densities of the producer and non-producer strain, we deploy a reaction-diffusion model enabling the explicit tracking of resource concentrations and population densities in both space and time. In particular let $N_p(x, t)$ and $N_n(x, t)$ denote the density of producers and non-producers, respectively, at time t and spatial location x, $x \in [0, l]$ with l denoting a positive constant. Then the model takes the following form

$$\frac{\delta S}{\delta t} = D_S \frac{\delta^2 S}{\delta x^2} - J^S(N_p + N_n) - Inv \cdot N_p \qquad (1a)$$

$$\frac{\delta H}{\delta t} = D_H \frac{\delta^2 H}{\delta x^2} - J^H(N_p + N_n) + 2Inv \cdot N_p \qquad (1b)$$

$$\frac{\delta N_p}{\delta t} = D_{N_p} \frac{\delta^2 N_P}{\delta x^2} + (1 - c)(\eta^H J^H + \eta^S J^S) N_p \qquad (1c)$$

$$\frac{\delta N_n}{\delta t} = D_{N_n} \frac{\delta^2 {}_{N_P}}{\delta x^2} + (\eta^H J^H + \eta^S J^S)\, N_n \qquad (1d)$$

where $\frac{\delta^2}{\delta x^2}$ is one-dimensional diffusion operator while D_* represent diffusion coefficients for sucrose (*S*), hexose (*H*) and cell biomass (*N*). Due to the molecular size we assume that the rate of movement of sucrose is twice as slow as that of hexose, while cells move at an even slower rate.

We impose no-flux boundary conditions in addition to the following initial conditions: $S(x, 0) = S_0$, where S_0 is a sucrose supply constant, $H(x, 0) = 0$ with $N_p\ (x, 0) = N_{p0}(x)$ and $N_n\ (x, 0) = N_{n0}(x)$ representing an initial distribution of producers and non-producers, respectively. The total initial population density is denoted by N_0 and an example of an initial spatial distribution of producers and non-producers is shown in Figure 2.10a. The model is simulated for different initial frequencies of producers and non-producers until all resources are exhausted and for each case we record the final total population size.

Next, we choose model parameter values that enable us to recover the result that the total population size is maximised for populations containing a mixture of producers and non-producers. These are listed in the table below while the model outcome is shown in Figure 2.10b.

To investigate whether the synergy between public-goods production and self-restraint drives the result shown in Figure 2.10b, we remove the self-restraint from the model by removing the assumption of the rate-efficiency trade-off leaving only the public-goods dilemma at play. In that case the model reverts to the classical finding that total population size is maximised for populations containing only producers (Figure 2.10c). This can be explained by the fact that when producers are common, the invertase production results in a large spike, both spatial and temporal, in hexose. This would enable rapid but inefficient growth. However if a fraction of non-producers is introduced into the population the hexose spike around producers that are in a vicinity of non-producers is smaller, so that the population burns finite resources more efficiently. The effects of the rate-efficiency trade-off can also be removed from the model by considering spatially homogeneous populations. In this

case both producers and non-producers share resources equally, and the boost of efficiency in resource consumption observed in the boundary between producers and non-producer in spatial environments will not be present here. Indeed, performing simulations of the model in spatially homogeneous environments we again recover the result that the total population size is maximised for a population containing only producers (Figure 2.10d).

V_{max}^{S}	11 [mmol sucrose/ (g protein x h)]
V_{max}^{H}	100 [mmol hexose/ (g protein x h)]
K_m^S	7 [mMol sucrose]
K_m^H	100 [mMol hexose]
inv	77 [mmol sugar / (g protein x h)]
c	0.004
S_0	29.2 [mMol]
N_0	3 x 10^{-5} [g protein/L]
D_S	0.005 [l^2 / h]
D_H	0.01 [l^2 / h]
D_N	0.0002 [l^2 / h]
η^S	0.01 [g protein/ mmol sucrose]
k	5 x 10^{-3} [mMol sucrose]
α_1	0.0176
α_2	0.0318
α_3	-2.2649
α_4	0.205

Chapter 3

Investigating the generality of Hamiltonian medicine failures with protein metabolism

3.1 Introduction

To test the generality of our findings with secreted invertase metabolism of sucrose, because fungal pathogens generate a wide range of secreted metabolic enzymes to break down polymeric nutrients (141, 161, 220), we asked if our contradiction of the principles of Hamiltonian medicine were applicable to other *M. oryzae* public-goods. Given that sucrose was found to be a principle carbon source to facilitate the proliferation, pathogenicity and fitness of *M. oryzae,* and hence the virulence imposed upon its host, we sought to test Hamiltonian medicine principles with an equally crucial public-good. We sought to generate a null mutant of a gene responsible for obtaining another essential element, nitrogen.

3.1.1 | Nitrogen metabolism in *M. oryzae*

As mentioned in Chapter 1, ammonium and L-glutamine are consumed as preferential nitrogen sources by *M. oryzae*, with secondary metabolic enzymes being repressed by nitrogen metabolite repression (NMR) under the control of *TPS1* (167, 181, 184). When preferred nitrogen sources are exhausted and so de-repression of NMR, expression of secondary metabolic genes to utilise less preferred N sources are activated (238). *NUT1* is the nitrogen regulatory gene responsible for controlling the utilisation of alternative nitrogen sources, such as complex proteins. Glucose is understood to be detected as glucose-6-phosphate by the sugar sensor *TPS1*, which in turn represses the NMR1-3 inhibitor proteins of *NUT1* (167, 239).

3.1.2 | Proteases of fungal plant pathogen

For plant pathogenic fungi, genes to exploit less preferred N sources include secreted proteases to depolymerise proteins to amino acids for absorption (161, 240). Proteolytic activity during pathogenesis could also have other functions. These include breaking down proteins involved in structural integrity or construction of plant cell walls (241, 242). Plants also produce antimicrobial proteins in defence against pathogen attack (243), to which pathogen derived proteases may be secreted to neutralise. These secreted proteases can also be implicated in host plant resistance. The secreted protease *AVR-Pita* of *M. oryzae* can elicit a hypersensitive response in rice plants by interacting with the gene product of plant cultivars expressing the *Pi-ta* resistance gene (9, 240, 244).

3.2 | Results

3.2.1 | Generating putative protease mutants

We sought to identify a public-good protease gene in *M. oryzae* by generating a deletion mutant with a deficiency in secreted proteolytic activity. We targeted a predicted aspartyl protease (MGG_09351, GenBank: XM_003720226.1, Uniprot: G4NI47) and serine protease (MGG_09246, GenBank: XM_003709825.1, Uniprot: G4MQ68) (Figure 3.1). As with invertase deletion, gene knockout was achieved by a split-marker gene deletion technique (145, 146) generating strains Δ*asp1* (MGG_09351) (Figure 3.1a-b) and Δ*ser1* (MGG_09351) (Figure 3.1 c-d).

Figure 3.1 a

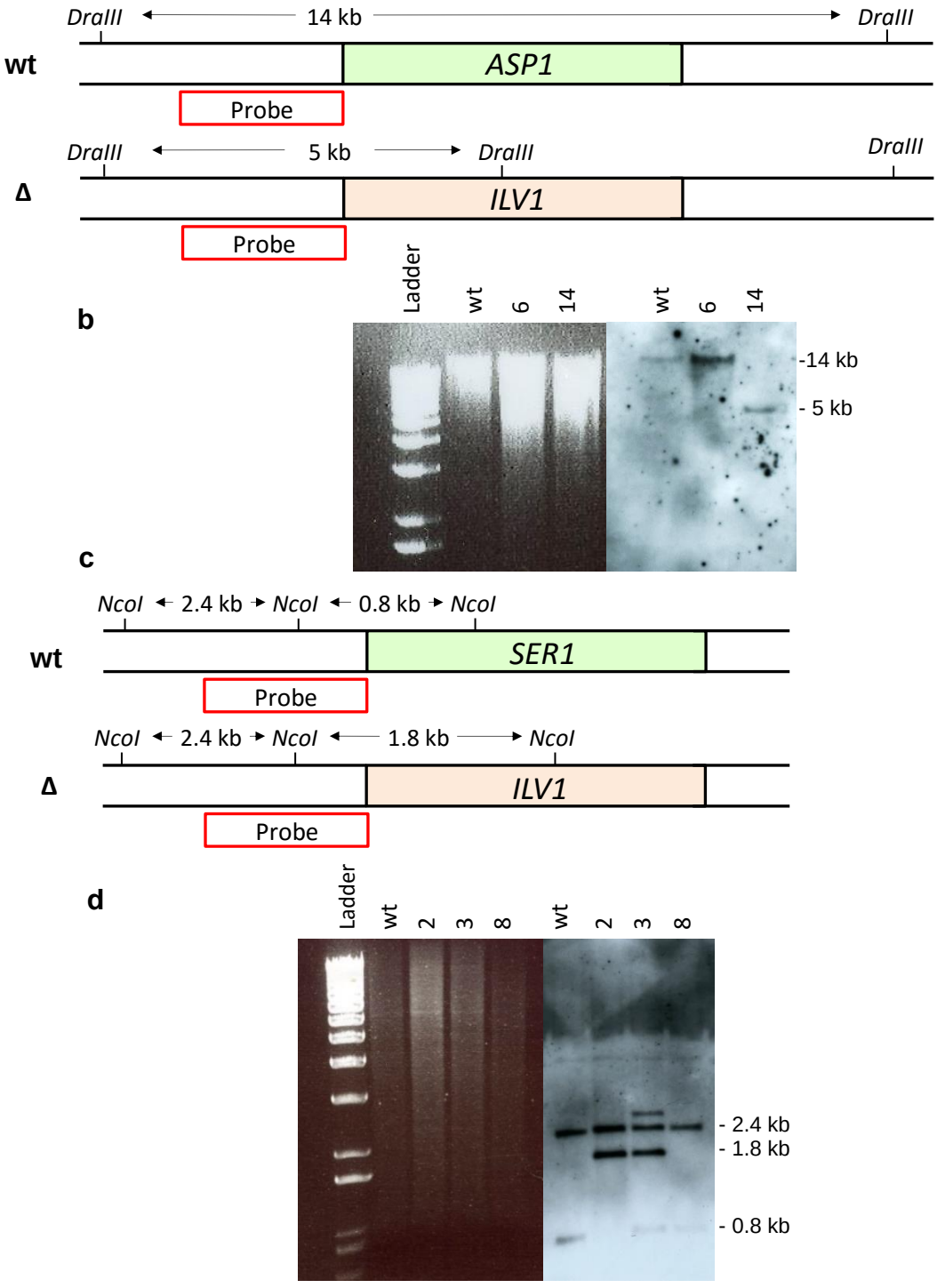

Figure 3.1 | Schematic of fusion PCR based split-marker targeted gene deletion of putative protease genes *ASP1* (MGG_09351) & *SER1* (MGG_09246) (a & c) and confirmation of gene replacement by Southern blot analysis (b & d). Gene replacements were achieved by replacing putative protease genes with a 2.8 kb sulfonylurea resistance allele (*ILV1)*. For each gene, in a first round of PCR, a 1 kb genomic fragment upstream (LF) and downstream (RF) of the ORF were amplified.

Separately, 1.6 kb overlapping fragments of the 5' and 3' end of the sulfonylurea resistance gene cassette (*ILV1*) were amplified. Amplicons produced were fused in a second round of PCR to produce two larger fragments of 2.6 kb. The constructs were used to transform *M. oryzae* (Strain *ToxA*:*SGFP* background Guy11) and gene replacement was achieved by homologous recombination. Gene replacements were confirmed by fragment size differentiation following restriction endonuclease digestion of gDNA with *DraIII* for *ASP1* and *NcoI* for *SER1*. Wild-type genotype band for *ASP1* was at 14 kb with mutants at 5 kb (transformant #14 shown here) (**b**). Both genotypes produced a band at 2.4 kb with an additional band; wild-type for *SER1* at 0.8 kb with mutants at 1.8 kb (transformant #2 shown here) (**d**).

The gene products of both *SER1* and *ASP1* are predicted to be secreted based on predictions made by the genomic assessment of the coding sequence (Table 3.1) and the identification of a signal peptide (Figure 3.2).

Figure 3.2

a **b**

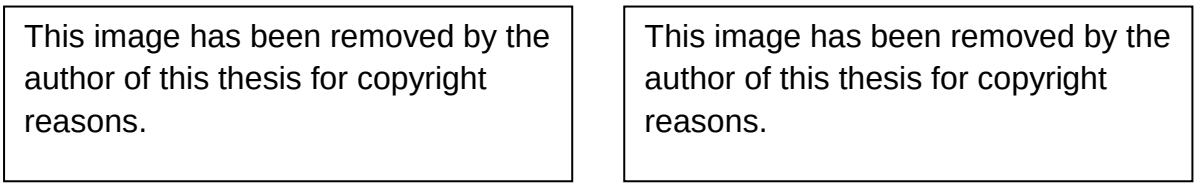

Figure 3.2 | Identification of predicted signal peptides on putative protease genes of *Magnaporthe oryzae* using SIGNALP 4.1 software (188). Both genes possess putative signal peptides with **a** MGG_09351 (*ASP1*) having a cleavage site between amino acids 19-20, with **b** MGG_09246 (*SER1*) having a cleavage site between amino acids 20-21. This suggests that both gene products are destined for the secretory pathway.

Table 3.1 | Subcellular localisation prediction of putative protease genes and yeast homologue of *ASP1* (*PEP4*) from Wolf PSORT software (187).

Gene	Wolf PSORT
MGG_09351 (*ASP1*)	extr: 23, mito: 1, cyto: 1
MGG_09246 (*SER1*)	extr: 27
PEP4 - YPL154C	extr: 18, golg: 4, E.R.: 2, vacu: 2

3.2.2 | The influence of putative protease deletion during infection

Spray inoculations were performed to examine the influence of protease deletion on pathogenicity of individual infections. We found that *ASP1* is required for full virulence due to reduced lesion sizes caused by Δ*asp1*, whereas *SER1* appears to be dispensable as no distinct virulence deficit was detected from infections by Δ*ser1* (Figure 3.3).

Figure 3.3

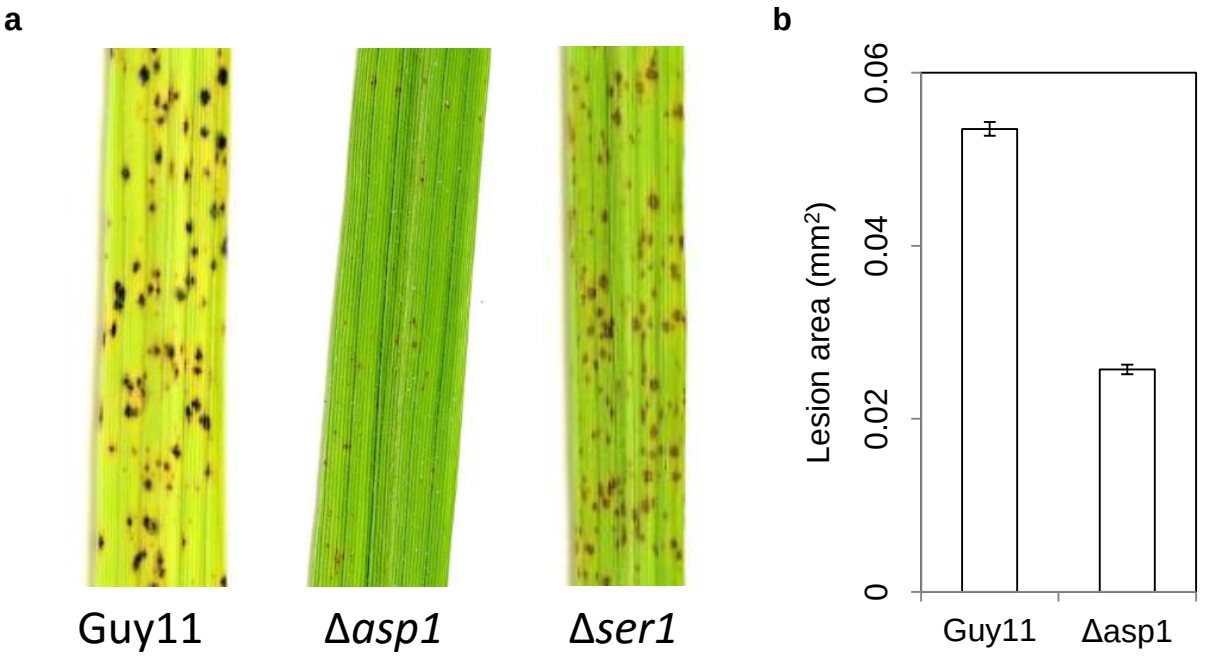

Figure 3.3 | Pathogenicity test of putative protease mutants by spray inoculation of susceptible rice cultivar CO39. a Δ*asp1* showed a virulence defect relative to the wild-type, whereas Δ*ser1* appeared dispensable for pathogenicity. **b** For Δ*asp1* this was quantified in terms of lesion area produced by image analysis using ImageJ software where we found that lesions were significantly smaller than the isogenic wild-type Guy11 ($p < 0.001$, $W = 12156433$ d.f. = 12143, Mann-Whitney U test).

Next, we performed leaf spot infections to examine if this virulence deficit translated into reduced pathogen population fitness during infection. Again, populations of *Δasp1* showed a reduction in fitness in terms of conidia production at the end of the infection cycle compared to the ancestral wild-type Guy11 strain (Figure 3.4). This is in contrast to the fungal plant pathogen *Botrytis cinerea* where deletion mutants of the major protease, also an aspartic proteinase, did not have any detected reduction in disease virulence (240).

Figure 3.4

a

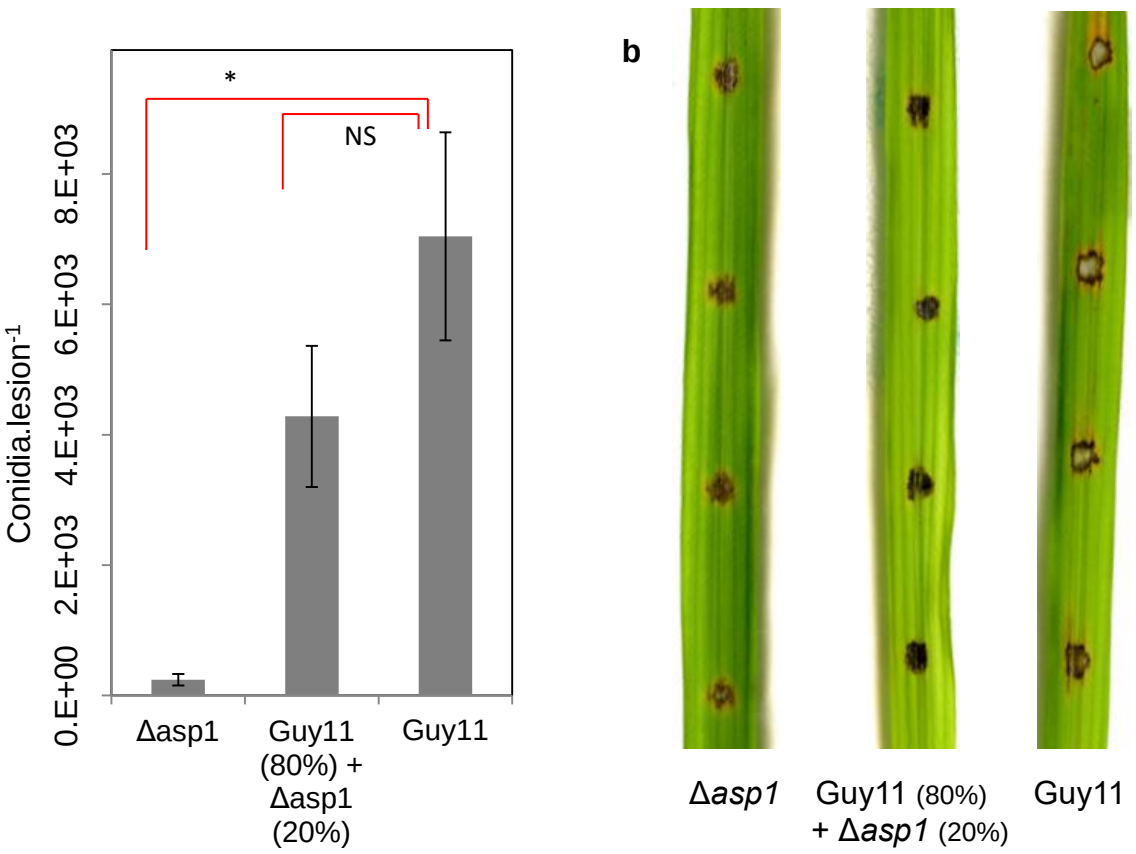

Figure 3.4 | Pathogen population fitness measured by conidia produced per lesion at the end of a disease cycle following leaf spot inoculation. a The numbers of conidia per lesion generated for infections with populations of pure Δ*asp1*, wild-type Guy11, and a mixed inoculation. Δ*asp1* produced significant fewer conidia per disease lesion than the wild-type Guy11 (*p < 0.001, W = 295, n = 44, d.f. = 86). A mixed infection with 80 % Guy11 + 20 % Δ*asp1* was not significantly different from populations purely of the wild-type virulence Guy11 strain (p = 0.5317, W = 603, d.f. = 72), (mean ± s.e.m.). **b** Representative images of lesions generated from which conidia were harvested 9 d.p.i., images captured at 7 d.p.i..

Based on the results we found with enhanced pathogen population fitness and virulence when a mixture of high virulence wild-type 'producer' strains were co-inoculated with a low virulence invertase 'non-producer' strain, we asked if a similar influence of mixed infections would be found with *Δasp1*. However, unlike with Δ*inv1*, coinfections with Δ*asp1* (at frequencies of 80% Guy11:20% Δ*asp1*) did not exhibit

enhanced pathogen population fitness in terms of conidia recovered per disease lesion (Figure 3.4)

3.2.3 | Examining the catabolic function of *ASP1*

We next sought to understand the cause behind the reduced virulence and fitness of Δ*asp1,* and why we did not find a similar trend with mixed strain infections as we had with Δ*inv1*. To do this we examined the function of *ASP1*. Firstly, we hypothesised that *ASP1* was involved in the metabolic breakdown of proteins. Δ*asp1* was assessed for growth defects *in vitro* on a range of complex nitrogen sources that require metabolic break down by protease. This was performed on MM-N or MM-NC (213), depending upon whether the wild-type Guy11 could form biomass in the absence of additional glucose. Nitrogen limited media was supplemented with different N-sources: + skimmed milk (fresh, 50% v/v), + BSA (1% w/v) & glucose (1% w/v), + gelatin (1% w/v). For the assay with skimmed milk, a zone of clearing was assessed as it is indicative of secreted protease activity (245). For *M. oryzae* secreted protease activity, a distinct ‘halo’ is not apparent around growing colonies as observed in other species such as *Aspergillus nidulans* (245). Therefore, colonies were inoculated onto filter paper discs on top of the media. Colonies could then be removed from the surface of the media to reveal zones of casein hydrolysis underneath (239). On all tested nitrogen sources, the Δ*asp1* mutant did not have a distinct growth deficiency compared to the isogenic wild-type strain. In case this resulted from the protein sources tested being of animal origin, the ability of the Δ*asp1* mutant to grow on rice-derived nutrient sources was tested. However, the Δ*asp1* mutant displayed no deficiency on either ground rice, soluble rice leaf proteins, or homogenised crude rice leaves (Figure 3.5).

Figure 3.5 | Testing for growth deficiencies of the Δ*asp1* mutant on complex nitrogen sources. a no distinct deficiencies were detected on a range of animal protein sources. MM-NC was used as a negative control. Growth on milk was assessed by forming a zone of clearing from where a growing colony of *M. oryzae* had been removed. **b** to test if this lack of deficiency resulted from the non-native source of protein, growth assays were performed on rice derived nutrient sources, again no distinct deficiency was detected.

Figure 3.5

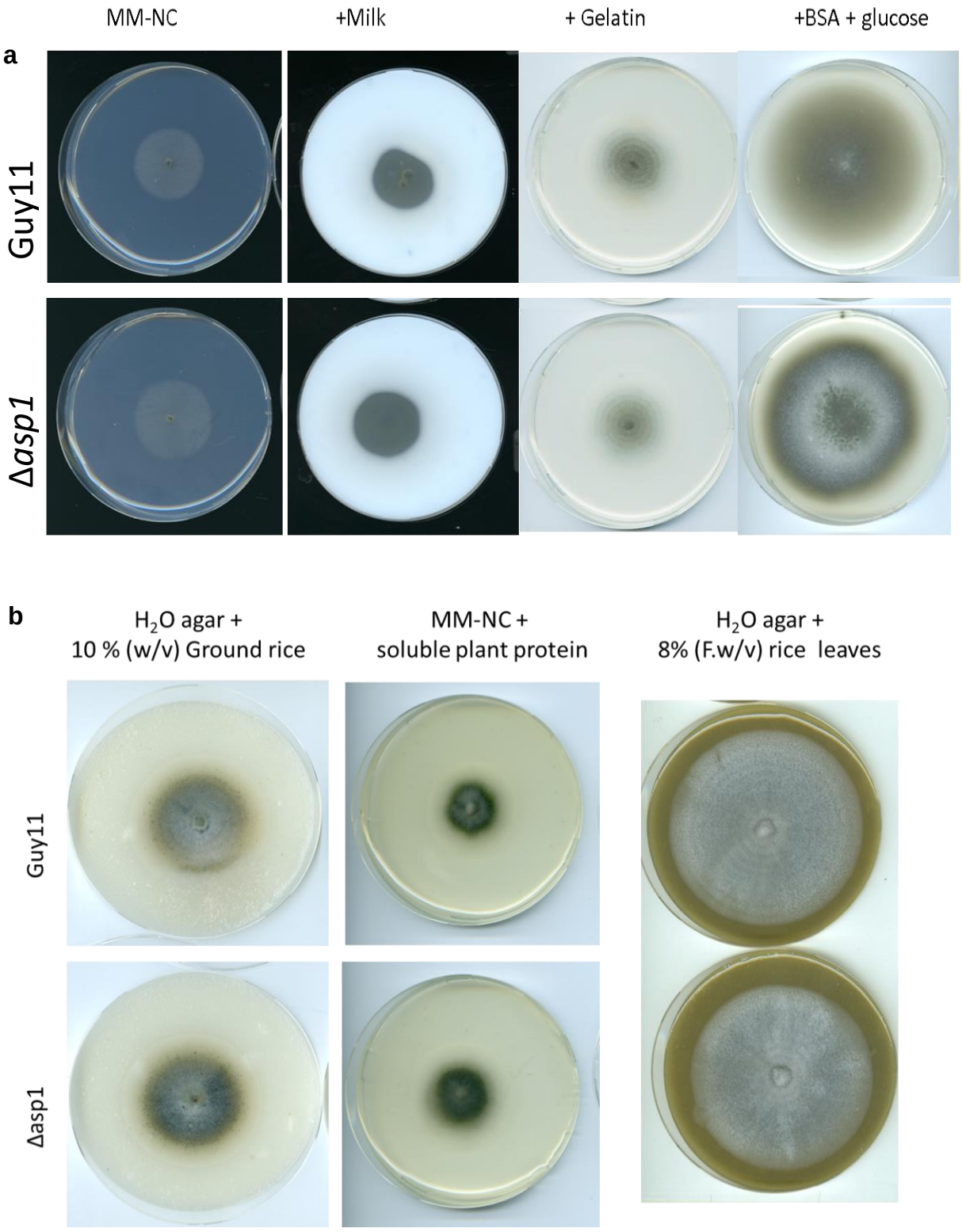
a
MM-NC
+Milk
+ Gelatin
+BSA + glucose
Guy11
Δasp1
b
H2O agar +
10 % (w/v) Ground rice
MM-NC +
soluble plant protein
H2O agar +
8% (F.w/v) rice leaves
Guy11
Δasp1

3.2.4 | The regulation of protease activity and testing for deficiencies in Δ*asp1*

Whether secreted protease activity was quantitatively reduced was examined by an enzymatic assay using the non-specific protease substrate azocasein (Sigma-Aldrich) based on a protocol described previously (246, 247). Initially the conditions under which wild-type *M. oryzae* protease expression is induced had to be determined. We found that protease expression was upregulated when the induction conditions lacked a carbon source, with expression highest in the absence of both a nitrogen and carbon source (Figure 3.6a).

Figure 3.6

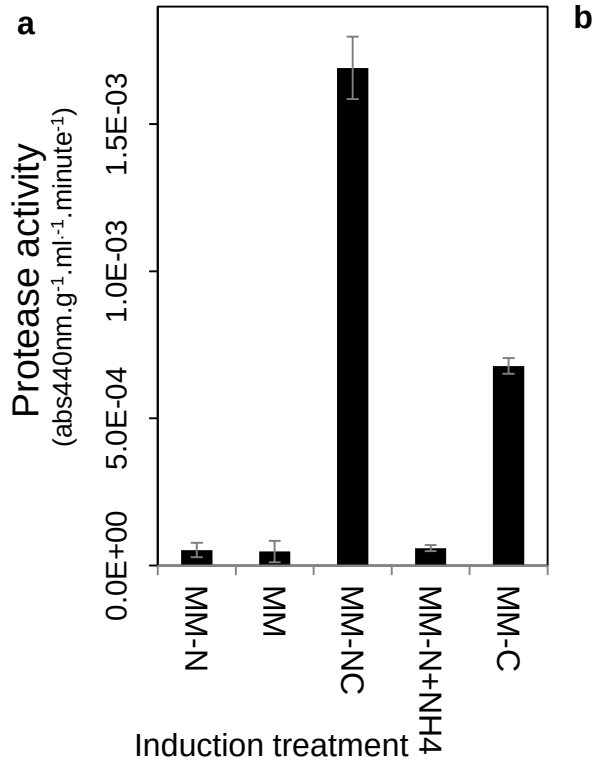

This image has been removed by the author of this thesis for copyright reasons.

Figure 3.6 | Regulation of protease activity in wild-type Guy11 *M. oryzae* in response to carbon and nitrogen environment. a Secreted protease activity was measured by enzymatic assay using a spectrophotometric stop reaction with the nonspecific protease substrate azocasein under a variety of induction conditions either lacking or supplemented with N or C sources. MM-NC lacks C and N, MM is supplemented with glucose and $NaNO_3$. MM-N and MM-C lack either glucose or $NaNO_3$. MM-N+NH_4 is supplemented with ammonium tartrate. Secreted activity was

measured on culture filtrate. Protease activity is repressed in the presence of glucose and upregulated in the absence of a nitrogen source. **b** model for control of carbon catabolite repression (CCR) and nitrogen metabolite repression (NMR) in response to glucose-6-phosphate (G6P) (taken from (167)). *NMR* genes are repressed by G6P sensing by *TPS1*. In agreement with results shown in **a**, this G6P sensing represses the utilisation of alternative N sources (Alt N), such as protease expression to exploit complex proteins, by repressing the GATA family transcriptional activator *NUT1*.

This finding of protease activity expression is in contrast to findings with *A. nidulans* where expression of extracellular protease was induced in media with glucose but lacking a nitrogen source (equivalent of MM-N). However in agreement, the addition of nitrogen sources such as NO_3^- repressed this expression (245, 246). This finding does support the model of combined CCR and NMR proposed for *M. oryzae* (Figure 3.6b) (167, 239). The Δ*asp1* mutant did not exhibit a significant reduction in the ability to liberate the azo dye from azocasein from its secreted enzyme fraction compared to Guy11 (Figure 3.7a).

Figure 3.7

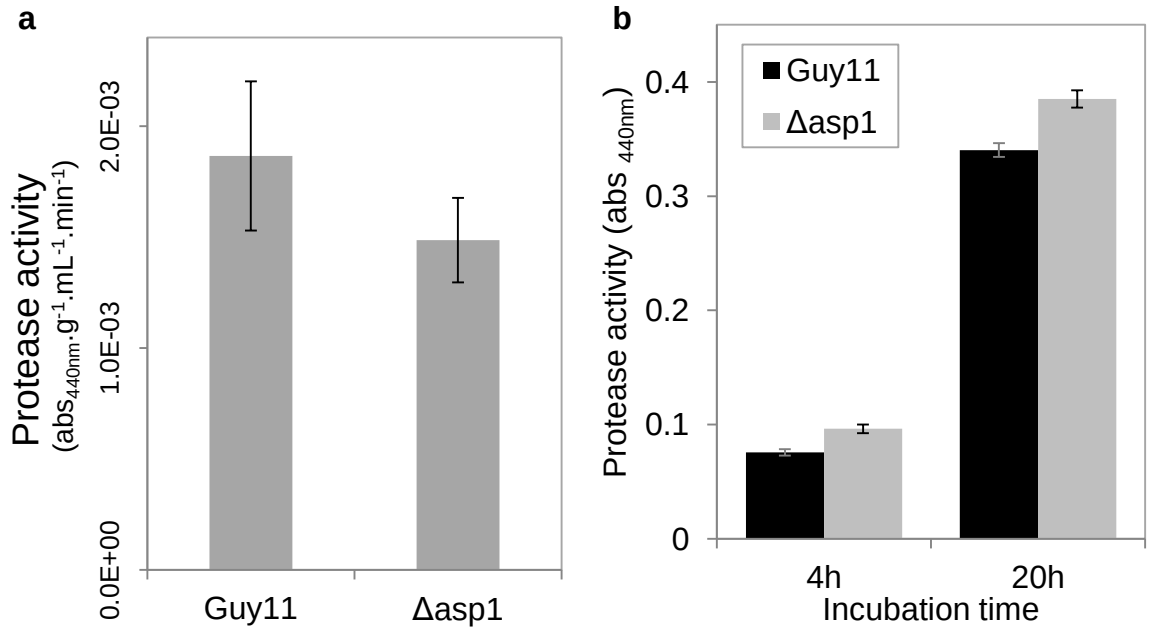

Figure 3.7 | Δ*asp1* did not show any reduced secreted (a) or intracellular (b) protease activity against azocasein compared to Guy11. Relative activity was measured by enzymatic assay using a spectrophotometric stop reaction on either culture filtrate (**a**) or homogenised mycelial biomass (**b**) after induction on MM-NC media. Protease activities are relative comparisons between strains with **a** being adjusted for time, biomass (dry weight) of fungi and volume of culture filtrate tested (mean ± s.e.m. n = 9); and **b** using absolute abs_{440nm} measurements of crude extract reactions with azocasein (mean ± s.e.m. n = 3) (see methods for details).

3.2.5 | The subcellular localisation of regulation of *ASP1*

In order to observe the subcellular localisation and expression of the *ASP1* gene, a C-terminal ASP1-mCherry fusion vector was constructed and transformed into the Δ*asp1* mutant generating strain *ASP1:mCherry*. This enabled both the sub-cellular localisation and regulation of ASP1-mCherry to be determined by epifluorescent microscopy. Expression was observed intracellularly during appressorium formation when conidia were inoculated onto hydrophobic *in vitro* surfaces (Figure 3.8a) as well as *in planta* when visualised infecting rice epidermal cells (Figure 3.8b). Expression was localised in punctate structures earlier in appressorium maturation (8 h) which appear to develop into larger elliptical structures which seem to arrange around the toroidal F-actin network formed during appressorium maturation (Figure 3.8a) (248). Substantial expression was not observed in primary invasive hyphae 48 h.p.i. (Figure 3.8b). This expression pattern in smaller punctate structures that develop into larger elliptical structures within the appressorium bears similarities to the localisation of the vacuole associated proteins *Vac8* (249) and an NADPH oxidase (*Nox2*) (250).

Figure 3.8 | Expression of ASP1-mCherry in the Δ*asp1* mutant during appressorium formation *in vitro* (a) and during rice infection (b). An ASP1-mCherry protein fusion expressed under control of the native promoter was constructed and transformed into the Δ*asp1* mutant. Expression and localisation were monitored by epifluorescent microscopy. **a** During appressorium formation on hydrophobic glass cover slips. After 8 h, ASP1-mCherry expression was observed in small punctate structures in the appressorium. Later (16-24 h), this was observed in larger elliptical structures. **b** Expression during infection was imaged by live cell imaging of leaf sheath epidermal cells. Expression was observed within similar structures in the appressorium up to 48 h.p.i., but not in primary invasive hyphae. Scale bar = 10 μm. DIC – mCherry – merged.

Figure 3.8

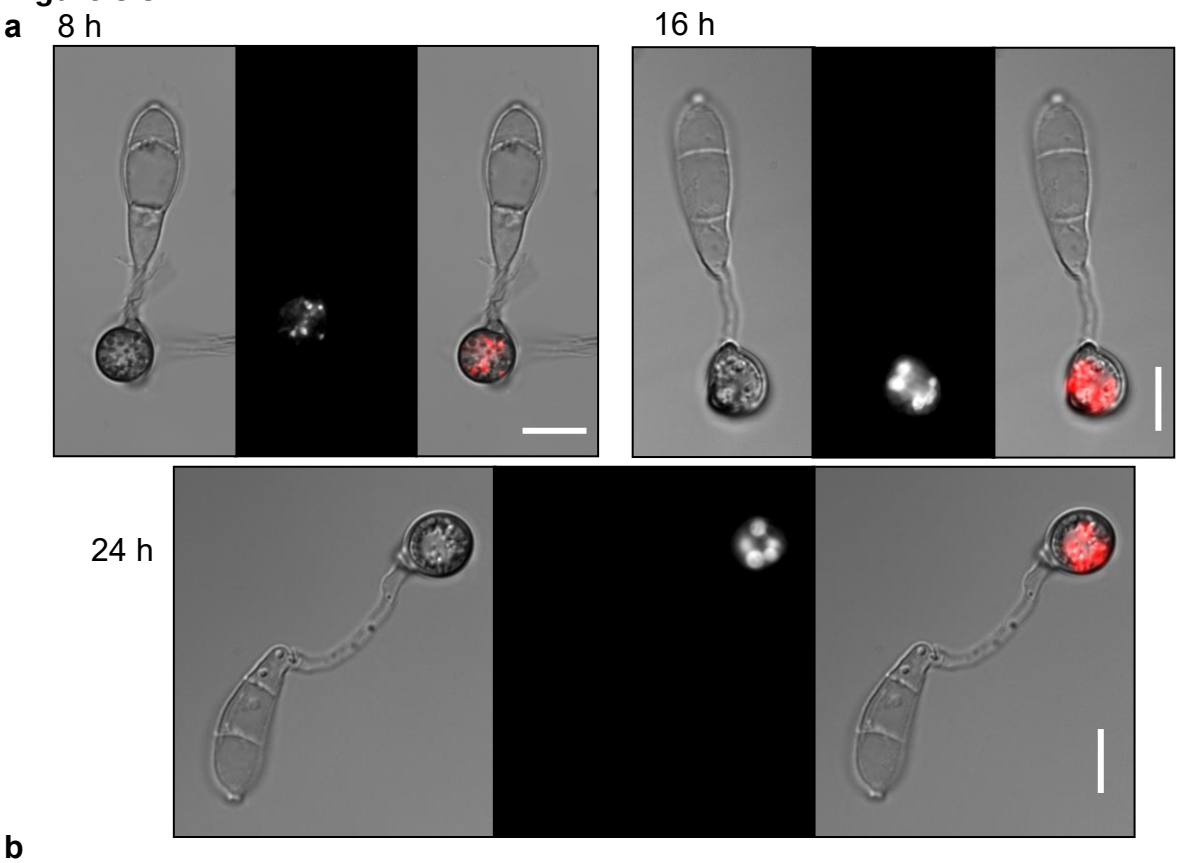

To confirm the sub-cellular structures in which the expression is located, we inoculated *ASP1:mCherry* on hydrophobic *in vitro* surfaces in the presence of CellTracker Blue CMAC (7-amino-4-chloromethylcoumarin; Invitrogen/Molecular Probes), which has been shown to specifically stains the acidic vacuolar compartment in the plant pathogenic fungus *U. maydis* (251). We found that the *ASP1* signal (mCherry) and the CMAC signal (DAPI) co-localised, suggesting that *ASP1* functions within the vacuole (Figure 3.9).

Figure 3.9

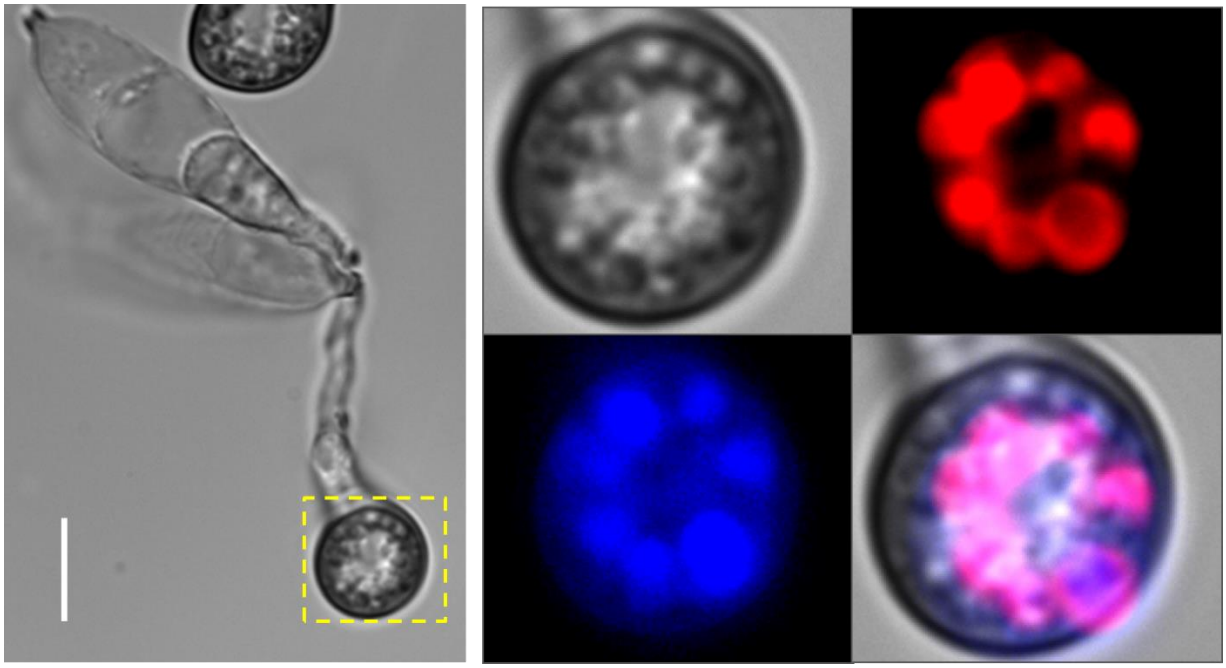

Figure 3.9 | ASP1 is localised within vacuoles of the appressorium. *ASP1:mCherry* conidia were inoculated on hydrophobic glass cover slips in the presence of CellTracker blue (CMAC) which specifically stains the vacuole. Images captured 24 h.p.i. show DIC (left) with magnified region of appressorium indicated (dashed lines). Magnified images show DIC (top left), mCherry (top right), DAPI (bottom left) and merged (bottom right). ASP1-mCherry co-localises with DAPI (magenta in merged image) indicating that ASP1 is located in the vacuole. Scale bar = 10 μm.

These results suggest that *ASP1* functions intracellularly, rather than extracellularly, in contrast to the bioinformatic predictions (Table 3.1 and Figure 3.2). Therefore, enzymatic assays were performed on the intracellular and cell wall bound fraction of Δ*asp1* cultures. However, again no reduction in protease activity was identified (Figure 3.7b). In case this resulted from low expression levels *in vitro*, an overexpression vector was constructed in the yeast expression vector GPDp:NEV-E (Figure 3.10a) as used and described previously in Chapter 1 for expression of *M. oryzae* invertase *INV1* in *S. cerevisiae* (Figure 1.7). Despite this vector having previously been shown to drive the expression of heterologous proteins, no increase in protease activity was detected (Figure 3.10b).

Figure 3.10

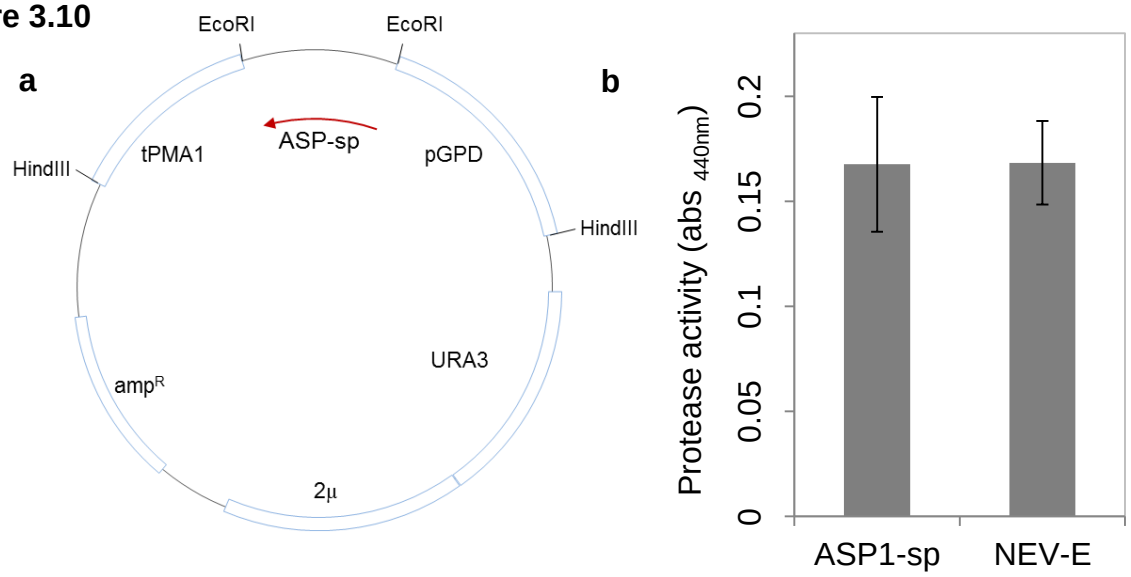

Figure 3.10 | Overexpression of *ASP1* in the yeast vector GPD$_p$:NEV-E shows no increased protease activity. The *ASP1* ORF with deleted signal-peptide (*ASP-sp*) was cloned into the GPD$_p$:NEV-E vector as an *EcoRI/EcoRI* fragment (**a)** and transformed in *S. cerevisiae* (DBY1034). **b** Protease activity of the *ASP1-sp* expressing strain showed no increase against the non-specific substrate azocasein. The empty vector was used as a negative control (NEV-E). Protease activity is relative activity displayed as abs. values from spectrophotometric assay (mean ± s.e.m., n = 9).

The protease enzyme assays collectively suggests that ASP1 does not have protease activity against azocasein. This may partly be caused by the protein being synthesised as an inactive zymogen as reported for the *S. cerevisiae* homologue *PEP4* (252, 253). Therefore, expression of *ASP1* may not be detected as protease activity in the absence of an additional activating protein from *M. oryzae.* Secondly this may also result from the absence of the native 3' UTR, which can have an important role in gene expression by influencing mRNA stability, export and translation efficiency (254). In addition, because of the downstream application, the protein extraction method from *S. cerevisiae* was performed in the absence of a protease inhibitor so the ASP1 protein synthesised may have been degraded and inactivated.

3.2.6 | Δ*asp1* for use in virulence reduction strategies by competitive exclusion

One reason that we do not observe synergy in pathogen fitness and virulence between the wild-type and the low virulence Δ*asp1* strain is because *ASP1* appears to function intracellularly, and therefore does not represent a public-good cooperative trait. This means that the Δ*asp1* mutant is unable to 'cheat' by energetically exploiting the wild-type producer and have the potential to alleviate a similar rate-efficiency trade-off as found with sucrose metabolism in Chapter 2. The sub-cellular localisation of *ASP1* also suggests that Δ*asp1* would not be a viable strain to implement for disease management by competitive exclusion and 'Hamiltonian medicine', as tested and implemented with less virulent strains of *C. difficile* (45)*, A. flavus* (47-51), *S. aureus* (87), and *P. auruginosa* (112). To confirm this with the Δ*asp1* mutant, mixed strain infections with the wild-type Guy11 were performed to assess the relative fitness of Δ*asp1* during disease. In contrast to the Δ*inv1* mutant (*v*

>1), the Δ*asp1* mutant was at a selective disadvantage (*v* < 1) relative to the wild-type in mixed infections (Figure 3.11). This suggests that the introduction of the less virulent Δ*asp1* strain into infections of the highly virulent wild-type strain, or natural gene disruptions or deletions, would result in the *ASP1* deficient strain being competitively excluded from the population. This means that any reduced pathogen population fitness or virulence would not be expected to persist over many generations of the polycyclic disease.

Figure 3.11

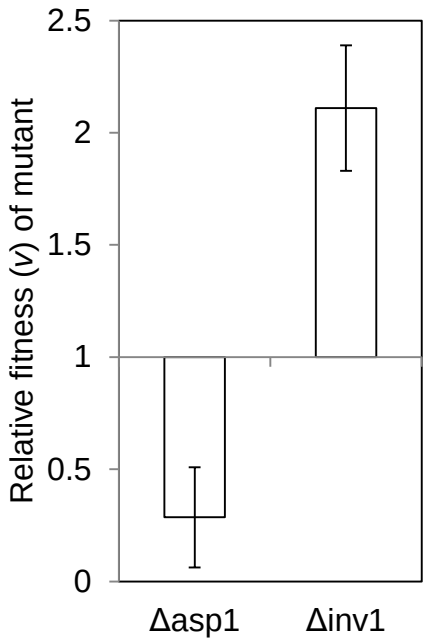

Figure 3.11 | The Δ*asp1* mutant is at a selective disadvantage relative to the wild-type Guy11 strain during mixed infections. Mixed infections of the Δ*asp1* or Δ*inv1* mutants were performed with the wild-type Guy11 strain and the relative fitness (*v* (204)) of strains was established from the number of conidia produced by each strain at the end of the disease cycle (9 d.p.i.). Strains were distinguished by a fluorescent tag (RFP or GFP) by epifluorescent microscopy. Infections were initiated with 10^3 conidia per infection with 80% Guy11 and 20% mutant strain. In contrast to the Δ*inv1* mutant (*v* >1), the Δ*asp1* mutant was at a selective disadvantage (*v* < 1) compared to Guy11.

3.2.7 | The role of *ASP1* within vacuoles of the appressorium

Having identified that *ASP1* leads to a reduction in disease virulence, we asked what function it has that leads to this result. Since *ASP1* localises to the vacuole, fungal gene homologues were identified that showed a similar localisation to help identify the function of *ASP1*. When assessing the yeast genome (*S. cerevisiase* S288c) the most significant alignment was found to be proteinase A (PrA), encoded by the *PEP4* gene (Accession NP_015171.1; e-value = 2e-25, identities = 28 %). *PEP4*, like *ASP1*, has been found to be a vacuolar enzyme. It is involved in the maturation and activation of other vacuolar hydrolases. Furthermore, it is encoded as an inactive preproenzyme that requires cleavage by a secondary protease (PrB) (252, 253). Therefore, if *ASP1* does share functional similarities with *PEP4,* which we have identified in terms of sub-cellular localisation, it may provide reasons as to why the nutritional and enzymatic assays performed with *M. oryzae* have not identified the reasons behind the pathogenicity deficiencies of the Δ*asp1* mutant. This is based on the evidence that it may not perform a catabolic function on nutrient resources, and overexpression in *S. cerevisiae* may not permit any species-specific activation of zymogens leading to a lack of detected protease activity. Notably, when the encoding sequence of *PEP4* was assessed using the subcellular localisation software WoLF PSORT (187), like *ASP1*, it was also predicted to be primarily localised extracellularly (Table 3.1), contrary to the localisation reported experimentally (255).

Another function of the *S. cerevisiae PEP4* gene is during the degradation of proteins during nitrogen starvation, and autophagy (256). The punctate *ASP1:mCherry* signal that was observed in developing appressoria bears similarities to fluorescence signal localised to autophagosomes by the *M. oryzae* gene *ATG8* (146). Therefore, the *M. oryzae* strains i) Guy11 expressing GFP-ATG8 - which labels autophagosomes and so is a marker for autophagy – and ii) Δ*atg8* - an autophagy deficient mutant (154) - were transformed with the *ASP1:mCherry* gene fusion (Figure 3.12). Early during appressorium maturation (8 h), the ASP1-mCherry signal was detected in the vicinity of autophagosomes in the appressorium (yellow asterisk). However, as the size of the vacuoles that contained the ASP1-mCherry signal increased by 24 h, there was an absence of signal from autophagosomes in the appressorium (yellow asterisk). This may indicate that autophagosomes are being degraded within the vacuoles where the ASP1-mCherry protein acts. *ASP1* may represent a protease which directly degrades protein portions of the autophagosomes or alternatively, analogous to the yeast homologue *PEP4, ASP1* may be involved in the proteolytic activation of other intravacuolar proteases (257). In the autophagy deficient mutant Δ*atg8*, mis-localisation of the ASP1-mCherry signal was detected at 8 h where the protein localised to the cortex of the appressorium. By 24 h the characteristic expression of ASP1-mCherry within vacuoles of the appressorium was not detected in the Δ*atg8* mutant. The aberrant expression in Δ*atg8* may be interpreted to suggest that the expression of *ASP1* is not induced in the absence of autophagy because it may function directly or indirectly in the breakdown of autophagomsomes. Alternatively, in the absence of autophagy, the fungus may be unable to metabolically fuel the synthesis of proteases given the absence of exogenous nutrients.

Figure 3.12 | Expression of ASP1-mCherry fusion construct in deletion mutant Δ*asp1*, the autophagosome labelled *GFP:ATG8* strain and the autophagy deficient mutant Δ*atg8.* Strains were transformed to express *ASP1:mCherry*. Conidia were inoculated onto glass cover slips and imaged after 8 h (Left) and 24 h (Right). Epifluorescent micrographs showing DIC – GFP (for *GFP:ATG8* only) – mCherry – merged panels. Localisation of ASP1-mCherry is in the appressorium within small punctate structures after 8 h, which merge into larger elliptical structures by 24 h. As we have shown in Figure 3.9 these represent vacuoles. Localisation of the GFP-ATG8 protein fusion show autophagosomes are present in the appressorium at 8 h (*), yet absent by 24h when the ASP1-mCherry signal within vacuoles is stronger. ASP1-mCherry appears mislocalised in the autophagy deficient mutant Δ*atg8* after 8 h when signal is detected at the cortex of the appressorium. By 24 h, ASP1-mCherry signal is absent in the Δ*atg8* mutant.

Figure 3.12

Δasp1

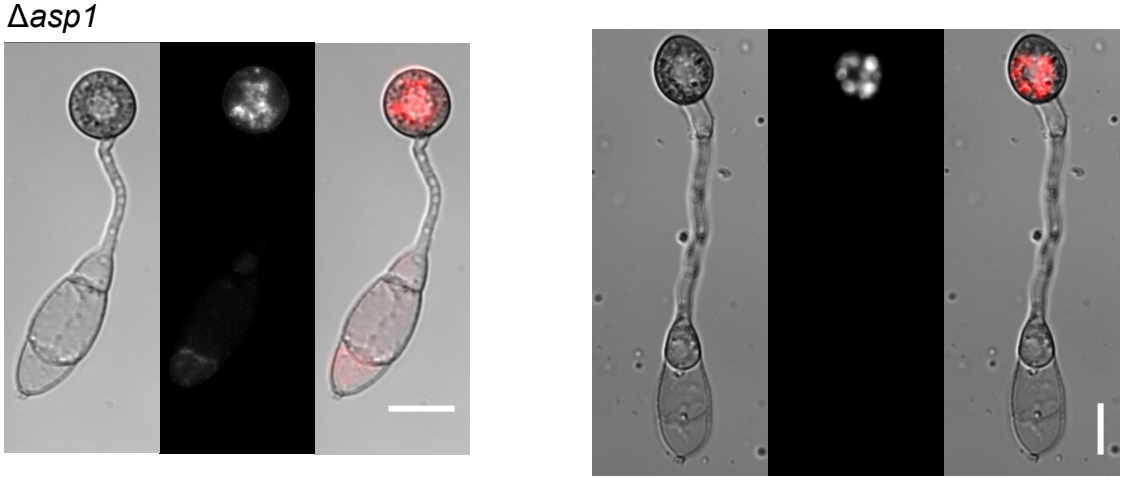

GFP:ATG8

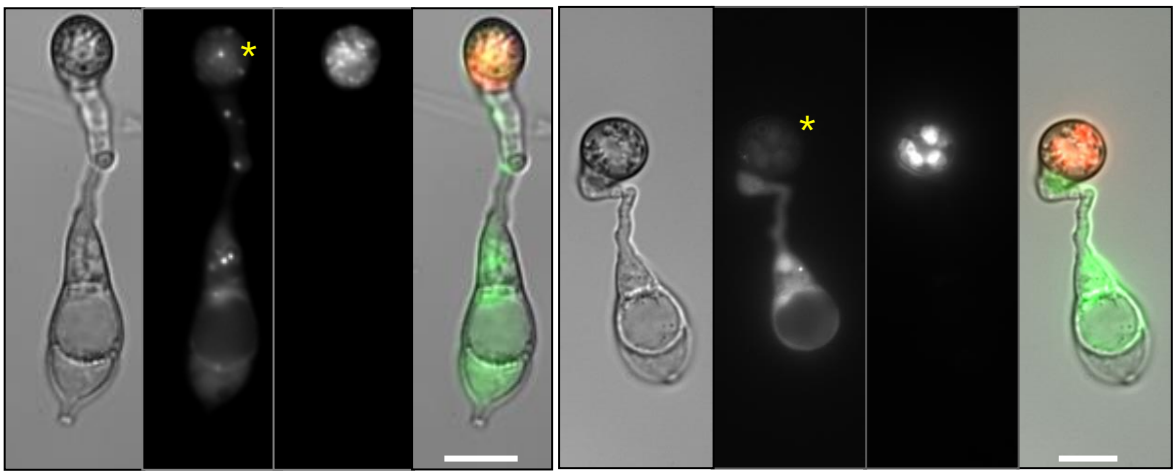

Δatg8

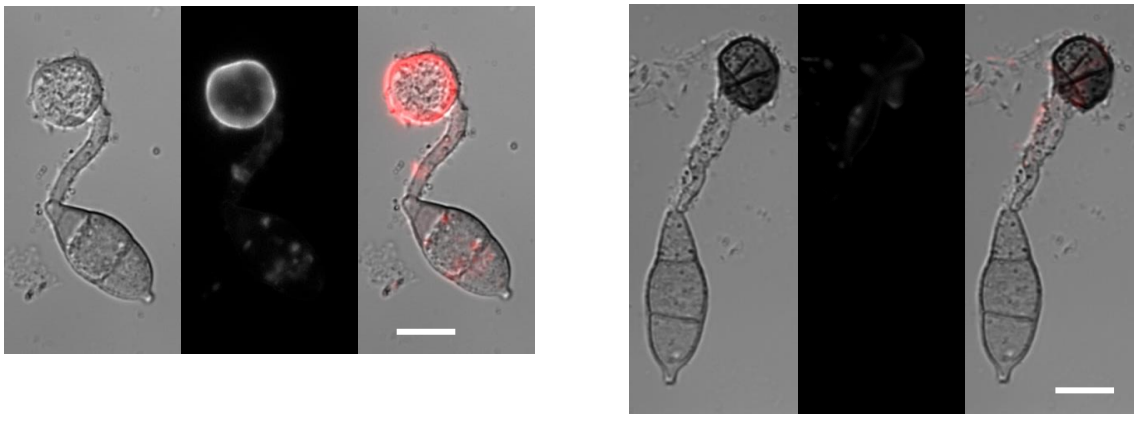

3.2.8 | Identifying the pathogenicity arrest phenotype of Δ*asp1*

Although we had found that deletion of *ASP1* results in reduced pathogenicity and virulence, we asked what precise phase of the disease cycle had been affected and when the 'arrested' phenotype occured. Based on RNA-seq data (Figure 3.13 ; M. Oses-Ruiz, X. Yan, D.M. Soanes and N.J.Talbot unpublished), *ASP1* is highly upregulated during appressorium formation (Figure 3.13a) and the earlier stages of infection, compared to conidia, and declines later (Figure 3.13b). The *in vitro* and earlier expression during infection is consistent with the imaging data obtained from the *ASP1:mCherry* strain where a signal was detectable in appressoria up to 48 h.p.i. (Figure 3.8). *ASP1* expression appears to be regulated by the *PMK1* MAP kinase signalling pathway (152) but not substantially by the downstream transcription factor *MST12* (150, 151).

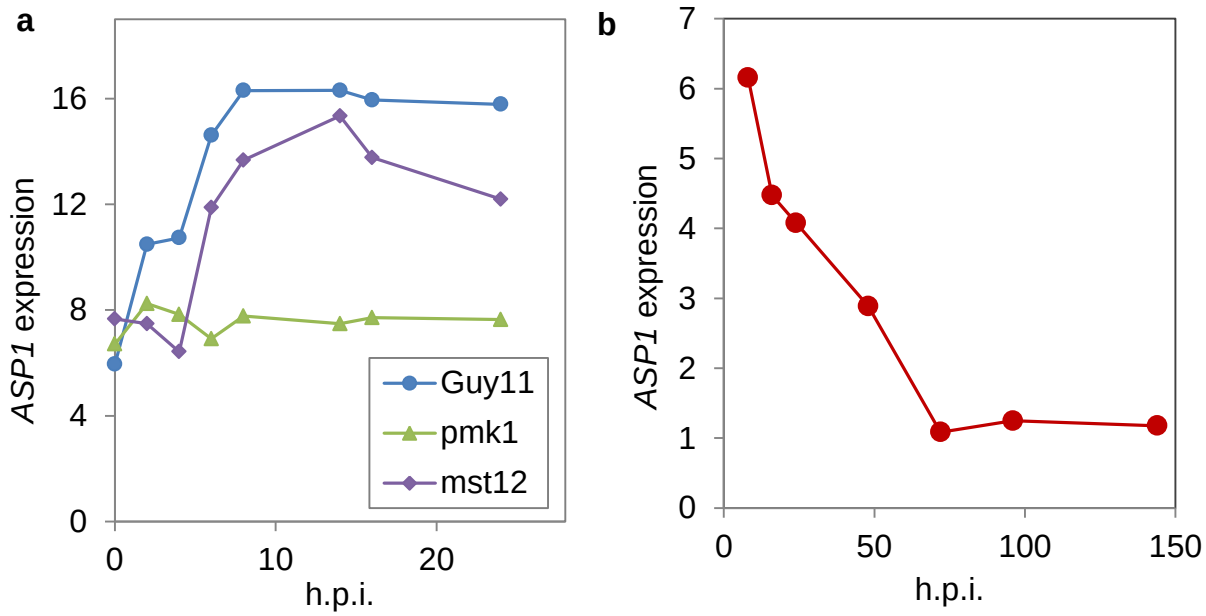

Figure 3.13 | Expression profile of *ASP1* during *in vitro* appressorium formation (a) and during rice leaf infection (b). Data acquired by RNA-seq by M. Oses-Ruiz, X. Yan, D.M. Soanes & N.J. Talbot unpublished. **a** Expression of *ASP1* in wild-type Guy11, the mutants of *pmk1* (MAP Kinase) and *mst12* (a transcription factor that is regulated by *PMK1*). Levels of expression are relative expression levels (log_2 base mean expression). **b** Levels of expression are shown as moderated log_2 ratio of transcript abundance compared to conidia (0 h.p.i.).

To investigate how deletion of *ASP1* affected the infection related phenotype of *M. oryzae,* firstly the ability of conidia of the Δ*asp1* mutant to successfully germinate and form appressoria was assessed. Relative to the isogenic wild-type strain, the Δ*asp1* mutant showed no reduced ability to form appressoria after 24 h *in vitro* (Figure 3.14a). To examine if these appressoria were functional, they were tested for the ability to penetrate yielding plant cuticles. Again they had no detectable reduction in the frequency at which they penetrated into the primary plant cells (Figure 3.14b). Using rice leaf sheath inoculations, the Δ*asp1* mutant was tested for its ability to invade beyond the primary cell. We found that the Δ*asp1* mutant had a significant ($p < 0.001$, $W = 13410$, Mann-Whitney U test), albeit small, reduction in its invasion rate after 40 h (Figure 3.14c).

Figure 3.14

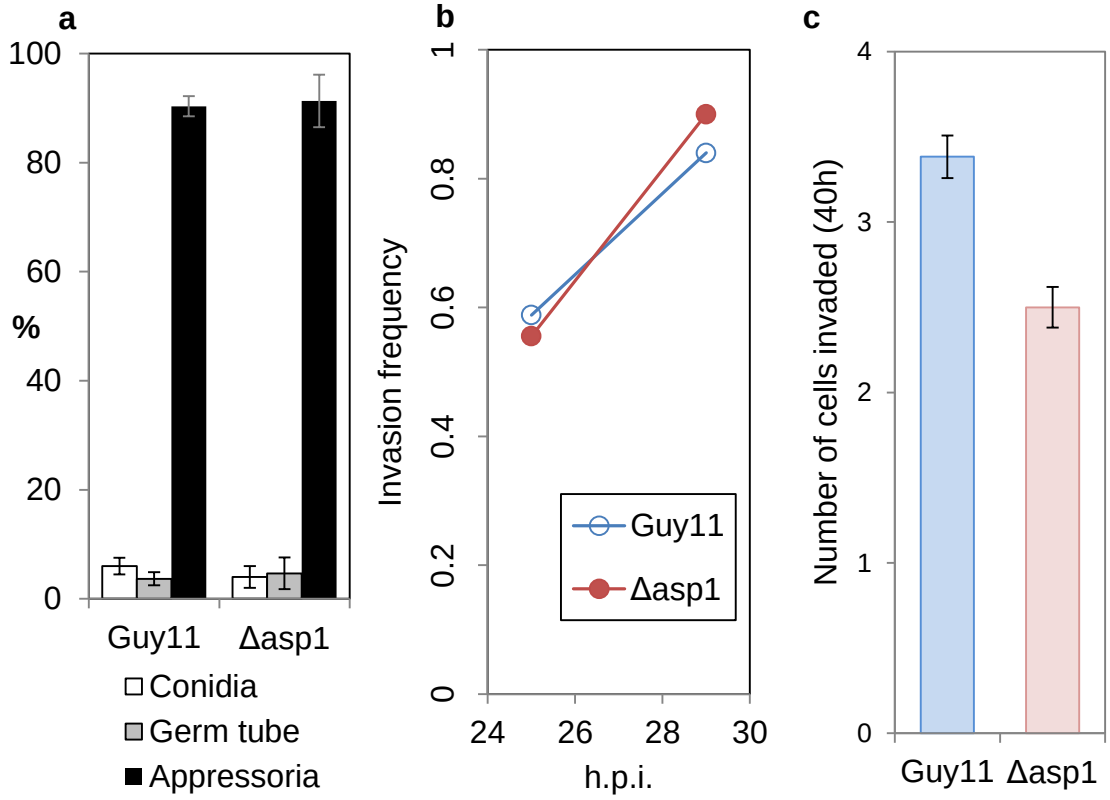

Figure 3.14 | The pathogenicity defect of the Δ*asp1* is post penetration. a The Δ*asp1* mutant is proficient in appressoria formation (> 75 % (196)), measured *in vitro*

on hydrophobic glass cover slips (mean ± s.e.m., n = 300) **b** Appressoria formed by the Δ*asp1* mutant can successfully penetrate plant cells (onion epidermis) at a comparable rate to Guy11 (invasion frequency is the frequency of appressoria formed that had successfully invaded the primary plant cell, n > 65). **c** The Δ*asp1* mutant had a decreased rate of invasion of rice leaf epidermal cells ($p < 0.001$, $W = 13410$, Mann-Whitney U test, n > 250). Results are pooled from three replicated experiments.

Together with the data revealing reduced disease lesion size and conidiation at the end of the disease cycle, these results indicate that the deficiency shown by the Δ*asp1* mutant occurs at some point after the fungus has entered the host. Given the similarities to the yeast gene *PEP4* and the experimental data developed in *M. oryzae*, this may result from reduced intracellular protein modification and nitrogen recycling by the pathogen. However, more experimental examination, such as using a yeast-2-hybrid screen to identify protein interactions, is needed to confirm the precise function of *ASP1*, but this is beyond the scope of this present thesis.

3.3 | Discussion

Our study set out to test the generality of the synergistic effect of mixed strain infections with a highly virulent wild-type strain and low virulence strain, which was deficient in a secreted metabolic enzyme, as we observed with invertase in Chapter 2. Given the finding with invertase and carbon metabolism, we targeted a gene that was involved in the metabolism of another abundant and vital nutrient resource; that of nitrogen metabolism. Based on RNA-seq data during rice infection, we identified an upregulated putative protease gene (Figure 3.13) that was predicted to act extracelluarly (Figure 3.2 and Table 3.1). This predicted secretion meant that these gene products had potential to act as a public-good trait, which could be open to exploitation by the deletion mutant. We found that deletion of the putative protease

ASP1 resulted in a pathogenicity defect in terms of virulence and pathogen fitness at the end of the disease cycle (Figure 3.3 and 3.4). However, during mixed strain infection with the wild-type, no synergistic effect between strains was detected (Figure 3.4). We also found that the protein of *ASP1* is not an exploitable social trait because the deletion mutant was unable to gain a selective advantage, during mixed-genotype infections, over a strain that produced it (Figure 3.11). From the perspective of virulence reduction strategies by competitive exclusion, this result means that it would not be viable to utilise this less virulent strain because it would soon be excluded from the population. When examining the reasons behind this finding, we identified that *ASP1* is intracellular and is located in vacuoles of the appressorium (Figure 3.9). Here, it may play a role in the degradation of proteins during autophagy, or in the activation of other proteolytic enzymes in the vacuole (Figure 3.12) (257). To examine this further, it would be interesting to see if autophagosomes accumulated in the vacuoles of the *Δasp1* mutant during appressorium formation due to an inability to degrade them. This could be achieved by introducing an RFP-ATG8 fusion protein into the Δ*asp1* mutant, but unfortunately this was beyond the scope of this current thesis. Enzymatic and growth assays did not reveal the cause behind the reduced pathogenicity of the Δ*asp1* mutant (Figure 3.5, 3.7 and 3.10), but do suggest that *ASP1* does not function in the direct catabolism of protein sources during vegetative growth. Instead, by visualising expression using an RFP fusion, *ASP1* appears to perform specific functions during appressorium formation and plant penetration (Figure 3.8). Altogether, these results reveal that no synergy was found in the mixed strain infections because the pathogenicity defect caused by the deletion of *ASP1* resulted from the inability to perform a private, non-social, function. Therefore, no social interactions were altered,

which are predicted to be crucial for the unexpected result that was observed with invertase in Chapter 2.

3.4 | Methods

3.4.1 | Generating protease deletion mutants

Protease genes were targeted using a PCR-based split-marker gene deletion technique (145, 146). The genes MGG_09351 (*ASP1*) and MGG_09246 (*SER1*) were targeted as putative secreted protease genes that were predicted to be important during infection. This was based upon protein family predictions and gene expression that had been found to be upregulated during rice plant infections and appressorium formation by RNA-seq (Figure 3.13) (M. Oses-Ruiz, X. Yan, D.M. Soanes and N.J.Talbot, unpublished), which possessed a signal-peptide sequence (Table 3.1 and Figure 3.2). LFs were amplified using primers 50.1 and M13F, RFs with 30.1 & M13R (Table 3.2).

Table 3.2 | Primers used for targeted gene deletion of putative protease genes from *M. oryzae.* Underlined regions indicate complementary regions for fusion PCR.

Primer name	Nucleotide sequence (5' - 3')
MGG_09246_50.1	AAGACTTTTTTTTTTCAACGACAC
MGG_09246_M13F	GTCGTGACTGGGAAAACCCTGGCGGATTAAGTTGTTGATGTTTTTGAG
MGG_09246_30.1	GTACTTAGGTGCATAGGAGAAATC
MGG_09246_M13R	TCCTGTGTGAAATTGTTATCCGCTGCTTTTTCATAACTGTCTTCATTT
MGG_09351_50.1	GCGCATGGTAGTAGTAGTAGTAAA
MGG_09351_M13F	GTCGTGACTGGGAAAACCCTGGCGAGGTACAACAAGTTGATGATAGAC
MGG_09351_30.1	AAAGATCTTGTACGAGTAGAGGGT
MGG_09351_M13R	TCCTGTGTGAAATTGTTATCCGCTAGAGTCTTGTTATTTTTTTTGGTG

As with the invertase deletion, transformants that exhibited sulfonylurea resistance were assessed by DIG-labelled Southern blot analysis and evaluated for fragment size differentiation following restriction endonuclease digestion of gDNA. For *ASP1* (MGG_09351), a DIG-labelled probe was constructed with primers MGG_09351_50.1 and MGG_09351_M13R (LF) and gDNA was fragmented with *DraIII* resulting in a wild-type band of 14 kb and positive gene replacement of 5 kb as found with transformant number 14. For *SER1* (MGG_09246) the DIG-labelled probe was constructed with primers MGG_09246_50.1 and MGG_09246_M13R (LF) and gDNA was fragmented with *NcoI* resulting in a wild-type band of 0.8 kb and positive gene replacement of 1.8 kb, with both strains possessing an additional band of 2.4 kb. Transformant number 2 was found to have a positive gene deletion (Figure 3.1).

3.4.2 | Growth assays of protease mutants

Plate assays to test for protease catabolic deficiencies were performed on a variety of protein sources. Media was MM-N or MM-NC (213), depending upon whether the wild-type Guy11 could form biomass in the absence of additional glucose. Nitrogen limited media was supplemented with different protein sources: + skimmed milk (fresh, 50% v/v), + BSA (1% w/v) & glucose (1% w/v), + gelatin (1% w/v). For the rice derived protein sources: ground rice (10% w/v) or homogenised rice leaves (8 % f.w/v ground in Liquid N_2) were added to H_2O agar (15 $g.L^{-1}$). Soluble rice leaf proteins were extracted by vortexing homogenised rice leaves in protein extraction buffer. Protein extraction buffer consisted of 1% (w/v) DMSO, 1 mM EDTA, 50 mM Tris/HCl (pH 8), 100mM NaCl and 1mM Dithiothreitol. Trichloroacetic acid was then added to a final concentration of 10% (w/v) to precipitate the protein content. The mixture was then subjected to centrifugation at 4000 r.p.m. for 10 min and the

supernatant discarded. The protein pellet was resuspended in sdH_2O, filter sterilised and added to MM-N.

3.4.3 | Enzymatic assay of secreted protease activity

Extracellular protease activity was assessed with the non-specific protease substrate azocasein (Sigma-Aldrich) based on a protocol described previously (246, 247). *M. oryzae* mycelial biomass was established in CM for 48 h, as described in methods. Mycelium was washed with sdH_2O and 1g wet weight was inoculated into 150 mL of the various induction treatments and incubated at 24 °C with 125 r.p.m. for 22 h. Mycelium was harvested at this point and dry weights established. Extracellular protease activities of culture media were assessed by combining 2 mL media with 1 mL azocasein (0.4% w/v in 100mM sodium orthophosphate buffer, pH 7.2) which was incubated at 37 °C for 4 h. The reaction was stopped by adding 2.5 mL trichloroacetic acid (10 % w/v) and insoluble material was spun down in a centrifuge at 4000 x *g* for 10 min. Absorbance of the supernatant was measured at 440 nm, blanked against uninoculated induction media, with protease activity expressed as abs_{440nm} per gram of dry weight fungal mycelium per mL, per min. Induction media consisted of MM (213), MM-N contains no sodium nitrate and MM-C has glucose omitted, MM-NC has both missing. MM-N+NH_4 is MM-N with 10 mM ammonium tartrate. On the basis of the data from the initial experiment to establish under which induction condition secreted protease activity was induced, to compare the relative protease activity of different strains MM-NC was used.

To test for internal protease activity of *M. oryzae,* the same procedure for culture preparation were used as for external activity, except for the mycelial biomass was extracted from the induction medium (MM-NC) after 5 h, washed with sdH_2O, snap

frozen in liquid N_2 and lypholised. Freeze-dried samples were then homogenized in liquid N_2 using a pestle and mortar to disrupt cell structure. Protein extraction buffer (2 mL) was added to the fine-powdered mycelium and the mixture was vortexed. Reaction tubes were subjected to centrifugation for 10 min at 4°C at 13,000 r.p.m. and the supernatant (1 mL) was used to test for internal protease activity as described above for the spent culture media to test for external activity.

3.4.4 | Constructing an *ASP1* overexpression vector

To enhance expression of the *ASP1* gene, the ORF was cloned into the overexpression yeast vector NEV-E (200) that we had previously modified with the GPD promoter and shown drives strong expression of heterologous genes of *M. oryzae* in *S. cerevisiae* with the invertase gene *INV1* (Figure 1.7b). Assessment of the coding sequence revealed a predicted 77 bp intron. Therefore, PCR amplification of the gene had to be performed on cDNA. As *ASP1* has been shown to show expression during appressorium formation (M. Oses Ruiz, X. Yan, D.M. Soanes and N.J.Talbot unpublished), cDNA was synthesised from RNA extracted from appressorium assays on *in vitro* hydrophobic surfaces after 14 h. This RNA was kindly provided by Dr. M. Oses Ruiz. cDNA was synthsized using an AffinityScript cDNA synthesis kit (Agilent Technologies) according to the manufacturer's instructions. The first strand cDNA synthesis reaction was performed by combining 10 µL of first-strand master mix (2x) with 3 µL of oligo(dT) primers (0.1 µg/ µL). To this, 1 µL of AffinityScript RT/RNase Block enzyme mixture was added with < 3 µg of RNA sample to a total of 20 µL. This reaction was mixed and incubated at 25 °C for 5 min to allow primer annealing. Reactions were then shifted to 42 °C for 15 min to allow cDNA synthesis, and subsequently terminated by 95 °C for 5 min. First-strand cDNA was used for amplification of the intronless *ASP1* ORF. To recover the

overexpressed *ASP1* gene product, the ORF was modified in order to keep it within the yeast cell. Using the protein localization software WoLF PSORT (187) and the signal peptide identifying software SIGNALP 4.1 (188), we identified the signal peptide sequence of the *ASP1* gene and deleted this (Figure 3.2a). The signal peptide cleavage site was found to be between amino acids 19 and 20 so the first methionine, and hence start codon, was retained and the amino acids 2-19 were omitted by using primer ASP1_F_-sp_IF to amplify the ORF from the cDNA. The PCR amplified *ASP1* minus signal peptide (*ASP1-sp*) fragment was cloned into the GDPp:NEV-E yeast expression vector by In-fusion cloning. Transformants were selected for based on ampicillin resistance and were screened for by colony PCR. The GPDp:ASP1-sp:NEV-E vector was then transformed into the *S. cerevisiae* strain DBY1034 (199) using *URA3* selection, generating strain DBY1034:ASP1-sp.

To screen *ASP1* for protease activity using the overexpression vector, *S. cerevisiae* was grown in SMM (minus-URA). Two millilitres of an overnight culture was inoculated into 50 mL fresh media and grown for 5 h. Cells were collected by centrifugation at 2000 r.p.m. for 5 min. Supernatant was discarded; cells were washed with 10 mL sdH_2O, and pelleted again at 2000 r.p.m. for 5 min. Cells were resuspended in 1 mL of protein extraction buffer and had 0.3 g of acid washed glass beads (425-600 µm) added. Suspensions were vortexed 5 x for 1 min with tubes stored on ice between intervals to retain protein viability. Tubes were then subjected to centrifugation for 10 min at 13,000 r.p.m., 4 °C and supernatant was collected for azocasein assay by combining 100 µL with 900 µL azocasein. Reactions were incubated at 37 °C for 20 h, stopped with the addition of 1 mL trichloroacetic acid (10 % w/v) and activity was assessed as described above. The empty vector (NEV-E) was used as a negative control.

3.4.5 | Localisation and regulation of *ASP1:mCherry* expression

To identify the subcellular expression of *ASP1*. a C-terminal *ASP1:mCherry* fusion vector was constructed and transformed into the Δ*asp1* mutant. This plasmid was constructed by In-Fusion cloning using the previously generated vector backbone pSC-INV1-BAR (Figure 1.11), linearized by digestion with *EcoRI/HindIII* to retain the *BAR* gene. The native *ASP1* promoter was retained by PCR amplifying a fragment from 1.8 kb upstream of the ORF, with the reverse primer excluding the stop codon using primers ASP1_C_F_IF and ASP1_C_R_IF (Table 3.3) . To this an *mCherry*:*trpCt* fragment, amplified using primers mCh_F_IF and TrpC_R_IF (Table 3.3), was cloned.

Figure 3.15

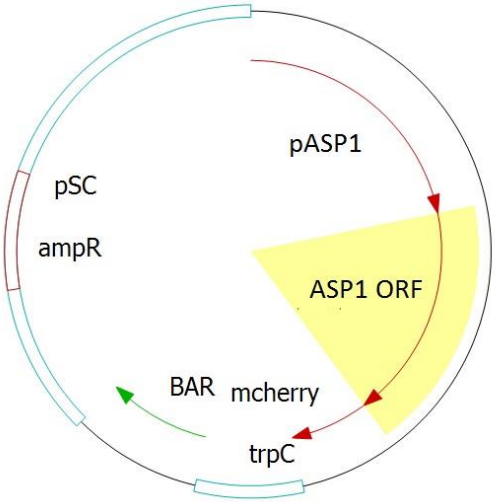

Figure 3.15 | Plasmid map for the ASP1-mCherry expression vector. The *ASP1* ORF with 1.8 kb upstream region to include the native promoter (pASP1) was cloned by In-fusion with an *mCherry*:*trpC* terminator fragment into the pSC-BAR vector backbone generated previously (Figure 1.11) to generate the ASP1-mCherry expression vector which was transformed into *M. oryzae*.

Table 3.3 | Primers used for generating the ASP1-mCherry fusion construct and the ASP1 overexpression vector. Underlined regions indicate complementary regions for In-fusion cloning.

Primer name	Nucleotide sequence (5' - 3')
mCh_F_IF	ATGGTGAGCAAGGGCGAGGA
TrpC_R_IF	GGTATCGATAAGCTTCTCGAGTGGAGATGTGGAGT
ASP1_C_F_IF	CCCAATGTGGAATTCTATAGTGTCTTGTCTGTCGC
ASP1_C_R_IF	GCCCTTGCTCACCATGACGGCGTGGTCGGCGATAC
ASP1_F_-sp_IF	AGTTAGTCTTGAATTCATGGCGCCGGCCAACAACCAGAA
ASP1_R_IF	CAATTCCCCGGAATTCTTAGACGGCGTGGTCGGCGATA

To identify the location of the RFP signal, *ASP1:mCherry* conidia were inoculated onto hydrophobic *in vitro* surfaces and allowed to germinate for 20 h. At this time, CellTracker Blue, CMAC (7-amino-4-chloromethylcoumarin; Invitrogen/Molecular Probes) was added to the inoculations at a final concentration of 0.1 mM. CMAC has been shown to specifically stain the acidic vacuolar compartment in the plant pathogenic fungus *U. maydis* (251). After 1 h, CMAC was washed away and the suspension fluid was replaced with sdH_2O. CMAC that had stained *M. oryzae* was visualised by fluorescence microscopy using the same wavelengths as DAPI (4',6-diamidino-2-phenylindole) staining which has a excitation wavelength of 358 nm with emission of 461 nm.

Chapter 4

Examining the implications of making sucrose metabolism 'private'

4.1 | Introduction

4.1.1 | The social dilemma of osmotrophy

As we have seen in Chapters 1 and 2, *M. oryzae* faces social dilemmas as a result of its osmotrophic feeding strategy. Individuals can exploit secreted depolymerising enzymes and the products they yield to gain a selective advantage. The secreted proteome of *M. oryzae* is understood to be complex, with 739 proteins predicted to be secreted, any of which could hypothetically be exploited by defecting or non-producing individuals (141, 161, 220). Osmotrophy is a feeding strategy employed throughout the kingdom of Fungi, as well as other eukaryotic groups including hypochytriomycetes and oomycetes, and even many bacteria (220). Considering that the strategy of external feeding is exploitable by individuals who avoid the cost of producing secreted products (66, 88, 206), why is it so apparently successful and widely persist in natural populations? The dilemma of public-good cooperation *per se* has been addressed in previous work, and earlier chapters of this thesis. For example, factors including negative frequency-dependent selection and population spatial structuring can make public-good producers favourable over defectors (58, 85, 204, 258). Yet the inclusive fitness of individuals may be restricted by cheats that exploit the cooperation of others, and the loss of public-goods that diffuse away into the environment. Therefore, we ask can making metabolism a 'private-good' enable the restriction upon fitness imposed by cheats to be alleviated?

The ability of fungi to feed by phagocytosis to make digestion a ‘private good’ was lost early in fungal evolution (259). Osmotrophs have adapted to limit the loss of public-goods to competitors and the environment with high affinity nutrient transporters (260, 261), and producing anti-competitor toxins (53, 54). Furthermore, osmotrophy is thought to yield advantages including more discerning absorption of substances, thus minimising toxin and pathogen uptake (220), and adaptability of enzyme and transporter expression to the presented nutritional requirements of variable substrates (262). Osmotrophy also enables the exploitation of macromolecules such as cellulose and lignin, which could not be consumed by direct absorption without prior external breakdown. However, there may be ways to avoid being exploited by ‘cheats’ with the consumption of compounds of an intermediate size such as the disaccharide sucrose. The plant pathogenic fungus *U. maydis* has a potential solution to exploitation by possessing a high-affinity, high-capacity sucrose transporter so that digestion can occur ‘privately’ in the cytoplasm. Though suggested to partly function as a mechanism to prevent defence responses in host plants resulting from glucose signalling, a highly unfavourable outcome for a biotrophic pathogen (172), firstly, we asked if this mode of sucrose metabolism provides the fungus with a mode of cheat suppression. Secondly, if internal digestion of sucrose can prevent exploitation, how does this feeding strategy fare in competition with those who digest externally? We also sought to examine the fitness costs associated with internal metabolism to help explain why osmotrophy is so prevelant amongst microbes.

4.1.2 | The importance and maintenance of diversity

By developing a system to examine the relative success of feeding strategies, we can also examine how the diversity of feeding strategies persists. Biodiversity in

general is important for ecosystem functions such as nutrient recycling (5) and, as we have seen in Chapter 2, diversity is important for virulence. Diversity also provides resilience and adaptability of the community to environmental change. Hardin's competitive exclusion principle (263) considers that at equilibrium multiple species are unable to coexist for a single limiting resource in spatially homogenous environments. Spatial structure can be important to buffer against competitive exclusion by creating different niches (264, 265). Yet biodiversity in spatially homogenous environments is understood to be maintained in part by fitness advantages when rare (negative frequency dependent fitness) and physiological trade-offs (237, 266, 267). In this study we present details of the physiological details underpinning one of these trade-offs, where diversity can be maintained by differing strategies of acquiring and utilising the same resource. This leads to a scenario where advantages can be gained at different population and environmental conditions, such as the inevitable temporal variations observed in nature as a result of consumption and proliferation. This mechanism of diversity has been observed previously through a combination of rate-affinity and rate-yield trade-offs in populations of *E. coli* (93). However, beyond trade-offs arising from biochemical pathways, we find that polymorphisms can be maintained based on the disparate benefits obtained through opposing nutrient acquisition strategies.

4.1.3 | Ecological factors on the evolution of cooperation

As shown in Chapter 2 and by others, population dynamics can influence the predicted evolution of public-goods cooperation (204, 268-270). It is also becoming increasingly apparent that ecological factors, such as the resource conditions and disturbance events, can influence the evolution of public-goods cooperation (271, 272). Furthermore, the majority of studies of public-good cooperation with microbes

have focussed on studying cooperators and cheats in isolation, as opposed to in the complex communities where they naturally live. The further competitive interactions that occur have implications for the evolution of cooperative traits (273-276). The outcome of these interactions on the relative success of cooperation appears to depend on how the competitor influences the communal environment. For instance, the success of cooperation depends on whether the competitor either exploits or contributes towards the public-good (274), or whether the competitor has a strategy to consume the communal resources 'privately' (275, 276).

4.2 | Results

4.2.1 | Developing a polymorphic system for sucrose metabolism

To overcome complications regarding disentangling relative fitness measurements across species, but rather focus on the specific traits they possess, we used strains of *S. cerevisiae* constructed in the same genetic background with modifications so that only the mode of sucrose metabolism was modified (Figure 4.1). *S. cerevisiae* has become established as a model organism for studying ecology and evolution (6). The strains used were the wild-type invertase (*SUC2*) secretor DBY1034 (from here on referred to as 'producer'). As an invertase defector, we used the *SUC2* deletion strain DBY1701 (from here on referred to as 'non producer') (199), which does not produce invertase, and so does not incur the associated metabolic cost, but can still benefit from secreted invertase produced by others. *SUC2* catalyses the hydrolysis of sucrose into its constituent monosaccharides, glucose and fructose, which are taken into the cell by hexose transporters to be internally metabolised by glycolysis (66).

To test internal sucrose metabolism in a common genetic background, the strain DBY2617 was employed, which has a signal sequence mutation *suc2-438*. This mutation, a deletion of amino acids 4-19, results in the production of a functional invertase that remains non-glycosylated, a feature of secreted proteins, and so remains cytoplasmic (199, 277). To this strain, the *U. maydis* sucrose transporter (*SRT1*, UM02374, UniProt: Q4PBY9) has been introduced, resulting in sucrose metabolism becoming a private-good (from here on this strain is referred to as 'transporter' (172) (see Methods for more information). This strain still possesses intact hexose transporters, so like the 'non-producer' it can also exploit hexoses liberated from sucrose by external invertase. Importantly, all three strains have the same prototrophic abilities for amino acids so no artificial additional 'cost of cooperation' was applied (as in (14, 269)).

Figure 4.1

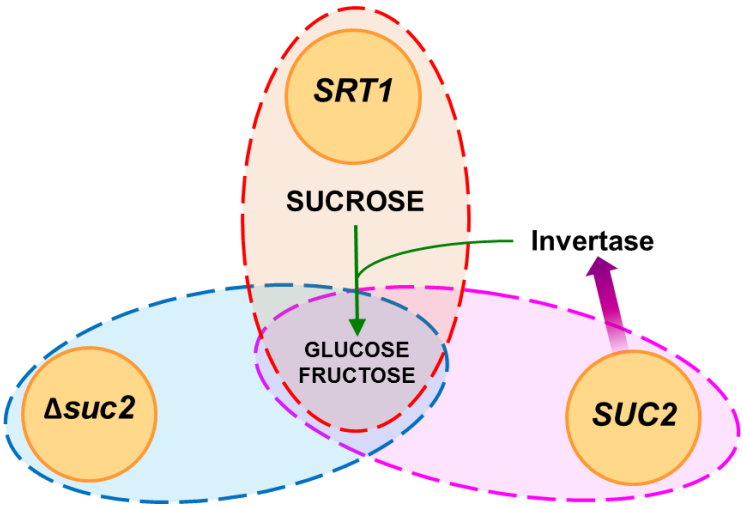

Figure 4.1 | Schematic of three *S. cerevisiae* strains with differing modes of sucrose metabolism. To feed on sucrose, wild-type *SUC2* strains (DBY1034) produce a secreted invertase that externally breaks down sucrose into its monosaccharides, glucose and fructose, which are taken up through hexose transporters for internal metabolism. For efficient growth, the 'non-producer' (Δ*suc*2, DBY1701) is reliant upon invertase secreted by others to access the monosaccharides from sucrose. The 'transporter' strain (*SRT1* in DBY2617) can directly take up sucrose and metabolise it internally. It can also exploit external hexoses that are generated in a mixed strain population. Shaded ellipses indicate the sugars that can be directly consumed by each strain.

4.2.2 | Identifying axenic phenotypes of sucrose metabolic polymorphisms

Firstly, we wanted to understand how the strains (Figure 4.1) act in axenic culture, with sucrose present as the sole carbon source, so that the influence of their sucrose feeding strategies on growth rates could be observed in isolation. We found that the invertase 'producer' had the highest growth rate in terms of maximal growth rate over a single batch culture, followed by the 'transporter'. The 'non-producer' had the slowest growth, yet could still proliferate to a degree despite lacking an invertase enzyme (Figure 4.2a & Table 4.1). The growth of the 'non-producer' is understood to result from slow and inefficient metabolism mediated by active sucrose H^+-symport (278) and internal maltase activity (279). This mode of sucrose metabolism is expected to contribute to growth of the producer, non-producer and transporter approximately equally, given that the strains are from a common ancestral strain and so possess the same capabilities in this pathway. These differences in growth rates on sucrose media were much reduced in glucose media (Figure 4.2b & Table 4.1), where all strains would directly take up the monosaccharide through hexose transporters for internal metabolism by glycolysis (66). The significant, yet relatively small, differences in growth rate that are apparent in glucose are thought to be attributed to the metabolic cost associated with invertase production, which is induced in low levels of glucose (280). This cost is incurred by both the 'producer' and the 'transporter'. The 'transporter' also experiences the additional cost of the *SRT1* sucrose transporter, expression of which is driven constitutively by the *PMA1* promoter (200). The benefit of invertase production in sucrose environments gives a more than three times increase in growth rate over non-producers (Figure 4.2a & Table 4.1). This is a much greater difference than from strains tested previously where a 20 % growth rate advantage was reported (85). This may be caused by the

different growth conditions employed, or different levels of sucrose uptake and metabolism by other means (278-279).

Figure 4.2

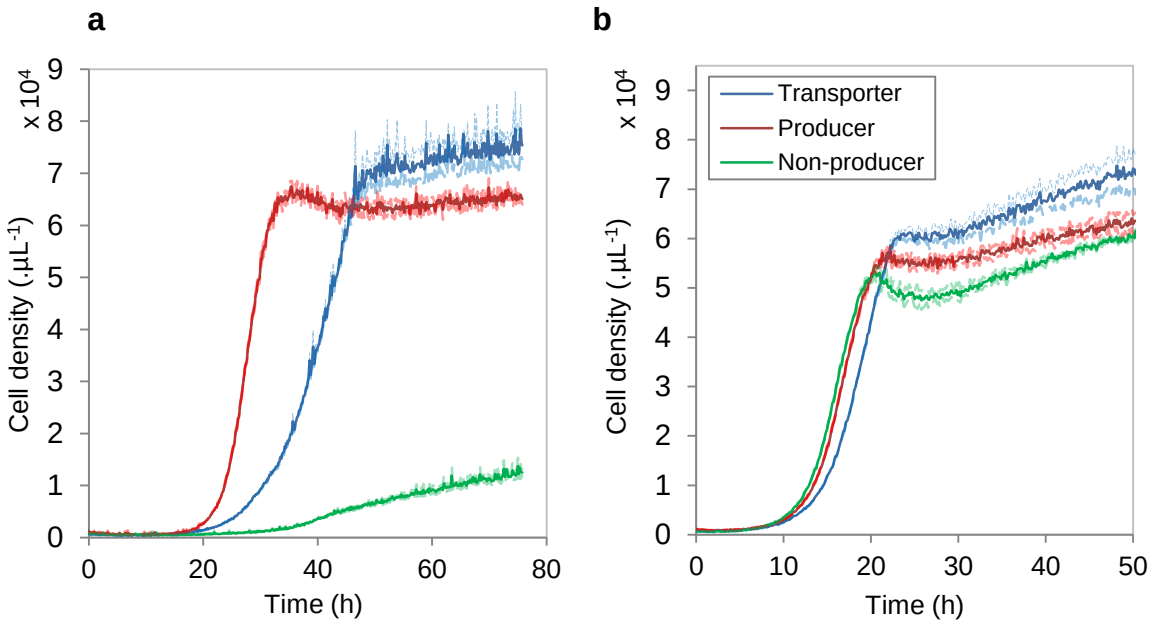

Figure 4.2 | Axenic growth curves to test growth phenotype of strains of *S. cerevisiae* with polymorphic sucrose metabolism. a in 25 mM (0.8557%) sucrose SMM. **b** in 0.8557% glucose SMM. Strains were inoculated in single strain cultures to observe growth rates in conditions that required invertase metabolism and conditions that do not. Calculated growth rates can be seen in Table 4.1. 'transporter' = blue, 'producer' = red, 'non-producer' = green. Mean ± s.e.m., n = 3.

Table 4.1 | Growth rates calculated from axenic growth experiments

Growth rate* (Malthusian growth parameter) in 0.8557 % (w/v) sugar SMM

Strain	Sucrose	Glucose
Invertase producer (DBY1034)	0.1987 ± 0.0004	0.3090 ± 0.0013
Invertase non-producer (DBY1701)	0.0607 ± 0.0006	0.3191 ± 0.0005
Sucrose transporter (DBY2617 + SRT1)	0.1359 ± 0.0009	0.2733 ± 0.0007

* All rates are significantly different ($p < 0.002$). Two-sided t-test. Growth rate measured from 0 h to the end of the exponential phase. Mean ± s.e.m. n = 3.

These axenic growth rates suggest that osmotrophy yields distinct advantages over the other feeding strategies, when interactions are only with clone mates. Another important finding of these simple growth experiments is that a trade-off between growth rate and final density exists, where a reduced rate of growth is compensated for by an increased yield in total density (77, 93) (Figure 4.3).

Figure 4.3

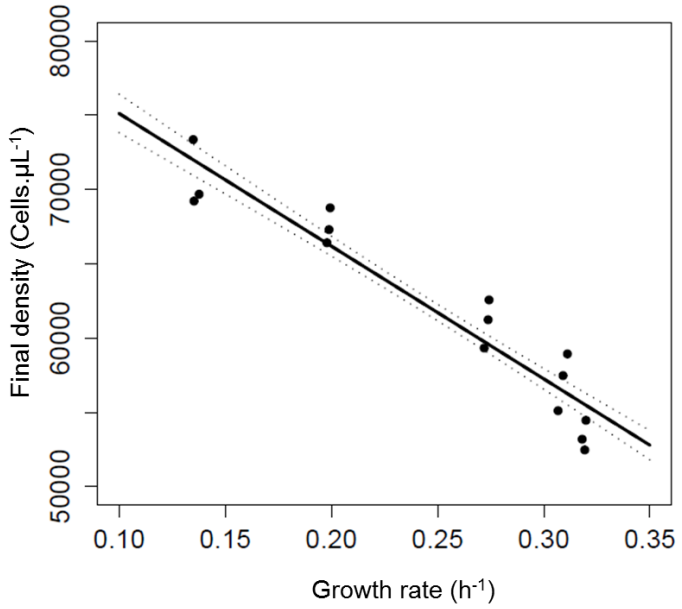

Figure 4.3 | A trade-off between rate and yield exists in *S. cerevisiae* strains with differing metabolism. A relationship between growth rate and final population density was observed in strains with differing metabolic strategies. Slower growth rates tended to have higher population yields ($p < 0.0001$, $\rho = -0.9428$, Spearman's rank correlation). Plotted are the population densities at the end of the exponential growth phase, against the growth rate over the same period. This data is compiled of the three strains, 'producer', 'non-producer' and 'transporter' in glucose media, and for 'producer' and 'transporter' in sucrose media (both at 0.8557 % w/v). 'Non-producer' in sucrose media was not included as it had not ceased exponential growth phase over the 75 h growth period, so final density could not be determined. Linear model fit ± s.e.m.

This trade-off highlights the importance of taking a holistic viewpoint of the fitness of traits, and organisms, as they are multi-faceted. Therefore, different proxies for fitness have to be considered within the framework of the organism's biotic and abiotic environment. For instance, when consuming a limited resource pool in the absence of competition, efficiency is favoured over rate to maximise reproductive output. However, in mixed strain environments, the rate of resource consumption and growth has distinct advantages for outcompeting competitors for a finite resource pool (77), analogous to social 'cheats' in Hardin's "tragedy of the commons" (96). Furthermore, the shift in the trade-off towards rate coincides with metabolising glucose by fermentation (77), which produces ethanol. Ethanol is toxic to many other microbes so this mode of metabolism has a secondary effect of excluding competitors. As the ethanol can later be metabolised when glucose is exhausted, this method of metabolising glucose has been termed the 'make-accumulate-consume' strategy (281).

4.2.3 | The fitness of sucrose feeding strategies in pairwise competition

We performed pairwise competition experiments to understand how interactions between pairs of strains in culture may influence their relative success in a mixed population. The competition between invertase 'producers' and 'non-producers' has been well characterised. It has been shown to exhibit the classical features of a public-good cooperative system. We confirmed that the 'producer' and 'non-producer' strains employed in this study displayed similar outcomes to those from previous experiments and cooperation theory (14, 66, 85). These characteristics include negative-frequency dependence, where either strain is fitter when rare in the population, suggesting a coexistence between the two strains (14, 58, 85) (Figure

4.4a), and density-dependent selection where ‘producers’ are fitter at low population densities, whereas ‘non-producers’ are fitter at high population densities (66) (Figure 4.4b).

Figure 4.4

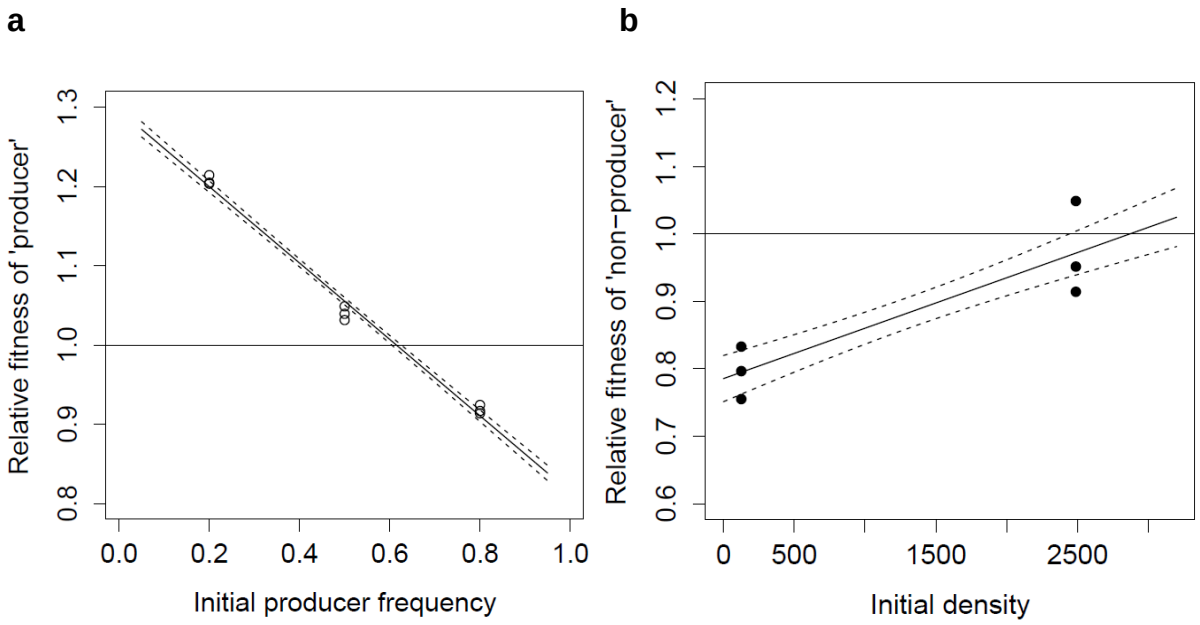

Figure 4.4 | Relative fitness of ‘producers’ to ‘non-producers shows frequency- and density-dependence. Pairwise competitions between ‘producers’ and ‘non-producers’ were performed in 25 mM sucrose SMM with different initial strain frequencies **(a)** and population densities **(b)**. **a** Negative-frequency dependence was found between strains meaning that they are relatively fitter when rarer in the population. Linear model ± s.e.m., $p < 0.0001$, $F_{(2,\ 6)}= 1360$. Initial density ≈ 125 cells.μL^{-1}. **b** High population density favours ‘non-producers’ (Linear model ± s.e.m., $p < 0.02$, $F_{(1,4)}= 14.77$) Density is cells per microlitre. Equal initial strain frequencies.

These two features, frequency and density dependent fitness, can interact to generate a feedback loop to maintain both strains at an eco-evolutionary equilibrium (269). Negative frequency-dependent and positive density-dependent fitness of public-good ‘non-producers’ relative to ‘producers’ arises from the opportunities

available for cheats to exploit cooperators, and non-linear benefits produced from increasing costly cooperation (282). In high density populations, the public-good availability relies more upon the average public-good production of individuals within social groups, rather than any single individual (270). When ‘non-producers’ are relatively rare in populations, again, they have more opportunities to exploit ‘producers’, leading to an advantage when there is strong selection for the cooperative trait, such as the growth advantage to the population when invertase is produced in sucrose environments (204).

Beyond density- and frequency-dependent selection, we found that ‘non-producers’ are fitter under higher resource concentrations (Figure 4.5). This is in contrast to previous studies to have examined the influence of resource supply on the fitness of public-good producers, where it was found that increasing resource supply preferentially helps producers. This previous result was thought to be caused by a reduced cost of cooperation (283). However, with invertase secretion to digest sucrose, because the additional resources are directly related to the cooperative trait in question, the ‘non-producers’ profit from an increased resource concentration. This is because in increased concentrations invertase mediated sucrose hydrolysis produces more hexoses, a larger proportion of which diffuse into the environment to be consumed by other members of the population (see below for quantification) (14). This, in turn, preferentially aids ‘non-producers’ who rely on the invertase activity of ‘producers’. Therefore, coexistence between producers and ‘non-producers’ results, in part, from producers getting preferential access to hexoses liberated from sucrose, which overcomes the costs related to the production of invertase. The results obtained for competition between ‘producers’ and ‘non-producers’ here are also in

agreement with those published previously using similar experimental conditions (106).

Figure 4.5

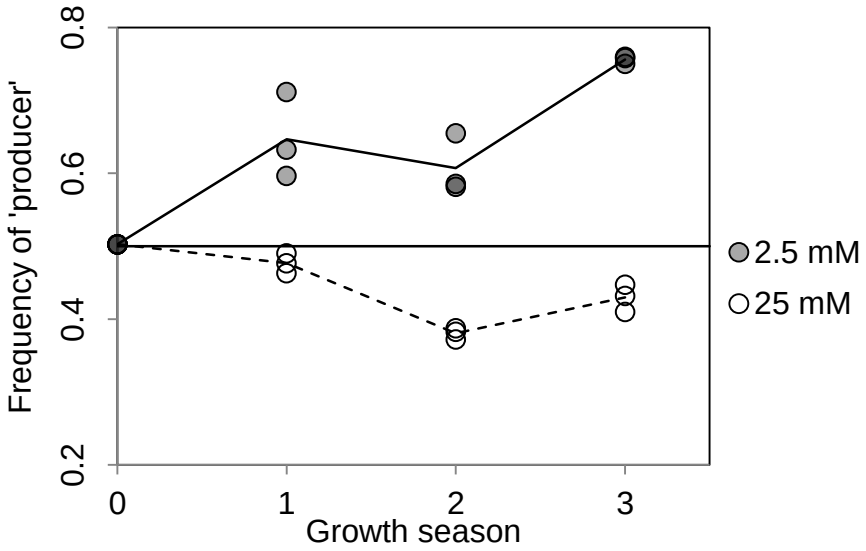

Figure 4.5 | The relative fitness of 'producers' versus 'non-producers' is dependent upon resource concentrations. Strains were competed from equal starting frequencies in 2.5 mM or 25 mM sucrose SMM. Transfers to fresh media were made every 48 h to allow saturation of population growth. Producers were relatively fitter in lower resource concentrations (2.5 mM), whereas this advantage was lost in higher resources (25 mM). n =3, line = mean.

Now that we have confirmed that the dynamics between the invertase 'producer' and 'non-producer' strains employed in this study, using our experimental set-up, are consistent with previous studies, we asked if making sucrose metabolism a 'private-good' could eliminate the incentive to 'cheat' by outcompeting 'non-producers'. To address this, mixed strain competitions between the 'transporters' and 'non-producers' were performed. As neither strain produces a secreted invertase, there is not expected to be any exploitation of external digestion. Hence, both strains metabolises sucrose internally and trophic interactions only occur in terms of direct competition for a limited resource pool. As predicted from the axenic growth rates (Figure 4.2) and intuitive predictions based on the interaction occurring, in all initial

frequencies of strains during pairwise competitions, the ‘transporter’ strain was at a selective advantage over the ‘non-producer’ (Figure 4.6a). During multiple season transfer experiments, this trend continued to the point where the ‘non-producer’ was not detectable by fluorescence intensity readings and was effectively excluded from the population (Figure 4.6b). Therefore, as expected, internal metabolism appears to be an effective feeding strategy to prevent ‘cheats’ from exploiting a metabolically costly enzyme.

Figure 4.6

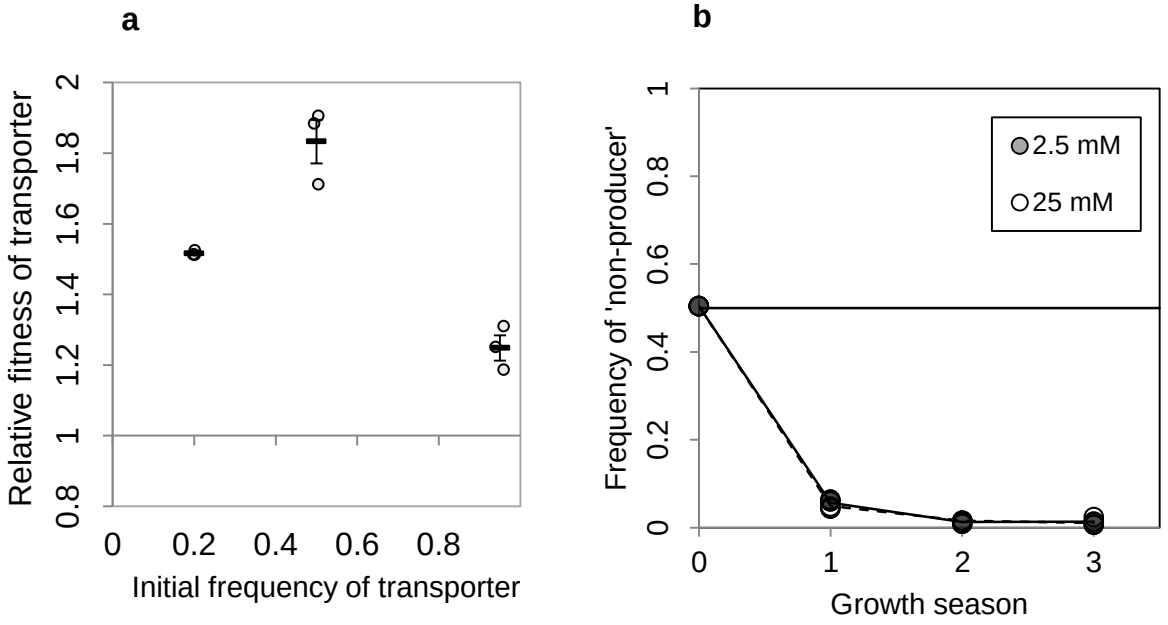

Figure 4.6 | Relative fitness of ‘transporter’ versus ‘non-producers’. a ‘Transporter’ strain has a higher relative fitness than the ‘non-producer’ over a range of starting intial frequencies in 25 mM sucrose SMM ($p < 0.02$ at each tested frequency, two-sided, one-sample t-test). Circles represent individual data points with artificial x-axis noise added to aid in visualising points. Initial frequencies were 0.25, 0.5 and 0.95. Dash = mean ± s.e.m.. **b** ‘Transporters’ all but excluded ‘non-producers’ from the mixed strain population after starting at equal frequences with transfers to fresh media made every 48 h in both 2.5 or 25 mM sucrose SMM. Line shows mean, n = 3.

We next sought to answer the question of why external digestion in microbes is so prevalent, given that it is exposed to social exploitation by cheats. To address this, firstly, we performed competitions between the invertase-secreting 'producer' and the 'transporter' to see if direct competition would reveal a dominant competitor. Since 'producers' have a higher axenic growth rate (Figure 4.2), would this be enough to outcompete 'transporters' in a mixed-genotype environment in the absence of spatial structure? We found that 'producers' had a selective advantage over 'transporters' at higher resource concentrations, yet 'transporters' dominated at lower resource concentrations (Figure 4.7a). Therefore, the selective advantage of internal sucrose metabolism appears to be dependent on the resource environment experienced.

Figure 4.7

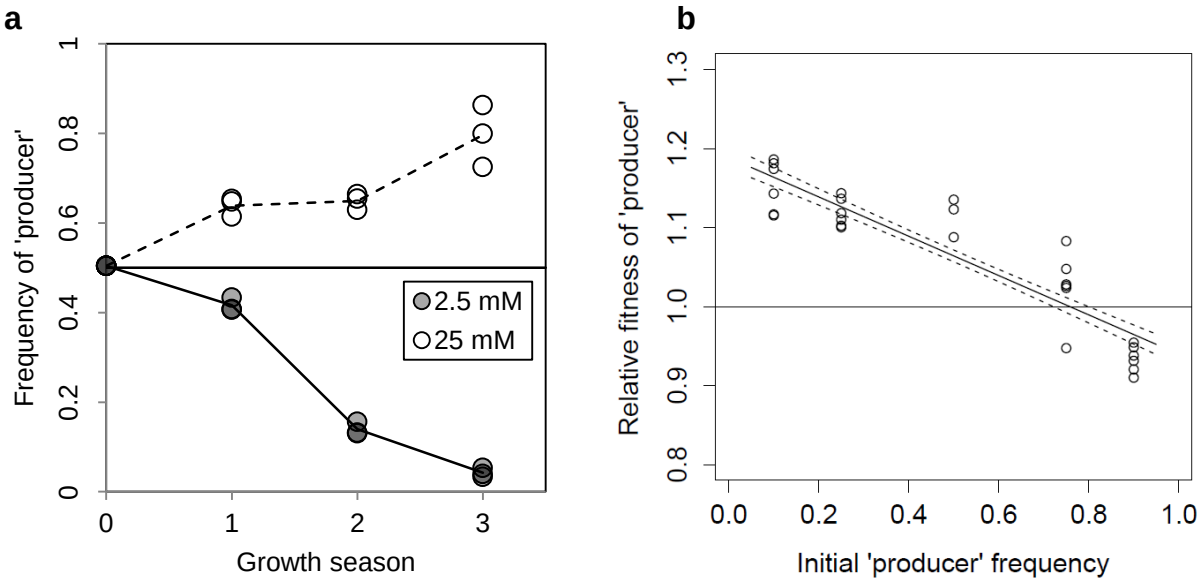

Figure 4.7 | Relative fitness of 'producer' versus 'transporter' strains. a Starting pairwise competitions from initially equal frequencies, 'transporters' have a competitive advantage at low resource concentrations (2.5 mM sucrose), whereas 'producers' dominate at high resource concentrations (25 mM sucrose). n= 3, line = mean. **b** In high resources (25 mM) 'producers' and 'transporters' exhibit negative frequency dependent fitness (Linear model: Adj. $R^2 = 0.808$, $\beta = -0.249$, $p < 0.0001$, $F_{(1, 25)} = 110.45$,) with either strain being fitter when rare, suggesting coexistence at intermediate frequencies, Line shows linear model ± s.e.m..

Negative-frequency dependent selection at the higher resource concentrations (25 mM) suggests coexistence between the strains in these conditions (Figure 4.7b). Since the ‘transporter’ strain is able to exploit invertase secretion in the same manner as the ‘non-producer’ strain, we consider the negative frequency-dependent selection, observed here, to be governed by a similar mechanism as between the ‘producer’ and ‘non-producer’ strains. This pairwise competition reveals how the selective advantages that differing feeding strategies bestow, are dependent upon the nutritional environment experienced, in addition to other conditions that favour public-good cooperation, such as spatial structure.

4.2.4 | The Allee effect resulting from secreted invertase sucrose metabolism

The negative frequency-dependent fitness observed in 25 mM sucrose was reversed, however, when the competitions were performed between the strains in 10 mM sucrose (Figure 4.8). This finding can be explained by the principles behind the Allee effect, where per capita growth rate is maximal at intermediate densities and reduced at lower densities (284) (Figure 4.9a). However, in the case with external sucrose metabolism, because the growth rate of the ‘producers’ depends on the interaction between catalysing periplasmic invertase of the yeast cell and extracellular sucrose, reducing the density (or concentration) of either will have the equivalent effect.

Figure 4.8

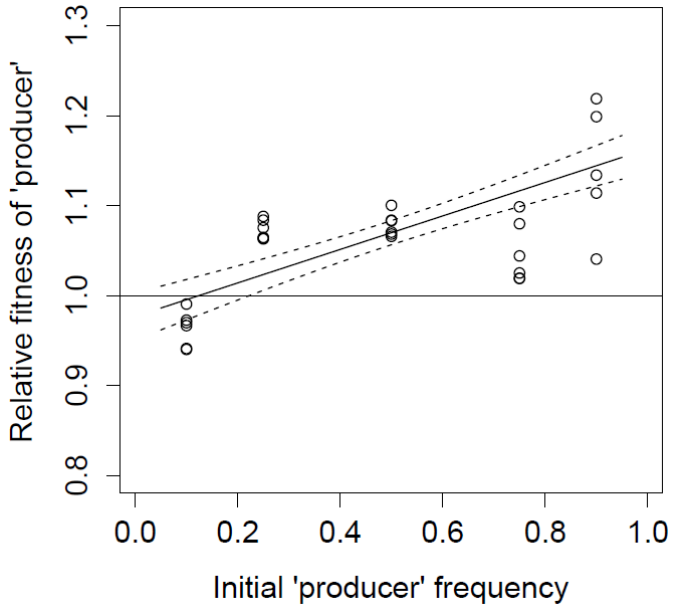

Figure 4.8 | Frequency dependent fitness of 'producers' vs 'transporters' reverses in lower resources. When competed in 10 mM sucrose SMM, 'producers' and 'transporters' exhibited positive frequency dependent fitness (Linear model: Adj. R^2= 0.357, β = 0.186, p < 0.001, $F_{(1, 28)}$ = 17.113). Line shows linear model ± s.e.m..

Figure 4.9

a

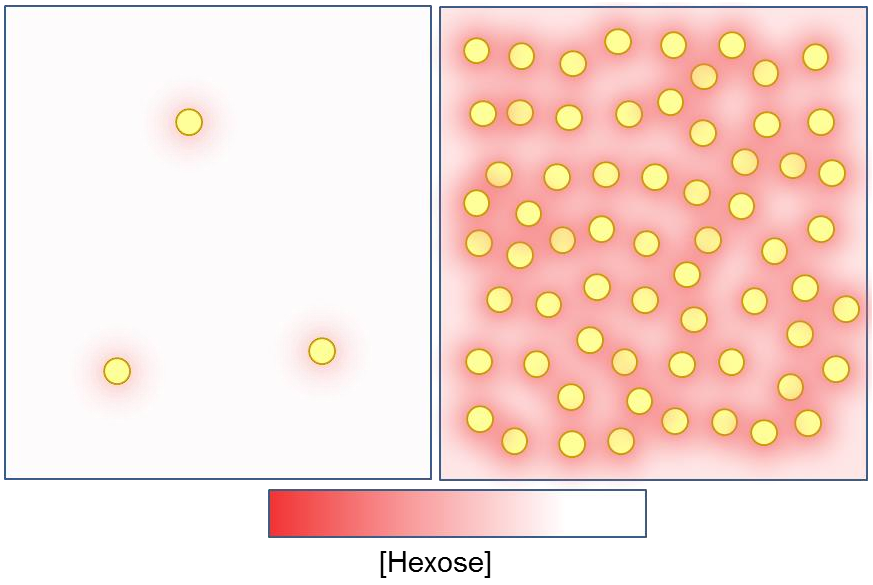

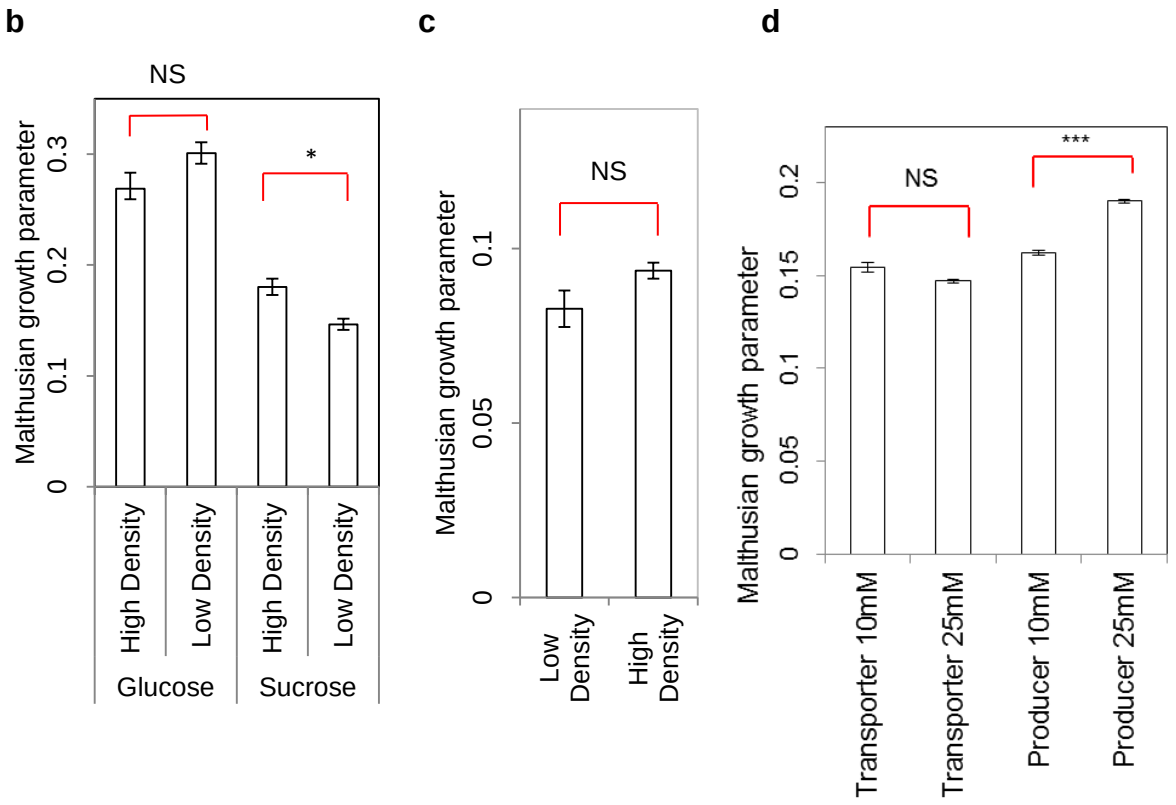

Figure 4.9 | Secreted invertase mediated sucrose metabolism experiences an Allee effect. a Schematic depicting the nature of the Allee effect experienced by 'producers'. Growth rate is higher for invertase secreting 'producers' when at higher population density (right) than low population density (left). This results from much of an individual's hexoses being obtained from the result of other's sucrose hydrolysis because a large proportion of the product is lost into the environment before it can be imported. Therefore, higher density leads to a higher external, and so communal, hexose concentration ([hexose]). This is in the absence of spatial structuring. **b** Evidence of this Allee effect was detected with 'producers' in sucrose SMM (2% w/v), where growth in low population density was significantly reduced compared to higher density (*$p < 0.02$, t-test assuming equal variance). This effect was lost in glucose SMM (2%) ($p > 0.05$, t-test assuming equal variance) mean ± s.e.m., n = 10. **c** An Allee effect was not detected in 'transporters' ($p > 0.05$ t-test assuming equal variance) mean ± s.e.m., n = 10. **d** Because the mechanism behind the Allee effect results from a reaction between an externally acting invertase and sucrose, reducing the external sucrose concentration has the same effect in 'producers' (***$p < 0.0001$, t-test assuming equal variances), which again is not detected with 'transporters' ($p > 0.05$, t-test assuming equal variance) mean ± s.e.m., n = 3. NS = not significantly different ($p > 0.05$).

Evidence of this Allee effect in the ‘producers’ was found in terms of both cell density and resource concentration. Whereas, for ‘transporters’ this effect was not detected (Figure 4.9b-d). This could be as a result of the mode of sucrose metabolism, because a large proportion of the products from external sucrose hydrolysis are lost into the environment. Therefore, the hexoses that an individual acquires are often produced by the social metabolic actions of others. At low population densities, there is a dearth of hexoses in the environment to capture, resulting in a low growth rate. This can be observed at low population frequencies, where the producers are at a selective disadvantage relative to the transporters (Figure 4.8). However, when the population density of invertase secretors increases, so does the experienced hexose concentration and hence the growth rate, leading to the ‘producers’ being relatively fitter than the ‘transporters’ (Figure 4.8). On the other hand, ‘transporters’ do not experience this Allee effect because their direct uptake and metabolism of sucrose is ‘private’. Despite the measured growth rate of the ‘producer’ being higher than the ‘transporter’ during the ‘low density’ measurement (Figure 4.9 b-c), the Allee effect that was detected suggests that the growth rate of the producer will have an exponential increase over the period during which these rates were calculated. The measurement used assumes a constant growth rate (299), therefore, does not capture the expected initial slow growth that is experienced while the external environment lacks hexoses. Unfortunately, the cell density where this slow growth is thought to occur is below the detection limit of the apparatus used, so was not empirically detected. The impact of the Allee effect is expected to have the most influence upon invertase-secreting ‘producers’ at the beginning of a seasonal batch culture. Here, population densities are particularly low and so the number of individuals generating communal hexoses will be small. Therefore, at this stage, the

hexose concentrations, the probability of up taking hexoses produced by others, and the subsequent growth rates will all be relatively low. The differing density dependent, or independent, growth rates of 'producers' and 'transporters' provides insight into the type of environments in which the opposing feeding strategies may be favoured.

4.2.5 | The benefits to public-good producers in low resources

To quantify the mechanism behind why 'producers' are fitter in low sucrose concentrations, as we have seen when in competition with either 'non-producers' (Figure 4.5) or in certain circumstances with 'transporters' (Figure 4.7b & 4.8), the differences in glucose capture efficiency in different resource concentrations were calculated. For simplicity, glucose is assumed to be equivalent to fructose. These calculations are based on hexose creation rate data, from (14), in different sucrose concentrations (*S*) and adapting calculations from (14) where, following Michaelis-Menten kinetics, the glucose creation rate per cell (sec^{-1}) is denoted by V and is given by

$$V = \frac{V_{max}[S]}{K_m + [S]} \quad \text{(i)}$$

where V_{max} denotes the maximal rate of the pathway and is given the value 4.8 x 10^8, and K_m denotes the Michaelis-Menten constant and is given the value 0.5 % (w/v) (14) (Figure 4.10).

The glucose capture efficiency ($\boldsymbol{\varepsilon}$) is defined by

$$\varepsilon = \frac{\Im_{in}}{V_i} \quad \text{(ii)}$$

where V_i is the glucose creation rate in a given (i) sucrose concentration, and the glucose flux into the cell, $\Im_{in}$, is estimated by

$$\Im_{in} = g \cdot r \quad \text{(iii)}$$

where g denotes the number of molecules of glucose required per cell, and is given by

$$g = \frac{h}{x_i - x_0} \quad \text{(iv)}$$

where h is the number of molecules of glucose (3.34258 x10^{15}.μL^{-1} in 0.1 % w/v) and x_i and x_0 are the initial and final cell densities.

r is the logarithmic growth rate, denoted by

$$r = \ln \frac{x_i}{x_0} / t \quad \text{(v)}$$

where t is time (h).

In 0.1 % (w/v) glucose, r = 0.186 h^{-1} ± 0.00144 s.e.m (n = 3).

The number of cells generated after all resources have been consumed in 0.1 % glucose (x_i - x_0) is 62274 ± 933 s.e.m. cells.μL^{-1} (n = 3).

g = 5.37 ± 0.08 s.e.m. x 10^{10} molecules of glucose per cell (n = 3).

So, $\Im_{in}$= 2.78 ± 0.61 s.e.m. x 10^6 molecules.sec^{-1} (n = 3).

Therefore, the estimate of glucose capture efficiency for producers and hence the preferential access they enjoy before the rest is lost to the communal environment in 25 mM sucrose $\mathcal{E}$ ≈ 0.917 %, whereas in 2.5 mM $\mathcal{E}$ ≈ 3.96 % (assuming V = 7.01 x 10^7 in 2.5 mM sucrose, and V = 3.03 x 10^8 in 25 mM from Figure 4.10 and equation

(i)). Therefore, invertase production becomes relatively more selfish in lower resource concentrations as a result of 'producers' being able to capture a larger portion of the hexoses generated before they diffuse into the environment to be used by neighbouring individuals. This is largely as a result of glucose creation rate being reduced in lower sucrose concentrations (Figure 4.10 and (14)), meaning that when hexose uptake is maximal, less excess monosaccharides are being generated and released into the environment.

Figure 4.10

Figure 4.10 | Glucose creation rate by invertase secreting *S. cerevisiae.* Data applied from (14) to estimate glucose creation rates in the experimental protocols applied in this current study. Glucose creation rates were estimated from Michaelis-Menten kinetics (equation (i)) to be 3.03×10^8 in 25mM (0.8557%) and 7.01×10^7 in 2.5 mM (0.08557%), providing an empirical explanation of why 'producers' can gain a selective advantage at low resource concentrations.

4.2.6 | Coexistence between polymorphic strains in spatially unstructured environments

Overall, in pairwise competitions between different sucrose feeding strategies at higher resource concentrations (25 mM sucrose) and certain initial frequencies and

densities, we found non-transitive hierarchies of competitiveness between the strains. With ‘transporter’ beating ‘non-producer’ (Figure 4.6), ‘producer’ beating ‘transporter’ (Figure 4.7) and ‘non producer’ beating ‘producer’ (Figure 4.5). These relative fitnesses suggest potential cyclical, so called ‘Rock-Paper-Scissors’, dynamics between the three strains in mixed culture (265, 276).

We found that three strains polymorphic for sucrose metabolism were able to coexist with a single limiting resource (Figure 4.11 a & c). This diversity in a spatially homogenous environment is understood to be maintained in part by fitness advantages when rare (negative frequency-dependent fitness) and by differing strategies of utilising the same resource where advantages can be gained at different population and environmental conditions experienced during this experimental set up. These deviations are comparable to the inevitable temporal variations observed in nature as a result of consumption and proliferation. This diversity is maintained by the way in which sucrose is metabolised. Sucrose can be digested either externally, to effectively create secondary resources (hexoses), or internally. This strain diversity was lost when strains were competing for glucose indicating that the polymorphisms in sucrose metabolism are the driving force behind this coexistence as a result of creating multiple niches (Figure 4.11 b & d).

Figure 4.11

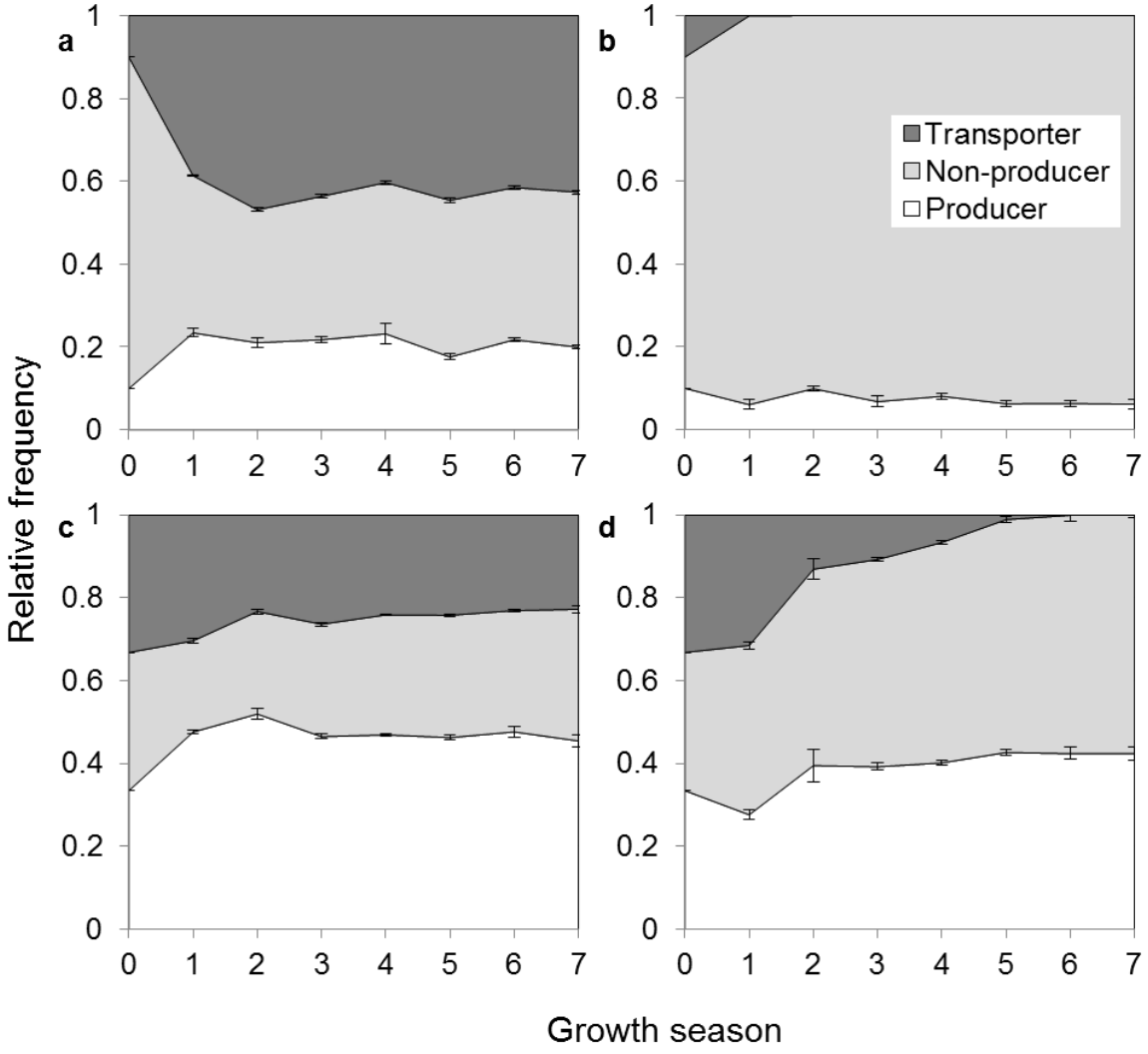

Figure 4.11 | Mixed-genotype cultures with three strains with polymorphisms in sucrose metabolism. Mixed cultures were started with 'producers', 'non-producers' and 'transporters' at initial frequencies of 1 : 8 : 1 (**a** & **b**) or 1 : 1 : 1 (**c** & **d**), respectively, in either 25 mM (0.8557 %) sucrose SMM (**a** & **c**) or 0.8557 % glucose SMM, n = 3. Strains coexisted over the course of the 7 d transfer experiment when they competed for sucrose, however 'transporters' were lost from the populations when competing for glucose. 'Non-producers' are expected to eventually exclude 'producers' when grown in glucose given that they have a competitive advantage (Relative fitness of producers in glucose = 0.932 ± 0.007 s.e.m., n = 4, $p < 0.003$, one-sample t-test). This advantage arises because 'non-producers' avoid the cost of invertase production, which is induced in low glucose concentrations (280). Initial density was ≈ 2.52 x 10^6 cells.mL^{-1} and transfers made every 24 h by which time population growth had saturated.

Polymorphic populations of *E. coli* on a single limiting resource, glucose, have been reported to result from strains adapting to feeding on metabolic intermediate products, such as acetate (285, 286). Our findings suggest that stable polymorphisms can also emerge from the way that strains utilise a single limiting resource. We have identified a physiological trait, that of polymorphic sucrose metabolism, which can drive diversity in temporal environments (287). Furthermore, a higher degree of diversity is theoretically possible if these forces act concurrently, such as if further adaptation to feeding on metabolic waste products and metabolic trade-offs between rate and yield or affinity exist (93, 286). Evidently, there are multiple factors that can contribute to stable polymorphisms in microbial populations competing for a single resource. Beyond metabolic polymorphisms, these include the reciprocal production and degradation of antagonistic chemicals (288). Gaining a further understanding of these factors contribute towards establishing a more comprehensive view of mechanisms that maintain diversity.

4.2.7 | The influence of a 'competitor' on the stability of public-goods cooperation

Having established this three 'species' community, and guided by the population dynamics of pairwise competitions, we asked how the added multi-species complexity could influence the competitiveness of public-good cooperation. As we have seen, stable coexistence between secreted invertase 'producers' and 'non-producers' can occur at intermediate frequencies (Figure 4.4). In addition to the influence of population dynamics on the evolution of cooperation, as we have seen, other ecological aspects can also have an effect, such as resource supply (Figure 4.5) (283). Furthermore, as microbes naturally exist in complex multi-strain/species communities, another important factor influencing the evolution of cooperation is the

presence of other competitors. These competitors can influence the abiotic conditions, such as the resource status of the environment, which we have previously shown can influence the relative fitness of ‘producers’ and ‘non-producers’ (Figure 4.5). It has been shown by others in a study of yeast invertase production, that the presence of a bacterial competitor, which was able to exploit the hexoses liberated from sucrose, enhances the fitness of the invertase producer relative to its social exploiter and so stabilizes cooperation (274). However in contrast, it was also found that the presence of a competitor, which also externally breaks down sucrose to produce hexoses, favours ‘non-producer’ strains over ‘producers’ (274). Given these differing results, we asked how this relationship would be influenced by the presence of a competitor for not only the ‘secondary’ resources from sucrose metabolism (i.e. hexoses) but also a direct competitor for the ‘primary’ resource (i.e. sucrose) that is consumed ‘privately’. For this type of competitor we used the ‘transporter’ strain. We found that the introduction of a competitor, for both primary and secondary resources, preferentially aided the ‘producers’ to enhance their relative fitness over ‘non-producers’ (Figure 4.12).

Figure 4.12

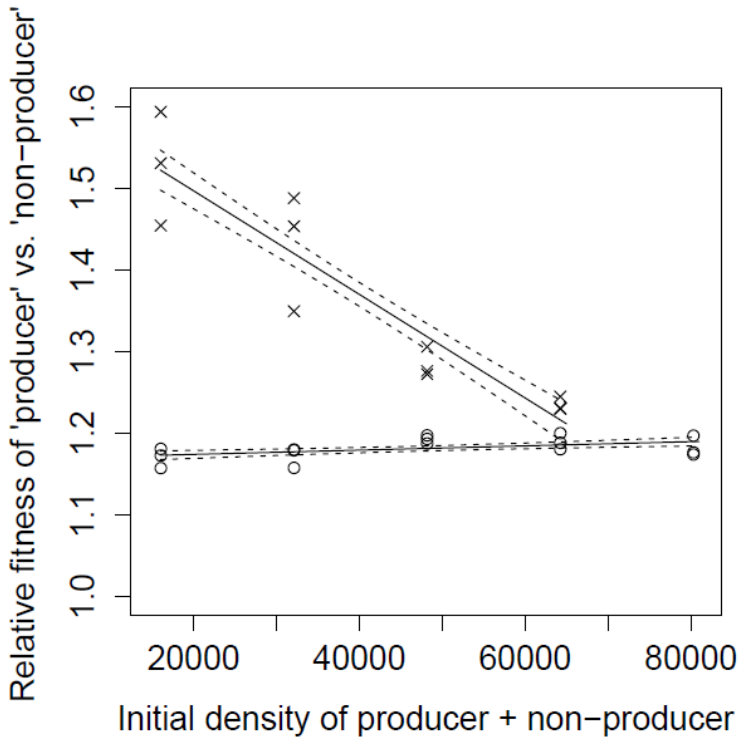

Figure 4.12 | The influence of the presence of a competitor on the relative fitness of 'producers' vs 'non-producers'. Competitions were initiated between 'producers' and 'non-producers' at equal initial frequency in the presence (x) or absence (o) of a competitor ('transporter'). Three strain populations were all initiated with an total starting density of ≈ 8 x10^4 cells, with the density of 'producer' + 'non-producers' indicated on the horizontal axis. Negative control (o) had just 'producer' + 'non-producer' strains to show that any effect observed with the presence of a 'competitor' was not caused purely by density-dependent effects. The presence of a 'competitor' significantly increased the fitness of 'producers' vs 'non-producers' ($p < 0.026$ at each starting density of 'producer' + 'non-producer', two-sided t-test) with increasing effect as the density of competitor increased ($p < 0.0001$, $\beta = -6.355$ e-06, adj. $R^2 = 0.844$, $F_{(1, 10)} = 60.52$), whereas in the absence of a 'competitor' there was no significant difference in fitness over the densities tested ($p > 0.05$, $F_{(1, 13)} = 3.665$).

To explain these results, we developed a previously established phenomenological model of the interactions between 'producers' and 'non-producers' (274), to incorporate the 'transporter' strain used in our study (Figure 4.13). As predicted from this model, introducing the 'transporter' strain firstly reduces the resource concentration by directly consuming sucrose, and secondly limits the total density of

the ‘producers’ + ‘non-producers’. This means that the ‘low density’ phase of the growth model is prominent and the period where ‘non-producers’ have a growth advantage over ‘producers’ is shortened (population density tends towards K_{new}). Evidence for this explanation can be seen when the starting density of the competitor (‘transporter’) is varied. When the ‘transporter’ is added at higher densities (moving left on the horizontal axis), which increasingly removes sucrose and limits the population density of the ‘producer’ + ‘non-producer’, the fitness of the ‘producer’ relative to the ‘non-producer’ increases (Figure 4.12). When the ‘transporters’ directly consume sucrose from the environment, they make ‘producers’ relatively more selfish (as described in section 4.2.5).This is because in a lower resource environment ‘producers’ capture a larger proportion of the hexoses that they generate before the hexoses are communally available. Therefore, in agreement with past studies investigating the influence of competitors on the evolution of cooperation, we find that the presence of a competitor preferentially aids cooperators (274). However, we elevate this finding to show that when the competitor is able to utilise both the primary resource privately and the secondary resource communally, this finding still holds. This is of importance because in a previous study the competitor was effectively acting as a ‘superior cheat’, as it could not utilise the primary resource alone (274). Whereas our study shows that competitors who are not reliant upon the cooperator for resources, as is arguably more common in natural systems, still confer a competitive benefit to cooperators. On the other hand, our results do contrast with findings investigating the influences of competitors on cooperation when the competitor can also consume the primary resource, sucrose (274). This contrast is caused by the fact that if the competitor consumes sucrose ‘privately’ it prevents exploitation by the ‘non-producers’.

Figure 4.13

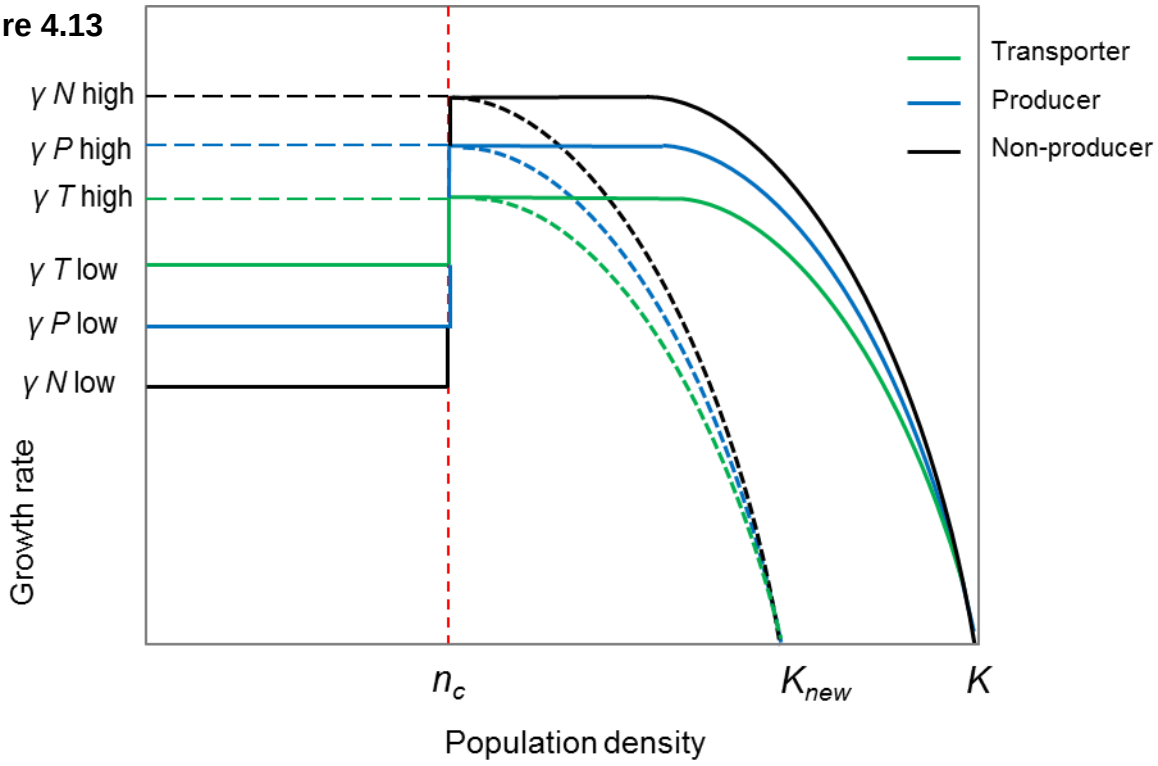

Figure 4.13 | Phenomenological model to describe the two-phase population growth model of polymorphic sucrose-metabolism in yeast. To model the population dynamics of three yeast strains with polymorphisms in sucrose utilisation, a growth model, generated to describe the dynamics of 'producer' and 'non-producer' strains alone (274), was extended in the present study to three strains. As shown experimentally in this study and previously, yeast growth by osmotrophic metabolism of sucrose is lower at low cell densities than at higher densities (Figure 4.9) (14, 274, 289). This results from the population level glucose/fructose creation rate from sucrose hydrolysis. At low densities, when the environment is lacking easily consumable hexoses produced from external catabolism, the 'producer' (γ*P* low) has a higher growth rate than the 'non-producer' (γ*N* low) (Figure 4.4) owing to the preferential access it gets to the hexoses it produces before they diffuse into the communal environment (in 25 mM sucrose ≈ 0.9 % whereas in 2.5 mM ≈ 4.0 %). The 'transporter' (γ*T* low) has a higher growth rate than the producer at low densities as it does not experience an Allee effect (its growth rate on sucrose does not depend on population density) like the 'producer' does (Figure 4.9).

When the population density reaches a threshold (n_c), growth rate is higher for all strains because hexoses are generated more rapidly as invertase secreting 'producers' accumulate (Figure 4.9). Past this critical density when monosaccharides have accumulated, growth rates are expected to more closely reflect those measured in glucose (i.e. 'Non-producer' > 'Producer' > 'Transporter') (Figure 4.2 & Table 4.1) owing to the cost of invertase production avoided by the 'Non-producer', and the additional cost of 'Transporter' production. The growth rates then decline logistically to zero as the population density reaches its carrying capacity (*K*), as

resources are exhausted. Alterations in the initial conditions of the batch cultures, therefore, influences the relative length of these two-phases during a batch culture, and hence the fitness of strains. This can include the initial cell density, relative frequencies and/or resource concentration. For instance, increasing resource concentration helps 'non-producers' by prolonging the length of the second phase, as well as reducing the differences in growth rate during the initial phase between 'non-producers' and 'producers' due to the proportion of hexose liberated for communal use being higher. Likewise, reducing the resource concentration will favour 'transporters' by curtailing the second phase because of a lower carrying capacity (K_{new}) (as indicated by dashed lines). Furthermore, these abiotic alterations can also result from the influence of the strains themselves. For instance, a high frequency of 'non-producers' will prolong the low-density period so enable the 'transporters' to persist in environments where they would otherwise be excluded by 'producers'.

4.2.8 | The impact of public-good cheats on diversity

Guided by pairwise competitions between 'producers' and 'transporters', we asked what impact the presence of 'non-producers' would have on the dynamic between competing strains for a single limiting resource. During pairwise competitions, we observed the reversal from negative frequency-dependent selection, suggesting coexistence between strains (Figure 4.7), to positive-frequency dependent selection, suggesting that either strain will dominate the other depending on the initial frequencies (Figure 4.8). Therefore, how will social cheats for secreted invertase influence this interaction? 'Producers' and 'transporters' were competed at 1:1 starting frequencies in an environment that during pairwise competitions resulted in 'producers' competitively excluding the 'transporters' (Figure 4.8). However, we found that when 'non-producers' were present in the population the three strains were able to coexist over the course of the 26 d transfer experiment (Figure 4.14). The 'non-producers' preferentially aided the 'transporters' by consuming hexoses, so reducing the communal resource pool, and increasing the length of the low density

growth phase and hence the period of low growth rate while the environment lacks easily available hexoses. This process is corroborated by the fact that with increasing density of ‘non-producers’, an increasing preference for selection in favour of the transporter occurs (Figure 4.14).

Figure 4.14

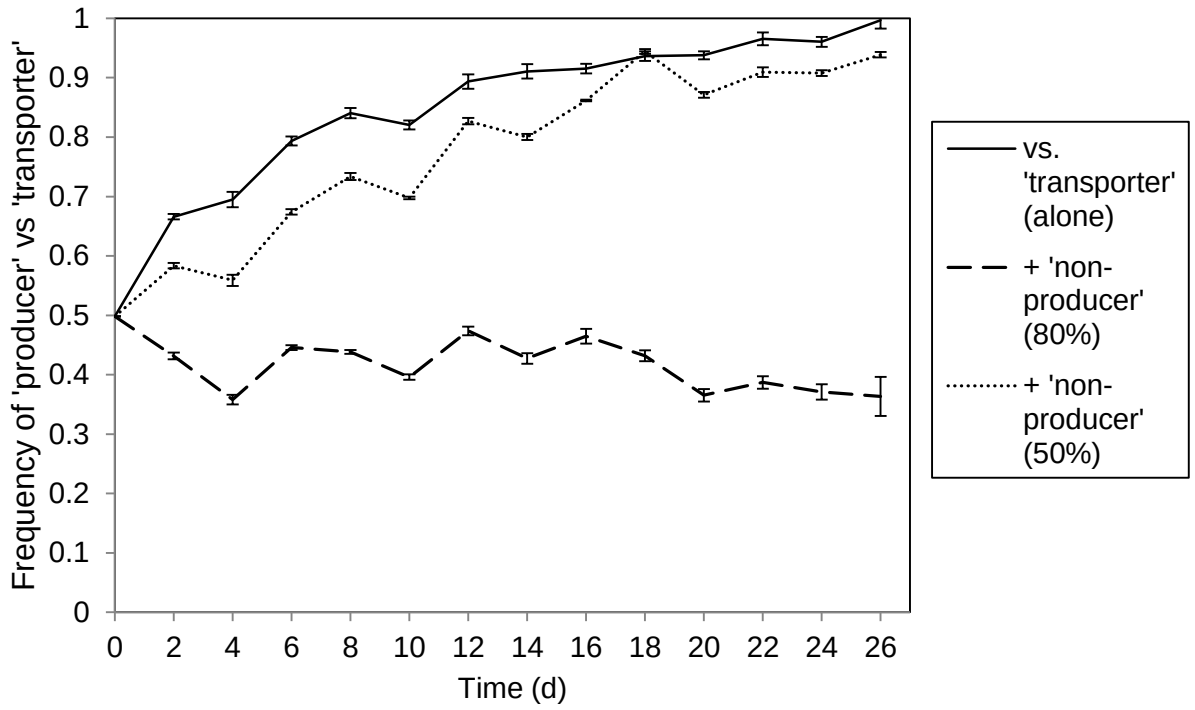

Figure 4.14 | The presence of a social ‘cheat’ (‘non-producer’) stabilises coexistence between two competitors. Mixed strain populations were initiated in 10 mM sucrose SMM, with ‘transporters’ + ‘producers’ at 1:1 initial frequencies, in the presence or absence of ‘non-producers’. All populations had equal starting total densities (≈ 1.26 x 10^5 cells.mL^{-1}). ‘Non-producers’, when present, were introduced at a starting frequency of either 50 or 80% of the total population. As expected from single season frequency dependence tests (Figure 4.8), when ‘producers’ and ‘transporters’ were competed alone from equal frequencies, ‘producers’ dominated and excluded ‘transporters’ from the population. However, when ‘non-producers’ were introduced they buffered the coexistence between ‘transporters’ and ‘producers’. Mean ± s.e.m., n = 3.

Moreover, when the resource concentration was artificially lowered in competition assays to simulate the effect ‘non-producers’ have upon the nutritional environment,

the ‘transporter’ outcompeted ‘producers’ at a range of initial frequencies (Figure 4.15). Therefore, these results suggest that social exploitation, commonly thought to be a damaging force to communities, can have the positive effect of promoting community diversity by limiting the power of an otherwise superior competitive force.

Figure 4.15

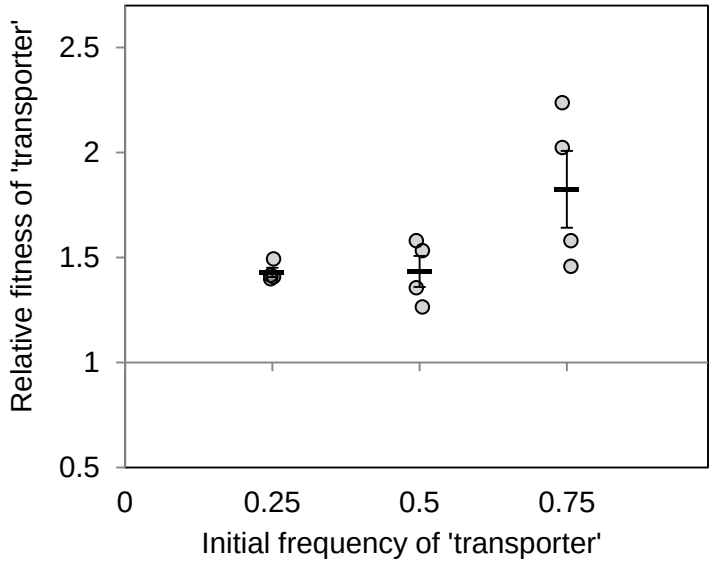

Figure 4.15 | Artificially simulating the influence that cheats have upon the nutritional environment displays that ‘non-producers’ favours selection for ‘transporters’. To mimic the influence of ‘non-producers’, pairwise competitions between ‘producers’ and ‘transporters’ were performed at a reduced resource concentration (2.5 mM sucrose). In this environment ‘transporters’ out-competed ‘producers’ over a range of initial frequencies ($p < 0.021$, one sample t-test at each initial frequency). Grey circles show each data point with added x-axis artificial noise to help visualise the points. Initial frequencies were 0.25, 0.5 and 0.75. Dashes show mean ± s.e.m., n = 4.

4.3 | Discussion

Our study has found that internalising sucrose metabolism, by shifting a public-good to a private-good, can successfully exclude cheats who would otherwise exploit cooperative extracellular digestion. Though generated artificially, we found that there were multiple fitness consequences of internalising sucrose metabolism in the *S.*

cerevisiae ‘transporter’ strain. The findings in our study provide insight into the reasons of why osmotrophy is such a widespread and seemingly successful feeding strategy. On the positive side, in addition to preventing social exploitation, in a spatially unstructured environment, internal metabolism is successful for low population density and resource concentrations as demonstrated when in direct competitions with secreted invertase ‘producers’ (Figure 4.7). Furthermore, resource use efficiency is amplified in ‘transporter’ strains as a consequence of the rate-efficiency trade-off experienced during consumption. Therefore, maximal population benefit may be favoured by internal metabolism (Figure 4.2 & 4.3).

Negatively, in terms of fitness of ‘transporters’, the consequences of internal metabolism includes a reduced growth rate in axenic culture (Figure 4.2 & Table 4.1). To see if this lower growth rate resulted from low expression of the *SRT1* gene, we constructed an expression vector for the *SRT1* gene under the regulation of the strong constitutive *GDP* promoter (201). However, no increase in growth rate over regulation by the *PMA1* promoter was observed (data not shown). Furthermore, at high population densities transporters, again, seem to be at a disadvantage once external hexoses have accumulated, a factor that is amplified when resources are plentiful. So overall, it appears that the competitiveness of either strategy is dependent upon the environment and the population demography.

Our finding of how the fitness of cooperators is dependent on the nutritional environment, leads to an evolutionary dilemma for the ‘producers’ in terms of evolving more efficient invertase genes. On the one hand, increasing efficiency is likely to support ‘producers’ in competition with ‘transporters’ as it reduces the negative influence of the Allee effect. However, in this three-genotype system,

increasing efficiency will concurrently increase the incentives for ‘non-producers’ to defect and rely upon the cooperative actions of others.

Furthermore, the *in vitro* nature of these experiments, coupled with the non-native or non-‘tuned’ gene regulation and efficiencies of an introduced transporter and the modified internalised invertase, may influence factors associated with adaptations to the natural conditions in which these strategies evolved. Therefore, to understand how this mode of nutrition acquisition influences fitness in a more natural context will require further examination, which we investigate in Chapter 5.

By generating a three-way polymorphic system to study sucrose metabolism, we were able to address questions concerning the evolution of cooperation and how diverse feeding strategies can be maintained. This was achieved whilst being able to understand the precise mechanisms behind the relative fitness of each strategy and the subsequent population-level dynamics. We found that in well-mixed environments, the presence of a competitor for a cooperatively metabolised resource can preferentially enhance the relative fitness of cooperators by increasing the relative ‘selfishness’ of public-goods (Figure 4.12 and section 4.2.5). We found this to result, firstly, from a larger proportion of the hexoses liberated from sucrose being captured by the ‘producer’, following reductions in the primary resource concentrations. Secondly, competitors aid cooperation by limiting the phase of the batch culture where population density and hexose concentrations are high, which preferentially favours ‘non-producers’ (14). Our finding is in contrast to a study examining the influence of a competitor who, like the cooperator, also externally metabolises sucrose (274). On the other hand, our finding is in agreement when the competitor only utilises the hexoses produced from sucrose hydrolysis (274).

Cooperative siderophore producing *P. aeruginosa* had their competitiveness enhanced over 'non-producers' by the presence of competing strains, who also generated their own 'private-good' to utilize a limiting resource (276). However, on the contrary, *S. aureus* competitors have been shown to cause increased siderophore production by *P. aeruginosa,* which favours 'non-producers' (275). As a result of these contrasting experimental findings, no general rule can be made about how all competitors will influence the stability of cooperation. Yet, previous findings in combination with those revealed by our study suggest that the competitor's impact on the nutritional environment is crucial. If the competitor generates a product, either directly or indirectly, which the 'non-producers' can exploit, then it preferentially helps social cheats (274, 275). On the other hand, if the competitor 'privately' consumes the limiting resource, as found with the 'transporter' strain in our study, it reduces the incentives to socially 'defect' (274, 276). Our study highlights the importance of understanding the nature of interactions involving competitors when examining their influence upon cooperation, because the details can drastically reverse the outcome.

The non-transitive hierarchical competitiveness of the three strains that we employed also reveals that the presence of social defectors can buffer the coexistence between strains with opposing feeding strategies, when otherwise one of the strains would dominate (Figure 4.14). This was found to be caused by reducing the 'power' of a superior competitor by amplifying the period where the 'producer', as a result of a social feeding strategy, suffers a low growth rate because of low population density and/or resource concentrations (Figure 4.13).

By establishing our results with modifications in particular metabolic strategies, in a common genetic background, we could pin-point the factors behind our findings without having to unravel complex interspecific fitness measures, and the associated

problems of antagonistic secondary metabolites (54) and pH intolerances (e.g. (274)). Our transporter strain is not unduly artificial. The sucrose transporter is from the fungal plant pathogen *U. maydis,* which possesses a yeast-like stage of its dimorphic life style (290). Furthermore, when treating the strains as 'species', the fact that the 'transporter' can utilise the public-goods of 'producers' is comparable to natural systems where the secreted products can be used across microbial species (274, 275). Our findings highlight that competition can both stabilize cooperation by decreasing incentives to cheat (Figure 4.12), and that cheats can also enable the coexistence of different metabolic polymorphisms by limiting the superiority of stronger competitors (Figure 4.14). Genetic diversity yields advantages to ecosystem processes, such as by facilitating nutrient recycling (5), as well as enhancing the relative competitiveness of populations through maximising efficiency (85), and antibiotic-mediated competitor exclusion (79). Consequently, understanding the forces that can influence diversity, such as those examined here, have importance for ecosystem processes that humans are reliant upon, as well as revealing forces that enhance the stability of cooperation.

4.4 | Methods

4.4.1 | Media and strain storage

Long term storage of strains was in 25 % glycerol stocks at -80 °C. Strains were routinely cultured on YPD media, which is 10 $g.L^{-1}$ yeast extract, 20 $g.L^{-1}$ peptone and 20 $g.L^{-1}$ glucose (± 16 $g.L^{-1}$ agar for solid media). For selection and growth experiments examining resource use and competitiveness, strains were grown in SMM (5 $g.L^{-1}$ ammonium sulfate, 1.7 $g.L^{-1}$ yeast nitrogen base (w/o ammonium

sulphate or amino acids), 20 mg.L^{-1} histidine, 50 mg.L^{-1} lysine) containing agar no.2 (16 g.L^{-1}), when necessary, and glucose (111mM) for routine growth, which was replaced with sucrose (or glucose), at varying specified concentrations depending on the experiment. This medium was used so that the carbon source could be easily manipulated and so that the media was lacking uracil to maintain selection on retention of the various modified NEV-E plasmids (containing *URA3*). Strains were revived on SMM + glucose agar plates at 30 °C.

4.4.2 | Yeast strains used in this study

Strains (Table 4.2) are all derived from the secreted invertase (*SUC2*, GenBank: CAA24618.1, UniProt: D5MS22) producing wild-type strain DBY1034 (a segregant from the ninth backcross of a series of backcrosses to introduce the *ura3-52* marker from Francois Lacroute strains into the S288c background, (Prof. Marian Carlson, Columbia University, personal communication, 20 Nov 2014). The invertase non-producing strain, DBY1701, was used as a 'non-producer' or cheat strain (199). A signal sequence mutation *suc2-438* was introduced in *SUC2,* resulting in a deletion from amino acid 4-19, so that invertase produced remained within the cytoplasm (199). To this strain (DBY2617) a sucrose transporter gene (*SRT1*) from the plant pathogenic fungus *U. maydis* had been introduced so that sucrose could be metabolised internally (172). *SRT1* had been introduced into DBY2617 using the shuttle vector NEV-E (Figure 4.16a), where expression was driven by the plasma membrane ATPase gene promoter (P_{PMA1}) (200) that contains the marker *URA3,* restoring uracil prototrophy. In order to observe the fitness consequences resulting from trophic interactions between strains during sucrose metabolism in a common environment, a method was developed to distinguish between strains and to establish the frequency of each from mixed populations. To maintain a common

genetic background of each strain, apart from their sucrose metabolism strategy, and to equal nutritional requirements in terms of amino acid auxotrophy and maintaining selection pressure upon the NEV-E:*SRT1* vector to ensure that it is not lost from strains, DBY1034 and DBY1701 were transformed with the same plasmid, NEV-E, containing the fluorescent proteins *eYFP* or *mCherry* respectively. The NEVE-E plasmid contains sequences of the 2µ plasmid, which include an origin of replication and a partitioning element. This sequence enables plasmids to be propagated with chromosome-like stability with a copy number of 40-60, and near equal distribution between mother and daughter cells (291, 292). Fluorescent protein expression was driven with the constitutive promoter of the glyceraldehyde-3-phosphate dehydrogenase gene (P_{GPD}) (201), replacing P_{PMA1} of the original NEV-E vector (200) (Figure 4.16b) because it did not drive sufficient expression to observe fluorescence signal after examination of transformed strains by epifluorescent microscopy.

Table 4.2 | Strains of *S. cerevisiae* used during this study

Strain name	Genotype	Reference
DBY1034 (‘producer’)	*MATa his4-539 lys2-801 ura3-52 SUC2*	(199)
DBY2617 (‘transporter’)	*MATa his4-539 lys2-801 ura3-52 suc2-438 SRT1*	(199) (172)
DBY1701 (‘non-producer’)	*MATa his4-539 lys2-801 ura3-52 SUC2-Δ9*	(199)

4.4.3 | Plasmid construction

The NEV-E plasmid (Figure 4.16a) was modified by conventional cloning with a ligation of a P_{GPD} *Hind*III/*Eco*RI fragment, *mCherry* or *eYFP Eco*RI/*Eco*RI fragment and a plasma membrane ATPase gene terminator (T_{PMA1}) *Eco*RI/*Bam*HI fragment

into the NEV-E backbone (Figure 4.16b & Table 4.2). Fragments were initially PCR amplified using proof-reading Phusion Taq Polymerase (NEB Inc., USA) and cloned using StrataClone PCR Cloning Kit (Stratagene). The fragments were ligated into the StrataClone Vector by combining 3 µL of StrataClone Cloning Buffer with 2 µL (5-50 ng) of PCR product and 1 µL of StrataClone Vector Mix. This reaction was incubated at room temperature for 5 mins. A 1-2 µL aliquot of this reaction mixture was mixed into a thawed tube of Strataclone SoloPack® Competant cells which was placed on ice for 20 mins. The transformation mixture was then heat-shocked at 42 °C for 45 sec then returned to ice for 2 min. A volume of 250 µL of 42 °C LB medium was added to the mixture that was incubated at 37 °C with 225-250 r.p.m. to allow the cells to recover. Cells were then plated onto LB-ampicillin plates overlaid with 40 µL of 2 % (w/v) X-gal (5-Bromo-4-chloro-3-indoyl-β-D-galactopyranoside in dimethylformamide) and incubated overnight at 37 °C. White or light blue transformants were assessed for plasmid DNA analysis by colony PCR and/or restriction digestion analysis of miniprep DNA to identify transformants possessing the correct plasmid. The desired fragments excised from the plasmid were then ligated into the NEV-E vector. Ligation was performed using T4 DNA ligase (Promega) according to manufacturer's instructions using a 3:1 molar ratio of insert:vector DNA for each fragment. Reactions were performed in a total volume of 10 µL with 100 ng of vector DNA, 3u of T4 DNA ligase and incubated for 3 h at room temperature. The resulting plasmid was transformed into StrataClone SoloPack® Competant cells. Thawed competent cells had 2 µL of the ligation reaction added to and gently mixed before being incubated on ice for 20 minutes. The transformation mixture was heat-shocked at 42 °C for 45 sec, then returned to ice for a further 2 min. A volume of 250 µL of LB at 42 °C was added to the mixture and the cells were

allowed to recover for 1 h at 37 °C with 225 r.p.m. The cells were plated onto LB-ampicillin and incubated overnight at 37 °C. Transformants were assessed by colony PCR with primers GPDp_F_Hindiii and mCherry_R_EcoRi to check for both the presence of the plasmid, and correct orientation of the *mCherry* or *eYFP* *Eco*RI/*Eco*RI fragment. This plasmid was transformed into strains DBY1034 and DBY1701. Transforms were assessed by colony PCR and fluorescence verified by epifluorescent microscopy (Olympus IX81) (Figure 4.16c).

Table 4.3 | Primer sequences used to construct plasmids for promoter driven fluorescent protein tags.

Primer name	Nucleotide sequence (5' - 3')
GPDp_F_Hindiii	AAGCTTTTACGTTGTAAAACGACGGCCA
GPDp_R_EcoRi	GAATTCAAGACTAACTATAAAAGTAGAA
mCherry_F_Ecori	GAATTCTTATGGTGAGCAAGGGCGAGGA
EYFP_F_Ecori	GAATTCTAATGGTGAGCAAGGGCGAGGA
eYFP_mCherry_R_EcoRI	GAATTCAATTACTTGTACAGCTCGTCCA

Figure 4.16

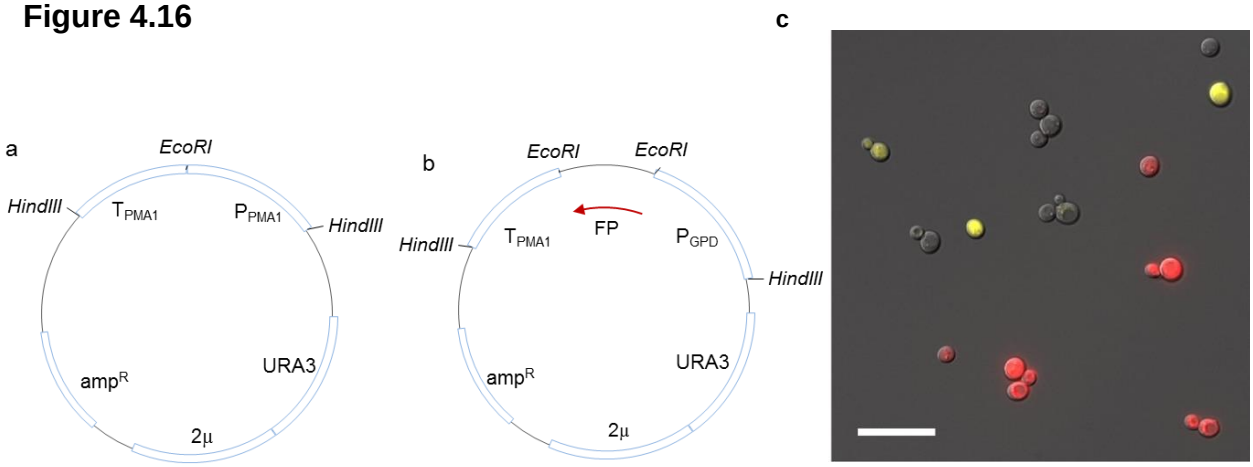

Figure 4.16 | Yeast strains were distinguished based on a fluorescent protein tag. a The original NEV-E shuttle vector (200), conferring ampicillin resistance (amp^R) and the *URA3* marker. **b** The modified vector developed for promoter driven fluorescence expression. The *PMA1* promoter (P_{PMA1}) was replaced with the GPD promoter (P_{GPD}). Fluorescent proteins (FP) were cloned into the *EcoRI* restriction site between the promoter and the PMA1 terminator (T_{PMA1}). **c** Epifluorescent micrograph of the mixed strain population showing the *eYFP* tagged DBY1034 invertase producing strain ('producer'), the *mCherry* tagged DBY1701 non-invertase producing strain ('non-producer') and the non-fluorecently tagged DBY2617 + P_{PMA1}:*SRT1* internal sucrose metabolising strain ('transporter'). Scale bar = 30 μm.

4.4.4 | Growth assessment and mixed strain competitions.

Cultures were initially grown overnight in 5 mL SMM + glucose inoculated from a single colony on an SMM + glucose agar plate. Cells were pelleted at 2000 r.p.m for 5 min., supernatant removed and resuspended in 10 mL of sdH_2O, subjected to centrifugation again at 2000 r.p.m. for 5 min and supernatant discarded again. The pellet was resuspended in 5 mL of SMM (+ C-source and concentration depending on experiment). This culture was diluted down until an optical density (620 nm) of 0.30 was achieved measured using a spectrophotometer (Jenway 7300). The starting culture was then prepared as a 1/20 dilution of this culture which equates to ≈ 1.26×10^5 cells.mL^{-1}, from which strain were mixed at the appropriate frequencies for each experiment. Competition cultures to test the influence of higher population density were initiated with ≈ 2.52×10^6 cells.mL^{-1}.

Growth experiments were performed in 48-well CELLSTAR® suspension multiwell plates (Greiner bio-one) using a volume of 640 µL per well at 30 °C with continuous shaking at 700 r.p.m., except when readings are being taken, in a FLUOstar OMEGA microplate reader (BMG Labtech). To minimise evaporation and prevent cross contamination between wells, the plate was covered with sterile polyester sealing

film (VWR international) that was pierced to permit gas exchange. Optical density (OD) was measured at a wavelength of 620 nm. Fluorescence intensity (FI) of *mCherry* was measured with excitation filter of 584 nm and emission 620 nm. FI of *eYFP* was measure with excitation filter of 500 nm and emission 540 nm. These fluorophores were selected as they have sufficiently distinct emission and excitation spectra so cross-talk was not detected (Figure 4.17a). For multiple season transfers, cultures were grown until population density had appeared to have saturated to allow maximal resources to be consumed. Seasons were either 24 h or 48 h depending on starting density and resource concentrations as specified with each experiment. The portion of the population that was transferred to fresh media each season was dependent upon the growth conditions but was calculated to approximately replicate the starting density of each initial season. For 'high density' treatments, 4 % of the population was transferred (25.6 μL per well). For 'low density' treatments 0.2 % of the population was transferred (1.28 μL), except for treatments with 2.5 mM sucrose where due to lower population growth 0.5 % was transferred (3.2 μL).

Frequency of strains was determined based on the presence of a constitutively expressed RFP (*mCherry*) or YFP (*eYFP*) with the proportions determined based on the equation:

$$X_1 = \frac{FI - (OD.FIB)}{(OD.FIF) - (OD.FIB)}$$

Where $X_1 = frequency\ of\ pNEV-E :: GPDp :: mCherry\ or\ eYFP\ carrying\ strain$

$FI = fluorescence\ intensity\ of\ population\ (mCherry\ or\ eYFP)$

$OD = optical\ density\ of\ population\ (620nm)$

$$FIB = fluorescence\ intensity\ of\ RFP/YFP\ blank\ population$$

$$FIF = fluorescence\ intensity\ of\ RFP/YFP\ population$$

When present, the remaining proportion of the population was designated as the non-fluorescent protein bearing 'transporter' strain DBY2617 + P_{PMA1}:*SRT1*.

Verification of this method for population composition was verified by combining actively growing populations of the three strains at equal densities (5.24 ± 0.03 s.e.m. x 10^4 cells.μL^{-1}) at known frequencies. The resulting populations were measured by the above method. For measurement against expected values of the *eYFP* expressing strain R^2 = 0.987 and for *mCherry* R^2 = 0.997 therefore corroborating this method of determining strain frequencies from mixed populations (Figure 4.17b).

The fluorescence signal expressed during the growth cycle was driven by the constitutive *GPD* promoter (201). It was found to drive strong expression during growth which was linear to population density. However, given that gene expression relies upon metabolic energy, this linear relationship was lost as population growth reached stationary phase (Figure 4.17c). Therefore populations were assessed for strain frequencies at a stage of the growth cycle where the relationship between fluorescence intensity and cell density were linear. This was at approximately 4.6 x 10^4 cells.μL^{-1}, except for when resources were < 10 mM [sucrose] (or equivalent (% w/v) glucose) when a density of approximately 3.2 x 10^4 cells.μL^{-1} was used as exponential growth ceased at lower total densities than at higher resources.

Given that the Δ*suc2* 'non-producer' strain does not proliferate substantially on sucrose media. Pure cultures to monitor fluorescence intensity were inoculated into

glucose media. Fluorescence measurements of the invertase producing strain were found to be equivalent on either carbon source (Figure 4.17d).

When growing untagged strains, we found that cells emitted a small degree of autofluorescence for *eYFP* measurements and had an absorptive effect on *mCherry* measurements (Figure 4.17e). Therefore, for blank measurements of the populations, in addition to using uninoculated media to monitor contamination, untagged 'transporter' strain was grown as a blank to correct for this noise. The FI measurements from the untagged 'transporter' strain were equivalent to the FI intensity of the FP tagged strains when measured under the opposing wavelengths to the FP they possessed. Therefore it was concluded that there was no detected cross-talk between fluorophores and that 'transporter' measurements could be used as a population 'blank' measurement.

Figure 4.17

a

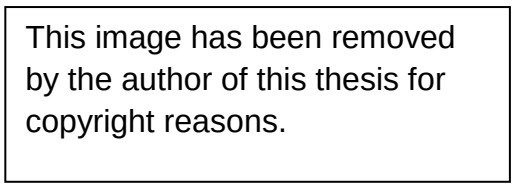

b

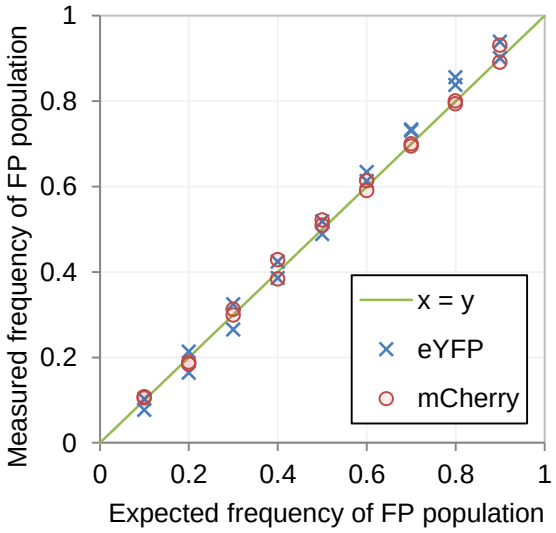

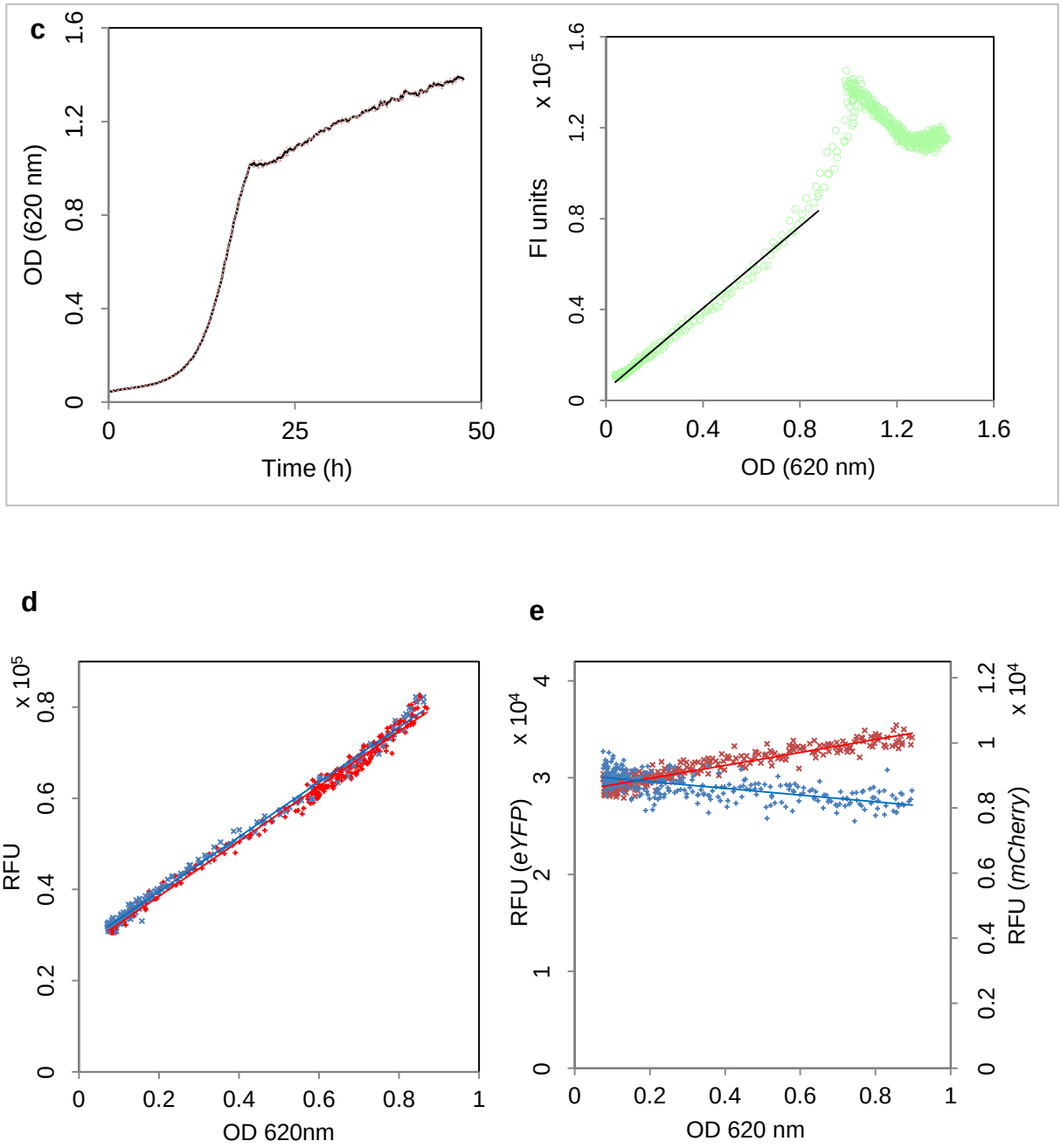

Figure 4.17 | Calibration and verification of method for determining strain frequencies based on fluorescent protein tags. a Fluorescence excitation and emission spectrum of fluorescent proteins used. The peaks of transmission (%T) are distinct between *eYFP* (dark) and *mCherry* (light) for the excitation (blue) and emission (red) spectrums. Fluorescence intensity (FI) of *mCherry* was measured with excitation filter of 584 nm and emission 620 nm. FI of *eYFP* was measure with excitation filter of 500 nm and emission 540 nm. Plot was generated using the 'Chroma Spectra Viewer' tool of the Chroma Technology Corporation (https://www.chroma.com/spectra-viewer). **b** Verification of the fluorescence intensity method to determine strain frequency. Measurement of mixed populations of known density and frequencies against expected values of the *eYFP* expressing strain R^2 =

0.987 and for *mCherry* R^2 = 0.997. **c** *GPD* promoter driven expression of *mCherry* in DBY1701 over growth cycle in glucose SMM. Fluorescence intensity (FI) increases linearly (as indicated with black line) up to approximately OD 0.8 which corresponds with the population approaching the end of exponential growth. Growth curve: mean ± s.e.m., n= 3. FI plot is combined data from three replicates. **d** Expression of *eYFP* in DBY1034 was equivalent in glucose (**+**) and sucrose (**x**) SMM, Relative fluorescent units (RFU). **e** untagged strains emitted a small degree of autofluorescence for *eYFP* measurements (**x**) and had an absorptive effect on *mCherry* measurements (**+**).

4.4.5 | Measurement of cell density

Cell density was calibrated to OD_{620nm} measurements using a method described previously (289). Populations of *S. cerevisiae* were grown to 2.46 x10^5 cells.μL^{-1} and then densities were prepared by 16 serial dilution steps of 0.75 of the original population to bring the density down to the lower limit detectable by the microtitre plate reader (Figure 4.18a). The initial population density was established by CFU count on YPD media. The OD_{620nm} measurement is linear with cell density up to approximately 0.3 above which it saturates towards a maximum reading. Cell density was subsequently calculated by transforming the OD_{620nm} measurements using the equation

$$OD_{real} = -\ln\left[1 - \frac{OD_{620nm} - OD_b}{OD_{max} - OD_b}\right](OD_{max} - OD_b)$$

Where OD_b is the blank measurement of media with no cells which in this measurement is 0.065, and OD_{max} is the maximum recording at saturating cell density which was found to be 1.707. OD_{real} is linear with cell density and OD_{real} 1 corresponds to approximately 4 x 10^4 cells.μL^{-1} (Figure 4.18b).

Figure 4.18 a **b**

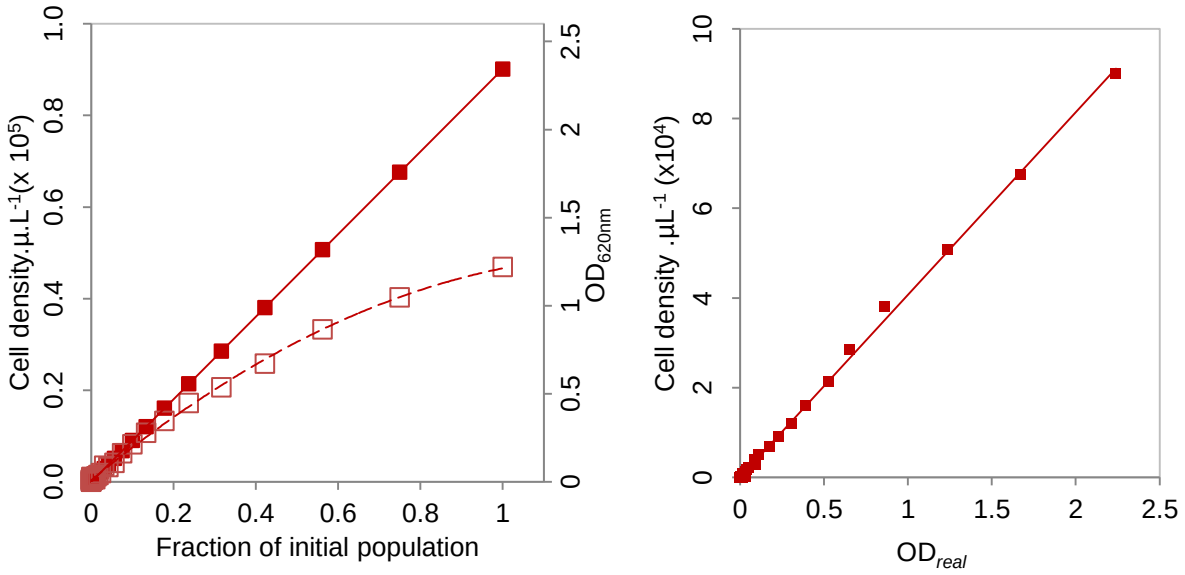

Figure 4.18 | Calibration of OD measurements and conversion to cell density. a Population densities were prepared by 16 serial dilutions of 0.75 from a high density population, the fraction of which is shown on the horizontal axis. OD measurements were taken (open squares) and converted to OD_{real} (solid squares) as described above. **b** After transformation, OD_{real} is linear with cell density (R^2 = 0.9986), OD_{real} = 1 corresponds to ≈ 4 x 10^5 cells.μL^{-1}.

4.4.6 | Determining growth rates of axenic strains

Overall growth rates of yeast strains in glucose and sucrose media were determined in pure strain cultures as described above with an initial density of ≈ 1.26 x 10^5 cells.mL^{-1}. Growth rates were calculated as the Malthusian growth parameter from inoculation to the point where population growth decelerates (measured at the following time points: Transporter *SRT1* strain: glucose = 22.5 h, sucrose = 46.4 h; Producer DBY1034: glucose = 19.3 h, sucrose = 30.7 h; Non-producer DBY1701: glucose = 18.7 h, sucrose = 75.8 h).

4.4.7 | Determining growth rates at ‘low’ density and ‘high’ density

Population density can be accurately determined using OD_{620nm} measurements in a plate reader when measurements are greater than ~ 0.1 which equates to ~ 1.4 x 10^3 cells.μL^{-1}. To measure the growth rate at lower densities, a series of 10 x 0.75 dilutions were performed from a culture of known density, confirmed by CFU count. These diluted populations were then allowed to multiply and the time taken to reach measureable densities by OD_{620nm} and hence Malthusian growth parameters were calculated. For high starting densities, 10 x dilutions from the same series, from OD_{620nm} > 0.1 were employed and growth rates over the equivalent initial periods as the low densities were calculated from absorbance measurements.

Chapter 5

Magnaporthe oryzae invertase as a 'private good'

5.1 | Introduction

The motivation of work in Chapter 5 follows a similar premise to that in Chapter 4, in terms of investigating public- versus private-goods. Therefore, for a more comprehensive introduction see section 4.1.

As shown in Chapters 1 & 2, *M. oryzae* secretes invertase to externally break down sucrose into its constituent monosaccharides to feed and proliferate. As a consequence, it is exposed to exploitation from social 'cheats'. In Chapter 4, we found that when sucrose metabolism was internalised in *S. cerevisiae,* the strain was able to prevent strains that avoided the cost of producing invertase from exploiting the internal invertase that it produced. This resulted in social cheats being competitively excluded from mixed strain populations (Figure 4.6). Given these results, we asked whether this principle could be extended to a fungal plant pathogen, *M. oryzae*. By internalising sucrose metabolism, we sought to examine both the influence of privatising invertase (*INV1*) on the population social dynamics with a 'cheat', but also whether filamentous fungi have evolutionarily 'opted' for an extracellular osmotrophic feeding strategy because of the fitness benefits it yields at the population level (Figure 5.1). Furthermore, we sought to examine the influence of internalising sucrose metabolism on the fitness of a fungal plant pathogen in its natural environment during infection of rice leaves.

Figure 5.1 a public-good b private-good

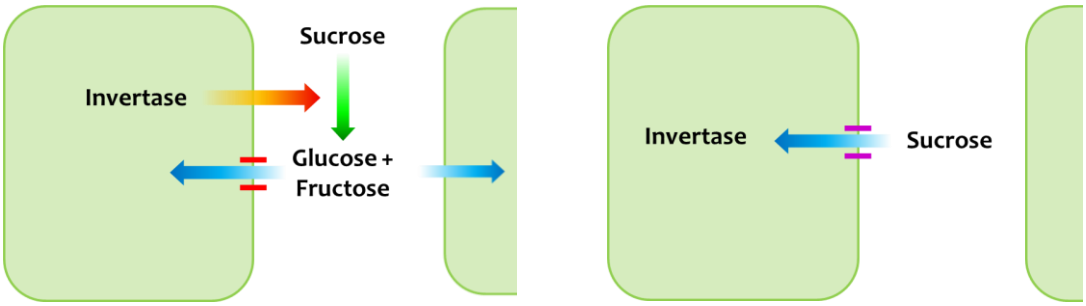

Figure 5.1 | Schematic of invertase mediated sucrose metabolism, a public- or private-good. a Wild-type *M. oryzae* feeds by osmotrophy where it secretes invertase to externally hydrolyses sucrose into its constituent monosaccharides glucose and fructose which are subsequently taken up for internal metabolism. These hexoses are available to social cheats. **b** This study aims to test the individual and population level consequences of internalising this process by not secreting invertase and directly taking up sucrose for internal metabolism to suppress social exploitation.

5.2 | Results

5.2.1 | Internalising invertase

To address these questions, we generated a strain of *M. oryzae*, designated *INV1-sp*, whose *INV1* gene had been modified so that it no longer possessed the signal peptide responsible for the protein to enter the secretory pathway. Signal peptides are found in the N-terminal portion of the amino-acid chain, which is cleaved off as the protein is being translocated through the membrane of the endoplasmic reticulum (293, 294). Deletions of these regions can lead to expression of novel functional intracellular forms of the protein (199).

5.2.2 | Deleting the *INV1* signal peptide affects growth on sucrose media

Phenotypic assessment of the *INV1-sp* strain revealed an altered growth morphology on sucrose minimal media, with a larger region of non-melanised hyphae around the expanding colony and a smaller melanised colony centre relative to the isogenic progenitor strain Guy11 (Figure 5.2). Melanin production can be induced by limiting nutrients to provide protection against environmental stresses (295). We propose that this is the cue in these conditions because otherwise its production could reduce the permeability of cell walls and so block nutrient uptake (295). Therefore, the morphology of *INV1-sp* may result from alterations in sucrose consumption caused by the internalising the invertase gene. In particular, if *INV1-sp* feeds on sucrose more slowly, then it may cause the colony centre to accumulate melanin more slowly, despite the colony diameter extending at a comparable rate to Guy11. This alteration in morphology was complemented when strains were supplied with glucose, which does not require invertase mediated catabolism (Figure 5.2).

Figure 5.2

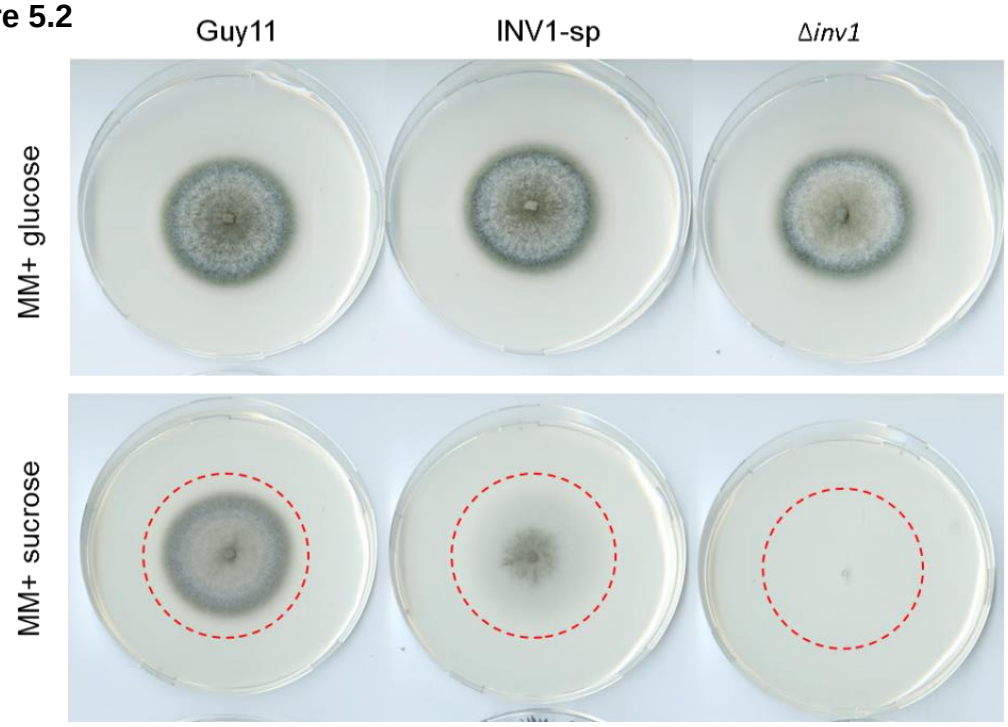

Figure 5.2 | Growth morphology of *INV1-sp*. *INV1-sp* has altered growth morphology on MM + sucrose which is intermediate between wild-type Guy11 and the Δ*inv1* mutant. *INV1-sp* has a relatively smaller melanised colony centre with a larger region of non-melanised hyphae around the expanding colony. This phenotype is functionally complemented on MM+glucose. Red-dashed line indicates the periphery of the fungal colony.

5.2.3 | Deleting the *INV1* signal peptide results in an internal invertase

Now that we had performed an allelic replacement of the *INV1* gene to remove the signal peptide, we tested if this deletion had the desired effect on the location of invertase activity in the *INV1-sp* strain. To examine this, we performed enzyme assays. Assays were designed to distinguish between external and internal activity by measuring the activity produced from the culture filtrate and disrupted mycelial biomass, respectively. We found that the *INV1-sp* strain had significantly reduced external, and increased internal, invertase activity compared to the wild-type Guy11 (Figure 5.3). This indicates that deletion of its signal peptide has resulted in the desired location of the invertase protein.

Figure 5.3

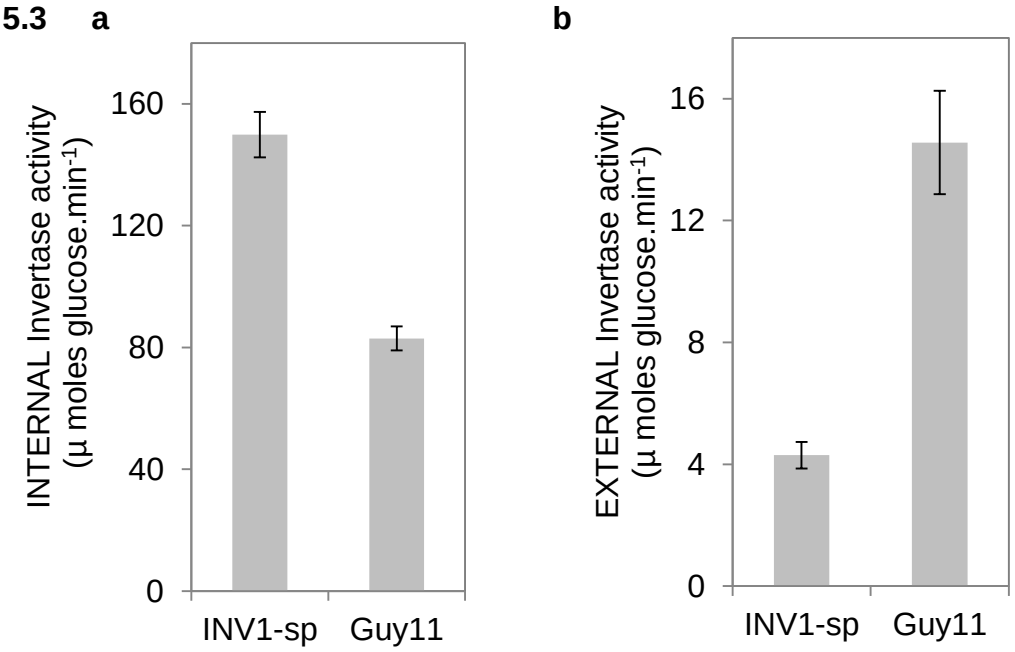

Figure 5.3 | Invertase assay to determine its location in the *INV1-sp* mutant. Enzymatic assays were performed on either the **a** 'internal' fraction (mycelial homogenate) or **b** 'external' fraction (culture filtrate) of liquid cultures of wild-type Guy11 and the signal peptide mutant *INV1-sp.* **a** *INV1-sp* has significantly higher internal invertase activity than Guy11 ($p < 0.003$, $t = 6.92$, two-sided t-test with equal variances) **b** yet Guy11 has significantly higher external activity than *INV1-sp* ($p < 0.005$, $t = 5.85$, two-sided t-test with equal variances). Mean ± s.e.m., n = 3. Note different y-axes scales.

During these enzyme assays, we detected some external activity in *INV1-sp* (Figure 5.3b). This may be attributed to the permeability of filamentous fungal hyphae leading to a portion of the enzyme leaking out, as found when enzymes of the intracellular quinate metabolic pathway were examined earlier in this thesis (Figure 2.6). However, given the significant increase in internal invertase activity in the *INV1-sp* strain, a large proportion of this enzyme is retained intracellularly (Figure 5.3a).

The wild-type strain also displayed substantial, though significantly reduced, invertase activity from the 'internal' assay (Figure 5.3a). This may be caused by protein that has been synthesised but yet to be secreted, or may mean that a portion of the external invertase localises in the periplasm (the space between the cell wall and the plasma membrane) similar to the invertase of *S. cerevisiae* (14, 296), which despite acting extracellularly, would not be differentiated by this assay. In addition, again similar to *S. cerevisiae*, *M. oryzae* may form different isoforms of invertase from a single gene, one secreted and one cytoplasmic (195).

Differing absolute levels of invertase activity, with much higher levels detected in the 'internal' fraction compared to the 'external' fraction (Figure 5.3), may be attributed to the experimental protocols employed. For the 'internal' assay, the fraction was relatively crude with other cell constituents not being excluded by dialysis, as with

the ‘external’ assay. This additional purification step may also have led to a loss of functional invertase (see methods for details).

Despite the enzymes assays that we performed revealing that deletion of the signal peptide of *INV1* did not result in an exclusively internal invertase, we deemed that the location of the invertase activity of *INV1-sp* was sufficient to test the principles of privatising sucrose metabolism, because of the different relative levels between strains.

5.2.4 | Transforming the *INV1-sp* strain with a high-affinity sucrose transporter

Now that we had internalised invertase in the *INV1-sp* strain, we next sought to introduce a permease gene, so that it could internalise sucrose for metabolism. To achieve this, we transformed the *INV1-sp* strain with the *U. maydis* sucrose transporter *SRT1* (172), which was codon optimised for expression in *M. oryzae* (designated *MoSRT1*). Sequence comparisons of *SRT1* against the *M. oryzae* genome gave moderate similarity (< 33 % identity) to a large family of sugar transporters, the majority of which are annotated as maltose or hexose transporters. Expression of this *SRT1* transporter was regulated by the *grg1* (glucose –repressible gene) promoter of *Neurospora crassa*, which has been shown to be highly induced in carbon poor environments (297), with expression still detected in uninduced conditions (298). This promoter was chosen so that expression of the *MoSRT1* transporter would be induced in response to limiting carbon resources so that overexpression did not impose excessive metabolic costs. We found that the *INV1-sp* strain was able to generate substantial biomass in liquid minimal media + sucrose (Figure 5.4). This is in contrast to the invertase deletion strain Δ*inv1*.

Figure 5.4 **a** **b**

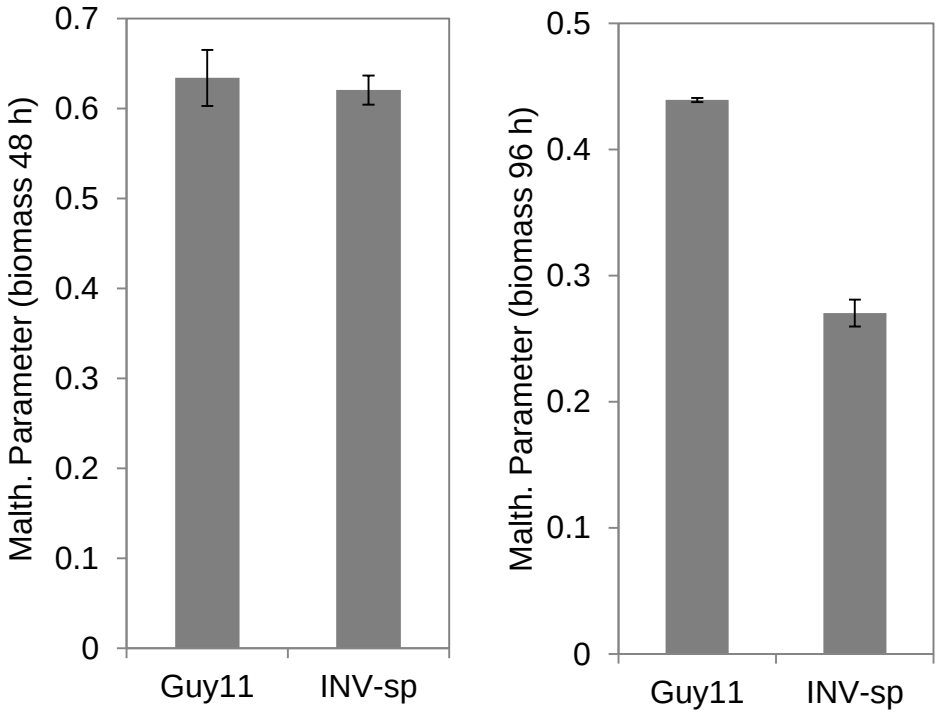

Figure 5.4 | Growth rate measurements of *INV1-sp* compared to Guy11 in sucrose media. Growth rates were measured in terms of dry weight biomass formation in liquid batch cultures of MM+ sucrose (1% w/v). Growth rates are comparable between strains after 48 h ($p > 0.79$, two-sided t-test with equal variances) (**a**) whereas wild-type strain Guy11 has a higher growth rate than *INV1-sp* by 96 h (**b**) ($p < 0.004$, $t = 15.82$, two-sided t-test with unequal variances). Growth rate calculated as Malthusian growth parameter (299) (which assumes constant growth rate). Mean ± s.e.m. **a**: n = 6, **b**: n = 3.

The addition of *MoSRT1* did not visually appear to alter the growth of the *INV1-sp* strain on sucrose agar media (not shown). Given its substantial growth capabilities in sucrose media (Figure 5.4), this was attributed to the *INV1-sp* strain not being limited in carbon resources. This could then lead to either the non-induction of the *MoSRT1* gene, or no substantial increase in resource uptake in these *in vitro* conditions, which may have led to a growth morphology more closely resembling the wild-type. *INV1-sp* may obtain resources by sucrose uptake through native *M. oryzae* transporters

leading to this lack of induction. The *U. maydis SRT1* transporter is highly specific for sucrose transport. To my knowledge the *M. oryzae* sugar transporters have not been functionally characterised, yet most classified transport proteins in plant associated fungi are specific for monosaccharides; primarily facilitating the uptake of glucose and fructose (168-171). These results suggest that *M. oryzae* has the ability to uptake sucrose through at least one of the many predicted sugar transporter genes it possesses (search term “sugar transport” on the *Magnaporthe oryzae* comparative Sequencing Project returned 484 possible matches). However, in a previous study it was reported that sucrose was not detected within mycelia of *M. oryzae,* based on carbohydrate analysis, suggesting that sucrose is not taken up without being hydrolysed first (173). However, interfering with *INV1,* as we have done in our study, may alter whether or not sucrose is taken up by the fungus.

5.2.5 | The ability of internalised sucrose metabolism to suppress invertase cheats in *M. oryzae*

Now that we had generated a strain which synthesised a ‘non-secreted’, internalised invertase, we asked if making invertase mediated sucrose metabolism a ‘private-good’ would be sufficient to stop the Δ*inv1* mutant from exploiting the invertase it produces? To test this we performed pairwise competitions *in vitro* with the Δ*inv1* mutant in conditions that required invertase metabolism (MM+ sucrose). We found that in contrast to the wild-type invertase secretor Guy11 ($m < 1$), *MoSRT1* was able to suppress the competitive advantage that the Δ*inv1* ‘cheat’ strain could gain by not producing invertase ($m > 1$). We found this to be the case over a range of initial frequencies of strains (Figure 5.5).

Figure 5.5

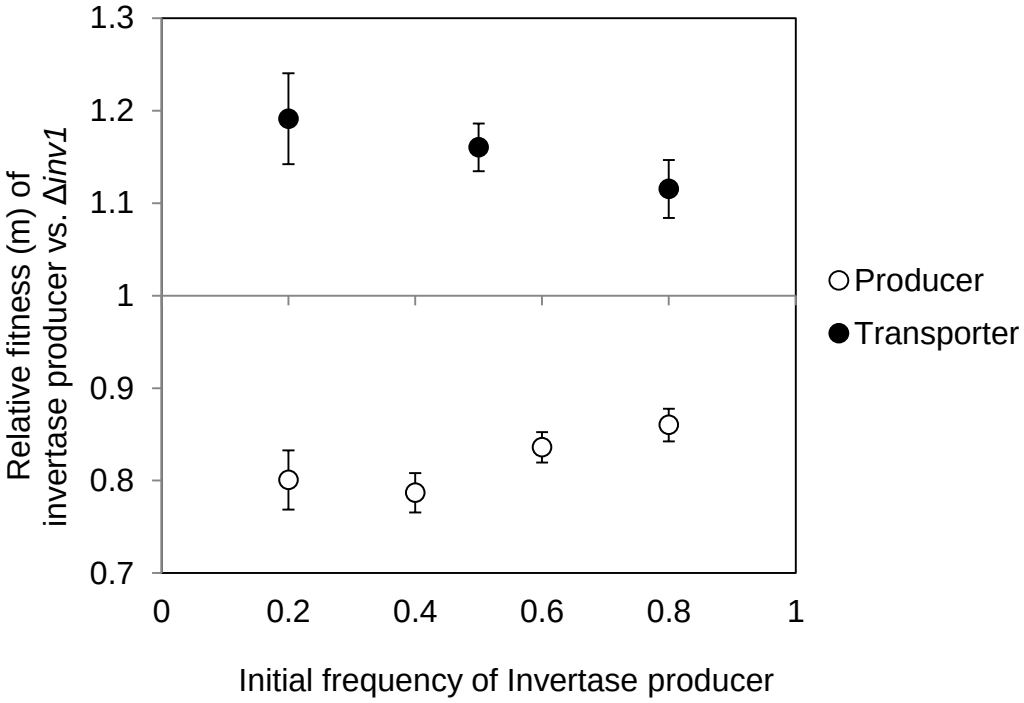

Figure 5.5 | The competitive ability of invertase secreting 'Producer' and non-secreting 'Transporter' strains against the Δ*inv1* deletion mutant. The Δ*inv1* mutant was competed against a strain that was either an invertase secretor (Guy11 – 'Producer') or an invertase non-secretor (*MoSRT1* – 'Transporter') on MM+ sucrose agar plates. The invertase secretor was at a selective disadvantage against the Δ*inv1* mutant ($m < 1$) ($p < 0.0003$, one-sample t-test, re-plot of data from Figure 2.4), whereas the invertase non-secretor (*MoSRT1*) could successfully suppress the exploitation by the Δ*inv1* mutant ($m > 1$) ($p < 0.026$, one-sample t-test). Mean ± s.e.m., $n \geq 3$.

5.2.6 | The Δ*inv1* mutant cannot exploit the invertase of *MoSRT1*

We next sought to verify the causes behind the competitive suppression of the Δ*inv1* mutant by *MoSRT1*. To achieve this we performed growth assays with the Δ*inv1* mutant in culture filtrate that had previously been inhabited by an invertase producing strain (and so contained any 'public-goods' that had been produced). The culture filtrate had been previously occupied by either the wild-type invertase secreting strain Guy11, or the internal invertase producer strain *MoSRT1*. The Δ*inv1*

mutant was found to have a significantly reduced growth rate ($p < 0.0007$, $t = 4.84$, $n = 6$, two-sided t-test with equal variance) when cultured in the supernatant of *MoSRT1* compared to growth on the supernatant of the invertase secreting wild-type strain (Figure 5.6). Furthermore, this growth was not found to be significantly different from growth on the supernatant of the non-invertase producing Δ*inv1* strain ($p > 0.414$, d.f.= 13, two-sided t-test with equal variance, comparison made against data from Figure 2.1). Therefore, together these results show that in pairwise interactions *MoSRT1* can suppress the competitive advantage of cheats by 'privatising' sucrose metabolism and preventing exploitation of its invertase.

Figure 5.6

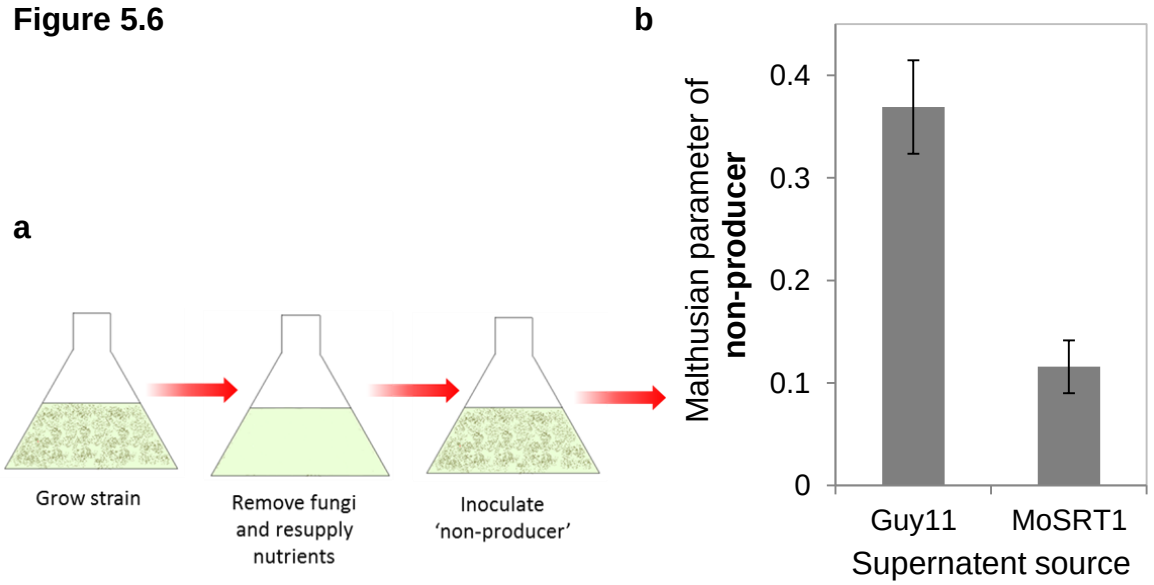

Figure 5.6 | Deletion of the *INV1* signal peptide means that the Δ*inv1* mutant is not able to exploit invertase production to the same extent as with the wild-type secreted invertase of Guy11. The Δ*inv1* mutant was cultured in the nutrient resupplied culture filtrate (MM+ sucrose) of either the invertase secreting Guy11 strain, or the non-secreting invertase producing *MoSRT1* strain, which contains any generated 'public-goods'. **a** Schematic representation of the experimental set up. **b** Malthusian growth parameter of the Δ*inv1* mutant in the resupplied culture filtrate (after 3 d) is significantly reduced with *MoSRT1* ($p < 0.0007$, $t = 4.84$, $n = 6$, two-sided t-test with equal variance). Mean ± s.e.m. data pooled from two repeated experiments.

5.2.7 | Privatising sucrose metabolism eliminates the synergy between invertase 'producers' and 'non-producers'

Having generated and characterised the *MoSRT1* strain, we then asked how making sucrose metabolism a non-cooperative 'private-good' would influence the population fitness in mixed strain populations with the Δ*inv1* mutant, considering the synergy that was observed between secreted invertase producers and non-producers (Figure 2.11a)? The predictions made by the mathematical model of our invertase system (Appendix 2.3 & Figure 2.10) suggest that it was crucial for invertase to be a public-good in order to generate the synergy between trains that we found experimentally (Figure 2.7, 2.8 and 2.11a). In support of our theoretical results, we found that when sucrose metabolism was internalised with the *MoSRT1* strain, the presence of the Δ*inv1* mutant did not result in maximal population fitness (Figure 5.7). Therefore, here we confirm that making invertase mediated sucrose metabolism a private good, and so removing one of the social traits, results in the synergy between strains being lost.

Figure 5.7

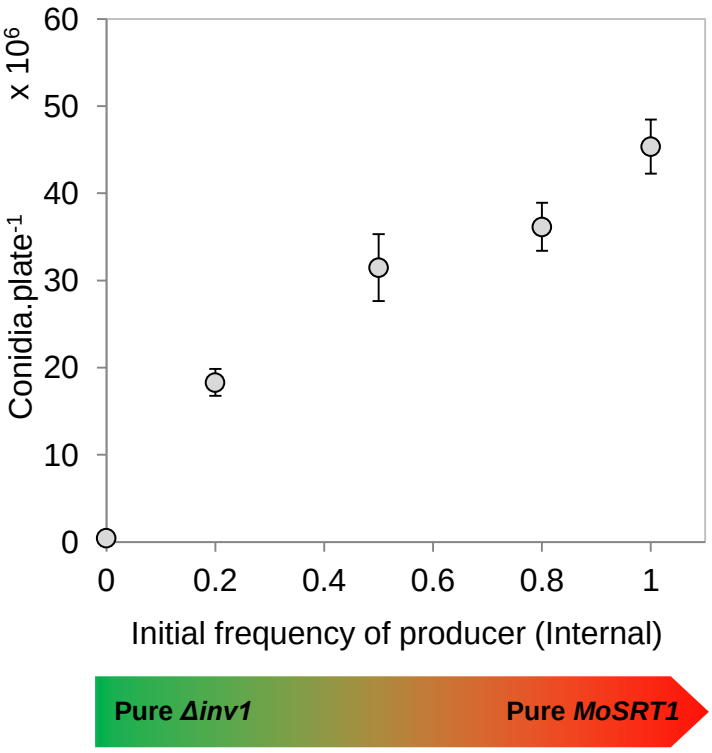

Figure 5.7 | Population fitness of Δ*inv1* and *MoSRT1* alone and in mixed populations. Fitness was measured as conidia generated per agar plate (MM+ sucrose). Unlike with the invertase secreting Guy11 strain, mixed populations of Δ*inv1* with an invertase producing strain did not result in population fitness being maximised when the Δ*inv1* was present with an internal invertase producing strain *MoSRT1.* In this case, population fitness was maximised in pure *MoSRT1* populations ($p < 0.043$, $F_{(4,34)} = 61.5$, one-way ANOVA with post-hoc Tukey's). Mean ± s.e.m.

5.2.8 | Internalising invertase increases resource use efficiency

If privatising a public-good can suppress cheats (Figure 5.5 and 5.6), we asked why *M. oryzae* secretes invertase if it is prone to exploitation? In addition, we asked if an evolutionary trade-off exists that means that secretion gave a competitive advantage over internal metabolism, thereby compensating for this loss to competitors? Firstly, the efficiency of sucrose use was examined in terms of conidia production. We found, however, that *MoSRT1* produced significantly more conidia on sucrose media than the invertase secretor Guy11 ($p < 0.012$, $t = 2.85$, two-sided t-test assuming equal variances, $n = 9$) (Figure 5.8).

Figure 5.8

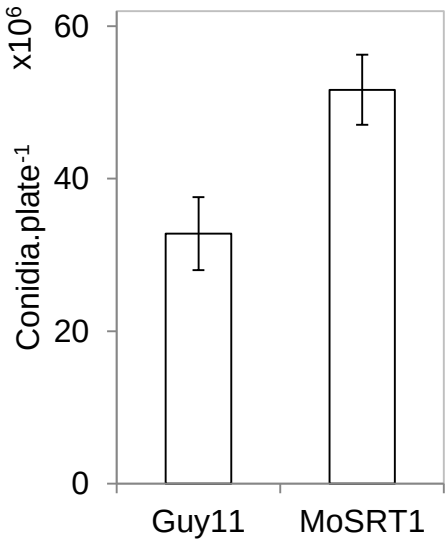

Figure 5.8 | Resource use efficiency in terms of spore production on sucrose media of the invertase secretor and non-secretor. Strains were inoculated onto MM+ sucrose (1% w/v) agar plates and fitness was assessed as the number of conidia produced per plate after 12 d. The invertase non-secretor *MoSRT1* produced significantly more conidia per plate than the invertase secretor Guy11 ($p < 0.02$, two-sided t-test assuming equal variances), n = 9, mean ± s.e.m., data pooled from three repeated experiments.

5.2.9 | The increased resource efficiency coincides with a reduced growth rate

To understand the reasons for the differences in resource use efficiency (Figure 5.8), because *M. oryzae* experiences a rate-efficiency trade-off, which we revealed in Chapter 2 (Figure 2.9), we performed growth rate assays by measuring biomass in liquid media (Figure 5.4). No difference in growth rate was found initially (up to 48 h) ($p > 0.79$, n = 6, t-test assuming unequal variances). However, the invertase secretor had a significantly higher growth rate later (up to 96 h, $p < 0.004$, $t = 15.82$, n = 3, t-test assuming unequal variances). This inconsistency can be explained by the influence of an Allee effect (284), as we found with experiments with invertase secretors of *S. cerevisiae* on sucrose media where growth rates are lower at low density than at intermediate density (Figure 4.9) (268). This density-dependent growth rate is caused by the nutritional environment experienced by the invertase secretor being dependent upon the collective actions of the population to form extracellular hexoses from secreted invertase. This is because much of the hexoses liberated from sucrose are lost to the environment (14). The density-dependent growth rate of the invertase secretor is in contrast to the invertase non-secretor, whose growth rate depends upon its ‘individual’ actions for internal metabolism. Therefore, at lower densities (up to 48 h) the growth rates are comparable (Figure 5.4a), whereas at higher density (up to 96 h) once a hexose rich extracellular

environment has been created, Guy11 has a distinctly higher growth rate (Figure 5.4b). The fact that *MoSRT1* is growing more slowly (Figure 5.4b), coupled with higher conidia production (Figure 5.8), suggests that its sucrose metabolism is shifting toward a higher efficiency in the rate-efficiency trade-off described in *M. oryzae* in Chapter 2 (Figure 2.9).

5.2.10 | The *in vivo* fitness consequences of a shift in the rate-efficiency trade-off

To test whether this increased efficiency of *MoSRT1* is an artefact of the *in vitro* experimental conditions, and that an increased growth rate is of more importance in the pathogen's natural *in planta* environment, fitness and virulence tests were performed during rice infection. We found that *MoSRT1* had increased fitness, in terms of conidia produced per lesion, and increased virulence, in terms of disease lesion area, over the isogenic wild-type Guy11 strain (Figure 5.9).

Figure 5.9

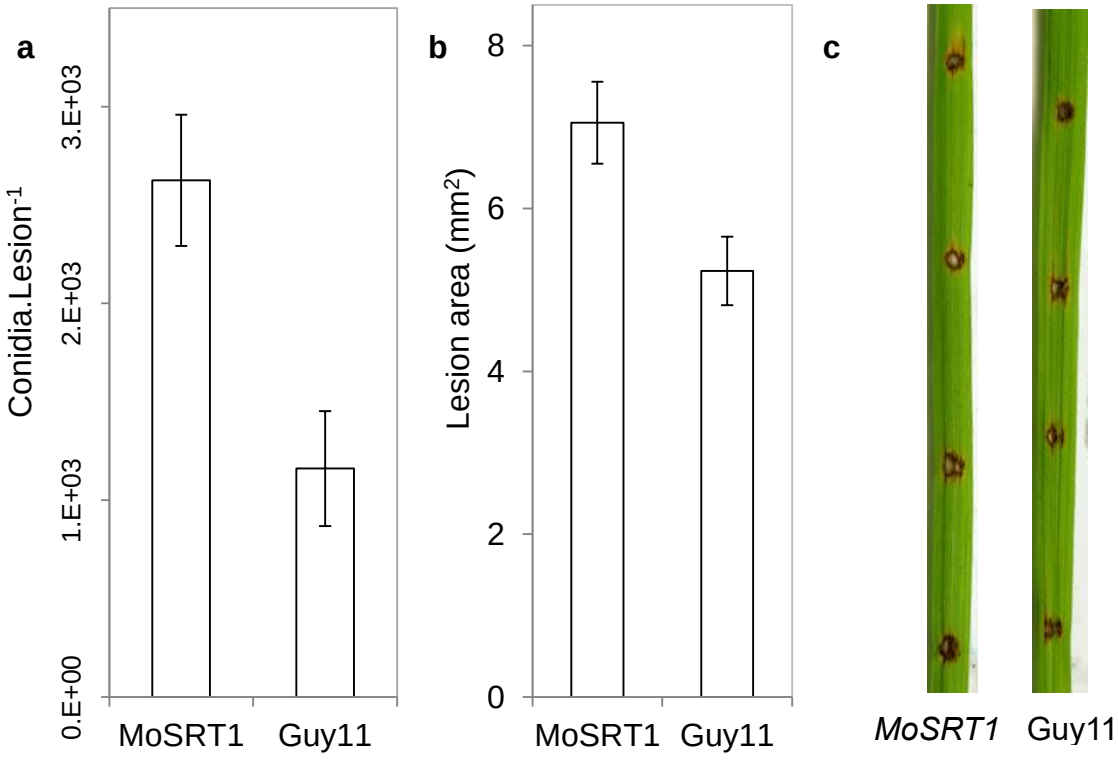

Figure 5.9 | Pathogen fitness and disease virulence of Guy11 and the *MoSRT1* mutant during infection by leaf spot inoculation. a *MoSRT1* has a higher fitness than Guy11 at the end of the disease cycle (9 d.p.i.) in terms of conidia produced per lesion ($p < 0.00172$, $t = 3.30$, two-sided t-test assuming equal variances, $n = 28$). **b** Enhanced fitness also translated into a more virulent infection in terms of lesion area ($p < 0.0086$, $t = 2.27$, two-sided t-test assuming equal variances, $n = 20$). Mean ± s.e.m., data pooled from two repeated experiments. **c** Example lesions from which data was collected.

5.2.11 | The competitiveness of internal versus external sucrose metabolism

So far, the fitness of *MoSRT1* compared to the wild-type has been assessed in single strain inoculations. Therefore, we next asked if the growth rate advantage exhibited by the wild-type strain over *MoSRT1* (Figure 5.4) would compensate for the reduced efficiency in resource use (Figure 5.8), during direct competition between the strains? However, we found that *MoSRT1* retained a fitness advantage over Guy11 during competition on sucrose media (Figure 5.10). Therefore, the fitness advantage gained by *MoSRT1,* through increased resource use efficiency and privatising sucrose metabolism, is greater than the increased growth rate achieved by the invertase secreting wild-type Guy11, with its public sucrose metabolising feeding strategy.

Figure 5.10

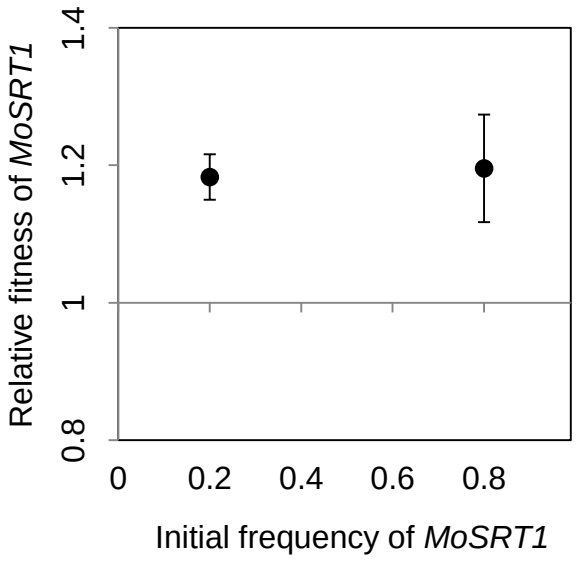

Figure 5.10 | Relative fitness of *MoSRT1* when in competition with Guy11. Mixed strain cultures were established on MM+ sucrose at two initial frequencies (0.2:0.8) and 0.8:0.2) and relative fitnesses were established based on the number of conidia generated. Strains were distinguished by Guy11 being tagged with a GFP (*ToxA:SGFP*). The internal sucrose metabolising *MoSRT1* was fitter than the external sucrose metabolising Guy11 at initial frequency of 0.2 ($p < 0.001$, $t = 5.53$, one-sample t-test) and 0.8 ($p < 0.04$, $t = 2.49$, one-sample t-test). Mean ± s.e.m., $n = 9$.

5.3 | Discussion

In Chapter 4, using a system with *S. cerevisiae*, we found that the fitness consequences of internalising sucrose metabolism depend on the environmental conditions under which the differing strategies are assessed. In Chapter 5, we aimed to test if the findings made with *S. cerevisiae* in Chapter 4 would translate into a filamentous fungal plant pathogen, *M. oryzae*. In this newly developed system, we could test the fitness of private- versus public-good feeding strategies in a more natural nutritional environment *in vivo*.

To test internalised sucrose metabolism in *M. oryzae,* we deleted the signal peptide sequence of the invertase gene, *INV1*. We found that the resulting strain, *INV1-sp*, had altered growth morphology on sucrose media (Figure 5.2) and a modified location of invertase activity, with a significant increase internally and decrease externally (Figure 5.3). Transforming *INV1-sp* with a codon optimised sucrose transporter from *U. maydis*, *MoSRT1,* did not substantially alter the strain's growth morphology on sucrose media. This suggests that *M. oryzae* may be able to uptake sucrose through other sugar transporters that it possesses.

Unlike with the wild-type invertase secretor, this 'private' metabolism enabled the strain to prevent a non-invertase producing strain (Δ*inv1*) from gaining a fitness

advantage over it by not paying the cost of invertase production (Figure 5.5). This exclusion was found to be caused by the Δ*inv1* not being able to exploit the invertase produced by others (Figure 5.6).

In Chapter 2, we experimentally found a synergistic effect between invertase secretors and non-producers. Our mathematical model predicted that public-good sucrose metabolism was crucial for this synergy. Using our internally metabolising strain, we were able to verify this prediction experimentally by eliminating the synergy between invertase producers and non-producers when sucrose is metabolised 'privately' (Figure 5.7).

We next examined the fitness of consequences of internalising sucrose metabolism for *M. oryzae*. We found that the internally metabolising strain has an increased efficiency in resource use (Figure 5.8), which coincides with a reduced growth rate (Figure 5.4). This suggests that as a consequence of a differing feeding strategy, the *MoSRT1* strain has shifted its position on the rate-efficiency trade-off towards higher efficiency. We, therefore, examined what this meant in terms of fitness consequences during infection and during direct competition with the invertase secreting strain, Guy11. We found that *MoSRT1* has an increased fitness and virulence during rice leaf infection (Figure 5.9) and a competitive advantage over the wild-type (Figure 5.10). The finding that *MoSRT1* has enhanced fitness during infection and imposes a more virulent infection (Figure 5.9), suggests that *M. oryzae* is sub-optimally adapted in terms of resource use efficiency when consuming sucrose during infection. In addition to increased resource use efficiency of the *MoSRT1* strain (Figure 5.8), which may be sufficient to explain the enhanced *in vivo* pathogen fitness and disease virulence, the finding may be compounded by a delay in the induction of plant defences against the non-invertase-secreting *MoSRT1*

strain. This is because plants have evolved means of sensing changes in apoplastic monosaccharide concentration brought about by pathogens' osmotrophic metabolism, which in turn switches on plant defence responses (300). So internalising sucrose metabolism, as we have generated in the *MoSRT1* strain, may partly mask the presence of the pathogen, resulting in a more successful infection. This will require more experimental work to verify if rice defences are indeed lessened during *MoSRT1* infection, which could be achieved by monitoring ROS production after staining with 3,3-diaminobenzidine tetrahydrochloride (DAB) as described previously (91).

The expression of the *MoSRT1* gene also requires further investigation to determine its contribution towards the fitness measures obtained in our study. The *U. maydis* sucrose transporter *SRT1*, has extremely high affinity to sucrose meaning that it can efficiently compete for sucrose in the environment. Whether the expression and affinity of this transporter is comparable in our transformed strain of *M. oryzae* will reveal how much of its competitive ability results from effectively sequestering sucrose from the environment and making it inaccessible to other competing strains. This could be achieved by measuring gene expression in the *MoSRT1* strain and relative uptake of radiolabelled sucrose.

Monoclonal populations of *M. oryzae* are fitter and more virulent when they feed by their non-native strategy of internal metabolism, demonstrating the efficiency constraints upon the wild-type when it feeds by osmotrophy. In order to gain further insight into the evolutionary fitness of osmotrophy for sucrose metabolism, it would be pertinent to perform mixed genotype infections with *MoSRT1* and Guy11. Such mixed inoculations would reveal if the outcomes of the *in vitro* competitions and the single strain infections from in this study are relevant to more complex and natural

environments. This would help to understand why wild-type strains of *M. oryzae* still feed by secreting invertase, given the flaws revealed in this study. The deletion of a signal peptide is a relatively simple genetic alteration, which could be expected to occur in nature from mutation, so further study would be required to reveal any negative impact of internalised invertase and why it is currently not known to exist in wild populations of *M. oryzae*.

5.4 | Methods

5.4.1 | Construction of the invertase non-secretor strain *INV1*-sp

Modification of the *M. oryzae INV1* gene was achieved by allelic replacement of the native ORF. This was performed by constructing a vector with a modified coding sequence that omitted the signal peptide, achieved by cloning four DNA fragments into the backbone vector pSC-B-amp/kan by In-fusion cloning. The signal peptide was identified using the identifying software SIGNALP 4.1 (188). Results indicated a cleavage site between amino acids 19 and 20 (Figure 1.4). PCR primers to amplify the DNA fragment containing the *INV1* gene were designed so the nucleotide sequence contained the ATG start codon followed by the sequence from amino acid 20. This fragment extended 0.5 kb beyond the stop codon to include the 3'UTR. Between this and a 1 kb RF region, a 2.8 kb sulfonylurea resistance selectable marker (*ILV1*)(202) was cloned. Upstream of the *INV1-sp* fragment was the native *INV1* promoter region (Figure 5.11 and Table 5.1). Prior to transformation into *M. oryzae* strain Guy11, the cloned four-fragment DNA sequence was excised from the vector with *EcoRI*. Allelic replacement was achieved by homologous recombination between the promoter and RF regions of the vector, and their corresponding

chromosomal regions. Transformants were screened for growth deficiencies on MM+ sucrose.

Figure 5.11

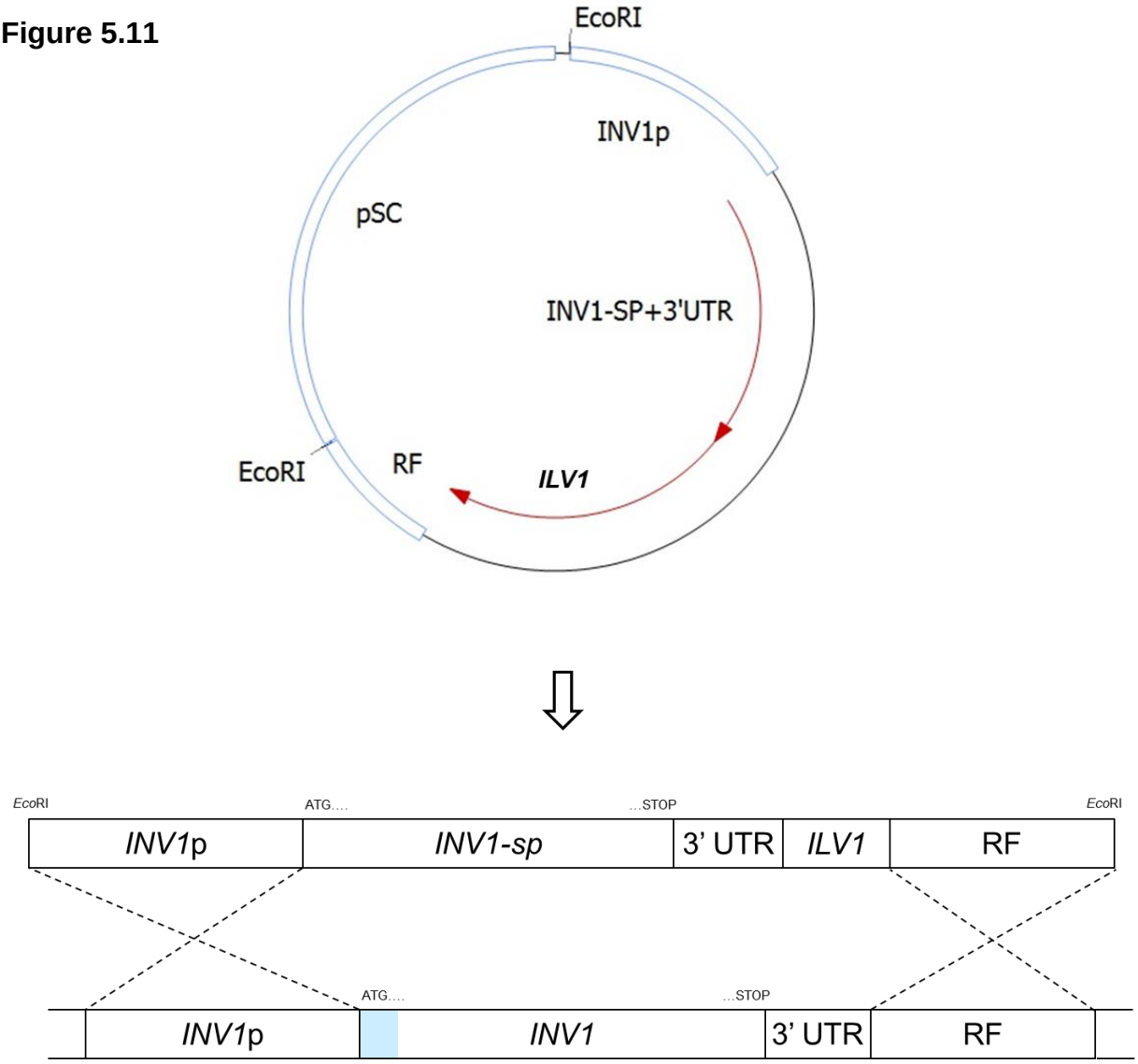

Figure 5.11 | Schematic of strategy to generate a strain with a non-secreted invertase (*INV1-sp*). Four fragments were cloned into the plasmid pSC-B-amp/kan by In-fusion cloning. These included a 1.8 kb native promoter region (INV1p), a sulfonylurea resistance allele (*ILV1*) for transformant selection, and a 1 kb right flank region (RF) to facilitate homologous recombination between the vector and complementary chromosomal regions of the genome. Internalisation of *INV1* was achieved by allelic replacement of the native *INV1* ORF with a fragment containing the native ORF minus the signal peptide (amino acids 2-19) (*INV1-sp*). The transformation vector was excised from the plasmid prior to transformation into *M. oryzae* (Guy11) by restriction digestion with *EcoRI.*

5.4.2 | Construction of the *MoSRT1* expression vector

The *U. maydis* sucrose transporter gene *SRT1* was codon optimised for expression in *M. oryzae* using the 'reverse translate' tool of the Sequence Manipulation Suite (http://www.bioinformatics.org/sms2/rev_trans.html) with the codon usage table for *M. oryzae* obtained from The Condon Usage Database (http://www.kazusa.or.jp/codon/). The resulting gene was called *MoSRT1* (see appendix 5.1 for nucleotide sequence). The DNA sequence was synthesised *de novo* and cloned into the plasmid pEX-K4 (eurofins Genomics), from which the sequence was amplified by PCR for downstream cloning. The *M. oryzae* codon optimised gene was cloned into an expression vector by In-fusion cloning (Figure 5.12). The vector was constructed in the plasmid 1284 (pNEB-Nat-Yeast) backbone. Expression was regulated by the *grg1* (glucose –repressible gene) promoter of *N. crassa* (297). This was followed by the *MoSRT1* ORF and the *trpC* terminator of *A. nidulans* (301, 302). Transformants were selected for based on resistance to bialophos (Basta) conferred by the phosphinothricin acetyltransferase gene (*BAR*) (202).

Figure 5.12

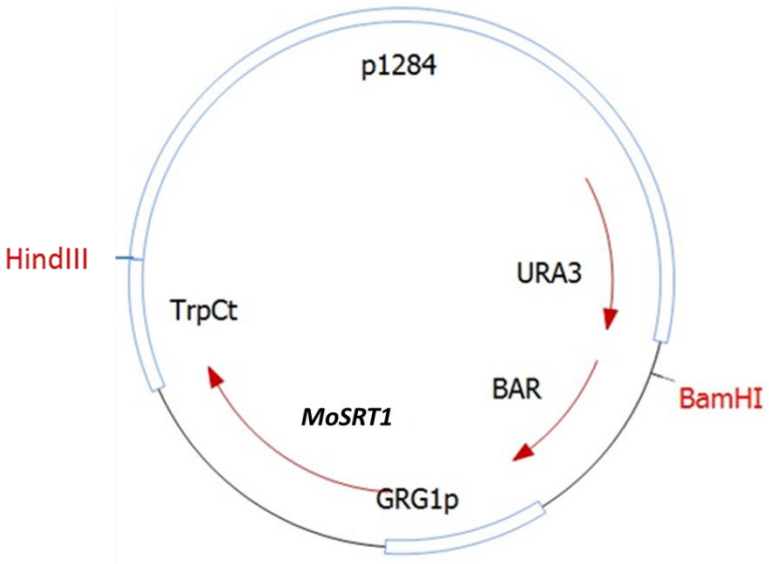

Figure 5.12 | Plasmid map of the vector constructed for the expression of the *M. oryzae* codon optimised *U. maydis* sucrose transporter *SRT1.* See text section 5.3.2 for construct details.

Table 5.1 | Primer sequences for generating the invertase secretion deficient strain *INV1-sp* and transformation of the *U. maydis* sucrose transporter *SRT1*
Underlined regions indicate complimentary regions for In-fusion cloning.

Primer name	Nucleotide sequence (5' - 3')
PINV1_F_pSC	ATCCACTGTGGAATTCCAGATTATGTGTATGGCGGC
PINV1_R_IF	CATCGTGCTGGTATTATTAA
INV1_ORF-SP_F	AATACCAGCACGATGCAAGCCCCTCCGGTGCCCCA
INV1_3UTR_R	ATGTCGGCTGTCTTTCTCCA
SUR_F_INV1	AAAGACAGCCGACATGTCGACGTGCCAACGCCACAGTGC
SUR_R	GTCGACGTGAGAGCATGCAATTCC
INV1_RF_F_SUR	TGCTCTCACGTCGACAGGGATGAATTTGTGATAATACCG
INV1_RF_R_pSC	GCCCAATGTGGAATTCCATGTTAAAATAAACTCTTGCCAC
BAR_F_p1284	GCAGGCATGCAAGCTGTCGACAGAAGATGATATTGAAG
BAR_R	GTCGACCTAAATCTCGGTGAC
GRG1p_F_BAR	GAGATTTAGGTCGACGGCCGCTAGAAGGAGCAGTC
GRG1p_R	ATTTGGTTGATGTGAGGGGTT
MoSRT1_F_GRG1	TCACATCAACCAAATATGGCTAGCAGCTCTCCTATC
MoSRT1_R	TTACTGGGGCGACGGTTGCA
TRPC_F_MoSRT1	CCGTCGCCCCAGTAACTGAAATCATCAAACAGCTTGA
TRPC_R_p1284	TGATTACGCCAAGCTAGTGGAGATGTGGAGTGG

Appendix 5.1 | Nucleotide sequence of the *MoSRT1* gene synthesis product:

5’ ATG GCT AGC AGC TCT CCT ATC CGT GAG TCC GTG TCC GTT ACT CCC TCG ATC TCC
TCG ACC CAG GCC AAG CCC AAG GTC TGG AGC ATC AGC GTC TTT GTT ACC GTC ATT ACC
ATC GCT CTC TCT GGT GCC ACC TAT GGC CTC GAG AAC TCG CTC ATG TCC CCT CTT GCG
GCC ATG CCG GAG TTT GTC AAG AAG TAC CAG GGC CTG AAC AGG GAG ACT CGC AAC
TAC ACC TTC ACC GCC CGC CAT CAG TCG ATG ATC TTC AGC ATC CCA CTC ACA GGA ACC
ATC GCT GGT GCC CTG GTT TCG CCC TAC CTT CAG AAC CGT CTG GGA CGT AAG TGG TCG
CTC TGT GCC GCC TAC ATG TTC TCG ATC CCC TCC ACG CAG CTC CAA CTG TGG GCG CCT
AAC CTC GCC GCG TTC ATT CTC GGT CGT GTT ATG AAC GGC CTT GCC TAC GGC TGT GCC
CTC TCT ATC GGC CCA CTC TAC CTC GCA GAT GTT GTC CCG ACA TCG ATT AGG GGC GGT
GCC GTT GCA TCG TCC AAC CTC CTC ACC ATC CTT GCC AAC CTC ATG GCC GCC ATC TGC
TGT TGG GCC ACT GAA GGC CAC TAT TCG GGC GCG AGG AAG TAC AAG ATC CCC TTG
GCG GTT CAG GCC GGA CTT CCC TTC CTC CTC CTG TTG CCG ACT CCC TTC TTG CCT GAA
TCG CCG GTG TGG TGT GTT CAG AAG GGT CGT ATT GGC GAA GCG CGC ATG GCT CTC
CAG CGC GTT CGT CCC GTC AGC GAT CGC GAG ATC GAG GAT GAG CTT CAG GAG ATT
GTC CGC GCT GAG CAA GAG CGT CGT ACG CTC GCC AAG GAC ACA AAG TTC ACC GAC
ATT TTC AGC CGT AAG CAC CTC TTG CGT ACG GTC GTT GCC GGT AGC TTC TTT AGC CTC
AAC CAG ATC TCG GGC ATC ATC CTC TCG ACC ACC TAT GCC ACC GTG TTC CTG ACC CAA
CTC GGC CTT GGT GAC CCT TTT GTC CTC ACT GTC TAC GCC TAC ATT TGC CAG GTC GTC
GGA GCT GCC CTG GCC ATC GTT GCG CTC GAG AAG GTC GGT CGC AGA TCG TTG GCT
CTC CCC GGT TTC GTC ATT CTG ACC ATC ATC GAC TTC GCA GCC GGT GTC CTC GCT TTC
TAC ACG AGC AAC CCG AAC GTC GCT AAG GCC ATC TCG GCC CTG GCC ATG GTC TTT AAC
TTT GTC TGG ACT CTC TGC TTC TAC AGC ATC TCG CTC CTT ATG CCA TCG GAG CTT CCG
ACG CAA CGC CTT AGG AAC TAC ACC ATG AGC TAC GCC ATT GGT TGG GGT CAG GCT ACC
GCC GTC GTC ACC ACC TTG GTC CTT CCC CAG ATC ACA GCT ACC GAC GCT GGC AAT CTG
GCT GCA AAG GCC TAC CTC ATC TTT GGT GGT TGT ATG CTT GTG ATC ACG ATC CTC GCG
TTC TTT CTC CTG CCG GAG ACT AGG GGT CGT ACG TTC TTC GAG ATT GAC CAG CTG TAC
TCC AAC AGA GTT CCC GCC TGG AGA TGG TCT AAG TTC GAG CTG GGC CGT ACC AGC
GGA TCG TTC CCT TCG GAA CAC GGT TCC TAC TTC GAG TCG GAT TCC CGT GCA GTC GGC
CTG ATT TCG GTC GAC AAG AAG TCC GGC TAT CAC ATT TCG CCC GAG ACT CTG CAA CCG
TCG CCC CAG TAA – 3’

Chapter 6 | General Discussion

Our study set out to address fundamental questions concerning microbial ecology and evolution. We aimed to gain a deeper understanding of the evolution of feeding strategies and metabolic polymorphisms in pathogens. We sought to test a nascent disease management strategy based on understanding of evolution and ecology, and the implications that these factors have for disease virulence. In order to overcome complications of unravelling the natural complexity of field experiments, model microbial systems for ecology were established and developed. We deployed a synthetic ecology approach where ecological theory was combined with molecular and genetic techniques to establish novel tractable and trackable synthetic microbial ecological systems. This enabled the study to pinpoint the genetic basis of the observations made. We could also manipulate the *in vitro* experimental conditions to verify predictions made by mathematical models, which were developed to explain the empirical findings. By being able to distinguish known genotypes of mixed strain populations, we could monitor their evolutionary trajectories to make longer term predictions about the populations, beyond the timescale of our experiments. Having established a model microbial system to study ecology in a plant pathogenic fungus, we were also able to bring back a degree of natural realism to our study by performing ecological experiments during infection. The environment in which the organism naturally exists could then be more closely replicated. As a result, the relevance of our model system was elevated beyond purely an *in vitro* environment, which often does not closely represent the natural conditions in which organisms evolved or adapted.

We aimed to test a promising virulence reduction strategy based on the principles of cooperation and competitive exclusion theory (2, 25, 26). We targeted a gene for

producing a socially available product that contributed to both the success of the pathogen, and the degree of damage that it inflicted upon its host plant. Given that fungi feed by secreting enzymes to externally digest complex molecules, the products of which are absorbed for metabolism (161, 220), we targeted an enzyme, invertase, which is responsible for digesting a primary carbon source for plant pathogenic fungi (164, 165). Using genomic data and genetic techniques established for targeted gene replacement (145, 146), a single invertase gene was identified and deleted. We found that this gene was responsible for the entire invertase activity of *M .oryzae* during standard *in vitro* growth conditions, which translated into a significant reduction in the fitness and virulence of the pathogen within its wild host. To our knowledge, this is the first functional identification and characterisation of invertase in what is considered the most scientifically and economically important fungal pathogen in molecular plant pathology (18).

Having developed an invertase null mutant Δ*inv1* in Chapter 1, in Chapter 2 we initiated mixed-strain infections of rice plants to test this novel disease management strategy based on competitive exclusion (2, 25, 26). However, contrary to existing theory and laboratory (87, 88, 112), agricultural (47-52) and clinical examples (45, 46) of the success of this strategy, we found that a mixture of the low-virulence mutants with the virulent wild-type actually amplified the fitness and virulence of the pathogen above infections initiated purely with the virulent wild-type strain. A mathematical model was generated to understand the reasons behind this unexpected result. We found that the pathogen has multiple interacting social traits, which influence fitness during sucrose metabolism. Our mathematical model predicts that it is the interaction between these traits that leads to the synergy that we observed between invertase producers and non-producers. In addition to the social

dilemma arising from public-good invertase production, we found that *M. oryzae* experiences a secondary social trait of prudent use of resources (76, 77). To verify the predictions of our model, we designed and performed experiments to test various assumptions of the model and the existing social evolutionary theory upon which this strategy is based (58).

We firstly experimentally confirmed that invertase production by *M. oryzae* represents a public-good trait as defined by existing theory, and that the fungus also experiences a resource use efficiency trade-off in relation to resource supply. To see if the interaction between these traits was sufficient to explain the synergy, using *in vitro* experiments to permit manipulation of the conditions, we firstly established an environment that recreated the synergy observed *in planta.* These conditions were then altered to remove or minimise various factors that were understood to be essential for the observed synergy. By altering the resource use inefficiency, spatial structuring or the necessity of public-good production, the synergy between strains was lost. Therefore, we verified the model developed and the mechanism behind our unexpected result.

Beyond our synthetic system, this finding has widespread applicability given how widespread multiple social traits are expected to be (35, 36, 85, 109, 211, 215). It is particularly pertinent to pathogens, including fungi, who feed by secreting a huge range depolymerising enzymes, which are predicted to coincide with a rate-efficiency trade-off, because they are considered to be unavoidable (77, 93, 141, 161, 220). Furthermore, with developing technologies in genetic manipulations, the idea of generating synthetic strains to be deployed for disease management represents a real possibility for future strategies (228).Therefore, this study provides a mechanistic framework for assessing potential new deployments of less-virulent

strains for disease management, and an understanding of how they can fail with potentially devastating consequences for infected hosts.

Building on Chapters 1 and 2, in Chapter 3 we sought to explore the generality of our finding with invertase of *M. oryzae,* by examining another metabolic enzyme, but this time for obtaining nitrogen from hosts. We generated a protease deletion mutant Δ*asp1.* We found that this mutant had a fitness and virulence defect during infection of rice plants. However, no synergy was observed between the deletion mutant and the wild-type like we had previously in Chapter 2 for *INV1*. As with invertase, we examined the physiological function of this gene. We found that, unlike invertase, the *ASP1* protease did not represent a public-good trait. Rather, it functioned intracellularly and so was a 'private-good'. As a consequence, the protease mutant did not represent a viable strain to implement for virulence reduction strategies by competitive exclusion. This is because it was unable to socially exploit the wild-type strain, so was outcompeted during plant infection and hence it is not expected to persist in the population. Despite this drawback, we examined the function of this protease. By generating a fluorescent protein fusion vector combined with fluorescent dye staining and live-cell imaging, we found *ASP1* to function within the vacuoles of the appressorium of *M. oryzae*. Here it is thought to function either as part of the autophagy machinery where it recycles cellular components to facilitate fungal proliferation in the absence of exogenous nutrients. Alternatively, given its homologue in *S. cerevisiae* (255-257), it may function as an activator of other hydrolytic enzymes in the vacuole. Identifying and characterising *M. oryzae* genes involved in successful infection will help build a broader understanding of the disease process. This in turn can help develop durable disease management strategies.

Considering how widespread extracellular feeding is in microbes, we next sought to address why the strategy is seemingly so successful given that it open to exploitation by social 'cheats', who do not pay a metabolic cost for its production. As we have seen previously in Chapter 2, polymorphisms in osmotrophic metabolism can result in maximal population fitness, but would it be possible to suppress 'cheats' by making sucrose metabolism an internal 'private-good'? Furthermore, how would an organism that feeds 'privately' fare in competition with the native 'public' feeder, and what would the population level consequences of these strategies be? To address these points, in Chapter 4 we developed a microbial ecological system in which the opposing strategies could be tested in a common genetic background, using the baker's yeast *S. cerevisiae.* As predicted, the internally metabolising 'transporter' strain successfully repressed 'non-producer' cheat strains. However, the competitiveness of the 'transporter' relative to the externally metabolising 'producer' was found to depend upon both the resource concentrations experienced as well as whether fitness was assessed in terms of growth rate or carrying capacity.

Now that we had characterised this three-way polymorphic system for sucrose metabolism, we next used it to answer other questions concerning the evolution of cooperation and the maintenance of diverse feeding strategies. Numerous factors have been examined and revealed to maintain cooperative traits, despite the fact that they are exposed to cheats who defect from paying the cost of cooperation (Section 1.1.7) (58-60, 107). These include frequency- (204) and density- (270) dependent selection and obtaining preferential access to the benefits generated from the cooperative behaviour (14). However, because public-good cooperation is often studied in isolation relative to an organism's naturally complex environment, we asked how the presence of a competitive 'species' for both 'primary' and 'secondary'

resources, yet who did not alter the common nutritional environment beyond depleting resources, would influence the success of being cooperative? Existing evidence for a consensus on the influence of competitors on cooperation is not obvious, because there are cases where both positive and negative effects have been reported (274-276). We found that the presence of our 'competitive species' enhances the relative fitness of cooperators by reducing resource concentrations. Reduced resource concentrations increased the 'selfishness' of cooperating by enabling cooperators to obtain a larger portion of the generated benefits and so reduce the incentives to socially defect. Therefore, the influence of competitors on the fitness of cooperators appears to depend on the details of the competitor. In particular, how the competitor alters the environment relative to the cooperative trait. If the presence of a competitor results in an increase in the 'public-good' then the cheat is helped (274, 275), whereas, if it depletes the environment's resources privately, as occurs with the 'transporter' strain that we used as a competitor, then the cooperator is fitter (274, 276).

When examining the fitness consequences of internal or external sucrose metabolism in *S. cerevisiae*, we found evidence of an Allee effect (284) present for external, but not internal metabolism. This stems from the fact that external digestion relies much upon the metabolic activities of other individuals in the population. This results in a transfer from negative to positive frequency-dependent selection with changing resource concentrations. This means that there was a shift from a situation where strains could coexist at an intermediate frequency, to where either strain would dominate and exclude the other depending on the initial frequencies. Therefore, we found that coexistence of otherwise excluding competitors could be established, or at least stabilised, by introducing cheats who exaggerated the

influence of the negatively acting Allee effect upon the otherwise superior invertase secreting ‘producer’.

Based upon the findings we made with the yeast polymorphic system in Chapter 4, we next sought to test what the implications of internalising sucrose metabolism would have in a fungal plant pathogen in Chapter 5. By examining internal metabolism in *M. oryzae* we could examine the fitness implications in conditions more closely resembling nature. This then aimed to reveal which feeding strategy was more favoured over the course of plant infection, given that either strategy appears to give different advantages in different environments. To do this, a strain of *M. oryzae* was generated with internalised sucrose metabolism, *MoSRT1*. As with *S. cerevisiae, MoSRT1* was able to suppress social exploiters and had a higher efficiency in resource use over the wild-type external invertase producer. This, again, came at the expense of a reduced growth rate. It was revealed that during infection, the increased efficiency of *MoSRT1* seemed to outweigh any cost of reduced growth rate, based on a more virulent infection and increased sporulation at the end of the disease cycle. This finding suggests that *M. oryzae* is sub-optimally adapted in resource use within hosts, which may be augmented by *MoSRT1* preventing host defence being triggered by extracellular glucose signalling (300), but this requires further investigation to confirm. Even in direct competition during *in vitro* experiments, the increased growth rate of the invertase secreting strain did not overcome the enhanced efficiency and capabilities of *MoSRT1* in exploiting that external digestion.

This study has revealed numerous benefits as to why a fungal plant pathogen should internalise its sucrose metabolism, yet it would appear from the apparent success of external digestion in fungal populations (165) that there are further benefits

bestowed upon them to explain this paradox, which have not been revealed by this current study.

This thesis has deployed molecular biology and genetic manipulations to gain an understanding of fungal feeding strategies from the perspective of both individuals, and using ecological understanding this has been extended to a population level. For the first time, we have functionally identified and characterised sucrose metabolism in the rice blast fungus. By developing this as a novel system to study microbial ecology, we have addressed questions concerning the use of cooperation and virulence theory against disease, and established an understanding of how and when these strategies can fail. We have explored the social nature of invertase production in detail with both yeast and a fungal plant pathogen to study the competitiveness of various feeding strategies and to reveal novel physiological traits that can stabilise diversity and cooperation. We also uncover a paradox in the success of secreted invertase production by *M. oryzae* where making the pathogen selfish, appears to improves its success.

Now that a novel system has been developed to study public-good production in a disease framework, future studies can look to reveal more complexities of feeding strategies during infection. This could include looking at longer term evolutionary dynamics of social ‘cheats’ and how populations will develop over numerous infection cycles. Despite these strains being generated synthetically in the lab, it would be of interest to see if wild strains that have been recovered from natural disease outbreaks possess any of the sucrose metabolism phenotypes that have been developed in this study, given that they can result in peak pathogen fitness.

Chapter 7 | Materials and methods

Chapter specific methods can be found at the end of their respective sections.

7.1 | Media and apparatus sterilisation

Sterilisation was routinely carried out by autoclaving at 121 °C for 15-20 min or filtration through 0.2 µm pore filters when heating was detrimental to substances.

7.2 | Growth and maintenance of *Magnaporthe oryzae* strains

Magnaporthe oryzae (303) strains used and constructed during this study are stored in the laboratory of N.J. Talbot (University of Exeter). Strains of *M. oryzae* used are derived from the wild-type Guy11 strain (304) and the subsequently generated GFP expressing (*ToxAp:SGFP*) strain (231). For long-term maintenance, Fungi were grown through filter paper discs (3MM, Whatman International), desiccated and frozen at -20 °C. Strains were routinely incubated in a temperature controlled room (24 °C) with 12h light/dark cycle. Except when specified, *M. oryzae* was grown on complete medium (CM) (305). CM comprises of 1 % (w/v) glucose, 0.2 % (w/v) peptone, 0.1 % (w/v) yeast extract, 0.1% (w/v) casamino acids, 0.1 % (v/v) trace elements (50 $mg.L^{-1}$ ethylenediaminetraacetic acid (EDTA), 22 $mg.L^{-1}$ zinc sulphate heptahydrate, 11 $mg.L^{-1}$ boric acid, 5 $mg.L^{-1}$ manganese (II) chloride tetrahydrate, 5 $mg.L^{-1}$ iron (II) sulphate heptahydrate, 1.7 $mg.L^{-1}$ cobalt (II) chloride hexahydrate, 1.6 $mg.L^{-1}$ copper (II) sulphate pentahydrate, 1.5 $mg.L^{-1}$ sodium molybdate dehydrate), 0.1 % (v/v) vitamin supplement (1 $mg.L^{-1}$ biotin, 1 $mg.L^{-1}$ nicotinic acid, 1 $mg.L^{-1}$ pyridoxine, 1 $mg.L^{-1}$ riboflavin, 1 $mg.L^{-1}$ thiamine), 6 $g.L^{-1}$ sodium nitrate, 0.5 $g.L^{-1}$ potassium chloride, 0.5 $g.L^{-1}$ magnesium sulfate, 1.5 $g.L^{-1}$ monopotassium

phosphate, pH to 6.5 with sodium hydroxide. When testing the metabolic influence of specific nutrients Minimal media (MM) was used (213) with carbon/nitrogen sources altered when appropriate. MM is 10 $g.L^{-1}$ glucose, 6 $g.L^{-1}$ sodium nitrate, 0.5 $g.L^{-1}$ potassium chloride, 0.5 $g.L^{-1}$ magnesium sulfate, 1.5 $g.L^{-1}$ potassium dihydrogen phosphate, 0.1 % (v/v) trace elements, pH to 6.5 with sodium hydroxide. Solid media was supplemented with 1.5 % (w/v) agar.

7.3 | *Magnaporthe oryzae* inoculum and *in vitro* fitness measures

Cultures were inoculated with mycelial agar plugs, fragments of filter paper discs overgrown with mycelia, or spore suspensions. Spore suspensions were generated from 12 d solid cultures that were flooded with sdH_2O. Aerial hyphae were disrupted with an L-shaped spreader before the suspension was filtered through sterile miracloth. The filtrate was subjected to centrifugation at 3700 r.p.m for 5 min to pellet the spores that were subsequently washed in 10 mL sdH_2O and spore frequency was established with a haemocytometer. For liquid cultures, 150 mL of CM was blended with 5 cm^2 plug of *M. oryzae* mycelia of a CM agar plate from the periphery of an actively growing culture in a commercial blender (Waring, Christison Scientific) for 20 sec then 10 sec and incubated in a temperature controlled room (24 °C) with 12h light/dark cycle on an orbital aerator (New Brunswick Scientific) with 125 r.p.m.

Sporulation was quantified *in vitro* from 25 mL MM (+ glucose/sucrose) agar plates. Plates were inoculated with 10^5 conidia and were harvested after 12 d by flooding with sdH_2O and agitating the culture surface. The liquid was then filtered to remove debris and conidia enumerated with a haemocytometer.

Biomass production was assessed by inoculating a 5 cm^2 plug of *M. oryzae* mycelium, from a CM agar plate from the periphery of an actively growing culture,

into 150 mL liquid CM and blended. Mycelia from these were extracted after 48 h, washed with sdH_2O, drained and 1 g wet weight (= 0.0635 g dry weight ± 0.00468 s.e.m.) transferred to 150 mL liquid minimal media (MM) with sucrose (10 $g.L^{-1}$) replacing glucose.

7.4 | *Magnaporthe oryzae* DNA Extraction

A small scale DNA extraction protocol was employed when, for example, analysing putative transformants. Nine-centimetre-diameter Petri dishes with solid CM were overlaid with cellophane (Lakeland) and inoculated with fungi and incubated for approximately 8 d until a mycelial mat had grown. The cellophane supporting the fungal mass was then peeled from the surface of the plate, placed into a mortar containing liquid nitrogen before being powdered and transferred to a 1.5 mL microcentrifuge tube and 500 µL pre-warmed (65 °C) 2 x CTAB buffer (0.7 M sodium chloride, 0.1 M Tris (Tris(hydroxymethyl)aminomethane), 7.8 mM EDTA, 5 mM hexadecyltrimethylammonium bromide (CTAB)) added and mixed. Samples were incubated at 65 °C with shaking every 10 min. After 30 min, 500 µL CIA (24:1 chloroform: iso-amyl alcohol) was added and tubes were placed on a shaking platform at 400 r.p.m. for 30 min, then subjected to centrifugation at 14000 x *g* for 20 min. The top aqueous phase was transferred to a new microcentrifuge tube, 500 µL CIA added, shaken at 400 r.p.m. for 5 min, before being subjected to centrifugation at 14000 x *g* for 10 min. The supernatant was then transferred to a fresh microcentrifuge tube and to precipitate the nucleic acids 1 mL of -20 °C isopropanol was added, mixed and incubated at -20 °C for at least 5 min. The tubes were then subjected to centrifugation at 14000 x *g* for 10 min and the supernatant discarded, leaving a pellet of DNA that was resuspended in 500 µL sdH_2O followed by the addition of 50 µL 3 M sodium acetate (pH 5.2) and 1 mL ethanol. Reaction tubes

were then incubated at -20 °C for 10 min to re-precipitate the nucleic acids. Samples were subsequently subjected to centrifugation at 14000 x *g* for 20 min and the purified nucleic acid pellet formed was washed again in 400 µL 70 % (v/v) ethanol after discarding the supernatant, and subjected to centrifugation at 14000 x *g* for 5 min after which the supernatant was removed and the nucleic acid pellet was air dried. This was then resuspended 100 µL sdH_2O containing 500 $\mu g.mL^{-1}$ RNase A. Nucleic acid concentrations were established using a NanoDrop spectrophotometer (Thermo Scientific). Samples were stored at -20 °C and gDNA quality was assessed for degradation by running 1 µL in a 0.8 % (w/v) agarose gel.

7.5 | DNA restriction digestions

DNA was digested with restriction endonucleases and supplied buffers (Promega UK Ltd., Southampton, UK; or New England Biolabs, Hitchen, UK). Reactions of 30 µL typically contained 0.2-1 µg DNA and 5-10 units of enzyme. For Southern blot analysis, 20 µg of DNA and 20 units of enzyme were used in a total volume of 50 µL. Reactions were incubated at 37 °C for 1-18 h.

7.6 | Polymerase Chain Reaction (PCR) DNA amplification

Amplification of DNA was performed by polymerase chain reaction (PCR) using a Techne TC-512 thermal cycler. Reaction volumes ranged from 25-50 µL and contained 0.4-0.5 µM of each primer and 10-250 ng DNA template (or a sample of individual transformant colony). DNA polymerases used were GoTaq® DNA polymerase (Promega), Phusion® High-Fidelity DNA polymerase (New England Biolabs), Thermo-Start® DNA polymerase (Thermo Scientific), SapphireAmp Fast PCR Master Mix (Clontech), DreamTaq Green PCR Master Mix (Thermo Scientific), or CloneAmp™ HiFi PCR Premix (Clontech) and manufacturers' instructions were

adhered to. GoTaq® DNA polymerase was used either in GoTaq® Green Master Mix or GoTaq® Flexi DNA polymerase at a concentration of 1.25 units per reaction with 0.2 mM of each dNTP, 1.5 mM magnesium chloride, 5X Green GoTaq® Flexi buffer and nuclease-free water to volume. With Phusion® High-Fidelity DNA polymerase, 1 unit enzyme per 50 µLreaction was used with 5 X Phusion HF or GC buffer, 0.2 mM of each dNTP, up to 3 % (v/v) DMSO for difficult to amplify regions, and nuclease free water to volume. When screening transformants by colony PCR, Thermo-Start® DNA polymerase (Thermo Scientific),SapphireAmp Fast PCR Master Mix (Clontech) or DreamTaq Green PCR Master Mix (Thermo Scientific) were used for higher sensitivity and faster reaction times. CloneAmp™ HiFi PCR Premix (Clontech) was used for difficult to amplify fragments for In-Fusion cloning. PCR reactions involved an initial denaturation step at 94-98 °C for 30 sec - 15 min, followed by 30-35 cycles of 94-98 °C for 5 sec - 1 min, 48-68°C for 5 sec – 1 min, 72 °C for 10 sec – 3 min, with a final hold at 4 °C.

7.7 | DNA gel electrophoresis

DNA fragments were separated according to size by gel electrophoresis in 0.8 % (w/v) agarose gel matrices with ethidium bromide (0.5 $\mu g.L^{-1}$) added to visualise DNA, in a 1 x TBE buffer (0.09 M Tris-borate, 2 mM EDTA). A 1 kb plus DNA Ladder (Invitrogen) was used as a size marker for fragments. Images of fluorescing gels were captured on a UV transilluminator with a gel documentation system (Image Master VDS, Fujifilm Thermal Imaging System FTI-500, Pharmacia Biotech).

7.8 | Purification of DNA fragments from agarose gel

Separated fragments of DNA from electrophoresis were extracted from agarose gels using Wizard® SV Gel and PCR Clean-Up System (Promega) according to the

manufacturer's protocol. While visualising on a UV transilluminator, DNA bands were cut from gels using a razor blade and transferred to a pre-weighed 30 mL universal container (Greiner bio-one), which was re-weighed and Membrane Binding Solution (4.5 M guanidine isothiocyanate, 0.5 M potassium acetate (pH 5)) added (10 µL per 10 mg of gel), briefly mixed then incubated at 65°C until the gel had completely melted. This was then transferred to an SV Minicolumn inserted into a Collection tube and incubated at ambient temperature for 1 min before centrifugation at 16000 x *g* for 1 min. The liquid was then discarded from the Collection Tube and the column was washed with 700 µL Membrane Wash Solution (80 % (v/v) ethanol, 10 mM potassium acetate (pH 5), 16.7 µM EDTA (pH 8)) and subjected to centrifugation at 16000 x *g* for 1 min. The wash was then repeated with 500 µL Membrane Wash Solution and subjected to centrifugation at 16000 x *g* for 5 min after emptying the Collection Tube. The SV Minicolumn was then moved to a fresh 1.5 mL microcentrifuge tube and 30 µL of Nuclease-Free water was applied to the column followed by incubation at ambient temperature for 1 min and centrifugation for 1 min at 16000 x *g* to recover the eluted DNA. Sample concentrations were quantified using a NanoDrop spectrophotometer (Thermo Scientific) and stored at -20 °C.

7.9 | Cloning

Escherichia coli was routinely used for cloning which was grown on Luria-Bertani (LB) medium. LB is 1 % (w/v) sodium chloride, 1 % (w/v) tryptone, 0.5 % (w/v) yeast extract, 2 % (w/v) agar for solid media, pH to 7 with sodium hydroxide. For selection 100 $\mu g.L^{-1}$ filter-sterilised ampicillin/kanamycin was added.

Various cloning methods were employed during this study depending on the necessary application and advances in standard laboratory procedures. These

include yeast recombination cloning, Blunt PCR cloning mediated by DNA topoisomerase I and Cre recombinase technologies (Agilent Technologies, USA), conventional cloning by restriction digestion and ligation, and In-Fusion® HD Cloning Plus (Clontech Laboratories, Inc, USA). The commercial kits were used according to manufacturers' instructions.

For the Blunt PCR cloning, DNA fragments were firstly PCR amplified using Phusion® High-Fidelity DNA Polymerase (NEB Inc., USA) and cloned into pSC-B-amp/kan vector. This was achieved by a ligation reaction with 3 µL StrataClone Blunt Cloning Buffer, 2 µL of PCR product (5-50 ng) and 1 µL StrataClone Blunt Vector Mix amp/kan. This ligation mixture was incubated at room temperature for 5 min. One microliter of this mixture was combined with thawed StrataClone SoloPack competent cells and incubated on ice for 20 min. The transformation mix was then heat-shocked at 42 °C for 45 sec before being returned to ice for 2 min. An aliquot of 250 µL of pre-warmed (42 °C) LB media was added and the culture was allowed to recover for 1 h at 225 r.p.m., 37 °C. Cells were screened for successful transformation by selection on LB -ampicillin plates with blue / white colour screening using X-gal (40 µL of 2% per plate). Transformants were screened after incubation overnight by colony PCR and restriction digest of plasmid DNA. Fragments excised from plasmids of positive transformants were then ligated into secondary vectors using T4 DNA ligase (Promega). Ligation was performed according to manufacturer's instructions using a 3:1 molar ratio of insert:vector DNA for each fragment. Reactions were performed in a total volume of 10 µL with 100 ng of vector DNA, 3u of T4 DNA ligase and incubated for 3 h at room temperature. This two-step cloning was later negated by using In-Fusion® HD Cloning Plus (Clontech Laboratories, Inc, USA), where only a single-step of PCR followed by a cloning

reaction into the desired linearised vector was required rather than into a specific vector as in the Blunt PCR Cloning. Furthermore, transformation efficiency was greater with very few false-positive transformants. In-Fusion cloning was performed by combining 2 µL 5X In-Fusion HD enzyme premix, with 50-200 ng of linearised vector and 10-200 ng of each PCR fragment in a total volume of 10 µL. The reaction was incubated at 50 °C for 15 min before being transformed into Stellar™ Competent Cells (Clontech Laboratories, Inc, USA). Transformation was performed by adding 2.5 µL of the In-Fusion reaction to 50 µL of thawed cells which were incubated on ice for 30 min, before being heat-shocked at 42 °C for 45 sec. The mix was then returned to ice for 1-2 min before having 450 µL of 37 °C SOC medium added. The culture was allowed to recover by incubation at 37 °C with 225 r.p.m. for 1 h, before being plated on selection plates of LB-ampicillin/kanamycin.

For high efficiency transformation of low yield and quality plasmids isolated from *S. cerevisiae*, XL10-Gold® Ultracompetent cells were used (Stratagene). An aliquot of 100 µL of thawed XL10-Gold® Ultracompetent cells were put into a pre-chilled 12 mL round-bottomed capped tubes (Greiner bio-one) to which 4 µL of XL10-Gold® β-Mercaptoethanol mix was added and gently mixed before being incubated on ice for 10 min with gentle shaking every 2 min. To this 0.1-50 ng DNA was added and tubes were gently swirled and incubated on ice for 30 min before being heat-shocked at 42 °C for 30 sec, followed by immediately being returned to ice for 2 min. The tubes were then supplemented with 0.9 mL of 42 °C NZY^+ broth (1 % (w/v) NZ amine (casein hydrolysate), 0.5 % (w/v) yeast extract, 0.5 % (w/v) sodium chloride, pH to 7.5 with sodium hydroxide, autoclaved followed by the addition of filter-sterilised 12.5 $mL.L^{-1}$ of 1 M magnesium chloride, 12.5 $mL.L^{-1}$ of 1 M magnesium sulfate and 20 $mL.L^{-1}$ of 20 % (w/v) glucose) and incubated at 37 °C for 1 h with shaking at 225

r.p.m. Portions were then plated on LB-ampicillin agar and incubated at 37 °C overnight.

7.10 | Plasmid DNA preparation and clone screening

Transformants that emerged were assess for correct construct by colony PCR and restriction digest analysis following extraction of plasmid DNA from bacterial cultures using a method adapted from (306). Colonies were initially inoculated into 5 mL LB ampicillin/kanamycin and grown overnight at 37 °C 225 r.p.m. A 1.5 mL portion of this culture was subjected to centrifugation for 5 min at 13,000 r.p.m. and the supernatant removed. The pellet was resuspended in 100 μL of lyse solution (0.08̇ M Tris/HCl pH 8, 0.0̇ M EDTA, 0.1 M sucrose) and vortexed. To this, 200 μL alkaline solution (0.2 M sodium hydroxide, 0.035 M SDS) was added, vortexed and stored on ice for 10 mins with occasional mixing. Then 150 μL of 3 M sodium acetate (pH 5.2) was added before the mixture was returned to ice for 10 min. This was then subjected to centrifugation at 13, 000 r.p.m. at 4 °C for 10 min and the supernatant was extracted to which 1 mL of ethanol was added and the resulting mix was stored on ice for 10 mins to allow the DNA to precipitate. DNA was collected following centrifugation at 13, 000 r.p.m. for 10 min and discarding the supernatant. The pellet was washed with 70 % ethanol before being resuspended in 30 µL containing 500 $\mu g.mL^{-1}$ RNase A. For restriction digest analysis 5 µL of this plasmid solution was used. Positive clones were retained for storage by mixing 500 μL of bacterial culture with 500 µL 50% (v/v) glycerol and snap frozen in liquid N_2 before being stored at -80°C.

To obtain a larger quantity of high quality plasmid DNA for further applications, clones were inoculated into 5 mL of liquid LB-ampicillin media overnight at 37 °C with

200 r.p.m. orbital shaking. A 100 µL aliquot of this overnight culture was used to inoculate 50 mL LB-ampicillin and grown overnight at 37 °C with 200 r.p.m. and plasmid DNA was isolated using PureYield™ Plasmid Midiprep System (Promega) to manufacturer's instructions. Cells were first pelleted at 5000 x *g* (Beckman JS-13.1) for 10 min and waste media removed before being resuspended in 3 mL Cell Resuspension Solution (50 mM Tris (pH 7.5), 10 mM EDTA, 300 µg RNase). To the suspension, Cell Lysis Solution (0.2 M NaOH, 1 % (w/v) SDS) was added; tubes were mixed by inversion and incubated for 3 min at ambient temperature, after which 5 mL of Neutralization Solution (4.09 M guanidine hydrochloride, 0.759 M potassium acetate, 2.12 M glacial acetic acid, total pH 4.2) was added followed by gently mixing by inversion. To separate aqueous and organic phases, the lysate was then subjected to centrifugation at 15000 x *g* (Beckman JS-13.1) for 15 min. The resulting supernatant was poured into a PureYield™ Clearing Column on top of a PureYield™ Binding Column placed onto a vacuum manifold and the vacuum was applied until the liquid had passed through both columns. The Clearing Column was then detached and 5 mL of Endotoxin Removal Wash was passed through the binding column followed by 20 mL of Column Wash Solution and the membrane was allowed to dry by applying the vacuum for a further 60 sec. Plasmid DNA was eluted by centrifugation by placing the binding column into a 50 mL Falcon tube (Becton Dickinson), adding 600 µL of nuclease-free water to the DNA binding membrane. After 1 min the tube was then subjected to centrifugation at 2000 x *g* (Centrifuge) for 5 min to collect the dissolved DNA.

7.11 | Split-marker targeted gene replacement of *M. oryzae*

Nucleotide sequences were obtained from the *Magnaporthe oryzae* comparative Sequencing Project, Broad Institute of Harvard and MIT (http://www.broadinstitute.org/).

Searching the *Magnaporthe comparative* Database*,* identified and provided sequences of genes that were targeted using a PCR-based split-marker gene deletion technique (145, 146) (Figure 7.1). Gene replacements were achieved by replacing putative invertase genes with a 2.8 kb sulfonylurea resistance allele (*ILV1)* which encodes aceolactate synthase, an enzyme involved in the synthesis of isoleucine and valine (202). For each gene, in a first round of PCR, a 1 kb genomic fragment upstream (LF) and downstream (RF) of the ORF were amplified. Separately, 1.6 kb overlapping fragments of the 5' and 3' end of the sulfonylurea resistance gene cassette (*ILV1*) were amplified. The upstream fragment, IL, was amplified with primers M13F and ILsplit, while with the downstream fragment, LV, primers LVsplit and M13R were used (See specific chapters for primer sequences). Amplicons produced were fused in a second round of PCR, with the LF fusing with IL and the RF with LV to produce two larger fragments of 2.6 Kb. This was achieved by complementary regions (M13F and M13R) being incorporated into the design of the primers used. The reverse primer for the upstream flanks and the forward primer for the downstream flanks contained 24 bp 5' overhangs complementary to M13 forward and reverse sequences contained in the IL and LV fragments. PCR was performed using Go Taq® Green Master Mix (Promega). The constructs; upstream flank fused with IL, and LV with the downstream flank; were used to transform *M. oryzae* (Strain *ToxA:SGFP* background Guy11) and gene replacement achieved by homologous

recombination between either flank and corresponding chromosomal regions, and unifying the selectable marker gene.

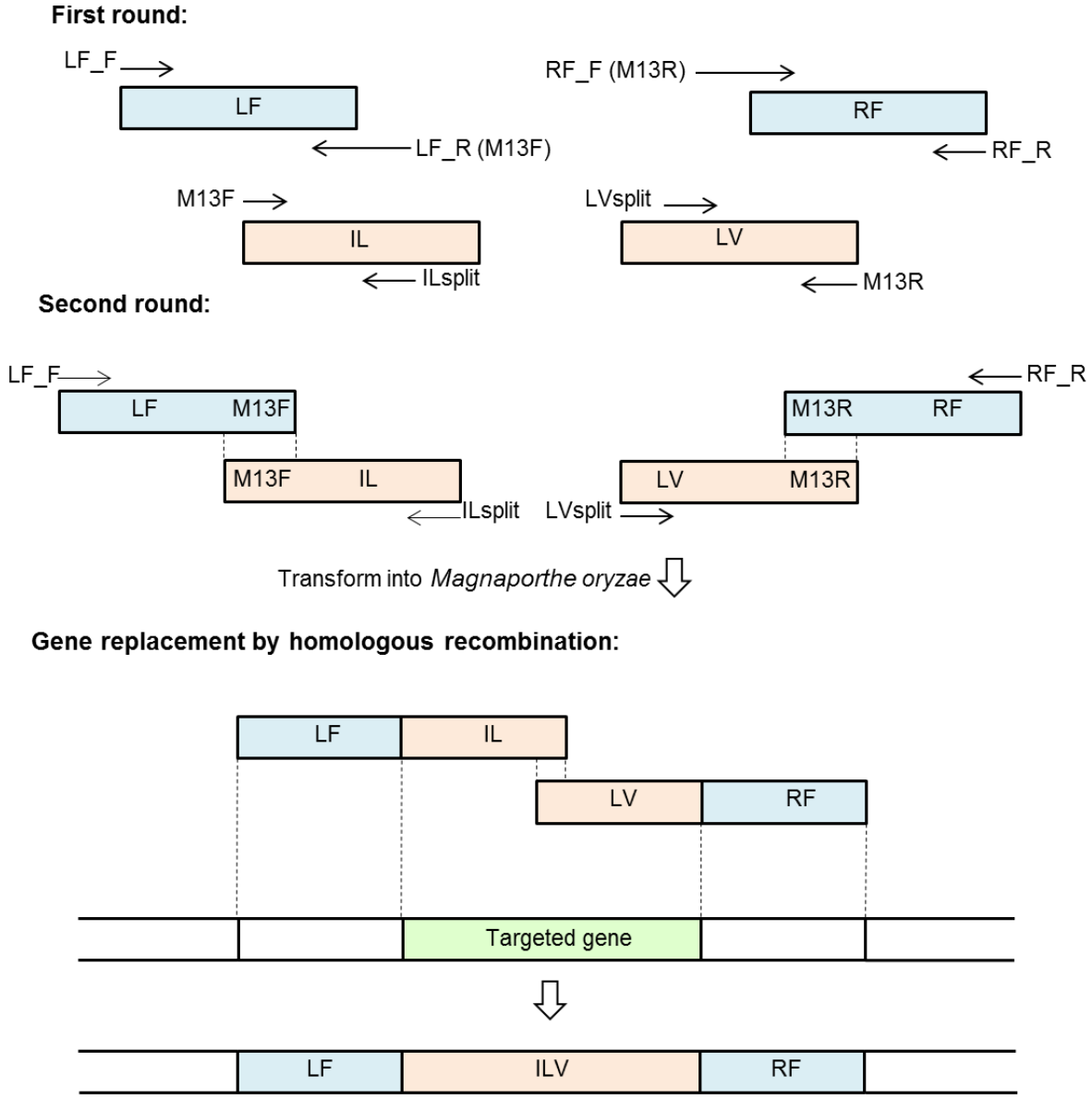

Figure 7.1 | Schematic for the principle of split-marker targeted gene replacement by double joint PCR. See text in section 7.11 for details.

7.12 | *M. oryzae* transformation

Liquid cultures of *M. oryzae* were prepared as described above and incubated for 48 h. The resulting fungal mass was harvested by filtration through sterile Miracloth (Calbiochem), washed with 100 mL sdH_2O and excess liquid removed by blotting with paper roll (Kimberley Clark Corporation). Mycelia were transferred to a 50 mL Falcon tube (Becton Dickinson) containing 40 mL filter-sterilized OM buffer (1.2 M magnesium sulphate, 10 mM sodium phosphate (pH 5.8), 1.2 % Glucanex (Novo Industries, Copenhagen) pH to 5.6 with disodium phosphate) and gently shaken to disperse fungal mass followed by incubating at 30 °C with 75 r.p.m. in an orbital incubator for 3h. The homogenate were subsequently transferred to a sterile polycarbonate Oakridge tube (Nalgene), overlaid drop-wise with one volume of cold ST buffer (0.6 M sorbitol, 0.1 M Tris-HCl (pH 7) and subjected to centrifugation at 5000 r.p.m. at 4 °C for 15 min in a swinging bucket rotor (Beckman JS-13.1) in a Beckman J2.MC centrifuge. Protoplasts were collected from the boundary between OM and ST buffer into a fresh Oakridge tube which was filled with STC buffer (1.2 M sorbitol, 10 mM calcium chloride, 10 mM Tris/HCl (pH 7.5)) and subjected to centrifugation at 3000 r.p.m. at 4 °C for 10 min (Beckman JS-13.1 rotor). After discarding supernatant, resuspended protoplasts were washed twice more with 10 mL of STC buffer and finally resuspended in 1 mL STC buffer and frequency of protoplasts was established using a haemocytometer. Fungal transformation was carried out by mixing 6-12 µg of DNA with 10^7 protoplasts (total volume 150 µL) and incubated at ambient temperature for 25 min. One millilitre of PTC buffer (60 % (w/v) polyethylene glycol 4000, 10 mM calcium chloride, 10 mM Tris-HCl (pH 7.5)) was added in two aliquots and mixed by inversion followed by incubation at ambient temperature for 20 min. The mixture was then added to 150 mL molten (45 °C)

BDCM (27.38 % (w/v) sucrose, 1 % (w/v) glucose, 0.2 % (w/v) ammonium nitrate, 0.1 % (w/v) asparagine, 0.17 % (w/v) yeast nitrogen base w/o amino acids and ammonium sulfate (Difco), pH to 6 with disodium phosphate, 1.5 % (w/v) agar) and poured into 9 cm diameter Petri dishes with 30 mL per plate and incubated for 16-24 h at 24 °C. For transformant selection plate cultures were overlaid with 15 mL BDCM but 1 % (w/v) agar, omitting sucrose, and containing either 150 $\mu g.mL^{-1}$ glufosinate-ammonium diluted from 100 $mg.mL^{-1}$ in sdH_2O stock for bialophos (Basta) resistant transformants, or 150 $\mu g.mL^{-1}$ chlorimuron ethyl (diluted from 100 $mg.mL^{-1}$ in N,N-dimethylformamide stock solution) for sulfonylurea resistant transformants. For plasmid mediated transformations, the STC/PTC/protoplast mix was initially combined with 3 mL TB3 buffer (20 % (w/v) sucrose, 1 % (w/v) glucose, 0.3 % (w/v) yeast nitrogen base w/o amino acids and ammonium sulphate) and incubated at 24 °C on an orbital aerator with 125 r.p.m. for 16-24 h before being transferred to the molten BDCM and once solidified, immediately overlaid with selection media. Plates were then incubated at 24 °C until transformants emerged (approximately 10 -14 days).

7.13 | Assessment of putative transformants for gene knockout

Transformants were selected for based on resistance to sulfonylurea (150 $\mu g.mL^{-1}$ chlorimuron ethyl) in overlay media. Emergent strains were sub-cultured onto fresh BDCM but 1 % (w/v) agar, omitting sucrose, containing 50 $\mu g.mL^{-1}$ chlorimuron ethyl to verify resistance phenotype. To confirm resistance correlated with gene replacement, putative transformants' and wild-type DNA was extracted as described above and genomes were assessed by digoxigenin-(DIG) labelled Southern blot analysis and evaluated for fragment size differentiation following restriction endonuclease digestion of gDNA. Strategies were devised by analysis of the *M.*

oryzae genome (141) via the *Magnaporthe comparative* Database (http://www.broadinstitute.org/annotation/genome/magnaporthe_comparative/MultiHome.html) whereby gDNA digestion would result in different sized fragments in the region of gene replacement compared with wild-type. Digested DNA samples were fractionated by gel electrophoresis and assessed by as described above.

7.14 | Southern blotting

Fragments of DNA separated in agarose gels were transferred to Hybond-NX (Amersham Biosciences) membranes by a capillary blotting technique of Southern (307). Prior to blotting, partial depurination of DNA molecules was performed to simplify base transfer by submerging the gel in 0.25 M HCl for 15 min with gentle rocking. Gels were then neutralised by replacing the HCl with 0.4 M NaOH and gently shaking for another 15 min. Blots were carried out using a 0.4 M NaOH transfer buffer that was drawn up through a wet paper wick (Whatman International) supported by a perspex panel onto which the agarose gel was placed. A sheet of Hybond-NX membrane was then laid upon the gel and positions of the wells were pencil marked. Parafilm strips were placed around the gel to enhance capillary action. Three layers of Whatman 3MM paper were then laid over the membrane followed by a stack of paper towels onto which a second perspex panel was placed. A 500 g weight was placed on top and the assembly was left to blot overnight, after which the nucleic acid was fixed to the membrane by UV crosslinking with an exposure of 120 millijoules.cm^{-2} in a BLX crosslinker (Bio-link).

7.15 | Membrane Hybridisation and Chemiluminescent detection of DIG-labelled nucleotides

The Hybond-NX membrane was incubated in a hybridisation bottle (Hybaid Ltd.) containing Southern hybridisation buffer (0.5 M sodium phosphate buffer (pH 7), 7 % (w/v) SDS) in a hybridisation oven (Hybaid Ltd.) at 62 °C with rotation for 30 min. The buffer was then poured off and the probe added before being returned to the oven for incubation at 62 °C overnight. The digoxigenin-(DIG) labelled probes were generated by PCR using Phusion® High-Fidelity DNA Polymerase and DIG DNA labelling mix (Roche Applied Science) (5 µL per 50 µL reaction). Amplicons were fractionated by gel electrophoresis and then purified from the agarose gel. Prior to hybridisation of Hybond-NX membranes, the purified probe was combined with 25-50 mL of Southern hybridisation buffer in a 50 mL Falcon tube and denatured at 100 °C for 10 min. Hybridisation was followed by washing the membrane twice with 20 mL Southern wash buffer (0.1 M sodium phosphate buffer (pH 7), 1 % (w/v) SDS) in the hybridisation bottle at 62 °C for15 min to remove unbound probe. DIG-labelled nucleic acids were visualised by chemiluminescence detection. Beforehand, the membrane was equilibrated in 20 mL DIG wash buffer (150 mM NaCl, 0.1 M maleic acid, pH to 7.5 with NaOH, 0.3 % (v/v) Tween 20) for 5 min at room temperature with gentle agitation. DIG wash buffer was then replaced with 40 mL Blocking solution (150 mM NaCl, 0.1 M maleic acid, pH to 7.5 with NaOH, 1 % (w/v) milk powder) for 30 min to quench background signal. Blocking solution was then discarded and the membrane was incubated with 40 mL antibody solution (0.0001 % (v/v) Anti-Digoxigenin-AP, Fab fragments (Roche) subjected to centrifugation for 20 min at 16000 x *g* prior to addition to prevent inclusion of small antibody aggregates, 150 mM NaCl, 0.1 M maleic acid, pH to 7.5 with NaOH, 1 % (w/v) milk powder) for 30

min. The membrane was then washed twice for 15 min with DIG wash buffer followed by being equilibrated in 20 mL DIG buffer (0.1 M Tris/HCl (pH 9.5), 0.1 M NaCl, 50 mM $MgCl_2$) for 5 min before chemiluminescence detection. The membrane was then transferred onto a polypropylene sheet and 1 mL CDP-*Star*® Chemiluminescent Substrate applied before being covered by a second layer of polypropylene to prevent desiccation and incubated for 5 min. Excess CDP- *Star*® was then drained and the membrane sealed in polypropylene before incubation at 37 °C for 30 min. Chemiluminescent detection was then achieved by exposing the membrane to X-ray film (Fuji Medical X-ray Film, Fuji Photo Film UK Ltd.) for 30 sec to 30 min at room temperature in an X-ray film cassette followed by developing in a OptiMax X-ray Processor (Protec).

7.16 | Yeast transformation

S. cerevisiae was stored in 25 % (v/v) glycerol stock and stored at -80 °C and revived by extracting a portion of the stock and plating onto YPD media (2 % (w/v) peptone, 2 % (w/v) glucose, 1 % (w/v) yeast extract 2 % (w/v) agar) and incubated inverted at 30 °C for 24 h. Strains that had been transformed with plasmids containing prototrophic markers were grown on supplemented minimal media (SMM) to maintain selection (5 $g.L^{-1}$ ammonium sulfate, 1.7 $g.L^{-1}$ yeast nitrogen base w/o amino acids or ammonium sulfate, 50 $mg.L^{-1}$ L-lysine and 20 $mg.L^{-1}$ L-histidine, 20 $g.L^{1}$ D-glucose, with 20 $g.L^{-1}$ agar).

For transformation, yeast cells from a single colony were inoculated into 3-5 mL liquid YPD and grown on an orbital incubator at 30 °C with 200 r.p.m. Two millilitres of this culture was inoculated into 50 mL liquid YPD and returned to the orbital incubator for 5 h before being transferred to a 50 mL Falcon tube and subjected to

centrifugation at 2200 r.p.m. for 5 min to recover the cells. After discarding the supernatant, the pellet was washed by resuspension in 10 mL sdH_2O followed by centrifugation at 2200 rpm for 5 min. The supernatant was removed and the pellet was then resuspended in 300 µL sdH_2O. Transformation was carried out in a 1.5 mL microcentrifuge tube by adding, in order; 100 µg in 50 µL sdH_2O of denatured herring sperm DNA, 600 ng of linearised or circular vector depending on application, 200 ng of each PCR amplified DNA fragment when applicable, and 50 µL of *S. cerevisiae* cells. To this 32 µL of 1 M lithium acetate and 240 µL of 50 % (w/v) polyethylene glycol 4000 was added and incubated for 30 min at 30 °C before being heat shocked at 45 °C for 15 min. Cells were then briefly pelleted by centrifugation at 2000 r.p.m. for 2 min, supernatant discarded and resuspended in 200 µL sdH_2O.

S. cerevisiae were plated onto yeast synthetic drop-out media (2 % (w/v) glucose, 2 % (w/v) agar, 0.5 % (w/v) ammonium sulphate, 0.5 % (w/v) casamino acids (Casein hydrolysate, Fluka), 0.17 % (w/v) yeast nitrogen base w/o amino acids, 0.002 % (w/v) adenine, 0.002 % (w/v) tryptophan) that specifically excludes uracil and uridine and so selects for transformants that have acquired the *URA3* gene from the 1284 or NEV-E vector, then inverted and incubated at 30 °C until colonies appeared.

Yeast transformants were screened for intended DNA sequences by PCR using Thermo-Start® DNA polymerase and yeast cells as template. DNA amplification of fragments of interest were analysed by gel electrophoresis. Colonies whose template returned correct sized bands were selected for further use.

To increase yield for transformation into *M. oryzae*, the plasmid was isolated from *S. cerevisiae* prior to transformation into *Escherichia coli* using XL10-Gold® Ultracompetent cells (Stratagene). Plasmid DNA was isolated from *S. cerevisiae*

according to a method developed from (306). Yeast was grown in 50 mL of liquid synthetic drop-out media at 30 °C with 200 r.p.m. overnight before being collected by centrifugation at 2000 x *g* for 5 min, removing the media and resuspending the pellet with 500 µL sdH_2O. Cells were transferred to a 1.5 mL microcentrifuge tube, subjected to centrifugation for 5 sec at 16000 x *g* and supernatant removed. To the cells were added, in order; 250 µL of yeast lysis buffer (2 % (v/v) Triton™ X-100, 1 % (w/v) SDS, 100 mM NaCl, 10 mM Tris, 1mM EDTA), 250 µL phenol: chloroform: isoamyl alcohol (25:24:21) and 300 µg of acid washed glass beads (425-600 µm). The tube was vortexed for 30 min followed by the addition of 250 µL of TE buffer (10 mM Tris-HCl pH 8, 1mM EDTA) and then subjected to centrifugation at 16000 x *g* for 15 min to separate the organic and aqueous phases. The supernatant was then extracted to a fresh 1.5 mL microcentrifuge tube before one tenth volume of 3 M sodium acetate (pH 5.5) and 1 mL of 96 % (v/v) ethanol was added and the mixture was incubated at -20 °C. The precipitated DNA was collected by centrifugation at 16000 x *g* and the supernatant discarded. The pellet was then resuspended in 400 µL of TE buffer with 40 µg RNase A and incubated at 37 °C for 10 min until dissolved followed by the addition of 10 µL of 4 M ammonium acetate and 1 mL of 96 % (v/v) ethanol. The tube was then subjected to centrifugation for 15 min at 16000 x *g* to collect precipitated DNA which was then washed with 500 µL of 70 % (v/v) ethanol after discarding the supernatant. This was then subjected to centrifugation at 16000 x *g* for 10 min, the ethanol removed and the pellet allowed to air dry before being resuspended in 50 µL of sdH_2O.

7.17 | Appressorium formation and penetration assay

To assess the ability of the conidia from mutant strains to germinate and develop the infection structure, the appressorium, an assay was performed based on that from (308). Conidia of *M. oryzae* germinate and form appressoria in response to environmental cues including a hard hydrophobic surface (148) and nutrient deprivation (149). Conidia (5×10^4.mL^{-1}), washed to remove residual nutrients, were inoculated onto borosilicate glass cover slips (Fisher Scientific UK Ltd.) and incubated in a damp chamber at 24°C. Samples were assessed for development after 24h by light microscopy. The assay was repeated three times and the data compiled.

To assess the ability of formed appressoria to penetrate plant cuticles, the same conidia suspensions were assessed on yellow onion epidermal strips as previously described(309). Prior to inoculation, 1 cm^2 epidermal strips (bulb scales) were washed with chloroform and thoroughly rinsed in sdH_2O to remove the fleshy bulb tissue and wax. These strips were placed on glass microscope slides and inoculated with the conidial suspension and incubated and assessed as above.

7.18 | Enzymatic assay of invertase

Secreted invertase activity was measured as a crude extract in used minimal media supplemented with varying carbon sources depending on experiment. Invertase activity was tested based on a spectrophotometric stop reaction where acid hydrazide generates yellow anions by reacting with reducing carbohydrates (glucose and fructose) in alkaline solutions (310, 311). Enzyme samples were established by preparing *M. oryzae* liquid cultures in 50 mL CM, incubating for 48 h before harvesting mycelia through sterile miracloth followed by washing was 100 mL sdH_2O

and blotting dry with paper towel. The fungal mass was subsequently transferred to fresh MM +/- carbon sources (1 % (w/v) where applicable) and incubated at 24 °C with orbital aeration of 125 r.p.m. for 18 h. The culture filtrate was then collected in a 50 mL Falcon tube by filtration through sterile miracloth and snap frozen in liquid nitrogen before being lypholised using a Heto PowerDry LL1500 freeze dryer (Thermo Electron Corporation). Desiccated samples were rehydrated with 2 mL sdH_2O and vigorously vortexed. Resuspended samples were then dialysed to exclude residual reducing sugars from samples while retaining larger proteins. This was performed at 4 °C using 1 mL sample, 10 k MWCO Snakeskin™ Dialysis tubing (Thermo Scientific), and 5 L 10 mM sodium acetate buffer (pH 5) that was replaced fresh once during the 24 h dialysis period. Invertase activity was measured by combining 100 µL of the dialysed sample with 900 µL sucrose substrate (1 % (w/v) in 100 mM sodium acetate buffer (pH 4.5)) at 55 °C for 20 min. Sucrose hydrolysis was determined by measuring liberated fructose and glucose molecules in the mixture after incubation by transferring 100 µL to 12 mL round bottomed capped tubes containing 2.9 mL 0.5 % (w/v) PAHBAH (p-Hydroxybenzhydrazide in 0.5 M NaOH), arresting invertase activity. Reaction mixtures were heated at 100 °C for 5 min, then cooled to room temperature and absorbance read at 410 nm using 1 mL cuvettes (Greiner Bio-one) in a spectrophotometer (Jenway 7300). Measurements were made against uninoculated blanks.

For internal invertase activity measures, the mycelia harvested after the 18h induction period were snap frozen in liquid N_2 and lypholised for 48 h. Freeze-dried mycelium (0.1 g) was ground to a fine powder with a pestle and mortar and transferred to a microcentrifuge tube. To this powder, 1 ml of protein extraction buffer (1% (w/v) DMSO, 1 mM EDTA, 50 mM Tris/HCl (pH 8), 100mM NaCl and 1mM

Dithiothreitol) was added. The mixtures were vortexed and subsequently centrifuged for 10 min at 13, 000 r.p.m., 4 °C. The resulting supernatant was assessed for invertase activity as described above for external activity. Measurements were made against samples with which reactions were immediately arrested with addition of PAHBAH in 0.5 M NaOH. This enabled both the inhibition of invertase activity and for any residual reducing sugars within the mycelial homogenate to be accounted for, because they had not been removed by dialysis like with the external activity measures.

7.19 | Pathogenicity and *in planta* fitness assay of *M. oryzae*

To test pathogenicity of *M. oryzae* strains, infections were performed on the susceptible indica rice cultivar CO39 (226). Plants were grown at 24 °C with 75-90 % relative humidity with 12 h light/dark cycle. Seedlings aged 3-4 weeks (approximately 3-leaf stage) were used for infection.

For the majority of infections a quantitative localized leaf spot infection assay was used. This enabled us to assess pathogen fitness and disease virulence so that the exact number of conidia in a specific area and the subsequent fitness of the pathogen could be determined, in addition to permitting intimate interactions between individuals of the infecting population. This was performed according to a previously described protocol (225), with the following modifications. Leaves of 3-4 week-old seedlings of rice cultivar CO39 were inoculated using intact seedlings because detached leaves may trigger defence responses and inhibit sink induction at infection sites and thus nutrient acquisition by the pathogen (91, 312). Each disease patch was initiated by inoculation with a 20 µL suspension of 5×10^4 conidia.mL^{-1} in 0.2 % (w/v) gelatine. This inoculum size was used as it was sufficient

to facilitate the full disease cycle to be completed so that the resulting population could be measured after sporulation. Lower inoculation levels led to unsuccessful infections and the pathogen producing no conidia. This inoculum size is realistic given that in the wild single disease lesions sporulate profusely to release thousands of conidia per day, which are transmitted to new host plants by dewdrop splash to reinitiate disease (157). Infected, attached leaves were incubated under high humidity to facilitate successful infection, which proceeded for 7 d, with the inoculation droplets blotted after the initial 26 h. Images of the infection lesions used for virulence quantification were captured at this time using an Epson Expression 1680 Pro scanner (1200 d.p.i.). The lesions were excised from leaves and placed under high humidity to induce sporulation for 48 h. Images of sporulating lesions were captured at this time by epifluorescence microscopy (Leica M205FA merged using ImageJ, National institutes of Health, USA). Conidia were extracted by flooding lesions with 200 µL sdH_2O, vortexed and lesion surfaces gently abraded, before the conidia were enumeration with a haemocytometer to establish total pathogen population fitness and the frequency of individual strains.

Pathogenicity and virulence of individual single site and single genotype infections were measured using spray inoculations as described previously (226) using 5 x 10^4 conidia.mL^{-1} in 5 mL 0.2% gelatine on rice seedlings. Spore suspensions were sprayed onto rice seedlings using an airbrush. Plants were watered and incubated under high humidity for 48 h, before being returned to normal growth regimen for a further 3 d. For lesion quantification, infected leaves were imaged 5 d after infection with an Epson Expression 1680 Pro scanner (1200 d.p.i.). Disease virulence in terms of lesion area from both leaf spot and spray inoculations was quantified using image analysis software (ImageJ, National institutes of Health, USA, see below for details).

Invasive growth rate and live-cell imaging during infection was assessed using leaf sheath inoculation assays based on those previously described (156) using a conidial suspension of 1-5 x 10^4.mL^{-1} in 0.2 % (w/v) gelatine. Infections were observed at specified time points, after dissection, by microscopy (Olympus IX81).

Single strain infections were tested using spray and leaf sheath inoculations as with these infection methods disease is measured on the basis of a single spore and hence genotype, assuming no systemic effects on the host from infection. The precise location and population demographic of each infection in a mixed genotype population could therefore not be determined with this assay and any mixed infection would likely consist of a series of metapopulations.

7.20 | Image analysis

Pathogen virulence was quantified by the area of the lesions formed during disease. Images (1200 d.p.i) were analysed to determine lesion area using ImageJ image analysis software (National institutes of Health, USA) using the following commands.

i) Images were cropped to exclude background:

ii) Colour channels were then split using command: Image > Color > Split channels. Blue channel was excluded as it did not add information to distinguish lesions from healthy leaf regions:

This image has been removed by the author of this thesis for copyright reasons.

iii) Green and red channels were then used to scale the images using the command: Process > Calculator plus, with the operation: Scale: i2 = i1 x k1 + k2, where i1 = Green channel, i2 = Red channel, and k1 & k2 are adjustable parameters applied to manually scale the image to desired degrees. These parameters were kept constant for each pathogenicity assay comparison reported (k1 = 3.0 and k2 = 1.0 in this example):

This image has been removed by the author of this thesis for copyright reasons.

iv) A threshold is then applied to distinguish lesions from background using the command: Image > Adjust > Threshold

This image has been removed by the author of this thesis for copyright reasons.

v) For analysis of leaf spot lesions, these lesions were closed and filled to ensure the entire area was measured using the command: Process > Binary > Close-, followed by Process > Binary > Fill Holes.

This image has been removed by the author of this thesis for copyright reasons.

vi) Lesion areas were then calculated from pixel numbers, established using the command: Analyze > Analyze particles, with the settings size (pixel^2): 0-infinity, Circularity: 0.00-1.00. It was established that 1 mm = 49.19 pixels.

7.21 | Fitness measurements

Fitness was calculated from Malthusian growth parameters (m) as described previously (299), where:

$$m = \ln\left[\frac{N(1)}{N(0)}\right]/d$$

when: $N(1) = final\ density$ $N(0) = initial\ density$ $d = time$

During *in planta* fitness measurements and *in vitro* measurements with Δ*qa* mutants, because some replicates returned zero values, violating the assumption of exponential growth in m, we employed a relative fitness (v) that compares changes in relative frequencies (204), where:

$$v = \frac{x_2(1 - x_1)}{x_1(1 - x_2)}$$

when: $x_2 = final\ frequency$ $x_1 = initial\ frequency$

7.22 | Microscopy

Epifluorescent microscopy was performed using either a Olympus IX81 inverted microscope with UPlanSApo x100/1.40 oil or x60/1.35 oil objectives, or a Leica M205FA stereo microscope. Images capturing fluorescent signals were merged using ImageJ image analysis software (National institutes of Health, USA).

7.23 | Data analysis

Plot generation and data analysis was performed in R version 3.1.1 or Microsoft Excel 2010. Pairwise statistical comparisons were made using t-tests. One-way ANOVA was used for comparing multiple groups, with post-hoc Tukey's test for pairwise comparisons of multiple groups. One-sample or two-sample t-tests (as specified) were performed depending on the experimental data being assessed. Two-sided t-tests were performed assuming equal variance when applicable, which was verified using an F-test Two-sample for variance. If data did not have equal variance then a t-test assuming unequal variance was used. For one-way ANOVA, standardised residuals were checked to be approximately normally distributed by plotting a histogram (Figure M2a) and a normal q-q plot (Figure M2b). Homogeneity of variance was verified by plotting standardised residuals against fitted values of the linear model (Figure M2c), and quantified using a Fligner-Killen test of homogeneity. The presence of overly influential data points was tested for by plotting standardised residuals against factor levels and seeing that all data points lie within the "Cook's distance" boundary (Figure M2d).

When experimental data did not conform to the assumptions of these parametric tests, non-parametric models were used. For pairwise comparisons of non-parametric data, a Mann Whitney U-test was performed. To test for differences between multiple groups of non-parametric data a Kruskal-Wallis test was used. For post-hoc pairwise analysis of non-parametric data, a Mann Whitney U-test was performed with Bonferroni correction.

Figure 7.2

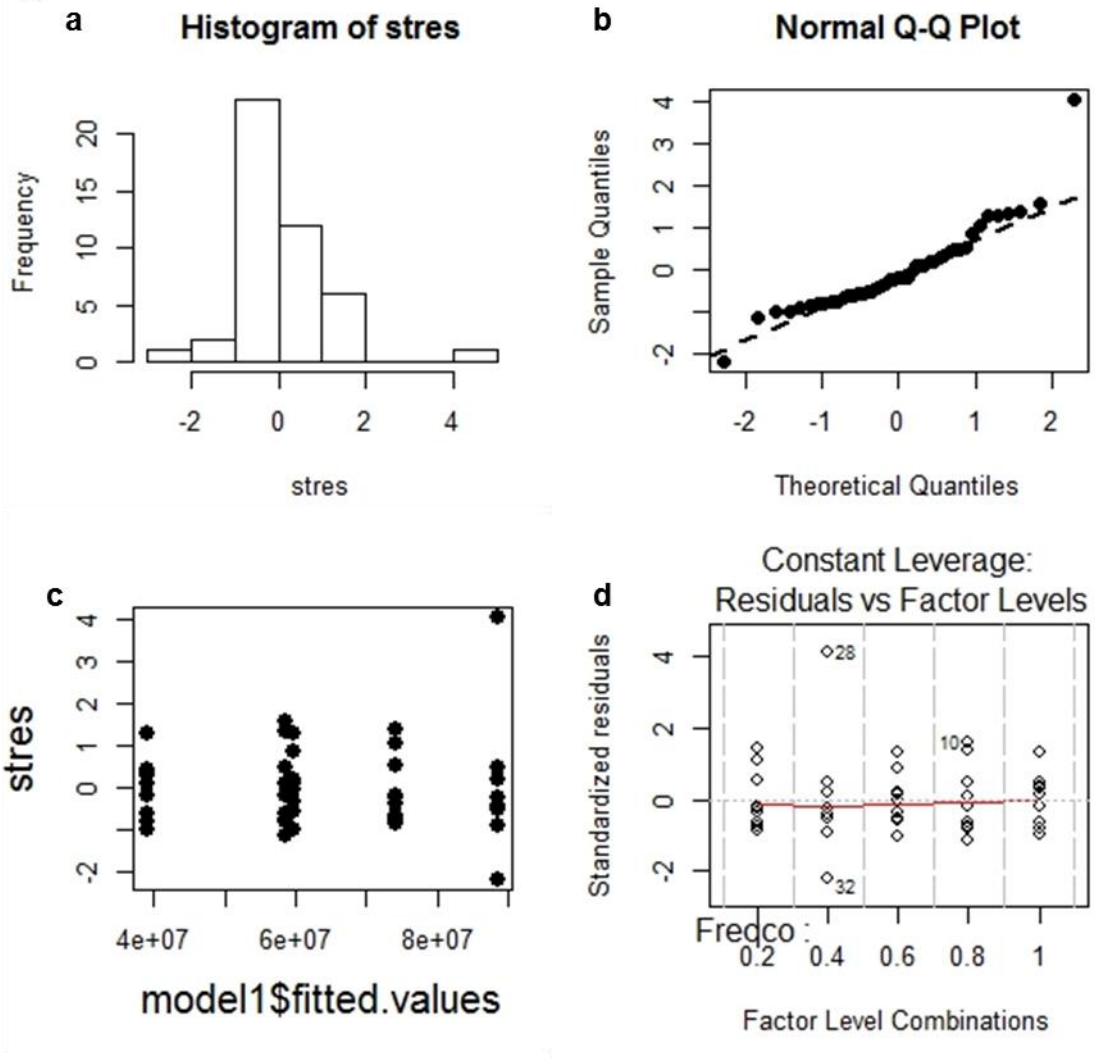

Figure 7.2 | Testing for the assumptions of parametric statistical tests performed in this study. Example plots of the statistical tests that were performed while checking the assumptions of parametric test used. The data in the examples shown is from Figure 2.11a when a one-way ANOVA was performed and assessed after being found to satisfy the associated assumptions of the test. These

assumptions include normally distributed residuals (**a** & **b**), that residuals do not show heteroscedasticity (**c**), and that there are no strongly influential observations (**d**).

7.24 | Protein sequence analysis

Sequence comparison analysis was performed using the BLASTP suite, U.S. National Library of Medicine (http://blast.ncbi.nlm.nih.gov/Blast.cgi?PAGE=Proteins). Comparisons were made against the *Magnaporthe oryzae,* strain 70-15 (141), using the non-redundant protein sequences (nr) database and a protein-protein BLAST algorithm. Nucleotide sequences were obtained from the *Magnaporthe oryzae* comparative Sequencing Project, Broad Institute of Harvard and MIT (http://www.broadinstitute.org/), the *Saccharomyces* Genome Database (313) (SGD, http://www.yeastgenome.org) and for *U. maydis,* MycoCosm, the Fungal Genomics Resource (http://genome.jgi.doe.gov/pages/search-for-genes.jsf?organism=Ustma1) (314).

References

1. Redecker D, Kodner R, Graham LE. Glomalean fungi from the Ordovician. *Science*. 2000;289(5486):1920-1.
2. Crespi B, Foster K, Ubeda F. First principles of Hamiltonian medicine. *Philos Trans R Soc Lond B Biol Sci*. 2014;369(1642):20130366.
3. Tabassum DP, Polyak K. Tumorigenesis: it takes a village. *Nat Rev Cancer*. 2015;15(8):473-83.
4. Schimel JP, Bennett J. Nitrogen mineralization: challenges of a changing paradigm. *Ecology*. 2004;85(3):591-602.
5. Kaiser C, Franklin O, Richter A, Dieckmann U. Social dynamics within decomposer communities lead to nitrogen retention and organic matter build-up in soils. *Nat Commun.* 2015;6:8960.
6. Replansky T, Koufopanou V, Greig D, Bell G. *Saccharomyces sensu stricto* as a model system for evolution and ecology. *Trends Ecol Evol*. 2008;23(9):494-501.
7. Jessup CM, Kassen R, Forde SE, Kerr B, Buckling A, Rainey PB*, et al*. Big questions, small worlds: microbial model systems in ecology. *Trends Ecol Evol*. 2004;19(4):189-97.
8. Goffeau A, Barrell BG, Bussey H, Davis RW, Dujon B, Feldmann H*, et al*. Life with 6000 genes. *Science*. 1996;274(5287):546, 63-7.
9. Ebbole DJ. *Magnaporthe* as a model for understanding host-pathogen interactions. *Annu Rev Phytopathol*. 2007;45:437-56.
10. Davies CM, Fairbrother E, Webster JP. Mixed strain schistosome infections of snails and the evolution of parasite virulence. *Parasitology*. 2002;124(Pt 1):31-8.
11. López-Villavicencio M, Courjol F, Gibson AK, Hood ME, Jonot O, Shykoff JA, *et al*. Competition, cooperation among kin, and virulence in multiple infections. *Evolution*. 2011;65(5):1357-66.
12. Wolf JB, Howie JA, Parkinson K, Gruenheit N, Melo D, Rozen D, *et al*. Fitness trade-offs result in the illusion of social success. *Curr Biol*. 2015;25(8):1086-90.
13. Chuang JS, Rivoire O, Leibler S. Simpson's paradox in a synthetic microbial system. *Science*. 2009;323(5911):272-5.
14. Gore J, Youk H, van Oudenaarden A. Snowdrift game dynamics and facultative cheating in yeast. *Nature*. 2009;459(7244):253-6.
15. Shou W, Ram S, Vilar JM. Synthetic cooperation in engineered yeast populations. *Proc Natl Acad Sci USA.* 2007;104(6):1877-82.
16. Blair JM, Webber MA, Baylay AJ, Ogbolu DO, Piddock LJ. Molecular mechanisms of antibiotic resistance. *Nat Rev Microbiol*. 2015;13(1):42-51.
17. Bush K, Courvalin P, Dantas G, Davies J, Eisenstein B, Huovinen P, *et al.* Tackling antibiotic resistance. *Nat Rev Microbiol.* 2011;9(12):894-6.
18. Dean R, Van Kan JA, Pretorius ZA, Hammond-Kosack KE, Di Pietro A, Spanu PD, *et al*. The Top 10 fungal pathogens in molecular plant pathology. *Mol Plant Pathol*. 2012;13(4):414-30.
19. Pennisi E. Armed and dangerous. *Science*. 2010;327(5967):804-5.
20. Bonman J.M. Durable resistance to rice blast disease - environmental influences. *Euphytica* 1992;63:115-23.
21. Godfray HC, Beddington JR, Crute IR, Haddad L, Lawrence D, Muir JF, *et al.* Food security: the challenge of feeding 9 billion people. *Science*. 2010;327(5967):812-8.
22. Payne DJ, Gwynn MN, Holmes DJ, Pompliano DL. Drugs for bad bugs: confronting the challenges of antibacterial discovery. *Nat Rev Drug Discov.* 2007;6(1):29-40.
23. Sawada H, Sugihara M, Takagaki M, Nagayama K. Monitoring and characterization of *Magnaporthe grisea* isolates with decreased sensitivity to scytalone dehydratase inhibitors. *Pest Manag Sci*. 2004;60(8):777-85.
24. Clatworthy AE, Pierson E, Hung DT. Targeting virulence: a new paradigm for antimicrobial therapy. *Nat Chem Biol.* 2007;3(9):541-8.
25. Korolev KS, Xavier JB, Gore J. Turning ecology and evolution against cancer. *Nat Rev Cancer*. 2014;14(5):371-80.
26. Foster KR. Hamiltonian medicine: why the social lives of pathogens matter. *Science*. 2005;308(5726):1269-70.
27. Jansen G, Gatenby R, Aktipis CA. Control vs. eradication: applying infectious disease treatment strategies to cancer. *Proc Natl Acad Sci USA*. 2015;112(4):937-8.
28. Adalja AA, Kellum JA. *Clostridium difficile*: moving beyond antimicrobial therapy. *Crit Care*. 2010;14(5):320.

29. Rasko DA, Sperandio V. Anti-virulence strategies to combat bacteria-mediated disease. *Nature Rev Drug Discov*. 2010;9(2):117-28.
30. López EL, Contrini MM, Glatstein E, González Ayala S, Santoro R, Allende D, *et al*. Safety and pharmacokinetics of urtoxazumab, a humanized monoclonal antibody, against Shiga-like toxin 2 in healthy adults and in pediatric patients infected with Shiga-like toxin-producing *Escherichia coli. Antimicrob Agents Chemother*. 2010;54(1):239-43.
31. Lowy I, Molrine DC, Leav BA, Blair BM, Baxter R, Gerding DN, *et al*. Treatment with monoclonal antibodies against *Clostridium difficile* toxins*. N Engl J Med*. 2010;362(3):197-205.
32. Ross-Gillespie A, Weigert M, Brown SP, Kümmerli R. Gallium-mediated siderophore quenching as an evolutionarily robust antibacterial treatment. *Evol Med Public Health*. 2014;2014(1):18-29.
33. LaSarre B, Federle MJ. Exploiting quorum sensing to confuse bacterial pathogens. *Microbiol Mol Biol Rev*. 2013;77(1):73-111.
34. Gilbert KB, Kim TH, Gupta R, Greenberg EP, Schuster M. Global position analysis of the *Pseudomonas aeruginosa* quorum-sensing transcription factor LasR. *Mol Microbiol.* 2009;73(6):1072-85.
35. Lee JH, Lee J. Indole as an intercellular signal in microbial communities. *FEMS Microbiol Rev*. 2010;34(4):426-44.
36. Pirhonen M, Flego D, Heikinheimo R, Palva ET. A small diffusible signal molecule is responsible for the global control of virulence and exoenzyme production in the plant pathogen *Erwinia carotovora*. *EMBO J.* 1993;12(6):2467-76.
37. Allen RC, Popat R, Diggle SP, Brown SP. Targeting virulence: can we make evolution-proof drugs? *Nat Rev Microbiol*. 2014;12(4):300-8.
38. García-Contreras R, Maeda T, Wood TK. Resistance to quorum-quenching compounds. *Appl Environ Microbiol*. 2013;79(22):6840-6.
39. García-Contreras R, Pérez-Eretza B, Lira-Silva E, Jasso-Chávez R, Coria-Jiménez R, Rangel-Vega A, *et al.* Gallium induces the production of virulence factors in *Pseudomonas aeruginosa. Pathog Dis.* 2014;70(1):95-8.
40. Köhler T, Perron GG, Buckling A, van Delden C. Quorum sensing inhibition selects for virulence and cooperation in *Pseudomonas aeruginosa*. *PLoS Pathog*. 2010;6(5):e1000883.
41. Pearson MN, Beever RE, Boine B, Arthur K. Mycoviruses of filamentous fungi and their relevance to plant pathology. *Mol Plant Pathol*. 2009;10(1):115-28.
42. Nuss DL. Hypovirulence: mycoviruses at the fungal-plant interface. *Nat Rev Microbiol.* 2005;3(8):632-42.
43. Williams GC, Nesse RM. The dawn of Darwinian medicine. *Q Rev Biol*. 1991;66(1):1-22.
44. Brown SP, West SA, Diggle SP, Griffin AS. Social evolution in micro-organisms and a Trojan horse approach to medical intervention strategies. *Philos Trans R Soc Lond B Biol Sci.* 2009;364(1533):3157-68.
45. Gerding DN, Meyer T, Lee C, Cohen SH, Murthy UK, Poirier A, *et al*. Administration of spores of nontoxigenic *Clostridium difficile* strain M3 for prevention of recurrent *C. difficile* infection: a randomized clinical trial. *JAMA*. 2015;313(17):1719-27.
46. Merrigan MM, Sambol SP, Johnson S, Gerding DN. Prevention of fatal *Clostridium difficile*-associated disease during continuous administration of clindamycin in hamsters. *J Infect Dis*. 2003;188(12):1922-7.
47. Cleveland TE, Dowd PF, Desjardins AE, Bhatnagar D, Cotty PJ. United States Department of Agriculture-Agricultural Research Service research on pre-harvest prevention of mycotoxins and mycotoxigenic fungi in US crops. *Pest Manag Sci.* 2003;59(6-7):629-42.
48. Pitt JI, Hocking AD. Mycotoxins in Australia: biocontrol of aflatoxin in peanuts. *Mycopathologia.* 2006;162(3):233-43.
49. Cotty P. Effect of atoxigenic strains of *Aspergillus flavus* on aflatoxin contamination of developing cottonseed. *Plant Disease*. 1990;74(3):233-5.
50. Cotty P, Bayman P. Competitive exclusion of a toxigenic strain of *Aspergillus flavus* by an atoxigenic strain. *Phytopathology*. 1993;83(12):1283-7.
51. Atehnkeng J, Ojiambo PS, Ikotun T, Sikora RA, Cotty PJ, Bandyopadhyay R. Evaluation of atoxigenic isolates of *Aspergillus flavus* as potential biocontrol agents for aflatoxin in maize. *Food Addit Contam Part A Chem Anal Control Expo Risk Assess.* 2008;25(10):1264-71.
52. Dorner JW. Efficacy of a biopesticide for control of aflatoxins in corn. *J Food Prot.* 2010;73(3):495-9.

53. Riley MA, Wertz JE. Bacteriocins: evolution, ecology, and application. *Annu Rev Microbiol*. 2002;56:117-37.
54. Leeder AC, Palma-Guerrero J, Glass NL. The social network: deciphering fungal language. *Nat Rev Microbiol*. 2011;9(6):440-51.
55. West SA, Griffin AS, Gardner A, Diggle SP. Social evolution theory for microorganisms. *Nat Rev Microbiol.* 2006;4(8):597-607.
56. Lehmann L, Keller L. The evolution of cooperation and altruism--a general framework and a classification of models*. J Evol Biol.* 2006;19(5):1365-76.
57. Sachs JL, Mueller UG, Wilcox TP, Bull JJ. The evolution of cooperation. *Q Rev Biol.* 2004;79(2):135-60.
58. Frank SA. *Foundations of Social Evolution*: Princeton University Press; 1998.
59. Hamilton WD. The genetical evolution of social behaviour. I. *J Theor Biol.* 1964;7(1):1-16.
60. Hamilton WD. The genetical evolution of social behaviour. II. *J Theor Biol.* 1964;7(1):17-52.
61. Hamilton WD. The evolution of altruistic behavior. *Am Nat.* 1963;97(896):354-6.
62. Celiker H, Gore J. Cellular cooperation: insights from microbes. *Trends Cell Biol.* 2013;23(1):9-15.
63. Crespi BJ. The evolution of social behavior in microorganisms. *Trends Ecol Evol.* 2001;16(4):178-83.
64. Velicer GJ. Social strife in the microbial world. *Trends Microbiol*. 2003;11(7):330-7.
65. West SA, Diggle SP, Buckling A, Gardner A, Griffin AS. The Social Lives of Microbes. *Annu Rev Ecol Evol Syst.* 2007;38(1):53-77.
66. Greig D, Travisano M. The Prisoner's Dilemma and polymorphism in yeast *SUC* genes. *Proc R Soc Lond B.* 2004;271 Suppl 3:S25-6.
67. Griffin AS, West SA, Buckling A. Cooperation and competition in pathogenic bacteria. *Nature*. 2004;430(7003):1024-7.
68. Buckling A, Harrison F, Vos M, Brockhurst MA, Gardner A, West SA, *et al.* Siderophore-mediated cooperation and virulence in *Pseudomonas aeruginosa. FEMS Microbiol Ecol.* 2007;62(2):135-41.
69. Diggle SP, Griffin AS, Campbell GS, West SA. Cooperation and conflict in quorum-sensing bacterial populations. *Nature*. 2007;450(7168):411-4.
70. Williams P, Camara M, Hardman A, Swift S, Milton D, Hope VJ, *et al.* Quorum sensing and the population-dependent control of virulence*. Philos Trans R Soc Lond B Biol Sci.* 2000;355(1397):667-80.
71. O'Loughlin EV, Robins-Browne RM. Effect of Shiga toxin and Shiga-like toxins on eukaryotic cells. *Microbes Infect*. 2001;3(6):493-507.
72. Raymond B, West SA, Griffin AS, Bonsall MB. The dynamics of cooperative bacterial virulence in the field. *Science*. 2012;337(6090):85-8.
73. Turner PE, Chao L. Prisoner's dilemma in an RNA virus. *Nature*. 1999;398(6726):441-3.
74. Velicer GJ, Kroos L, Lenski RE. Developmental cheating in the social bacterium *Myxococcus xanthus. Nature.* 2000;404(6778):598-601.
75. Strassmann JE, Zhu Y, Queller DC. Altruism and social cheating in the social amoeba *Dictyostelium discoideum. Nature.* 2000;408(6815):965-7.
76. MacLean RC, Gudelj I. Resource competition and social conflict in experimental populations of yeast. *Nature*. 2006;441(7092):498-501.
77. Pfeiffer T, Schuster S, Bonhoeffer S. Cooperation and competition in the evolution of ATP-producing pathways. *Science*. 2001;292:504.
78. Ackermann M, Stecher B, Freed NE, Songhet P, Hardt WD, Doebeli M. Self-destructive cooperation mediated by phenotypic noise. *Nature*. 2008;454(7207):987-90.
79. Cordero OX, Wildschutte H, Kirkup B, Proehl S, Ngo L, Hussain F, *et al.* Ecological populations of bacteria act as socially cohesive units of antibiotic production and resistance. *Science*. 2012;337(6099):1228-31.
80. Lewis K. Persister cells, dormancy and infectious disease. *Nat Rev Microbiol*. 2007;5(1):48-56.
81. Kolter R, Greenberg EP. Microbial sciences: the superficial life of microbes. *Nature*. 2006;441(7091):300-2.
82. Lee HH, Molla MN, Cantor CR, Collins JJ. Bacterial charity work leads to population-wide resistance. *Nature*. 2010;467(7311):82-5.
83. Chapman A, Fernandez del Ama L, Ferguson J, Kamarashev J, Wellbrock C, Hurlstone A. Heterogeneous tumor subpopulations cooperate to drive invasion. *Cell Rep*. 2014;8(3):688-95.

84. Jiricny N, Diggle SP, West SA, Evans BA, Ballantyne G, Ross-Gillespie A, *et al.* Fitness correlates with the extent of cheating in a bacterium*. J Evol Biol.* 2010;23(4):738-47.
85. MacLean RC, Fuentes-Hernandez A, Greig D, Hurst LD, Gudelj I. A mixture of "cheats" and "co-operators" can enable maximal group benefit. *PLoS Biol.* 2010;8(9): e1000486.
86. West SA, Buckling A. Cooperation, virulence and siderophore production in bacterial parasites. *Proc R Soc Lond B.* 2003;270(1510):37-44.
87. Pollitt EJ, West SA, Crusz SA, Burton-Chellew MN, Diggle SP. Cooperation, quorum sensing, and evolution of virulence in *Staphylococcus aureus*. *Infect Immun*. 2014;82(3):1045-51.
88. Harrison F, Browning LE, Vos M, Buckling A. Cooperation and virulence in acute *Pseudomonas aeruginosa* infections. *BMC Biol*. 2006;4:21.
89. Rainey PB, Rainey K. Evolution of cooperation and conflict in experimental bacterial populations. *Nature*. 2003;425:72.
90. Zhang S, Xu JR. Effectors and effector delivery in *Magnaporthe oryzae. PLoS Pathog.* 2014;10(1):e1003826.
91. Parker D, Beckmann M, Zubair H, Enot DP, Caracuel-Rios Z, Overy DP, *et al*. Metabolomic analysis reveals a common pattern of metabolic re-programming during invasion of three host plant species by Ma*gnaporthe grisea*. *Plant J*. 2009;59(5):723-37.
92. Patkar RN, Benke PI, Qu Z, Chen YY, Yang F, Swarup S, *et al.* A fungal monooxygenase-derived jasmonate attenuates host innate immunity. *Nat Chem Biol.* 2015;11(9):733-40.
93. Meyer JR, Gudelj I, Beardmore R. Biophysical mechanisms that maintain biodiversity through trade-offs. *Nat Commun.* 2015;6:6278.
94. Axelrod R, Hamilton WD. The evolution of cooperation. *Science*. 1981;211(4489):1390-6.
95. Trivers RL. The evolution of reciprocal altruism. *Q Rev Biol.* 1971:35-57.
96. Hardin G. The tragedy of the commons. *Science*. 1968;162:1243.
97. West SA, Griffin AS, Gardner A. Social semantics: altruism, cooperation, mutualism, strong reciprocity and group selection. *J Evol Biol*. 2007;20(2):415-32.
98. Maynard-Smith J. Group selection and kin selection. *Nature*. 1964;201:1145-7.
99. Mitteldorf J, Wilson DS. Population viscosity and the evolution of altruism. *J Theor Biol*. 2000;204(4):481-96.
100. Kümmerli R, Gardner A, West SA, Griffin AS. Limited dispersal, budding dispersal, and cooperation: an experimental study. *Evolution*. 2009;63(4):939-49.
101. Li SI, Purugganan MD. The cooperative amoeba: *Dictyostelium* as a model for social evolution. *Trends Genet*. 2011;27(2):48-54.
102. Xavier JB, Foster KR. Cooperation and conflict in microbial biofilms. *Proc Natl Acad Sci USA.* 2007;104(3):876-81.
103. Strassmann JE, Gilbert OM, Queller DC. Kin discrimination and cooperation in microbes. *Annu Rev Microbiol.* 2011;65:349-67.
104. Smukalla S, Caldara M, Pochet N, Beauvais A, Guadagnini S, Yan C, *et al*. *FLO1* is a variable green beard gene that drives biofilm-like cooperation in budding yeast. *Cell*. 2008;135(4):726-37.
105. Queller DC, Ponte E, Bozzaro S, Strassmann JE. Single-gene greenbeard effects in the social amoeba *Dictyostelium discoideum. Science*. 2003;299(5603):105-6.
106. Koschwanez JH, Foster KR, Murray AW. Sucrose utilization in budding yeast as a model for the origin of undifferentiated multicellularity. *PLoS Biol*. 2011;9(8):e1001122.
107. Wilson DS. A theory of group selection. *Proc Natl Acad Sci USA.* 1975;72(1):143-6.
108. Blyth CR. On Simpson's paradox and the sure-thing principle*. JASA.* 1972;67(338):364-6.
109. Harrison F, Buckling A. Siderophore production and biofilm formation as linked social traits. *ISME J.* 2009;3(5):632-4.
110. Dandekar AA, Chugani S, Greenberg EP. Bacterial quorum sensing and metabolic incentives to cooperate. *Science*. 2012;338(6104):264-6.
111. Foster KR, Shaulsky G, Strassmann JE, Queller DC, Thompson CR. Pleiotropy as a mechanism to stabilize cooperation. *Nature*. 2004;431(7009):693-6.
112. Rumbaugh KP, Diggle SP, Watters CM, Ross-Gillespie A, Griffin AS, West SA. Quorum sensing and the social evolution of bacterial virulence. *Curr Biol.* 2009;19(4):341-5.
113. Köhler T, Buckling A, van Delden C. Cooperation and virulence of clinical *Pseudomonas aeruginosa* populations*. Proc Natl Acad Sci USA*. 2009;106(15):6339-44.
114. Brown SP, Hochberg ME, Grenfell BT. Does multiple infection select for raised virulence? *Trends Microbiol*. 2002;10(9):401-5.
115. Buckling A, Brockhurst MA. Kin selection and the evolution of virulence. *Heredity*. 2008;100(5):484-8.

116. Anderson RM, May RM. Coevolution of hosts and parasites. *Parasitology*. 1982;85 (Pt 2):411-26.
117. Bremermann HJ, Pickering J. A game-theoretical model of parasite virulence. *J Theor Biol.* 1983;100(3):411-26.
118. Nowak MA, May RM. Superinfection and the evolution of parasite virulence. *Proc R Soc Lond B*. 1994;255(1342):81-9.
119. Frank SA. Models of parasite virulence. *Q Rev Biol*. 1996;71(1):37-78.
120. Ebert D, Bull JJ. Challenging the trade-off model for the evolution of virulence: is virulence management feasible? *Trends Microbiol*. 2003;11(1):15-20.
121. Read AF, Taylor LH. The ecology of genetically diverse infections. *Science*. 2001;292(5519):1099-102.
122. Hood ME. Dynamics of multiple infection and within-host competition by the anther-smut pathogen. *Am Nat*. 2003;162(1):122-33.
123. Balmer O, Tanner M. Prevalence and implications of multiple-strain infections. *Lancet Infect Dis*. 2011;11(11):868-78.
124. Staves PA, Knell RJ. Virulence and competitiveness: testing the relationship during inter- and intraspecific mixed infections. *Evolution*. 2010;64(9):2643-52.
125. Ben-Ami F, Mouton L, Ebert D. The effects of multiple infections on the expression and evolution of virulence in a *Daphnia*-endoparasite system. *Evolution*. 2008;62(7):1700-11.
126. de Roode JC, Helinski ME, Anwar MA, Read AF. Dynamics of multiple infection and within-host competition in genetically diverse malaria infections. *Am Nat*. 2005;166(5):531-42.
127. Chao L, Hanley KA, Burch CL, Dahlberg C, Turner PE. Kin selection and parasite evolution: higher and lower virulence with hard and soft selection. *Q Rev Biol*. 2000;75(3):261-75.
128. Brown SP, Johnstone RA. Cooperation in the dark: signalling and collective action in quorum-sensing bacteria. *Proc R Soc Lond B*. 2001;268(1470):961-5.
129. Brown SP. Collective action in an RNA virus. *J Evol Biol*. 2001;14(5):821-8.
130. Zelikovich N, Eyal Z. Reduction in pycnidial coverage after inoculation of wheat with mixtures of isolates of *Septoria tritici. Plant Disease*. 1991;75(9):907-10.
131. Eyal Z. The response of field-inoculated wheat cultivars to mixtures of *Septoria tritici* isolates. *Euphytica*. 1992;61(1):25-35.
132. Schürch S, Roy BA. Comparing single-vs. mixed-genotype infections of *Mycosphaerella graminicola* on wheat: effects on pathogen virulence and host tolerance. *Evol Ecol*. 2004;18(1):1-14.
133. Maltby A, Mihail J. Competition among *Sclerotinia sclerotiorum* genotypes within canola stems. *Can J Bot*. 1997;75(3):462-8.
134. Vizoso DB, Ebert D. Mixed inoculations of a microsporidian parasite with horizontal and vertical infections. *Oecologia*. 2005;143(1):157-66.
135. Vardo-Zalik AM, Schall JJ. Clonal diversity alters the infection dynamics of a malaria parasite (*Plasmodium mexicanum*) in its vertebrate host. *Ecology*. 2009;90(2):529-36.
136. Bashey F, Reynolds C, Sarin T, Young SK. Virulence and competitive ability in an obligately killing parasite. *Oikos*. 2011;120(10):1539-45.
137. Schmid-Hempel P, Puhr K, Kruger N, Reber C, Schmid-Hempel R. Dynamic and genetic consequences of variation in horizontal transmission for a microparasitic infection. *Evolution*. 1999:426-34.
138. De Roode JC, Read AF, Chan BH, Mackinnon MJ. Rodent malaria parasites suffer from the presence of conspecific clones in three-clone *Plasmodium chabaudi* infections. *Parasitology*. 2003;127(Pt 5):411-8.
139. Choisy M, de Roode JC. Mixed infections and the evolution of virulence: effects of resource competition, parasite plasticity, and impaired host immunity. *Am Nat*. 2010;175(5):E105-18.
140. Talbot NJ. On the trail of a cereal killer: Exploring the biology of *Magnaporthe grisea. Annu Rev Microbiol.* 2003;57:177-202.
141. Dean RA, Talbot NJ, Ebbole DJ, Farman ML, Mitchell TK, Orbach MJ*, et al*. The genome sequence of the rice blast fungus *Magnaporthe grisea. Nature*. 2005;434(7036):980-6.
142. Ou S. Pathogen variability and host resistance in rice blast disease. *Ann rev phytopath*. 1980;18(1):167-87.
143. Jeon J, Park SY, Chi MH, Choi J, Park J, Rho HS, *et al.* Genome-wide functional analysis of pathogenicity genes in the rice blast fungus. *Nat Genet*. 2007;39(4):561-5.
144. Martin-Urdiroz M, Oses-Ruiz M, Ryder LS, Talbot NJ. Investigating the biology of plant infection by the rice blast fungus *Magnaporthe oryzae*. *Fungal Genet Biol*. 2015.

145. Yu JH, Hamari Z, Han KH, Seo JA, Reyes-Domínguez Y, Scazzocchio C. Double-joint PCR: a PCR-based molecular tool for gene manipulations in filamentous fungi. *Fungal Genet Biol.* 2004;41(11):973-81.
146. Kershaw MJ, Talbot NJ. Genome-wide functional analysis reveals that infection-associated fungal autophagy is necessary for rice blast disease. *Proc Natl Acad Sci USA*. 2009;106(37):15967-72.
147. Mentlak TA, Kombrink A, Shinya T, Ryder LS, Otomo I, Saitoh H, *et al*. Effector-mediated suppression of chitin-triggered immunity by *Magnaporthe oryzae* is necessary for rice blast disease. *Plant Cell*. 2012;24(1):322-35.
148. Gilbert R, Johnson A, Dean RA. Chemical signals responsible for appressorium formation in the rice blast fungus *Magnaporthe grisea*. *Physiol Mol Plant Pathol*. 1996;48(5):335-46.
149. Jelitto TC, Page HA, Read ND. Role of external signals in regulating the pre-penetration phase of infection by the rice blast fungus, *Magnaporthe grisea. Planta.* 1994;194(4):471-7.
150. Park G, Xue C, Zheng L, Lam S, Xu JR. *MST12* regulates infectious growth but not appressorium formation in the rice blast fungus *Magnaporthe grisea. Mol Plant Microbe Interact*. 2002;15(3):183-92.
151. Park G, Bruno KS, Staiger CJ, Talbot NJ, Xu JR. Independent genetic mechanisms mediate turgor generation and penetration peg formation during plant infection in the rice blast fungus. *Mol Microbiol*. 2004;53(6):1695-707.
152. Xu JR, Hamer JE. MAP kinase and cAMP signaling regulate infection structure formation and pathogenic growth in the rice blast fungus *Magnaporthe grisea. Genes Dev*. 1996;10(21):2696-706.
153. de Jong JC, McCormack BJ, Smirnoff N, Talbot NJ. Glycerol generates turgor in rice blast. *Nature*. 1997;389(6648):244-.
154. Veneault-Fourrey C, Barooah M, Egan M, Wakley G, Talbot NJ. Autophagic fungal cell death is necessary for infection by the rice blast fungus. *Science*. 2006;312(5773):580-3.
155. Deng Y, Qu Z, Naqvi NI. Role of macroautophagy in nutrient homeostasis during fungal development and pathogenesis. *Cells*. 2012;1(3):449-63.
156. Kankanala P, Czymmek K, Valent B. Roles for rice membrane dynamics and plasmodesmata during biotrophic invasion by the blast fungus. *Plant Cell*. 2007;19(2):706-24.
157. Wilson RA, Talbot NJ. Under pressure: investigating the biology of plant infection by *Magnaporthe oryzae*. *Nat Rev Microbiol*. 2009;7(3):185-95.
158. Mekwatanakarn P, Kositratana W, Levy M, Zeigler R. Pathotype and avirulence gene diversity of *Pyricularia grisea* in Thailand as determined by rice lines near-isogenic for major resistance genes. *Plant Disease*. 2000;84(1):60-70.
159. Kumar J, Nelson RJ, Zeigler RS. Population structure and dynamics of *Magnaporthe grisea* in the Indian Himalayas. *Genetics*. 1999;152(3):971-84.
160. Mendgen K, Hahn M. Plant infection and the establishment of fungal biotrophy. *Trends Plant Sci.* 2002;7(8):352-6.
161. Talbot NJ. Living the sweet life: how does a plant pathogenic fungus acquire sugar from plants? *PLoS Biol*. 2010;8(2):e1000308.
162. Kubicek CP, Starr TL, Glass NL. Plant cell wall-degrading enzymes and their secretion in plant-pathogenic fungi. *Annu Rev Phytopathol*. 2014;52:427-51.
163. Lim JD, Cho JI, Park YI, Hahn TR, Choi SB, Jeon JS. Sucrose transport from source to sink seeds in rice. *Physiologia Plantarum*. 2006;126(4):572-84.
164. Weber H, Roitsch T. Invertases and life beyond sucrose cleavage. *Trends Plant Sci*. 2000;5(2):47-8.
165. Parrent JL, James TY, Vasaitis R, Taylor AF. Friend or foe? Evolutionary history of glycoside hydrolase family 32 genes encoding for sucrolytic activity in fungi and its implications for plant-fungal symbioses. *BMC Evol Biol*. 2009;9:148.
166. Dallagnol L, Rodrigues F, Chaves AdM, Vale F, DaMatta F. Photosynthesis and sugar concentration are impaired by the defective active silicon uptake in rice plants infected with *Bipolaris oryzae*. *Plant Pathol*. 2013;62(1):120-9.
167. Fernandez J, Wright JD, Hartline D, Quispe CF, Madayiputhiya N, Wilson RA. Principles of carbon catabolite repression in the rice blast fungus: *Tps1*, *Nmr1-3*, and a MATE-family pump regulate glucose metabolism during infection. *PLoS Genet*. 2012;8(5):e1002673.
168. Voegele RT, Struck C, Hahn M, Mendgen K. The role of haustoria in sugar supply during infection of broad bean by the rust fungus *Uromyces fabae*. *Proc Natl Acad Sci USA*. 2001;98(14):8133-8.

169. Doehlemann G, Molitor F, Hahn M. Molecular and functional characterization of a fructose specific transporter from the gray mold fungus *Botrytis cinerea. Fungal Genet Biol.* 2005;42(7):601-10.
170. Schüssler A, Martin H, Cohen D, Fitz M, Wipf D. Characterization of a carbohydrate transporter from symbiotic glomeromycotan fungi. *Nature*. 2006;444(7121):933-6.
171. Polidori E, Ceccaroli P, Saltarelli R, Guescini M, Menotta M, Agostini D, *et al*. Hexose uptake in the plant symbiotic ascomycete *Tuber borchii* Vittadini: biochemical features and expression pattern of the transporter *TBHXT1*. *Fungal Genet Biol*. 2007;44(3):187-98.
172. Wahl R, Wippel K, Goos S, Kämper J, Sauer N. A novel high-affinity sucrose transporter is required for virulence of the plant pathogen *Ustilago maydis. PLoS Biol*. 2010;8(2):e1000303.
173. Hwang BK, Kim KD, Kim YB. Carbohydrate composition and acid invertase activity in rice leaves infected with *Pyricularia oryzae*. *J Phytopathol*. 1989;125(2):124-32.
174. Doidy J, Grace E, Kühn C, Simon-Plas F, Casieri L, Wipf D. Sugar transporters in plants and in their interactions with fungi. *Trends Plant Sci*. 2012;17(7):413-22.
175. Sutton PN, Gilbert MJ, Williams LE, Hall J. Powdery mildew infection of wheat leaves changes host solute transport and invertase activity. *Physiologia Plantarum*. 2007;129(4):787-95.
176. Cho JI, Lee SK, Ko S, Kim HK, Jun SH, Lee YH, *et al*. Molecular cloning and expression analysis of the cell-wall invertase gene family in rice (*Oryza sativa* L.). *Plant Cell Rep.* 2005;24(4):225-36.
177. Voegele RT, Mendgen KW. Nutrient uptake in rust fungi: how sweet is parasitic life? *Euphytica*. 2011;179(1):41-55.
178. Ruiz E, Ruffner H. Immunodetection of *Botrytis*-specific invertase in infected grapes*. J Phytopathol*. 2002;150(2):76-85.
179. Voegele RT, Wirsel S, Möll U, Lechner M, Mendgen K. Cloning and characterization of a novel invertase from the obligate biotroph *Uromyces fabae* and analysis of expression patterns of host and pathogen invertases in the course of infection. *Mol Plant Microbe Interact.* 2006;19(6):625-34.
180. Wilson RA, Fernandez J, Quispe CF, Gradnigo J, Seng A, Moriyama E*, et al*. Towards defining nutrient conditions encountered by the rice blast fungus during host infection. *PLoS One*. 2012;7(10):e47392.
181. Wilson RA, Jenkinson JM, Gibson RP, Littlechild JA, Wang ZY, Talbot NJ. *Tps1* regulates the pentose phosphate pathway, nitrogen metabolism and fungal virulence. *EMBO J*. 2007;26(15):3673-85.
182. Tanzer MM, Arst HN, Skalchunes AR, Coffin M, Darveaux BA, Heiniger RW, *et al*. Global nutritional profiling for mutant and chemical mode-of-action analysis in filamentous fungi. *Funct Integr Genomics*. 2003;3(4):160-70.
183. Wilson RA, Gibson RP, Quispe CF, Littlechild JA, Talbot NJ. An NADPH-dependent genetic switch regulates plant infection by the rice blast fungus. *Proc Natl Acad Sci USA*. 2010;107(50):21902-7.
184. Fernandez J, Wilson RA. The sugar sensor, trehalose-6-phosphate synthase (*Tps1*), regulates primary and secondary metabolism during infection by the rice blast fungus: Will *Magnaporthe oryzae'*s “sweet tooth” become its “Achilles’ heel”? *Mycology*. 2011;2(1):46-53.
185. Franceschetti M, Bueno E, Wilson RA, Tucker SL, Gómez-Mena C, Calder G, *et al*. Fungal virulence and development is regulated by alternative pre-mRNA 3'end processing in *Magnaporthe oryzae*. *PLoS Pathog*. 2011;7(12):e1002441.
186. Lombard V, Golaconda Ramulu H, Drula E, Coutinho PM, Henrissat B. The carbohydrate-active enzymes database (CAZy) in 2013. *Nucleic Acids Res*. 2014;42(Database issue):D490-5.
187. Horton P, Park K-J, Obayashi T, Fujita N, Harada H, Adams-Collier C, *et al*. WoLF PSORT: protein localization predictor. *Nucleic Acids Res*. 2007;35(suppl 2):W585-W7.
188. Petersen TN, Brunak S, von Heijne G, Nielsen H. SignalP 4.0: discriminating signal peptides from transmembrane regions. *Nature methods*. 2011;8(10):785-6.
189. Vainstein MH, Peberdy JF. Regulation of invertase in *Aspergillus nidulans*: effect of different carbon sources. *J Gen Microbiol*. 1991;137(2):315-21.
190. Chen W-c, Liu C-h. Production of β-fructofuranosidase by *Aspergillus japonicus. Enzyme Microb Technol*. 1996;18(2):153-60.
191. Rubio M, Navarro A. Regulation of invertase synthesis in *Aspergillus niger*. *Enzyme Microb Technol.* 2006;39(4):601-6.

192. Dodyk F, Rothstein A. Factors influencing the appearance of invertase in *Saccharomyces cerevisiae. Arch Biochem Biophys*. 1964;104:478-86.
193. Neigeborn L, Carlson M. Genes affecting the regulation of *SUC2* gene expression by glucose repression in *Saccharomyces cerevisiae. Genetics*. 1984;108(4):845-58.
194. Giraldo MC, Dagdas YF, Gupta YK, Mentlak TA, Yi M, Martinez-Rocha AL*, et al*. Two distinct secretion systems facilitate tissue invasion by the rice blast fungus *Magnaporthe oryzae. Nat Commun*. 2013;4:1996.
195. Perlman D, Raney P, Halvorson HO. Cytoplasmic and secreted *Saccharomyces cerevisiae* invertase mRNAs encoded by one gene can be differentially or coordinately regulated. *Mol Cell Biol*. 1984;4(9):1682-8.
196. Parker D, Beckmann M, Enot DP, Overy DP, Rios ZC, Gilbert M*, et al*. Rice blast infection of *Brachypodium distachyon* as a model system to study dynamic host/pathogen interactions. *Nat Protoc*. 2008;3(3):435-45.
197. Roitsch T, Balibrea ME, Hofmann M, Proels R, Sinha AK. Extracellular invertase: key metabolic enzyme and PR protein. *J Exp Bot*. 2003;54(382):513-24.
198. Rolland F, Baena-Gonzalez E, Sheen J. Sugar sensing and signaling in plants: conserved and novel mechanisms. *Annu Rev Plant Biol*. 2006;57:675-709.
199. Kaiser CA, Botstein D. Secretion-defective mutations in the signal sequence for *Saccharomyces cerevisiae* invertase*. Mol Cell Biol.* 1986;6(7):2382-91.
200. Sauer N, Stolz J. *SUC1* and *SUC2*: two sucrose transporters from *Arabidopsis thaliana*; expression and characterization in baker's yeast and identification of the histidine-tagged protein. *Plant J.* 1994;6(1):67-77.
201. Bitter GA, Egan KM. Expression of heterologous genes in *Saccharomyces cerevisiae* from vectors utilizing the glyceraldehyde-3-phosphate dehydrogenase gene promoter. *Gene*. 1984;32(3):263-74.
202. Sweigard JA, Chumley F, Carroll A, Farrall L, Valent B. A series of vectors for fungal transformation. *Fungal Genet NewsI*. 1997:52-3.
203. Naumov GI, Naumova ES, Sancho ED, Korhola MP. Polymeric *SUC* genes in natural populations of *Saccharomyces cerevisiae. FEMS Microbiol Lett*. 1996;135(1):31-5.
204. Ross-Gillespie A, Gardner A, West SA, Griffin AS. Frequency dependence and cooperation: theory and a test with bacteria*. Am Nat*. 2007;170(3):331-42.
205. Ribeck N, Lenski RE. Modeling and quantifying frequency-dependent fitness in microbial populations with cross-feeding interactions. *Evolution*. 2015;69(5):1313-20.
206. Drescher K, Nadell CD, Stone HA, Wingreen NS, Bassler BL. Solutions to the public goods dilemma in bacterial biofilms. *Curr Biol.* 2014;24(1):50-5.
207. Soanes DM, Chakrabarti A, Paszkiewicz KH, Dawe AL, Talbot NJ. Genome-wide transcriptional profiling of appressorium development by the rice blast fungus *Magnaporthe oryzae. PLoS Pathog.* 2012;8(2):e1002514.
208. Lamb HK, Hawkins AR, Smith M, Harvey IJ, Brown J, Turner G, *et al.* Spatial and biological characterisation of the complete quinic acid utilisation gene cluster in *Aspergillus nidulans. Mol Gen Genet.* 1990;223(1):17-23.
209. Glass NL, Rasmussen C, Roca MG, Read ND. Hyphal homing, fusion and mycelial interconnectedness. *Trends Microbiol*. 2004;12(3):135-41.
210. Inglis RF, Brown SP, Buckling A. Spite versus cheats: competition among social strategies shapes virulence in *Pseudomonas aeruginosa. Evolution*. 2012;66(11):3472-84.
211. Brown SP, Taylor PD. Joint evolution of multiple social traits: a kin selection analysis*. Proc R Soc B*. 2009:rspb20091480.
212. Saitoh H, Hirabuchi A, Fujisawa S, Mitsuoka C, Terauchi R, Takano Y. *MoST1* encoding a hexose transporter-like protein is involved in both conidiation and mycelial melanization of *Magnaporthe oryzae. FEMS Microbiol Lett*. 2014;352(1):104-13.
213. Talbot NJ, McCafferty HRK, Ma M, Moore K, Hamer JE. Nitrogen starvation of the rice blast fungus *Magnaporthe grisea* may act as an environmental cue for disease symptom expression. *Physiol Mol Plant P*. 1997;50(3):179-95.
214. Frey P, Prior P, Marie C, Kotoujansky A, Trigalet-Demery D, Trigalet A. Hrp$^-$ mutants of *Pseudomonas solanacearum* as potential biocontrol agents of tomato bacterial wilt. *Appl Environ Microbiol.* 1994;60(9):3175-81.
215. Hirakawa H, Kodama T, Takumi-Kobayashi A, Honda T, Yamaguchi A. Secreted indole serves as a signal for expression of type III secretion system translocators in enterohaemorrhagic *Escherichia coli* O157:H7. *Microbiology*. 2009;155(Pt 2):541-50.

216. Driscoll WW, Pepper JW, Pierson LS, Pierson EA. Spontaneous Gac mutants of *Pseudomonas* biological control strains: cheaters or mutualists? *Appl Environ Microbiol*. 2011;77(20):7227-35.
217. Alizon S, de Roode JC, Michalakis Y. Multiple infections and the evolution of virulence. *Ecol Lett.* 2013;16(4):556-67.
218. Nagy JD, Armbruster D. Evolution of uncontrolled proliferation and the angiogenic switch in cancer. *Math Biosci Eng*. 2012;9(4):843-76.
219. Gillies RJ, Gatenby RA. Adaptive landscapes and emergent phenotypes: why do cancers have high glycolysis? *J Bioenerg Biomembr*. 2007;39(3):251-7.
220. Richards TA, Talbot NJ. Horizontal gene transfer in osmotrophs: playing with public goods. *Nat Rev Microbiol.* 2013;11(10):720-7.
221. Farman ML, Eto Y, Nakao T, Tosa Y, Nakayashiki H, Mayama S, *et al.* Analysis of the structure of the *AVR1-CO39* avirulence locus in virulent rice-infecting isolates of *Magnaporthe grisea. Mol Plant Microbe Interact*. 2002;15(1):6-16.
222. Kang S, Lebrun MH, Farrall L, Valent B. Gain of virulence caused by insertion of a Pot3 transposon in a *Magnaporthe grisea* avirulence gene. *Mol Plant Microbe Interact*. 2001;14(5):671-4.
223. El-Said A. Mycotoxins and invertase enzyme of the mycoflora of molasses in Upper Egypt. *Mycobiology*. 2002;30(3):170-4.
224. Natarajan M, Walk ST, Young VB, Aronoff DM. A clinical and epidemiological review of non-toxigenic *Clostridium difficile. Anaerobe*. 2013;22:1-5.
225. Jia Y, Valent B, Lee F. Determination of host responses to *Magnaporthe grisea* on detached rice leaves using a spot inoculation method. *Plant Disease*. 2003;87(2):129-33.
226. Valent B, Farrall L, Chumley FG. *Magnaporthe grisea* genes for pathogenicity and virulence identified through a series of backcrosses. *Genetics*. 1991;127(1):87-101.
227. Prabhu AS, Filippi MC, Silva GB, Lobo VLS, Morais OP. An unprecedented outbreak of rice blast on a newly released cultivar BRS Colosso in Brazil. In: *Advances in Genetics, Genomics and Control of Rice Blast Disease*. Springer; 2009. p. 257-66.
228. Liu R, Chen L, Jiang Y, Zhou Z, Zou G. Efficient genome editing in filamentous fungus *Trichoderma reesei* using the CRISPR/Cas9 system. *Cell Discovery*. 2015;1.
229. Jones JD, Dangl JL. The plant immune system. *Nature*. 2006;444(7117):323-9.
230. Conrath U, Pieterse CM, Mauch-Mani B. Priming in plant-pathogen interactions. *Trends Plant Sci.* 2002;7(5):210-6.
231. Sesma A, Osbourn AE. The rice leaf blast pathogen undergoes developmental processes typical of root-infecting fungi. *Nature*. 2004;431(7008):582-6.
232. Lorang JM, Tuori R, Martinez J, Sawyer T, Redman R, Rollins J, *et al*. Green fluorescent protein is lighting up fungal biology. *Appl Environ Microbiol*. 2001;67(5):1987-94.
233. Schuster M, Lipowsky R, Assmann M-A, Lenz P, Steinberg G. Transient binding of dynein controls bidirectional long-range motility of early endosomes. *Proc of the Natl Acad Sci USA*. 2011;108(9):3618-23.
234. Zhang H, Wu Z, Wang C, Li Y, Xu JR. Germination and infectivity of microconidia in the rice blast fungus *Magnaporthe oryzae*. *Nat Commun*. 2014;5:4518.
235. Pringle A, Taylor J. The fitness of filamentous fungi. *Trends Microbiol*. 2002;10(10):474-81.
236. Bauchop T, Elsden SR. The growth of micro-organisms in relation to their energy supply. *J Gen Microbiol.* 1960;23:457-69.
237. Beardmore RE, Gudelj I, Lipson DA, Hurst LD. Metabolic trade-offs and the maintenance of the fittest and the flattest. *Nature*. 2011;472(7343):342-6.
238. Wilson RA, Arst HN. Mutational analysis of *AREA*, a transcriptional activator mediating nitrogen metabolite repression in *Aspergillus nidulans* and a member of the "streetwise" GATA family of transcription factors. *Microbiol Mol Biol Rev*. 1998;62(3):586-96.
239. Froeliger EH, Carpenter BE. *NUT1*, a major nitrogen regulatory gene in *Magnaporthe grisea*, is dispensable for pathogenicity. *Mol Gen Genet*. 1996;251(6):647-56.
240. ten Have A, Espino JJ, Dekkers E, Van Sluyter SC, Brito N, Kay J*, et al*. The *Botrytis cinerea* aspartic proteinase family. *Fungal Genet Biol*. 2010;47(1):53-65.
241. Showalter AM. Structure and function of plant cell wall proteins. *Plant Cell*. 1993;5(1):9-23.
242. Hall Q, Cannon MC. The cell wall hydroxyproline-rich glycoprotein RSH is essential for normal embryo development in *Arabidopsis*. *Plant Cell*. 2002;14(5):1161-72.
243. van Loon LC, Rep M, Pieterse CM. Significance of inducible defense-related proteins in infected plants. *Annu Rev Phytopathol*. 2006;44:135-62.

244. Jia Y, McAdams SA, Bryan GT, Hershey HP, Valent B. Direct interaction of resistance gene and avirulence gene products confers rice blast resistance*. EMBO J.* 2000;19(15):4004-14.
245. Cohen B. Ammonium repression of extracellular protease in *Aspergillus nidulans*. *Microbiology*. 1972;71(2):293-9.
246. Hynes MJ. Effects of ammonium, L-glutamate, and L-glutamine on nitrogen catabolism in *Aspergillus nidulans. J Bacteriol*. 1974;120(3):1116-23.
247. Hynes MJ, Kelly JM. Pleiotropic mutants of *Aspergillus nidulans* altered in carbon metabolism. *Mol Gen Genet*. 1977;150(2):193-204.
248. Dagdas YF, Yoshino K, Dagdas G, Ryder LS, Bielska E, Steinberg G, *et al*. Septin-mediated plant cell invasion by the rice blast fungus, *Magnaporthe oryzae. Science*. 2012;336(6088):1590-5.
249. He M, Kershaw MJ, Soanes DM, Xia Y, Talbot NJ. Infection-associated nuclear degeneration in the rice blast fungus *Magnaporthe oryzae* requires non-selective macro-autophagy. *PLoS One*. 2012;7(3):e33270.
250. Ryder LS, Dagdas YF, Mentlak TA, Kershaw MJ, Thornton CR, Schuster M*, et al*. NADPH oxidases regulate septin-mediated cytoskeletal remodeling during plant infection by the rice blast fungus. *Proc Natl Acad Sci USA*. 2013;110(8):3179-84.
251. Steinberg G, Schliwa M, Lehmler C, Bölker M, Kahmann R, McIntosh JR. Kinesin from the plant pathogenic fungus *Ustilago maydis* is involved in vacuole formation and cytoplasmic migration. *J Cell Sci*. 1998;111 (Pt 15):2235-46.
252. Wolff AM, Din N, Petersen JG. Vacuolar and extracellular maturation of *Saccharomyces cerevisiae* proteinase A. *Yeast.* 1996;12(9):823-32.
253. Ammerer G, Hunter CP, Rothman JH, Saari GC, Valls LA, Stevens TH. *PEP4* gene of *Saccharomyces cerevisiae* encodes proteinase A, a vacuolar enzyme required for processing of vacuolar precursors. *Mol Cell Biol*. 1986;6(7):2490-9.
254. Barrett LW, Fletcher S, Wilton SD. Regulation of eukaryotic gene expression by the untranslated gene regions and other non-coding elements. *Cell Mol Life Sci*. 2012;69(21):3613-34.
255. Parr CL, Keates RA, Bryksa BC, Ogawa M, Yada RY. The structure and function of *Saccharomyces cerevisiae* proteinase A. *Yeast*. 2007;24(6):467-80.
256. Takeshige K, Baba M, Tsuboi S, Noda T, Ohsumi Y. Autophagy in yeast demonstrated with proteinase-deficient mutants and conditions for its induction. *J Cell Biol*. 1992;119(2):301-11.
257. Jones EW. Three proteolytic systems in the yeast *Saccharomyces cerevisiae. J Biol Chem*. 1991;266(13):7963-6.
258. Nadell CD, Foster KR, Xavier JB. Emergence of spatial structure in cell groups and the evolution of cooperation. *PLoS Comput Biol.* 2010;6(3):e1000716.
259. James TY, Kauff F, Schoch CL, Matheny PB, Hofstetter V, Cox CJ, *et al*. Reconstructing the early evolution of Fungi using a six-gene phylogeny. *Nature*. 2006;443(7113):818-22.
260. Brown CJ, Todd KM, Rosenzweig RF. Multiple duplications of yeast hexose transport genes in response to selection in a glucose-limited environment. *Mol Biol Evol*. 1998;15(8):931-42.
261. Galeote V, Novo M, Salema-Oom M, Brion C, Valério E, Gonçalves P, *et al*. *FSY1*, a horizontally transferred gene in the *Saccharomyces cerevisiae* EC1118 wine yeast strain, encodes a high-affinity fructose/H+ symporter. *Microbiology*. 2010;156(Pt 12):3754-61.
262. Bermudez Moretti M, Perullini AM, Batlle A, Correa Garcia S. Expression of the *UGA4* gene encoding the delta-aminolevulinic and gamma-aminobutyric acids permease in *Saccharomyces cerevisiae* is controlled by amino acid-sensing systems. *Arch Microbiol*. 2005;184(2):137-40.
263. Hardin G. The competitive exclusion principle. *Science*. 1960;131(3409):1292-7.
264. Kim HJ, Boedicker JQ, Choi JW, Ismagilov RF. Defined spatial structure stabilizes a synthetic multispecies bacterial community. *Proc Natl Acad Sci USA*. 2008;105(47):18188-93.
265. Kerr B, Riley MA, Feldman MW, Bohannan BJ. Local dispersal promotes biodiversity in a real-life game of rock-paper-scissors. *Nature*. 2002;418(6894):171-4.
266. Gudelj I, Beardmore RE, Arkin SS, MacLean RC. Constraints on microbial metabolism drive evolutionary diversification in homogeneous environments. *J Evol Biol*. 2007;20(5):1882-9.
267. Cordero OX, Polz MF. Explaining microbial genomic diversity in light of evolutionary ecology. *Nat Rev Microbiol*. 2014;12(4):263-73.
268. Datta MS, Korolev KS, Cvijovic I, Dudley C, Gore J. Range expansion promotes cooperation in an experimental microbial metapopulation. *Proc Natl Acad Sci USA*. 2013;110(18):7354-9.
269. Sanchez A, Gore J. Feedback between population and evolutionary dynamics determines the fate of social microbial populations. *PLoS Biol*. 2013;11(4):e1001547.

270. Ross-Gillespie A, Gardner A, Buckling A, West SA, Griffin AS. Density dependence and cooperation: theory and a test with bacteria. *Evolution*. 2009;63(9):2315-25.
271. Brockhurst MA, Buckling A, Gardner A. Cooperation peaks at intermediate disturbance. *Curr Biol.* 2007;17(9):761-5.
272. Brockhurst MA, Habets MG, Libberton B, Buckling A, Gardner A. Ecological drivers of the evolution of public-goods cooperation in bacteria. *Ecology*. 2010;91(2):334-40.
273. Little AE, Robinson CJ, Peterson SB, Raffa KF, Handelsman J. Rules of engagement: interspecies interactions that regulate microbial communities. *Annu Rev Microbiol.* 2008;62:375-401.
274. Celiker H, Gore J. Competition between species can stabilize public-goods cooperation within a species. *Mol Syst Biol.* 2012;8:621.
275. Harrison F, Paul J, Massey RC, Buckling A. Interspecific competition and siderophore-mediated cooperation in *Pseudomonas aeruginosa. ISME J.* 2008;2(1):49-55.
276. Inglis RF, Biernaskie JM, Gardner A, Kümmerli R. Presence of a loner strain maintains cooperation and diversity in well-mixed bacterial communities. *Proc R Soc Lond B*. 2016;283(1822).
277. Preuss D, Mulholland J, Kaiser CA, Orlean P, Albright C, Rose MD*, et al.* Structure of the yeast endoplasmic reticulum: localization of ER proteins using immunofluorescence and immunoelectron microscopy. *Yeast*. 1991;7(9):891-911.
278. Stambuk BU, Batista AS, De Araujo PS. Kinetics of active sucrose transport in *Saccharomyces cerevisiae. J Biosci Bioeng*. 2000;89(2):212-4.
279. Khan NA, Zimmermann FK, Eaton NR. Genetic and biochemical evidence of sucrose fermentation by maltase in yeast. *Mol Gen Genet*. 1973;123(1):43-50.
280. Ozcan S, Vallier LG, Flick JS, Carlson M, Johnston M. Expression of the *SUC2* gene of *Saccharomyces cerevisiae* is induced by low levels of glucose. *Yeast*. 1997;13(2):127-37.
281. Piskur J, Rozpedowska E, Polakova S, Merico A, Compagno C. How did *Saccharomyces* evolve to become a good brewer? *Trends Genet*. 2006;22(4):183-6.
282. Archetti M, Scheuring I. Review: Game theory of public goods in one-shot social dilemmas without assortment. *J Theor Biol*. 2012;299:9-20.
283. Brockhurst MA, Buckling A, Racey D, Gardner A. Resource supply and the evolution of public-goods cooperation in bacteria. *BMC Biol.* 2008;6:20.
284. Allee WC, Park O, Emerson AE, Park T, Schmidt KP. Principles of animal ecology: WB Saundere Co. Ltd.; 1949.
285. Pfeiffer T, Bonhoeffer S. Evolution of cross-feeding in microbial populations. *Am Nat*. 2004;163(6):E126-35.
286. Rosenzweig RF, Sharp RR, Treves DS, Adams J. Microbial evolution in a simple unstructured environment: genetic differentiation in *Escherichia coli. Genetics*. 1994;137(4):903-17.
287. Butler G, Hsu S, Waltman P. A mathematical model of the chemostat with periodic washout rate. SIAM Journal on Applied Mathematics. 1985;45(3):435-49.
288. Kelsic ED, Zhao J, Vetsigian K, Kishony R. Counteraction of antibiotic production and degradation stabilizes microbial communities. *Nature*. 2015;521(7553):516-9.
289. Dai L, Vorselen D, Korolev KS, Gore J. Generic indicators for loss of resilience before a tipping point leading to population collapse. Science. 2012;336(6085):1175-7.
290. Steinberg G. On the move: endosomes in fungal growth and pathogenicity. *Nat Rev Microbiol*. 2007;5(4):309-16.
291. Ghosh SK, Hajra S, Paek A, Jayaram M. Mechanisms for chromosome and plasmid segregation. *Annu Rev Biochem*. 2006;75:211-41.
292. Futcher AB. The 2 micron circle plasmid of *Saccharomyces cerevisiae. Yeast.* 1988;4(1):27-40.
293. Rapoport TA. Transport of proteins across the endoplasmic reticulum membrane. *Science*. 1992;258(5084):931-6.
294. Nielsen H, Engelbrecht J, Brunak S, von Heijne G. Identification of prokaryotic and eukaryotic signal peptides and prediction of their cleavage sites. *Protein Eng.* 1997;10(1):1-6.
295. Henson JM, Butler MJ, Day AW. The dark side of the mycelium: melanins of phytopathogenic fungi. *Annu Rev Phytopathol*. 1999;37:447-71.
296. Tanino T, Matsumoto T, Fukuda H, Kondo A. Construction of system for localization of target protein in yeast periplasm using invertase. *J Mol Catal B: Enzym*. 2004;28(4):259-64.
297. McNally MT, Free SJ. Isolation and characterization of a *Neurospora* glucose-repressible gene. *Curr Genet*. 1988;14(6):545-51.

298. Freitag M, Hickey PC, Raju NB, Selker EU, Read ND. GFP as a tool to analyze the organization, dynamics and function of nuclei and microtubules in *Neurospora crassa. Fungal Genet Biol.* 2004;41(10):897-910.
299. Lenski RE, Rose MR, Simpson SC, Tadler SC. Long-term experimental evolution in *Escherichia coli.* I. Adaptation and divergence during 2,000 generations. *Am Nat*. 1991;138(6):1315-41.
300. Ehness R, Ecker M, Godt DE, Roitsch T. Glucose and stress independently regulate source and sink metabolism and defense mechanisms via signal transduction pathways involving protein phosphorylation. *Plant Cell*. 1997;9(10):1825-41.
301. Mullaney EJ, Hamer JE, Roberti KA, Yelton MM, Timberlake WE. Primary structure of the *trpC* gene from *Aspergillus nidulans*. *Mol Gen Genet*. 1985;199(1):37-45.
302. Punt PJ, Oliver RP, Dingemanse MA, Pouwels PH, van den Hondel CA. Transformation of *Aspergillus* based on the hygromycin B resistance marker from *Escherichia coli*. *Gene*. 1987;56(1):117-24.
303. Couch BC, Kohn LM. A multilocus gene genealogy concordant with host preference indicates segregation of a new species, *Magnaporthe oryzae, from M. grisea. Mycologia*. 2002;94(4):683-93.
304. Leung H, Lehtinen U, Karjalainen R, Skinner D, Tooley P, Leong S, *et al.* Transformation of the rice blast fungus *Magnaporthe grisea* to hygromycin B resistance. Curr Genet. 1990;17(5):409-11.
305. Talbot NJ, Ebbole DJ, Hamer JE. Identification and characterization of *MPG1*, a gene involved in pathogenicity from the rice blast fungus *Magnaporthe grisea*. *Plant Cell*. 1993;5(11):1575-90.
306. Sambrook J, Fritsch EF, Maniatis T. *Molecular cloning : a laboratory manual*. Cold Spring Harbor: Cold Spring Harbor Laboratory Press; 1989.
307. Southern EM. Detection of specific sequences among DNA fragments separated by gel electrophoresis. *J Mol Biol*. 1975;98(3):503-17.
308. Hamer JE, Howard RJ, Chumley FG, Valent B. A mechanism for surface attachment in spores of a plant pathogenic fungus. *Science*. 1988;239(4837):288-90.
309. Thines E, Weber RW, Talbot NJ. MAP kinase and protein kinase A-dependent mobilization of triacylglycerol and glycogen during appressorium turgor generation by *Magnaporthe grisea. Plant Cell.* 2000;12(9):1703-18.
310. Bacon JSD. Methods for measuring transglycosylase activity of invertases. In: *Methods in enzymology I*. New York: Academic Press, New York; 1955. 258-62.
311. Lever M. A new reaction for colorimetric determination of carbohydrates*. Anal Biochem.* 1972;47(1):273-9.
312. Liu G, Kennedy R, Greenshields DL, Peng G, Forseille L, Selvaraj G, *et al*. Detached and attached *Arabidopsis* leaf assays reveal distinctive defense responses against hemibiotrophic *Colletotrichum* spp. *Mol Plant Microbe Interact*. 2007;20(10):1308-19.
313. Cherry JM, Hong EL, Amundsen C, Balakrishnan R, Binkley G, Chan ET, *et al.* *Saccharomyces* Genome Database: the genomics resource of budding yeast. *Nucleic Acids Res.* 2012;40(Database issue):D700-5.
314. Kämper J, Kahmann R, Bölker M, Ma LJ, Brefort T, Saville BJ, *et al.* Insights from the genome of the biotrophic fungal plant pathogen *Ustilago maydis. Nature*. 2006;444(7115):97-101.